UNIVERSITY OF CALIFORNIA SAN DIEGO

Measuring Changes in Algal-Derived Metabolites in Marine and Freshwater Systems

A dissertation submitted in partial satisfaction of the requirements for the degree Doctor of Philosophy

in

Chemistry

by

Jonathan Scott Sauer

Committee in charge:

Professor Kimberly Prather, Chair
Professor Daniel Donoghue
Professor Susan Golden
Professor Andrew Kummel
Professor Robert Pomeroy
Professor Wei Xiong

2020

The Dissertation of Jonathan Scott Sauer is approved, and it is acceptable in quality and form for publication on microfilm and electronically:

_____

_____

_____

_____

_____

_____

Chair

University of California San Diego

2020

DEDICATION

To my incredible, and supporting family and
those I've met, loved, and learned from along the way.

EPIGRAPH

"If a mixture of different kinds of electrified atoms is moving along in one stream, then when electric and magnetic forces are applied to the stream simultaneously, the different kinds of atoms are sorted out, and the original stream is divided up into a number of smaller streams separated from each other. The particles in any one of the smaller streams are all of the same kind."

-Sir J.J. Thompson, *The Atomic Theory (1914)*

TABLE OF CONTENTS

LIST OF ABBREVIATIONS AND SYMBOLS

AFM	atomic force microscopy
APCI	atmospheric pressure chemical ionization
APS	aerodynamic particle sizer
AVOC	algal volatile organic compound
BEAST	biological effects on air sea transfer
BTEX	benzene toluene ethylbenzene xylene
BVOC	biogenic volatile organic compound
(S)CCM	(standard) cubic centimeters per second
CCN	cloud condensation nuclei
Chl A	chlorophyll a
CIMS	chemical ionization mass spectrometry
CI-TOFMS	chemical ionization time of flight mass spectrometry
CPC	condensation particle counter
CR_{MeSH}	methanethiol conversion ratio
DNA	deoxyribonucleic acid
DMDS	dimethyl disulfide
DMS	dimethyl sulfide
DMSP	dimethylsulfiopropionate
$DMSP_d$	dissolved dimethylsulfoniopropionate
$DMSP_P$	particulate dimethylsulfoniopropionate
DOC	dissolved organic carbon
DOM	dissolved organic matter

EDOC	exchangeable dissolved organic carbon
ESI	electrospray ionization
ESP	environmental sample processor
FCM	flow cytometry
FEP	fluorinated ethylene-propylene
$F_{Triglyceride}$	triglyceride fragmentation ratio
GC	gas chromatography
GCxGC	2-dimensional gas chromatography
GC/MS	gas chromatography mass spectrometry
GNPS	global natural products social molecular networking
HB	heterotrophic bacteria
HEPA	high efficiency particulate air
HESI	heated electrospray ionization
hetSSA	heterogeneously aged sea spray aerosol
HGG1	heterolobosean amoeba
HRMS	high resolution mass spectrometry
ICP-MS	inductively coupled plasma mass spectrometry
IMPACTS	investigations into marine particle chemistry and transfer science
IMR	ion molecule reaction
IMS	imaging mass spectrometry
IN	ice nuclei
INP	ice nucleating particle
ISV	isolated sampling vessel

LC/MS	liquid chromatography mass spectrometry
LIT	linear ion trap
(S)LPM	(standard) liters per minute
LS-APGD	liquid sampling atmospheric pressure glow discharge
MALDI	matrix assisted laser desorption ionization
MART	marine aerosol reference tank
mDOM	marine dissolved organic matter
MeOH	methanol
MeSH	methanethiol
MOUDI	micro orifice uniform deposit impactor
MS	mass spectrometry
MS/MS	product ion mass spectrometry
m/z	mass to charge ratio
OFR	oxidative flow reactors
ORP	open raceway pond
OSC	organo-sulfur compound
PA	proton affinity
PAM-OFR	potential aerosol mass oxidative flow reactor
PBR	photobioreactor
PTFE	polytetrafluoroethylene
qPCR	quantitative polymerase chain reaction
RF	radio frequency
SeaSCAPE	sea spray chemistry and particle evolution

SMA	secondary marine aerosol
SOARS	Scripps ocean atmosphere research simulator
sOTU	single nucleotide resolution
SPE	solid phase extraction
SPME	solid phase micro extraction
SRFA	suwannee river fulvic acid
SSA	sea spray aerosol
TCa	tricaprin
TCy	tricaprylin
TLa	trilaurin
TM	trimyristan
TP	tripalmitin
VOC	volatile organic compound

LIST OF FIGURES

LIST OF TABLES

ACKNOWLEDGEMENTS

I would like to begin by thanking Professor Kimberly Prather for the incredible opportunities and mentoring she has provided as my advisor. Kim has given me ultimate freedom to operate countless powerful, and amazing, and expensive devices to my heart's content. She has constantly challenged me to focus on the big picture and led by example in doing so herself. I owe Kim a massive deal of thanks to her patience in trusting me to improve and giving me a big second chance. I would like to also specifically mention Dr. Robert Pomeroy, who made special time for extended conversations in his office, car, and the hallway about science and life. I would also like to thank my remaining doctoral committee members Professor Andrew Kummel, Professor Wei Xiong, Professor Daniel Donoghue, and Professor Susan Golden for the opportunities, advice, critique, and dialog as I have progressed through my thesis.

The Prather research group is a special place where I have made friends for life. There is something to be said about the bonds that are formed in mutual struggle, and the care of high-performance analytical instrumentation is a real struggle. I am incredibly indebted to the brilliant graduate student and postdoc mentors who showed me how to get experiments to work and take my struggles in stride. I am grateful for the opportunities I have had to pass this knowledge down to those after me, while still watching with perspective as they inevitably make the same mistakes I did. I appreciate all their support that has come in weekly presentations, preparations for exams, writing of manuscripts, and staying sane at the end of a long day. Thank you to: Alexia Moore, Ben Rico, Brock Mitts, Dr. Camille Sultana, Charlotte Beale, Dr. Christopher Lee, Clare Morris, Dr. Daniel Petras, Dr. Douglas Collins, Dr. Gavin Cornwell, Hashim Al-Mashat, John Connor, Joseph Manson, Dr. Julie Dinasquet, Kathryn Mayer, Ke'La Kimble, Dr. Louise Kristensen, Lucia Cancelada, Matthew Pendergraft, Mitchell Santander, Dr. Olivia Ryder, Dr. Rebecca Simpson,

Robin Richardson, and Dr. Xiaofei Wang. I'd also like to specifically thank Joe Mayer, who has given me invaluable help with fabricating and maintaining instrumentation as well as showing me how technical skill is almost more art than science. His can-do attitude has inspired me to keep my hands dirty and look in all directions for solutions to difficult problems. I'd also like to thank Monica Castrejon, whose brilliance in organizing people and tasks made the experiments I did truly possible.

Outside of the Prather research group, I'd like to thank the collaborators who have helped in large field experiments and been pivotal to better improving my work. Thanks to: Dr. Carolyn Fisher, Emily Barnes, Dr. Gordon Novak, Kathryn Moore, Luis Camarda, Michael Alves, Michael Vermuel, Dr. Ryan Simkovsky, Summer Sherman, and Dr. Todd Lane. I'd like to specifically thank Dr. Timothy Bertram who helped me immensely with the troubleshooting and advice on my primary analytical technique.

Lastly, I could have not made it very far without the support of my family. My father Scott, stepmother Carmen, and mother Roxanne have done everything they could to make sure I was happy, supported, and doing what I loved. My siblings, Amanda, Brett, and Breanna have been incredible cheerleaders that I am truly blessed to call my family.

Chapter 2, in full, is currently being prepared for resubmission to Journal of Geophysical Research: Biogeosciences. Sauer, J.S., Minich, J.J., Dinasquet, J., Malfatti, F., Mayer, K.J., Santander, M.D., Pendergraft, M.A., Mitts, B., Lee, C., Wang, X., Rico, B., Knight, R., Bertram, T.H, Prather, K.A. (2020). "Production of Dimethyl Sulfide, Methanethiol, and Dimethyl Disulfide During Controlled Phytoplankton-Bacterial Mesocosm Experiments." Journal of Geophysical Research: Biogeosciences (2020) The dissertation author is the primary investigator and author of this manuscript.

Chapter 3, in full, is currently being prepared for submission for publication of the material. Nguyen, D.D., Sauer, J.S., Camarda, L.P., Sherman, S., Prather, K.A., Golden, S.S., Pomeroy, R., Dorrestein, P.C., Simkovsky, R. (2020), "Multi-scale Examination of Grazer-Induced Changes in Molecular Signatures of Cyanobacteria" Dr. Don G. Nguyen and the dissertation author are co-first authors of this manuscript.

Chapter 4, in full, is currently being prepared for submission for publication of the material. Sauer, J.S., Simkovsky, R.S., Moore, A., Camarda, L., Prather, K.A., Pomeroy, R. "Early Detection of Algal Grazing with Rapid, Continuous Measurements of Volatile Gases" The dissertation author is the primary investigator and author of this manuscript.

Chapter 5, in full, is a reprint of material as it appears in Analytical Chemistry. Alves, M.R., Sauer, J.S., Prather, K.A., Grassian, V.H., Wilkins, C.L. (2020). "Liquid Sampling-Atmospheric Pressure Glow Discharge Ionization as a Technique for the Characterization of Salt-Containing Organic Samples." Anal. Chem., 92, 8845-8851. Reproduced with permission of the American Chemical Society. Michael R. Alves and the dissertation author are co-first authors of this manuscript.

Chapter 6, in full, is currently being prepared for submission for publication of the material. Sauer, J.S., Mayer, K.J., Lee, C., Crocker, D.R., A., Alves, M.R., Amiri, S., Barnes, E., Crocker, D.R., Dinasquet, J., Kaluarachchi, C.P., Dang, D., Glicker, H., Kilgour, D., Lawler, M.J., Mitts, B.A., Morris, C.K., Moore, A.N., Tumminello, P.R., Walker, J.L., Goldstein, A.H., Grassian, V.H., Jaffe, J., Malfatti, F., Martz, T.R., Tivanski, A.V.,Cappa, C.D., Bertram, T.H., Prather, K.A. "The Sea Spray Chemistry and Particle Evolution Study (SeaSCAPE): Overview and Experimental Methods", Kathryn J. Mayer, Christopher Lee, and the dissertation author are co-first authors of this manuscript.

Chapter 7, in full, is a reprint of material as it appears in Accounts of Chemical Research. Mayer, K.J, Sauer, J.S., Dinasquet, J., Prather, K.A. (2020). "CAICE Studies: Insights from a Decade of Ocean–Atmosphere Experiments in the Laboratory" Acc. Chem. Res., 92, 8845-8851. Reproduced with permission of the American Chemical Society. Kathryn J. Mayer and the dissertation author are co-first authors of this manuscript.

VITA

2014 Bachelor of Science, University of Wisconsin Stevens Point

2014-2020 Research Assistant, University of California San Diego

2020 Doctor of Philosophy, University of California San Diego

PUBLICATIONS

[*]Mayer, K. J., [*]Sauer, J. S., Dinasquet, J. and Prather, K. A.: CAICE Studies: Insights from a Decade of Ocean–Atmosphere Experiments in the Laboratory, Acc. Chem. Res., doi:10.1021/acs.accounts.0c00504, 2020.

[*]Alves, M. R., [*]Sauer, J. S., Prather, K. A., Grassian, V. H. and Wilkins, C. L.: Liquid Sampling-Atmospheric Pressure Glow Discharge Ionization as a Technique for the Characterization of Salt-Containing Organic Samples, Anal. Chem., 92(13), 8845–8851, doi:10.1021/acs.analchem.0c00361, 2020.

Hasenecz, E. S., Jayarathne, T., Pendergraft, M. A., Santander, M. V., Mayer, K. J., Sauer, J. S., Lee, C., Gibson, W., Kruse, S., Malfatti, F., Prather, K. A. and Stone, E.: Marine bacteria affects saccharide enrichment in sea spray aerosol during a phytoplankton bloom, ACS Earth Sp. Chem., 4(9), 1638–1649 doi:https://doi.org/10.1021/acsearthspacechem.0c00167, 2020.

Widner, D. L., Knauf, Q. R., Merucci, M. T., Fritz, T. R., Sauer, J. S., Speetzen, E. D., Bosch, E. and Bowling, N. P.: Intramolecular halogen bonding supported by an aryldiyne linker, J. Org. Chem., 79(13), 6269–6278, doi:10.1021/jo501015x, 2014.

Hamm, D. C., Braun, L. A., Burazin, A. N., Gauthier, A. M., Ness, K. O., Biebel, C. E., Sauer, J. S., Tanke, R., Noll, B. C., Bosch, E. and Bowling, N. P.: Conjugated metallorganic macrocycles: Opportunities for coordination-driven planarization of bidentate, pyridine-based ligands, Dalt. Trans., 42(4), 948–958, doi:10.1039/c2dt31914d, 2013.

Ren, Q., Reedy, C. G., Terrell, E. A., Wieting, J. M., Wagie, R. W., Asplin, J. P., Doyle, L. M., Long, S. J., Everard, M. T., Sauer, J. S., Baumgart, C. E., D'Acchioli, J. S. and Bowling, N. P.: Evidence of enhanced conjugation in ortho -arylene ethynylenes with transition metal coordination, J. Org. Chem., 77(5), 2571–2577, doi:10.1021/jo300034h, 2012.

[*]Co-first authors.

PRESENTATIONS

Sauer, J.S., Simkovsky, R., Moore, A.N., Prather, K. A., Pomeroy, R., (2020) Application of Chemical Ionization Mass Spectrometry for Rapid Multivessel Monitoring of Algal Health and Grazer Infection State; Algae Biomass Summit, Online Meeting, September 2020

Sauer, J., Minich, J., Dinasquet, J., Mayer, K.,; Santander, M.V., Malfatti; Francesca, M., Pendergraft, M., Rico, B., Mitts, B., Wang X.,Bertram, T., Knight, R., Prather, K., Factors Controlling the Release of Methylated Sulfur Species from Laboratory Mesocosm Experiments in Coastal Seawater; AGU Fall Meeting, San Francisco, Ca, 2019

Sauer, J., Lee, C., Michaud, J., Ryder, O., Prather, K.A. Changes in Chemical Composition of Sea Spray Aerosol In Response to Bulk Enzymatic Processing; ACS San Diego April 2016

Sauer, J., Nelson, N., Schlapper, A., Metabolomic Analysis of Potato Glower Volatiles; American Society for Biochemistry and Molecular Biology Annual Meeting, San Diego, CA, April 2014

ABSTRACT OF THE DISSERTATION

Measuring Changes in Algal-Derived Metabolites in Marine and Freshwater Systems

by

Jonathan Scott Sauer

Doctor of Philosophy in Chemistry

University of California San Diego, 2020

Professor Kim Prather, Chair

Metabolites produced by microalgae profoundly affect the natural environment as the dominant organic carbon source in the ocean and the dominant organic sulfur source to the atmosphere. Of particular interest to this dissertation is the production of algal metabolites in response to changes in organism health and biological community turnover. In this dissertation, algal metabolites are investigated in highly complex marine and in controlled commercial-oriented environments. Measurements of organosulfur gases dimethyl sulfide, methanethiol, and dimethyl disulfide during marine mesocosm experiments show that the production of highly reactive non-dimethyl sulfide organosulfur compounds can comprise a far larger fraction of total sulfur released from the ocean than previously understood. This production was found to depend on the bacterial assemblages present in each mesocosm in combination with the biochemistry of the water. To more accurately measure algal metabolites in the natural environment, a new ionization method

for high resolution mass spectrometry of high-salt organic samples was applied to analysis of marine samples. This method demonstrated the ability to analyze unprocessed seawater for the first time. To produce systems which replicate the turnover of natural marine algae, a review of the ocean-atmosphere simulator approach is given. As an exemplar of this approach, an intensive experiment utilizing an ocean atmosphere simulator is given which discusses the system performance and mesocosm characteristics. As microalgae are increasingly used commercially as a source of renewable biomass, understanding the production of metabolites in response to deleterious factors such as grazing is needed. The connection between algal grazing and production of grazing-specific metabolites was investigated by combining the results from imaging mass spectrometry, liquid chromatography mass spectrometry, and gas chromatography mass spectrometry. These studies found chlorophyll-a related breakdown products in the solid and liquid phases which were connected to measurements of volatile gases. Continuous measurements of volatile gases from microalgae by chemical ionization mass spectrometry were performed to understand the timescale in which gas production in response to grazing occurs. Chemical ionization mass spectrometry was found to be able to detect grazing in algal cultures 24-72 hours faster than current best methods, opening a new monitoring approach for commercial microalgae.

Chapter 1. Introduction

1.1 Algae

Across the Earth's oceans, lakes, rivers, and land a productive group of organisms called algae live in and transform their surroundings. While the term "algae" has no formal connection to specific taxonomy, it is frequently used to refer to a broad assemblage of photosynthetic organisms which are structurally differentiated from plants (Barsanti and Gualtieri, 2014a). Algae span a large range of sizes, from small single-celled phytoplankton to large macroalgae which can be up to 60 m in length. These organisms occupy a wide range of habitats where they often comprise the base of the surrounding food web. Algae significantly impact the chemical composition of the environment through their participation in the phosphorus, nitrogen, silicon, sulfur, and oxygen-carbon cycles (Barsanti and Gualtieri, 2014b). Marine algae alone produce approximately 50% of the oxygen that we breathe. Historically, algae have drastically altered the composition of the atmosphere since the evolution of oxygenic photosynthesis by cyanobacteria, transforming the composition of the Earth's atmosphere from 80% N_2, 10% CO/CO_2, and 10% H_2 (by volume) to 78% N_2, 21% O_2, and 0.036% CO_2 during the great oxidation transition 3.0-2.3 billion years ago (Lyons et al., 2014). Understanding the impact of algae's chemical influence on the environment has been extensively studied to date, however significant questions remain as the type, quantity, and reasons these chemicals are released, and their behaviors of these chemicals once they enter the environment.

1.2 Chemicals Produced by Algae

Algae synthesize a highly diverse range of chemicals required for their survival in the environments they inhabit. To construct the physical structures of their cell bodies, algae synthesize carbohydrate, lipid, protein, or mineralized exteriors (Domozych et al., 2012;

Hildebrand et al., 2018). Within the cells, algae produce a vast variety of chemicals, including proteins (amino acids), nucleic acids (purines, pyrimidines), lipids (fatty acids, triglycerides), isoprenoids (terpenoids, steroids, carotenoids), polysaccharides, halogenated compounds, amines, organosulfur, and inorganic gases (Achyuthan et al., 2017; Cardozo et al., 2007; Carpenter et al., 2012). These compounds carry out numerous roles in algal metabolism, from photosynthesis to defense against pathogenic attack (Zuo, 2019). Consequently, many of these chemical species are released from algal cells into the external environment as waste-products, functional entities (signaling etc.), or inadvertently due to cell senescence. Once released into the environment, these chemicals can be further turned over by oxidation and consumption by other organisms or can transfer across interfaces as volatile gases.

1.3 Algal Organics in the Marine Environment

The chemical composition of the ocean is diverse and variable in time. Inputs from biological activity, especially algae, combine with geochemical processes and contributions from anthropogenic sources. These inputs not only influence the biochemical and inorganic behavior of ocean itself, but also the marine atmosphere as these chemicals are aerosolized as sea spray aerosol (SSA) or volatilized by evaporation.

One of the most important organic constituents of natural seawater is marine dissolved organic matter (mDOM), which has a total reservoir of $6.62*10^{14}$ kg C (Hansell et al., 2009). mDOM is operationally defined as organic material that passes through filtration at 0.2 μm, discriminating it from particulate organic matter (POM) which is retained between filters of 0.7 to 0.2 μm (Lønborg et al., 2020). mDOM molecules can be further described by their content of dissolved organic carbon (DOC), nitrogen, phosphorus, sulfur, complexed metals, and other elements.

Sources of DOC in the marine environment can be either autochthonous or allochthonous, meaning produced within the system or externally. For autochthonous DOC, the most important producers are phytoplankton (microalgae) and macroalgae, which release extracellular DOC as 5-30% of their total primary production. Phytoplankton also produce DOC during stress, autolysis, and grazing by zooplankton and bacteria. (Van Boekel et al., 1992) Furthermore, sloppy feeding, excretion, and defecation by grazers consuming algae contribute to release of DOC, showing the entire lifecycle of algae lead to various contributions in the DOC pool. (Lampert, 1978)

Further operational refinement of DOC can discriminate it into a volatile fraction which is capable of air sea exchange, known EDOC, which has been shown to be up to one third of DOC in surface waters (Dachs et al., 2005). This fraction is frequently referred to as volatile organic compounds (VOC), but can also contain non-organic volatile species such as ammonia (Facchini et al., 2008). VOCs released from microorganisms into the surrounding aqueous environment transfer into the atmosphere depending on a variety of factors which include the properties of the VOC itself (molecular weight, vapor pressure, henry's law constant), the properties of the water (salinity, temperature) and turbulent mixing forces such as wind and bubble bursting (Brooks et al., 2009; Johnson, 2010). While significant work has been achieved towards better understanding the mDOM, factors which affect the composition, quantity, and dynamics of the production of algal metabolites which comprise mDOM are still poorly understood.

1.4 Algal Organosulfur in the Marine Environment

One of the most studied algal metabolites in mDOM is dimethylsulfoniopropionate (DMSP). DMSP ($C_5H_{10}O_2S$) is a zwitterionic organosulfur compound (OSC) which is utilized primarily by algae as an osmolyte but also fulfills several other biochemical roles (DeBose et al., 2008; Kiene et al., 2000). When released from algal cells, DMSP can be metabolized through

enzymatic breakdown to produce volatile OSCs, primarily dimethyl sulfide (DMS) and methanethiol (MeSH) (Reisch et al., 2011). The breakdown of extracellular DMSP is mediated by the presence of marine heterotrophic bacteria which utilize the sulfur and carbon in DMSP for their own metabolic needs (Sun et al., 2016). Due to the low solubility, fairly high concentration, and widespread presence of these dissolved gases in marine surface waters (~0.1-10nM), air-sea transfer of these gases is a notable source of both organic carbon and sulfur in the marine boundary layer (Kettle et al., 2001). In the case of dimethyl sulfide, 28 Tg $S \cdot yr^{-1}$ are emitted from the oceans, the largest natural source of sulfur emission into the atmosphere (Lee and Brimblecombe, 2016).

Following transfer, DMS and MeSH are oxidized in the marine atmosphere by OH radical, sunlight, and other oxidants, into end products H2SO4 and methanesulfonic acid. Due to their low volatility and high water solubility, these compounds will partition into the aerosol phase, either through condensation onto pre-existing particles or formation of new particles (Kroll and Seinfeld, 2008). The incorporation of oxidized sulfur mass into aerosol particles significantly influences the aerosol budget in the marine atmosphere, leading to significant changes in the number of cloud condensation nuclei (CCN): particles which accumulate water and form cloud droplets which compose clouds (Fitzgerald, 1991). For these reasons, the connections between algal ecology, biochemistry, and cloud cover over the ocean have been intensely studied over the last 50 years to better understand and predict dynamics in climate and precipitation (Quinn and Bates, 2011).

While significant progress has been made towards understanding the atmospheric behavior of OSCs (Hoffmann et al., 2016; Veres et al., 2020), significant questions still remain over the relative emissions between different OSCs depending on the biological taxa present and the environmental conditions which influence them (Pinhassi et al., 2005; Simo, 2001; Varaljay et al., 2015).

1.5 Algae in the Commercial Sector

Algae are commercially cultivated for valuable products derived from their biomass. The utilization of algae is a promising "green" technology that is still maturing as innovations to develop new products and cultivation methods increase profitability. The production of algae for biofuels is the most well-known example, with U.S. production of biofuels at ~7 billion liters in 2018 (EIA, 2020). In addition, algal production of animal feeds, pharmaceuticals, dyes, nutraceuticals, and high value small molecules represent other promising opportunities for this technology. (Burkart and Mayfield, 2013; Hu et al., 2008; Jones and Mayfield, 2012). Current technology for full-scale algal cultivation is split between two methods: closed photobioreactors (PBRs) and open raceway ponds (ORPs) (Richardson et al., 2014). While PBRs maintain superior culture cleanliness and better control conditions such as temperature, light, and nutrients, the enhanced yields from PBRs are offset by their high up-front and operational costs. Conversely, open raceway ponds are comparatively cheap to construct at large scale, but their weaknesses include a vulnerability to unpredictable environmental conditions and the unwanted introduction of biological contaminants known as grazers (Richardson et al., 2014). Studies suggest that up to 30% algae biomass is lost due to grazing in commercial operations (Deore et al., 2020). Algal grazers, sometimes called predators, comprise a variety of different taxonomic groups which can include fungi, viruses, zooplankton such as copepods, rotifers, dinoflagellates, amoeba, ciliates, and bacteria (Di Caprio, 2020; Deore et al., 2020). Their effect on algal ponds can be highly deleterious, with some grazer infections capable of eliminating all algal biomass within 48 hours of introduction. This challenge is expanded by the growth dynamics of algal grazers which occur on exponential timescales, meaning the window to detect infections by current methods is on the order of hours (Forehead and O'Kelly, 2013). The current methods of grazer detection are optical

microscopy and flow cytometry, which have been inadequate in their ability to detect grazer contamination early enough to prevent significant commercial biomass losses. Further research on grazer detection and mitigation strategies is warranted.

1.6 Volatile Gases Produced by Algae in Response to Grazing

The measurement of VOCs produced by commercial microalgae has recently received more attention as a method to monitor algal state of health as well as detect metabolites produced by grazing (Achyuthan et al., 2017; Fisher et al., 2020; Reese et al., 2019). While most prior research has focused on VOCs obtained from lysed algae, there has been little investigation of in situ VOC production that would occur in cultured ponds. Known algal VOC classes include alcohols, alkanes, alkenes, aldehydes, ketones, sulfides, amines, halogenated VOCs, terpenes, and other oxygenated VOCs (Achyuthan et al., 2017). In a pilot experiment, Reese et al. showed enhanced production of carotenoid breakdown products, trans β-ionone and β-cyclocitral from grazer infected Microchloropsis salina, showing the promise of these gases as tools to monitor biomass production and prevent pond crashes. Utilizing a different VOC sampling method for the same algae/grazer pair, Fisher et al. (2019) discovered several small VOCs indicating algal grazing with little overlap between the VOCs observed with their sampling method to work in Reese et al. While these experiments break important ground, several important questions remain to be answered as to how algal VOC production responds to grazing.

1.7 Mass Spectrometry for the Detection of Algal Metabolites

In mass spectrometry (MS), ions are generated from organic or inorganic compounds, separated from each other by differing mass to charge ratios (m/z), and detected by their respective m/z and abundance (Gross, 2011). The specific ionization method for any MS instrument is often the defining feature which limits the physical phase, chemical composition, and speed with which

analytes can be introduced and detected. This dissertation will discuss various MS methods, the purpose and capability of which are described here.

1.7.1 Gas Chromatography Mass Spectrometry

Historically, the predominant method for determination of molecular identity of volatile organic compounds (VOCs) has been gas chromatography mass spectrometry (GC/MS). In GC/MS, a sample of volatile analytes (either liquid or gas phase) is injected onto a narrow diameter capillary column where carrier gases are passed through the column which direct the chemical mixture towards the electron impact (EI) ionization source and mass spectrometer detector. Depending on the analyte volatility and polarity as well as the column temperature, different gas molecules adhere to the capillary column stationary phase material with differing efficiency, leading to spatial separation of analytes on the column. This separation leads to differing arrival times of analytes at the mass spectrometer, allowing for unambiguous detection of molecular species by their precursor mass and fragmentation pattern (McMaster, 2008). Notably, GC/MS traditionally suffers from slow sample throughput (~45 min/sample) when a large variety of analytes must be observed. For the GC/MS analysis of VOCs in this work, VOC samples were taken using solid phase microextraction (SPME) fibers. In SPME, headspace VOCs are exposed to a thin (40-100 μm) sampling fiber which has a distinct chemical surface functionality which allows for the adsorption of sample VOCs onto the fiber. These VOCs are then thermally desorbed off the SPME fiber in the GC/MS sampling inlet for analysis (Souza-Silva et al., 2015).

1.7.2 High Resolution Mass Spectrometry

In high resolution mass spectrometry (HRMS), mass spectra of ionized analytes are acquired with highly accurate and precise m/z values through the usage of high performance mass analyzers (Marshall and Hendrickson, 2008). In HRMS, samples are ionized through a variety of

different methods, usually with the intention of maintaining the intact molecular ion. This contrasts with EI, which leads to a high degree of fragmentation. High mass resolution and mass accuracy allows for the calculation of accurate molecular formulae for the observed ions. Further identification can be achieved through tandem mass spectrometry, also known as MS/MS, wherein the mass-specific fragmentation of the precursor ion is coupled with high-resolution mass analysis of the product ions (Fenselau, 1992). The information obtained from MS/MS can be analyzed using molecular networking algorithms, which identify similarity relationships between fragmentation patterns and aid in the interpretation of complex mass spectra (Wang et al., 2016).

Currently, HRMS analysis of analytes dissolved in seawater is large challenge due to its salinity (~35g kg^{-1}) (Millero et al., 2008). Salts interfere with ionization, cause corrosion, and deposit onto instrument surfaces, potentially damaging them. Frequently, extraction methods to separate dissolved organic compounds from salts in marine samples are utilized; however, their sample recovery rates can be highly variable and a large fraction of organic species in a sample are not analyzed (Kruger et al., 2011).

1.7.3 Chemical Ionization Mass Spectrometry

To begin, we draw a distinction between chemical ionization utilized as an alternative ionization method for GC/MS instruments instead of EI. In the context of this thesis, chemical ionization mass spectrometry is defined as an analysis method whereby the complete analyte gas mixture is sampled into the ionization region without pre-separation and the constituents detected by mass spectrometry. To generate analyte ions, a reagent ion gas is cointroduced to the ionization source with the analyte gas, and provided the chemical energetics between the reagent ions and analyte gases allow for ionization reactions in the residence time of the ionization source, analyte product ions are generated (Bertram et al., 2011). In this dissertation, the reagent ions utilized are

protonated water clusters, (H2O)nH+ where n = 1,2,3,…, and benzene cluster cations (C6H6)n+ where n = 1,2 which ionize primarily by proton transfer and charge transfer respectively (Aljawhary et al., 2013; Kim et al., 2016). For each ionization chemistry, the chemical energetics necessary for analyte ionization: a higher proton affinity than $(H_2O)_nH^+$ (691, 694, 730, 769 kJ mol-1) or a lower ionization potential than $(C_6H_6)_n^+$ (9.2 eV) results in an ionization selectivity which limits each ionization chemistry to detect certain classes of chemical compounds. For $(H_2O)_nH^+$, organic compounds with a low degree of oxygenation—aliphatic ketones, aldehydes, and amines—are detected with high sensitivity (Aljawhary et al., 2013). For $(C_6H_6)_n^+$, select biogenic VOCs with lower ionization energies such as organosulfur compounds, and amines can be detected (Kim et al., 2016; Lavi et al., 2017). This chemical selectivity is a significant advantage to CIMS which allows for direct sampling of air masses without producing an over-complicated mass spectrum that would be observed with a more generalist ionization method such as EI. From the chemical selectivity of the ionization, the defining characteristic of CIMS is the high sampling speed (up to 10 Hz) which allows for real-time sampling of complete air masses continuously for days or weeks with minimal interruption. The data product of CIMS is time-series mass spectra of gas composition that can extend over comparatively long durations (>30 days) to other forms of chemical analysis. This distinct characteristic of CIMS has been mostly applied towards questions in the atmospheric sciences as covarying factors with gas composition like wind, temperature, and turnover of biological organisms (Carpenter et al., 2012; Kim et al., 2015, 2017).

1.8 Systems to replicate the complexity of marine microbiology and chemical turnover

Field measurements in the marine environment can capture the full complexity of atmospheric aerosols and gases, but frequently struggle to disentangle the numerous factors which contribute to their properties. Conversely, many laboratory studies utilize overly simplistic model

systems which do not capture the behavior of real-world systems. Towards these challenges, new devices have been constructed which simulate the complexity of the marine environment by holding natural seawater in closed systems and generating sea spray aerosol (SSA) for chemical analysis. Marine aerosol reference tanks (MARTs) and wave channels produce SSA through plunging waterfalls and wave breaking respectively which match the aerosol size distribution of SSA observed in the marine environment (Prather et al., 2013; Stokes et al., 2013, 2016). These vessels are suited for natural marine mesocosms, which contain the entire microbial loop (phytoplankton, bacteria, viruses) through the addition of nutrients. This allows for studies which assess the impacts of biological turnover and dynamics on aerosol composition, trace gas production, and other atmospherically relevant processes (Wang et al., 2015). These aerosol generation devices have already succeeded in advancing the simulated ocean-atmosphere approach and have aided in the identification of numerous new processes in atmospheric chemistry.

1.9 Goals of dissertation

This dissertation focuses upon changes in production of organic and volatile species by microalgae in both natural-simulated and commercial contexts. Furthermore, for natural systems, special attention is paid towards the simulation of real-world chemical and biological complexity. The main questions that will be addressed include:

1. What is the partitioning between different volatile organosulfur compounds in natural marine mesocosm experiments? How is this partitioning related to, and affected by the chemical and biological factors that define each mesocosm?
2. What molecules are produced when commercial microalgae interact with grazers? Can molecular relationships obtained from these analyses inform the analytes that one would observe in the gas phase?

3. In what timescales do commercial algae change their production of gases in response to grazing? Can high frequency composition measurements be utilized to detect grazer infections?
4. In the dissolved phase, can new methods of sample introduction and ionization be utilized to measure algal-related metabolites without pre-existing salt removal?
5. What are the properties of aerosols and gases observed in large mesocosm experimental devices such as wave channels?
6. What are the merits, weaknesses, and successes of the ocean-atmosphere experimental approach? What advancements to this approach need to be made to better simulate the natural marine environment?

1.10 Synopsis of dissertation

This dissertation attempts to address these questions by combing laboratory experiments which span a range of compositional measurement techniques. Chapter 2 shows that the production of non-DMS organosulfur gases—methanethiol and dimethyl disulfide—can greatly exceed production of DMS in coastal mesocosm experiments. Measurements of these gases in tandem with biological sequencing uncovered relationships between bacterial taxa and OSC formation, which were further contextualized by comparisons to the biochemical state of the water over the course of each bloom. These findings were applied to an atmospheric model which showed the influence of non-DMS OSCs can be significant to sulfate aerosol formation in the marine atmosphere, thus affecting cloud formation and the Earth's radiative budget.

Chapter 3 of this dissertation investigates the production of chemical markers by algae at three different scales as they are infected with amoeba grazers. Using imaging mass spectrometry (IMS) for algae mounted on solid agar substrate and infected with amoeba, specific ions were

mapped to regions where grazing occurred. Using the spatially correlated ions from IMS solid-phase analysis, liquid chromatography mass spectrometry was performed on aqueous samples and molecular networking was applied to ascertain the identity of the matching molecular species. From this analysis, several metabolites related to chlorophyll-a breakdown were identified to be indicators of amoeba grazing. Specifically, pheophorbide A, pyropheophorbide, and pyropheophytin were found to be grazing-specific metabolites, differing from the precursor metabolite pheophytin A by removal of phytol and methyl formate moieties. Given the relatively high volatility of phytol and methyl formate, further analyses of the gas phase of grazer infected algae was performed to see if those species were identifiable. While small quantities of a phytol-adjacent metabolite, phytol ketone, were observed, no methyl formate was identified by gas chromatography mass spectrometry or chemical ionization mass spectrometry. However, multiple volatile gases not predicted by the IMS/LCMS were found to be produced by grazer infected algae, showing promise for the usage of VOC measurement for early grazer detection.

Chapter 4 of this dissertation investigates the usage of chemical ionization time of flight mass spectrometry (CI-TOFMS) for online analysis of multiple algal culture headspaces to investigate grazer contamination. Using protonated water cluster chemical ionization, several (>40) distinct ions were identified in 40 L algal cultures which quickly equilibrated to the instrument and tubing surfaces within ~12s of sampling each vessel. After addition of grazers to a final concentration of 0.1 cells/mL to algal cultures, CI-TOFMS analysis observed changes in production of several (>20) volatile gases significantly faster (25-76 hours) than microscopy could detect grazers. Further analysis of algal gas time series indicated that enhanced production or cessation of certain species is consistent with larger algal biomass densities, an interesting result

which suggests additional applications for the use of gas phase analysis in monitoring the health of commercial algae ponds.

Chapter 5 of this dissertation describes the application of a liquid sampling atmospheric pressure glow discharge (LS-APGD) ionization source for the high-resolution mass spectrometric analysis of high salinity organic samples. An investigation of LS-APGD ionization behaviors for a triglyceride mixture was performed to ascertain the impacts of varying salt concentration on analyte sensitivity and fragmentation susceptibility in comparison to electrospray ionization. Highly complex samples of marine dissolved organic matter were further investigated using the LS-APGD in contrast to ESI with particular attention payed towards the degree of chemical functionality of analytes detected by each ionization method. Lastly, for the first time, samples of organic-rich raw seawater were directly analyzed as a demonstration of the capabilities of LS-APGD.

Chapter 6 of this dissertation describes the characterization of the Scripps Institution of Oceanography wave channel which was recently utilized for a large experimental intensive: The Sea Spray Chemistry and Particle Evolution Study (SeaSCAPE). The extensive control experiments conducted to assess the wave channel's production of sea spray aerosols, air flow characteristics, and cleanliness to anthropogenic contaminants are discussed. The wave channel accurately reproduces the aerosol size distribution of marine sea spray aerosol; however, challenges with maintaining system cleanliness inform future improvements to headspace introduction and building materials. Lastly, the SeaSCAPE intensive campaign is outlined with attention paid towards the production of biologically representative algal-bacterial mesocosms.

Finally, Chapter 7 presents a review of the ocean-atmosphere experimental method which seeks to replicate the biological and chemical complexity of the ocean. Details regarding

investigations of sea spray composition, reactivity, and climate relevant properties are discussed which demonstrate the utility of the ocean atmosphere approach. Lastly, future directions of the ocean atmosphere approach are outlined which detail the incorporation of detailed atmospheric aging processes. Overall, the contents of this dissertation provide insight into the production, measurement, and implications of VOC production from microalgae.

1.11 Acknowledgements

Ryan Simkovsky and Kathryn Mayer are acknowledged for their assistance in editing this chapter.

1.12 References

Achyuthan, K. E., Harper, J. C., Manginell, R. P. and Moorman, M. W.: Volatile metabolites emission by in vivo microalgae—an overlooked opportunity?, Metabolites, 7(3), doi:10.3390/metabo7030039, 2017.

Aljawhary, D., Lee, A. K. Y. and Abbatt, J. P. D.: High-resolution chemical ionization mass spectrometry (ToF-CIMS): Application to study SOA composition and processing, Atmos. Meas. Tech., 6(11), 3211–3224, doi:10.5194/amt-6-3211-2013, 2013.

Barsanti, L. and Gualtieri, P.: Biogeochemical Role of Algae, Algae, 2, 199–220, doi:10.1201/b16544-6, 2014.

Bertram, T. H., Kimmel, J. R., Crisp, T. A., Ryder, O. S., Yatavelli, R. L. N., Thornton, J. A., Cubison, M. J., Gonin, M. and Worsnop, D. R.: A field-deployable, chemical ionization time-of-flight mass spectrometer, Atmos. Meas. Tech., 4(7), 1471–1479, doi:10.5194/amt-4-1471-2011, 2011.

Van Boekel, W. H. M., Hansen, F. C., Riegman, R. and Bak, R. P. M.: Lysis-induced decline of a Phaeocystis spring bloom and coupling with the microbial foodweb, Mar. Ecol. Prog. Ser., 81(3), 269–276, doi:10.3354/meps081269, 1992.

Burkart, M. D. and Mayfield, S. P.: Biofuels for the 21st century, Curr. Opin. Chem. Biol., 17(3), 436–438, doi:10.1016/j.cbpa.2013.05.003, 2013.

Di Caprio, F.: Methods to quantify biological contaminants in microalgae cultures, Algal Res., 49(March), 101943, doi:10.1016/j.algal.2020.101943, 2020.

Cardozo, K. H. M., Guaratini, T., Barros, M. P., Falcão, V. R., Tonon, A. P., Lopes, N. P., Campos, S., Torres, M. A., Souza, A. O., Colepicolo, P. and Pinto, E.: Metabolites from algae with economical impact, Comp. Biochem. Physiol. - C Toxicol. Pharmacol., 146(1-2 SPEC. ISS.), 60–78, doi:10.1016/j.cbpc.2006.05.007, 2007.

Carpenter, L. J., Archer, S. D. and Beale, R.: Ocean-atmosphere trace gas exchange, Chem. Soc. Rev., 41(19), 6473–6506, doi:10.1039/c2cs35121h, 2012.

Dachs, J., Calleja, M. L., Duarte, C. M., del Vento, S., Turpin, B., Polidori, A., Herndl, G. J. and Agustí, S.: High atmosphere-ocean exchange of organic carbon in the NE subtropical Atlantic, Geophys. Res. Lett., 32(21), 1–4, doi:10.1029/2005GL023799, 2005.

DeBose, J. L., Lema, S. C. and Nevitt, G. A.: Dimethylsulfoniopropionate as a foraging cue for reef fishes, Science (80-.)., 319(5868), 1356, doi:10.1126/science.1151109, 2008.

Deore, P., Beardall, J. and Noronha, S.: A perspective on the current status of approaches for early detection of microalgal grazing, J. Appl. Phycol., doi:10.1007/s10811-020-02241-x, 2020.

Domozych, D. S., Ciancia, M., Fangel, J. U., Mikkelsen, M. D., Ulvskov, P. and Willats, W. G. T.: The cell walls of green algae: A journey through evolution and diversity, Front. Plant Sci., 3(MAY), 1–7, doi:10.3389/fpls.2012.00082, 2012.

EIA: Monthly Biodiesel Production Report, , 10, 2020.

Facchini, M. C., Decesari, S., Rinaldo, M., Carbone, C., Finessi, E., Mircea, M., Fuzzi, S., Moretti, F., Tagliavini, E., Ceburnis, D. and O'Dowd, C. D.: Important source of marine secondary organic aerosol from biogenic amines, Environ. Sci. Technol., 42(24), 9116–9121, doi:10.1021/es8018385, 2008.

Fenselau, C.: Tandem mass spectrometry: The competitive edge of pharmacology, Annu. Rev. Pharmacol. Toxicol., 32(c), 555–578, doi:10.1146/annurev.pharmtox.32.1.555, 1992.

Fisher, C. L., Lane, P. D., Russell, M., Maddalena, R. and Lane, T. W.: Low molecular weight volatile organic compounds indicate grazing by the marine rotifer brachionus plicatilis on the microalgae microchloropsis salina, Metabolites, 10(9), 1–20, doi:10.3390/metabo10090361, 2020.

Fitzgerald, J. W.: Marine aerosols: A review, Atmos. Environ. Part A, Gen. Top., 25(3–4), 533–545, doi:10.1016/0960-1686(91)90050-H, 1991.

Forehead, H. I. and O'Kelly, C. J.: Small doses, big troubles: Modeling growth dynamics of organisms affecting microalgal production cultures in closed photobioreactors, Bioresour. Technol., 129, 329–334, doi:10.1016/j.biortech.2012.11.082, 2013.

Gross, J. H.: Mass spectrometry: A textbook: Second edition, Mass Spectrom. A Textb. Second Ed., 1–753, doi:10.1007/978-3-642-10711-5, 2011.

Hansell, D. A., Carlson, C. A., Repeta, D. J. and Schlitzer, R.: Dissolved organic matter in the ocean, Oceanography, 22(SPL.ISS. 4), 202–211, doi:10.5670/oceanog.2009.109, 2009.

Hildebrand, M., Lerch, S. J. L. and Shrestha, R. P.: Understanding diatom cell wall silicification-moving forward, Front. Mar. Sci., 5(APR), 1–19, doi:10.3389/fmars.2018.00125, 2018.

Hoffmann, E. H., Tilgner, A., Schrödner, R., Bräuer, P., Wolke, R. and Herrmann, H.: An advanced modeling study on the impacts and atmospheric implications of multiphase dimethyl sulfide chemistry, Proc. Natl. Acad. Sci. U. S. A., 113(42), 11776–11781, doi:10.1073/pnas.1606320113, 2016.

Hu, Q., Sommerfeld, M., Jarvis, E., Ghirardi, M., Posewitz, M., Seibert, M. and Darzins, A.: Microalgal triacylglycerols as feedstocks for biofuel production: Perspectives and advances, Plant J., 54(4), 621–639, doi:10.1111/j.1365-313X.2008.03492.x, 2008.

Jones, C. S. and Mayfield, S. P.: Algae biofuels: Versatility for the future of bioenergy, Curr. Opin. Biotechnol., 23(3), 346–351, doi:10.1016/j.copbio.2011.10.013, 2012.

Kettle, A. J., Rhee, T. S., Von Hobe, M., Poulton, A., Aiken, J. and Andreae, M. O.: Assessing the flux of different volatile sulfur gases from the ocean to the atmosphere, J. Geophys. Res. Atmos., 106(D11), 12193–12209, doi:10.1029/2000JD900630, 2001.

Kiene, R. P., Linn, L. J. and Bruton, J. A.: New and important roles for DMSP in marine microbial communities, J. Sea Res., 43(3–4), 209–224, doi:10.1016/S1385-1101(00)00023-X, 2000.

Kim, M. J., Michaud, J. M., Williams, R., Sherwood, B. P., Pomeroy, R., Azam, F., Burkart, M. and Bertram, T. H.: Bacterial-driven production of nitrates in seawater, Geophys. Res. Lett., 42(2), 1–8, doi:10.1002/2014GL062865., 2015.

Kim, M. J., Zoerb, M. C., Campbell, N. R., Zimmermann, K. J., Blomquist, B. W., Huebert, B. J. and Bertram, T. H.: Revisiting benzene cluster cations for the chemical ionization of dimethyl sulfide and select volatile organic compounds, Atmos. Meas. Tech., 9(4), 1473–1484, doi:10.5194/amt-9-1473-2016, 2016.

Kim, M. J., Novak, G. A., Zoerb, M. C., Yang, M., Blomquist, B. W., Huebert, B. J., Cappa, C. D. and Bertram, T. H.: Air-Sea exchange of biogenic volatile organic compounds and the impact on aerosol particle size distributions, Geophys. Res. Lett., 44(8), 3887–3896, doi:10.1002/2017GL072975, 2017.

Kroll, J. H. and Seinfeld, J. H.: Chemistry of secondary organic aerosol: Formation and evolution of low-volatility organics in the atmosphere, Atmos. Environ., 42(16), 3593–3624, doi:10.1016/j.atmosenv.2008.01.003, 2008.

Kruger, B. R., Dalzell, B. J. and Minor, E. C.: Effect of organic matter source and salinity on dissolved organic matter isolation via ultrafiltration and solid phase extraction, Aquat. Sci., 73(3), 405–417, doi:10.1007/s00027-011-0189-4, 2011.

Lampert, W.: Release of dissolved organic carbon by grazing zooplankton, Limnol. Oceanogr., 23(4), 831–834, doi:10.4319/lo.1978.23.4.0831, 1978.

Lavi, A., Vermeuel, M. P., Novak, G. A. and Bertram, T. H.: The sensitivity of benzene cluster cation chemical ionization mass spectrometry to select biogenic terpenes, Atmos. Meas. Tech. Discuss., 3251–3262, doi:10.5194/amt-2017-408, 2017.

Lee, C. L. and Brimblecombe, P.: Anthropogenic contributions to global carbonyl sulfide, carbon disulfide and organosulfides fluxes, Earth-Science Rev., 160, 1–18, doi:10.1016/j.earscirev.2016.06.005, 2016.

Lønborg, C., Carreira, C., Jickells, T. and Álvarez-Salgado, X. A.: Impacts of Global Change on Ocean Dissolved Organic Carbon (DOC) Cycling, Front. Mar. Sci., 7(June), 1–24, doi:10.3389/fmars.2020.00466, 2020.

Lyons, T. W., Reinhard, C. T. and Planavsky, N. J.: The rise of oxygen in Earth's early ocean and atmosphere, Nature, 506(7488), 307–315, doi:10.1038/nature13068, 2014.

Marshall, A. G. and Hendrickson, C. L.: High-resolution mass spectrometers, Annu. Rev. Anal. Chem., 1(1), 579–599, doi:10.1146/annurev.anchem.1.031207.112945, 2008.

McMaster, M. C.: GC / MS A Practical User's Guide., 2008.

Millero, F. J., Feistel, R., Wright, D. G. and McDougall, T. J.: The composition of Standard Seawater and the definition of the Reference-Composition Salinity Scale, Deep. Res. Part I Oceanogr. Res. Pap., 55(1), 50–72, doi:10.1016/j.dsr.2007.10.001, 2008.

Pinhassi, J., Simó, R., González, J. M., Vila, M., Alonso-Sáez, L., Kiene, R. P., Moran, M. A. and Pedrós-Alió, C.: Dimethylsulfoniopropionate turnover is linked to the composition and dynamics of the bacterioplankton assemblage during a microcosm phytoplankton bloom, Appl. Environ. Microbiol., 71(12), 7650–7660, doi:10.1128/AEM.71.12.7650-7660.2005, 2005.

Prather, K. a, Bertram, T. H., Grassian, V. H., Deane, G. B., Stokes, M. D., Demott, P. J., Aluwihare, L. I., Palenik, B. P., Azam, F., Seinfeld, J. H., Moffet, R. C., Molina, M. J., Cappa, C. D., Geiger, F. M., Roberts, G. C., Russell, L. M., Ault, A. P., Baltrusaitis, J., Collins, D. B., Corrigan, C. E., Cuadra-Rodriguez, L. a, Ebben, C. J., Forestieri, S. D., Guasco, T. L., Hersey, S. P., Kim, M. J., Lambert, W. F., Modini, R. L., Mui, W., Pedler, B. E., Ruppel, M. J., Ryder, O. S., Schoepp, N. G., Sullivan, R. C. and Zhao, D.: Bringing the ocean into the laboratory to probe the chemical complexity of sea spray aerosol., Proc. Natl. Acad. Sci. U. S. A., 110(19), 7550–7555, doi:10.1073/pnas.1300262110, 2013.

Quinn, P. K. and Bates, T. S.: The case against climate regulation via oceanic phytoplankton sulphur emissions, Nature, 480(7375), 51–56, doi:10.1038/nature10580, 2011.

Reese, K. L., Fisher, C. L., Lane, P. D., Jaryenneh, J. D., Moorman, M. W., Jones, A. D., Frank, M. and Lane, T. W.: Chemical Profiling of Volatile Organic Compounds in the Headspace of Algal Cultures as Early Biomarkers of Algal Pond Crashes, Sci. Rep., 9(1), 1–10, doi:10.1038/s41598-019-50125-z, 2019.

Reisch, C. R., Moran, M. A. and Whitman, W. B.: Bacterial catabolism of dimethylsulfoniopropionate (DMSP), Front. Microbiol., 2(AUG), 1–12, doi:10.3389/fmicb.2011.00172, 2011.

Richardson, J. W., Johnson, M. D., Zhang, X., Zemke, P., Chen, W. and Hu, Q.: A financial assessment of two alternative cultivation systems and their contributions to algae biofuel economic viability, Algal Res., 4(1), 96–104, doi:10.1016/j.algal.2013.12.003, 2014.

Simo, R.: Production of atmospheric sulfur by oceanic plankton: Biogeochemical, ecological and evolutionary links, Trends Ecol. Evol., 16(6), 287–294, doi:10.1016/S0169-5347(01)02152-8, 2001.

Souza-Silva, É. A., Jiang, R., Rodríguez-Lafuente, A., Gionfriddo, E. and Pawliszyn, J.: A critical review of the state of the art of solid-phase microextraction of complex matrices I.

Environmental analysis, TrAC - Trends Anal. Chem., 71, 224–235, doi:10.1016/j.trac.2015.04.016, 2015.

Stokes, M. D., Deane, G. B., Prather, K., Bertram, T. H., Ruppel, M. J., Ryder, O. S., Brady, J. M. and Zhao, D.: A Marine Aerosol Reference Tank system as a breaking wave analogue for the production of foam and sea-spray aerosols, Atmos. Meas. Tech., 6(4), 1085–1094, doi:10.5194/amt-6-1085-2013, 2013.

Stokes, M. D., Deane, G., Collins, D. B., Cappa, C., Bertram, T., Dommer, A., Schill, S., Forestieri, S. and Survilo, M.: A miniature Marine Aerosol Reference Tank (miniMART) as a compact breaking wave analogue, Atmos. Meas. Tech., 9(9), 4257–4267, doi:10.5194/amt-9-4257-2016, 2016.

Sun, J., Todd, J. D., Thrash, J. C., Qian, Y., Qian, M. C., Temperton, B., Guo, J., Fowler, E. K., Aldrich, J. T., Nicora, C. D., Lipton, M. S., Smith, R. D., De Leenheer, P., Payne, S. H., Johnston, A. W. B., Davie-Martin, C. L., Halsey, K. H. and Giovannoni, S. J.: The abundant marine bacterium Pelagibacter simultaneously catabolizes dimethylsulfoniopropionate to the gases dimethyl sulfide and methanethiol, Nat. Microbiol., 1(8), 6–10, doi:10.1038/nmicrobiol.2016.65, 2016.

Varaljay, V. A., Robidart, J., Preston, C. M., Gifford, S. M., Durham, B. P., Burns, A. S., Ryan, J. P., Marin, R., Kiene, R. P., Zehr, J. P., Scholin, C. A. and Moran, M. A.: Single-taxon field measurements of bacterial gene regulation controlling DMSP fate, ISME J., 9(7), 1677–1686, doi:10.1038/ismej.2015.23, 2015.

Veres, P. R., Andrew Neuman, J., Bertram, T. H., Assaf, E., Wolfe, G. M., Williamson, C. J., Weinzierl, B., Tilmes, S., Thompson, C. R., Thames, A. B., Schroder, J. C., Saiz-Lopez, A., Rollins, A. W., Roberts, J. M., Price, D., Peischl, J., Nault, B. A., Møller, K. H., Miller, D. O., Meinardi, S., Li, Q., Lamarque, J. F., Kupc, A., Kjaergaard, H. G., Kinnison, D., Jimenez, J. L., Jernigan, C. M., Hornbrook, R. S., Hills, A., Dollner, M., Day, D. A., Cuevas, C. A., Campuzano-Jost, P., Burkholder, J., Paul Bui, T., Brune, W. H., Brown, S. S., Brock, C. A., Bourgeois, I., Blake, D. R., Apel, E. C. and Ryerson, T. B.: Global airborne sampling reveals a previously unobserved dimethyl sulfide oxidation mechanism in the marine atmosphere, Proc. Natl. Acad. Sci. U. S. A., 117(9), 4505–4510, doi:10.1073/pnas.1919344117, 2020.

Wang, M., Carver, J. J., Phelan, V. V., Sanchez, L. M., Garg, N., Peng, Y., Nguyen, D. D., Watrous, J., Kapono, C. A., Luzzatto-Knaan, T., Porto, C., Bouslimani, A., Melnik, A. V., Meehan, M. J., Liu, W. T., Crüsemann, M., Boudreau, P. D., Esquenazi, E., Sandoval-Calderón, M., Kersten, R. D., Pace, L. A., Quinn, R. A., Duncan, K. R., Hsu, C. C., Floros, D. J., Gavilan, R. G., Kleigrewe, K., Northen, T., Dutton, R. J., Parrot, D., Carlson, E. E., Aigle, B., Michelsen, C. F., Jelsbak, L., Sohlenkamp, C., Pevzner, P., Edlund, A., McLean, J., Piel, J., Murphy, B. T., Gerwick, L., Liaw, C. C., Yang, Y. L., Humpf, H. U., Maansson, M., Keyzers, R. A., Sims, A. C., Johnson, A. R., Sidebottom, A. M., Sedio, B. E., Klitgaard, A., Larson, C. B., Boya, C. A. P., Torres-Mendoza, D., Gonzalez, D. J., Silva, D. B., Marques, L. M., Demarque, D. P., Pociute, E., O'Neill, E. C., Briand, E., Helfrich, E. J.

N., Granatosky, E. A., Glukhov, E., Ryffel, F., Houson, H., Mohimani, H., Kharbush, J. J., Zeng, Y., Vorholt, J. A., Kurita, K. L., Charusanti, P., McPhail, K. L., Nielsen, K. F., Vuong, L., Elfeki, M., Traxler, M. F., Engene, N., Koyama, N., Vining, O. B., Baric, R., Silva, R. R., Mascuch, S. J., Tomasi, S., Jenkins, S., Macherla, V., Hoffman, T., Agarwal, V., Williams, P. G., Dai, J., Neupane, R., Gurr, J., Rodríguez, A. M. C., Lamsa, A., Zhang, C., Dorrestein, K., Duggan, B. M., Almaliti, J., Allard, P. M., et al.: Sharing and community curation of mass spectrometry data with Global Natural Products Social Molecular Networking, Nat. Biotechnol., 34(8), 828–837, doi:10.1038/nbt.3597, 2016.

Wang, X., Sultana, C. M., Trueblood, J., Hill, T. C. J., Malfatti, F., Lee, C., Laskina, O., Moore, K. A., Beall, C. M., McCluskey, C. S., Cornwell, G. C., Zhou, Y., Cox, J. L., Pendergraft, M. A., Santander, M. V., Bertram, T. H., Cappa, C. D., Azam, F., DeMott, P. J., Grassian, V. H. and Prather, K. A.: Microbial Control of Sea Spray Aerosol Composition: A Tale of Two Blooms, ACS Cent. Sci., 1(3), 124–131, doi:10.1021/acscentsci.5b00148, 2015.

Zuo, Z.: Why algae release volatile organic compounds - The emission and roles, Front. Microbiol., 10(MAR), 1–7, doi:10.3389/fmicb.2019.00491, 2019.

Chapter 2. Production of Dimethyl Sulfide, Methanethiol, and Dimethyl Disulfide During Controlled Phytoplankton-Bacterial Mesocosm Experiments

2.1 Abstract

The oceans cover nearly three-quarters of the Earth's surface, yet we understand far less about biogenic volatile organic compounds (BVOCs) emissions from the ocean compared to land. The most studied marine BVOC is dimethyl sulfide (DMS) due to its role in forming sulfate aerosols which seed clouds and affect climate. Compared to DMS, far fewer measurements exist of other reactive organosulfur compounds due to their highly reactive nature. Here, in an isolated ocean/atmosphere wave channel, we directly measured the temporal evolution of DMS, methanethiol (MeSH) and dimethyldisulfide (DMDS) in the clean head space over the course of three phytoplankton-bacterial blooms. Notably, the concentrations of MeSH and DMDS can rival or even exceed that of DMS. Furthermore, both BVOCs display different temporal trends with MeSH and DMDS peaking after DMS. These differences can be explained by changes in the utilization of sulfur by marine bacteria. Amplicon sequencing of the bacterial communities present during each bloom show different populations are correlated with DMS and MeSH emissions. Lastly, a model comparison using experimental (MeSH+DMDS)/DMS) production ratios with existing measurements in the literature supports that under certain conditions MeSH and DMDS production can in fact dominate in marine environments, including coastal waters. This study suggests that in order to fully explain the impacts of the ocean on clouds and climate, more reactive sulfur species in marine environments must be taken into account.

2.2 Introduction

2.2.1 Relevance of Organosulfur Species in the Atmosphere

The composition of the atmosphere is significantly impacted by emissions of organosulfur compounds (OSCs) from the ocean. Biogenic production of OSCs in marine environments revolves around the multifunctional osmolyte dimethylsulfoniopropionate (DMSP), synthesized by marine phytoplankton, being released during senescence, followed by enzymatic cleavage of aqueous DMSP yields DMS (Simo, 2001). A minor fraction (~10%) of aqueous DMS is ventilated into the atmosphere at an estimated annual flux ranging between 17.6-34.4 Tg(S) yr^{-1} (Figure 2.1) (Lana et al., 2011). In the marine boundary layer, OSCs, including DMS, have short atmospheric lifetimes (<1-2 days) as they become quickly oxidized by hydroxyl radical (Wine et al., 1981). DMS oxidation products partition to the aerosol phase either through condensation onto existing aerosols, or through the formation of new particles (O'Dowd & De Leeuw, 2007). Direct scattering of solar radiation by sulfate aerosols and their ability to form cloud droplets in the marine boundary layer significantly contribute to Earth's energy balance (France et al., 2013). Over the past 4 decades, a significant effort has been placed on quantitatively constraining marine biogenic emissions of OSCs and identifying possible biogeochemical feedback mechanisms. These efforts have continued to uncover complex biochemical processes that form and consume OSC. Nevertheless, to fully explain the spatiotemporal patterns of OSC concentrations, further insight into the biogeochemical pathways leading to OSC species in the marine atmosphere are needed.

2.2.2 Field Measurements of MeSH and DMDS

In the atmosphere, the lifetimes of DMS, MeSH, and DMDS are 33h, 4.1h, and 0.7h respectively, at diurnally averaged OH radical concentrations ($[OH]^*_{avg} = 2\times10^6$ molecules cm^{-3}) (Wine et al., 1981). As a result of this, comparatively low steady state concentrations of MeSH and DMDS are expected in the atmosphere, which have mostly limited detailed observations to

the aqueous phase. Unfortunately, the chemical reactivity and difficulty of measuring MeSH e.g. generating calibration standards effectively has led to a significant lack of measurements.

In Kettle et al. (2001), field measurements transecting the Atlantic Ocean calculated (MeSH/(MeSH+DMS)) flux ratios using their experimentally derived dissolved concentrations. These flux ratios averaged to 0.16, with occasional high MeSH relative fluxes (MeSH/DMS ≈1) observed in coastal regions or during upwelling events where high bacterial growth rates often occur. In the North Sea, Baltic Sea, and Kattegat, (MeSH/(MeSH+DMS)) average flux ratios were found to be 0.11, 0.05, and 0.04 respectively. More recent measurements of dissolved MeSH in the North East Pacific and atmospheric MeSH in the southwest Pacific have generally agreed with these findings, with MeSH:DMS aqueous concentration ratios of 0.19-0.50 and (MeSH/(MeSH+DMS)) flux ratios of 0.14-0.24 in each of these regions of the Pacific (R. Kiene et al., 2017; Lawson et al., 2020). From these studies, correlations of MeSH to DMS and MeSH to DMSP have shown mixed, but generally positive relationships indicating a common, but decoupled metabolic connection between these species. The factors that drive the wide variability in MeSH production are still poorly understood, but more recent investigations of the biochemistry of dissolved organosulfur have begun to shed new light as discussed in the next section.

There are even fewer field measurements of DMDS than MeSH in the marine environment. In the first quantitative field measurements of DMDS, Tanzer and Heumann (1992) along the Atlantic Ocean from Northern Europe to South Africa measured dissolved DMDS concentrations ranging from <0.015-0.229 nM which were significantly lower than DMS concentrations measured over the same study (0.3-8 nM). In the Baltic Sea, Kattegat/Skagerrak, and North Seas dissolved DMDS:DMS ratios ranged from 0.006-0.011 with concentrations of DMDS varying between 10-50 pM (Leck & Rodhe, 1991). In both studies, correlations between DMDS and other

factors were not found. No other measurements of marine atmospheric DMDS have been reported except for two previous brief mentions of estimates of concentrations below 3 pptv (Grenfell et al., 1999; Persson & Leck, 1994). In general, the consensus from existing field measurements point to DMS as the dominant marine OSC emitted as ~83% of mass, with MeSH occupying the remainder of the balance with trace levels of DMDS. In some cases, this picture changes in more productive zones with MeSH taking a greater role.

2.2.3 Biology and Biochemistry of DMSP

Production of DMS has been primarily studied through investigations of its main precursor DMSP which is released during the growth and senescence of marine primary producers (Reisch et al., 2011). Aqueous DMSP is degraded by heterotrophic bacteria through two different pathways: demethylation to 3-methiolpropionate which is further demethiolated to methanethiol (MeSH), or cleavage of DMSP to DMS and acrylic acid (Kiene & Linn, 2000). Depending on the biological and chemical states of the ocean, a "bacterial switch" between the partitioning of DMSP catabolism through the demethylation and cleavage pathways may occur, leading to different ratios of breakdown products (Pinhassi et al., 2005; Simo, 2001). In cases where dissolved DMSP release is high compared to bacterial sulfur demand, DMSP cleavage to DMS is the preferred pathway. When DMSP release is low compared to bacterial sulfur demand, MeSH production is the preferred pathway. Interestingly, while many observations have shown that the demethylation pathway generally dominates DMSP catabolism (34-100%) (Figure 2.3.1), DMS has the highest concentration of dissolved OSCs on average due to the extremely fast rate of MeSH uptake by heterotrophic bacteria (Kiene, 1996). Furthermore, significant variability in MeSH uptake rates and the presence of compounds inhibiting MeSH incorporation indicate that in some cases, MeSH

consumption may decrease to rates where production significantly exceeds loss (Kiene, 1996; Kiene et al., 1999).

2.2.4 Dimethyl Disulfide

The origin of DMDS in marine surface waters is thought to be from abiotic MeSH oxidation, although kinetics and details on the factors that control this process in seawater are not known. The formation of DMDS from MeSH in freshwater is known to proceed rapidly, on the order of hours, especially in the presence of dissolved catalytic species such as Cu^{2+}, Fe^{3+}, and ascorbic acid (Chin & Lindsay, 1994a; Higgins et al., 2012). MeSH oxidation to DMDS is also known to occur on various surfaces which includes activated carbon and stainless steel (Bashkova et al., 2002; Perraud et al., 2016). Biotic production of DMDS through enzymatic activity has been investigated in food chemistry, however no enzymatic processes in marine microorganisms have been reported to date (Chin & Lindsay, 1994b). While the abiotic degradation of DMDS has been shown to be extremely slow in dark conditions, actinic flux should strongly influence the breakdown of DMDS based on strong absorption by the sulfur-sulfur bond (Buchshtav et al., 2019). Biotically, DMDS has been used as a potent DMS consumption inhibitor in bacteria. DMDS is also vulnerable to consumption, however the rates are not known (Wolfe & Kiene, 1993; Wolfe et al., 2002). This study focuses on advancing this limited understanding of the production mechanisms, biochemical influence, and lifetime of DMDS in natural seawater.

Here, we report the results from three mesocosm incubation experiments during the Biological Effects on Air Sea Transfer (BEAST) experiment which used coastal seawater to directly measure the temporal evolution of the production of OSCs during a phytoplankton-bacterial bloom. Through a combination of atmospheric and seawater measurements, the evolution of OSC concentrations are measured over the bloom lifecycle and connect these phenomena with

the bacterial communities and metabolic pathways that control these processes. Our observations suggest that if DMS, MeSH and DMDS are present in the open ocean at ratios similar to those measured in this experiment, that MeSH and DMDS may contribute significantly to the production of sulfate aerosol.

2.3 Materials and Methods

2.3.1 Preparation of Mesocosm Incubation Experiments

Seawater was obtained from Ellen Browning Scripps Pier (La Jolla, CA; 32°51´56.8"N: 117° 15´38.48"W) and pumped from an inlet 5 meters below the ocean surface. The seawater was filtered with a 50 µm nitex mesh to remove larger debris and zooplankton before addition to an outdoor 2400 L PTFE tank. To eliminate the introduction of large detritus (insects, leaves, etc), a thin polyethylene sheet was suspended ~1 m above the outdoor mesocosm tank reservoir. Sunlight irradiated the water surface along the natural hours of the experiment. The seawater was periodically monitored for temperature to ensure conditions were consistent with coastal San Diego in mid-summer. The tank was aerated and mixed using bubbled air passed through HEPA-filters at ~10 LPM into Tygon tubing held ~0.5 m below the water line. For all three sequential mesocosm incubation experiments, the outdoor tank was acclimated overnight after initial filling, before nutrient addition the following morning. Seawater was supplemented with f/2 algal growth medium (Proline, Aquatic Eco-Systems, Apopka, FL), diluted 50x with added 9 µM sodium metasilicate to induce a phytoplankton bloom. Bloom progress was tracked using a handheld fluorimeter (Aquafluor, Turner Designs, San Jose, CA) daily. For all three mesocosm experiments (Figure 2.3.6) water was transferred each morning from the outdoor tank reservoir to three marine aerosol reference tanks (MARTs) (Stokes et al., 2013)**.** Subsequently, each morning after the first day, the water was transferred back from the MARTs into the outdoor tank before the MARTs

were re-filled for that morning. After the phytoplankton peak in each bloom, as indicated by daily fluorescence measurements, the water was kept in all three MART tanks with no further transfers until the end of the experiments. This methodology was implemented due to gradual shearing of phytoplankton biomass by the MART centrifugal pump which can prematurely halt phytoplankton blooms. Therefore, keeping the mesocosm water in a less-stressful environment allowed the experiment to measure the evolution of OSC species over the entire bloom lifecycle utilizing a MART system. The use of MARTs was chosen for these experiments as several other measurements were also performed at the same time and required the production of sea spray aerosol. The results and findings of those measurements will be published elsewhere.

2.3.2 Marine Aerosol Reference Tank Operation

The MART systems used in this study were filled with ~110 L of seawater and a plunging sheet of water with a free-falling distance of ~10 cm. The size distribution of the resultant bubble plume acquired by hydrophone (ITC 1089d) was referenced to preexisting size distributions to ensure the proper physical production pathways of SSA. MARTs were plunged on a cycle of 4 seconds with the centrifugal pump on, and 10 seconds of no pumping to permit flume degassing and foam creation. Clean air obtained continuously from a zero-air generator (Sabio 1001) was introduced to the MART headspace at a flow rate of 6.6 standard liters per minute (SLPM). The temperature of each MART was maintained at ~26 °C by circulating water through a 316 stainless steel chiller coil immersed in the tank water.

2.3.3 Heterotrophic Bacterial Abundance and Composition

Bulk seawater was collected in 5 ml cryovials from the MARTs via a stainless steel side port ~10 cm from the bottom (see Stokes et al. 2013 for MART details) For bacteria counts, samples were preserved with glutaraldehyde at 0.05% final concentration and stored at -80 C after

flash freezing (Noble & Fuhrman, 1998). Microbial abundances for heterotrophic bacteria for all experiments were obtained using flow cytometry at The Scripps Research Institute (TSRI) Flow Core Facility with a BIO-RAD, ZE5 Cell Analyzer. Samples were diluted (1:10) in 1×TE buffer (pH 8), then stained with SYBR Green I at room temperature for 10 min in the dark. (Gasol & Del Giorgio, 2000) Bacterial growth rates were calculated using the daily concentrations as previously described. (Fuhrman & Azam, 1980). For amplicon sequencing, 400 µL seawater was sampled every day from the MART and immediately frozen at -80 ^{o} C to preserve microbiome integrity. (Song et al., 2016) Samples were processed following the Earth Microbiome Project protocols (http://wwwearthmicrobiome.org) with modifications for low biomass input (Caporaso et al., 2012). DNA was extracted from samples using the KatharoSeq lowbiomass methodology, (Minich et al., 2019; Minich, Zhu, et al., 2018). Specifically, water samples were thawed on ice for 30 minutes, vortexed, and then 400 µl was transferred into individual bead beating tubes. After extraction, 50 µl of eluted DNA was transferred to 384 well plates. The miniaturized PCR protocol was used to generate NGS libraries with a final reaction volume of 5 µl (0.2 ul gDNA, 0.2 µl barcoded primers).(Minich, Humphrey, et al., 2018) For sequencing, an equal volume of amplicon was pooled across all samples, followed by a cleanup using the QIAquick PCR purification kit (Qiagen, Cat# 28106). Pre-processing of sequences was performed using the Qiita platform with statistical analysis then performed with Qiime 2 (Bolyen et al., 2019; Gonzalez et al., 2018). Unique 150 base pair sequences were generated using the deblur algorithm yielding de novo, sub-Operational-Taxonomic-Units Units at single nucleotide resolution (sOTUs). (Amir et al., 2017) PCoA plots were generated with UniFrac distances using Emperor (Lozupone & Knight, 2005; Vázquez-Baeza et al., 2013). Additional statistical analyses were performed using PRISM 8. Rarefaction levels were empirically determined by calculating the sample exclusion cutoff at

which 90% of the sequences from DNA extraction positive controls mapped to the known or expected organism (Zymo mock community), which in this case resulted in 1840 reads (Figure 2.14). To determine which microbial sOTUs were associated with DMS and MeSH production, the Spearman correlation with discrete false-discovery rate within the Calour tool was used (Xu et al., 2019). Sample success was calculated to occur at 1840 reads: therefore, samples with less than 1840 reads were excluded from analysis (Figure 2.14a).

Functional genes associated with the cleavage pathway (dddP) and demethylation pathway (dmdA) of DMSP were quantified by q-PCR following previously described protocols (Levine et al., 2012; Zeng et al., 2016). Briefly, universal primers dddP 874F/971R and dmdA 282F/591R were used to quantify dddP and dmdA respectively. Quantification were performed on a AriaMx (Agilent) using SsoAdvanced Sybr Green universal supermix (BioRad). Technical triplicates were run for each sample. Seven-fold serially diluted standard curves and no template controls were run in triplicates on each plate. Genomic DNA from a Rhodobacterales strain isolated off Scripps Pier was used as standard for both genes. Single amplifications were confirmed by melt curve for each run.

2.3.4 Chemical Ionization Time-of-Flight Mass Spectrometry

BVOC measurements were made using a chemical ionization time-of-flight mass spectrometer (CI-TOFMS) using benzene cluster ion chemistry, as described in (Kim et al., 2016). Benzene ion clusters were chosen as the reagent ion due to its high sensitivity towards the detection of reactive sulfur species. Briefly, ~300 ppm benzene gas is prepared via a flow of 10 standard cubic centimeters per minute (sscm) medical grade N_2 over a cylinder of liquid benzene (LCMS Grade, Sigma Aldrich). Benzene vapor was then diluted by N_2 and passed through a 20mCi Po-210 ionizer. Through N_2 collisions with alpha particles produced by Po-210, benzene cluster

cations are generated and delivered into the ion-molecule region (IMR) of the CI-TOFMS instrument via an inline critical orifice (O'Keefe) at a flow of 1.8 SLPM (Veres et al., 2008). Sample headspace was pulled into the IMR through another orifice at 1.8 SLPM. A secondary bypass pump was utilized to increase sample flow to 2.6 SLPM to reduce the gas residence time in the ~2 m (3.175mm ID) fluorinated ethylene propylene (FEP) tubing which connected the headspace of each MART to the CI-TOFMS. A sintered glass RH probe (Vaisala) was connected in-line between a sampling tee near the CI-TOFMS inlet and bypass pump to continuously measure the relative humidity and temperature of the MART headspace. The IMR, based on the design by Kercher et al., 2009, was maintained at empirically derived conditions, 50 °C via heat tape, a pressure of 60 Torr, and 250V DC. Analyte ions produced via chemical ionization with benzene cluster cations were passed into a custom-built electrodynamic ion funnel which collects and focuses the ion beam and gently de-clusters ions that may have excess benzene or water molecules attached. A commercial RF-only quadrupole (TOFWERK) transfers the ions into an orthogonal extraction time of flight mass spectrometer. Data acquisition was performed using ToFDAQ software (TOFWERK), with co-summed spectra saved at a rate of ~1 Hz. Data analysis was performed in TOFWARE, (TOFWERK) a graphical interface plugin for IGOR (Wavemetrics), in which mass calibration and baselining procedures were applied to the raw data. Daily ion intensities from each MART tank were normalized to the summed intensity of benzene and its dimer (m/z 78, 156) and averaged for quantitation. During sampling periods in which analyte ion intensity exceeded more than 10% of reagent ion intensity, the sampled MART headspace was diluted by humidified zero air at a tee before the CI-TOFMS inlet. On each day, at least 30 minutes of mass spectra were averaged from each MART tank. For both DMS and DMDS, external calibrations of each gas using permeation tubes (VICI Metronics) were performed across the

humidity range to account for the humidity-dependent sensitivities of each compound. For MeSH, an external calibration was performed after the mesocosm experiments using a 1 ppm MeSH in N2 calibrated gas canister (Airgas) in dry and humid conditions diluted between 0.1 – 80 ppbv matching the MART experiments. The sensitivity for DMS at the water vapor mixing ratio of the MART tanks (17.0 g/kg) was found to be 9.8 normalized counts per second (ncps)/pptv, DMDS 21.2 ncps/pptv, and MeSH 0.3 ncps/pptv. DMS was measured as $[M]^+$ as m/z 62, MeSH as a benzene adduct $[M+78]^+$ at m/z 126, and DMDS as $[M]^+$ at m/z 94. Given the lower-mass resolution of the CI-TOFMS (<1200 full width at half maximum) ion assignments were made using unit mass resolution leading to possibility of unknown ions contributing to ion intensity at the same unit mass. During periods of high OSC ion intensity, isotope ratios for ^{34}S were used to verify the identity of each OSC compound. All three MART tanks daily mass spectra were averaged for phytoplankton blooms 1 and 2. For mesocosm 3, only one MART was used.

2.4 Results

2.4.1 Bloom Progression, OSC Concentrations

Each of the blooms progressed through 3 distinct phases: exponential growth, peak bloom, and senescence as indicated by changes in bulk fluorescence (Figure 2.3.2a, b). Notably, all three blooms reached different levels of peak fluorescence, which converts through externally calibrated chlorophyll a levels (chl. a) ranging from 2.3 – 11.5 μg L^{-1}. These values fall within previous measurements of chl. a made at this ocean sampling location (La Jolla, CA) which range from 0.1-20 μg L^{-1}, where the 95% quantile resides below 7.73 μg L^{-1} (McGowan et al., 2017). At the start of each experiment, heterotrophic bacteria (HB) counts decreased after the first day, likely in response to the water transfer and adaptation to new conditions. (Figure 2.3b, d). After the initial decline, HB counts increased steadily during the bloom lifecycle reaching a max 3.3-9.4 times

their minimum concentrations until leveling off or decreasing after the senescent phase. Daily average measurements of headspace DMS, MeSH, and DMDS (Figure 2.3 a, b) showed significant concentration variations (40-80x) over the bloom lifetimes. The observed peak headspace concentrations of each OSC are significantly higher than marine field measurements, due to ventilation caused by the plunging waterfall of the MART, combined with the relatively low flow of zero air through the MART headspace (Davis et al., 1998). The Henry's Law solubility constants for DMS, DMDS, and MeSH, 5.0×10^{-3} mol m^{-3} Pa^{-1}, 7.0×10^{-3} mol m^{-3} Pa^{-1} and 3.8×10^{-3} mol m^{-3} Pa^{-1} respectively, are nominally similar, indicating that the measured headspace ratios of DMDS and MeSH to DMS are not likely caused by disproportionate ventilation effects (Sander, 2015). Consequently, we expect that the headspace ratios of each OSC roughly correspond to the relative concentrations of these compounds in seawater. DMS concentrations tracked the peak of each bloom (Figure 2.3a, c), which is consistent with field and laboratory observations (Van Duyl et al., 1998; Kwint et al., 1993; Lizotte et al., 2008). In contrast, MeSH and DMDS increase quickly during the death phase of each bloom commensurate with the subsequent rise of heterotrophic bacteria abundance (Figure 2.3.2b, d). Bacterial specific growth rates, calculated from daily changes in bacteria abundance, directly correspond to an increase in MeSH concentrations in bloom 1 ($r^2 = 0.85$), however the observed link between these concentrations is not as strong during blooms 2 and 3 ($r^2 = 0.28, 0.01$), providing evidence other factors are controlling non-DMS OSCs. The measured concentration ratios of MeSH:DMS for all three blooms/experiments span multiple orders of magnitude ranging from values of ~0.2-50. Compared to the literature, the upper end of these values is significantly higher, and likely due to the combination of the rich bloom conditions coupled with the coastal seawater microbial community (Leck & Rodhe, 1991). Despite this, MeSH:DMS concentration ratios were still comparatively high (~10) at the onset of each bloom

before the growth phase, suggesting the concentration ratio of MeSH:DMS can reach surprisingly high levels in coastal environments, consistent with ratios observed in marine sediments (Sorensen, 1988; Visscher et al., 1991).

2.4.2 Dimethyl Disulfide

The high levels of DMDS observed in these mesocosm experiments was initially surprising given the lack of previous reports of DMDS in the literature (Leck & Rodhe, 1991; Tanzer & Heumann, 1992). One concern was DMDS arising as an artifact of the experimental design. To assess whether DMDS was artificially being produced by oxidation in the ~20 cm stainless CI-TOFMS inlet, several control experiments were performed (Supplementary Methods 2.8.1) (Perraud et al., 2016). These controls found as much as ~35% of MeSH could be converted to DMDS in the instrument inlet (Figure 2.9). Through changing the CI-TOFMS inlet to PFA, the conversion ratio was decreased to ~11-15% implicating the remaining DMDS was created by upstream dimerization in the gas regulator or by conversion on the walls of the CI-TOFMS IMR chamber itself. To contextualize these controls within the mesocosm experiments, the control-obtained conversion ratio (35%) was utilized to calculate the expected MeSH and subsequent DMDS concentrations under the expectation that only the CI-TOFMS inlet was responsible for MeSH dimerization. We found that on 9 of the 27 days of the mesocosm experiments, DMDS concentrations were 50% higher than those expected by MeSH dimerization on the inlet alone, indicating that DMDS was indeed being formed naturally during the experiments (Figure 2.11).

To eliminate whether the submerged stainless steel chiller coil in the MART impacted MeSH oxidation in the liquid phase, aqueous samples of seawater obtained directly from the outdoor tank were bubbled in separate borosilicate bottles and the ventilated gases were measured by CI-TOFMS (Figure 2.10a). From these experiments, MeSH:DMDS concentration ratios

closely matched those obtained from the MARTs, indicating the 1-hour residence time of the mesocosm water in the MART with the stainless steel coil prior to sampling had negligible impact on MeSH dimerization (Figure 2.10b). Our findings also agree with recent investigations of OSC measurements which highlight the importance of using materials which limit MeSH conversion to DMDS on instrument and sampling vessel surfaces (Perraud et al., 2016).

2.4.3 Bacterial Community Dynamics

In order to understand how marine bacteria affect the fate of DMSP, the dynamics of the bacterial communities and correlations to OSCs were studied over the course of three blooms (Moran & Durham, 2019; Reisch et al., 2011). The succession of bacterial taxa observed for each experiment was typical of communities responding to a phytoplankton bloom progression, with the relative abundance of more opportunistic fast-growing bacteria (e.g. Bacteriodetes and Rhodobacterales) increasing over time (Fig. 2 a, b). (Buchan et al., 2014). The production of both DMS (Figure 2.12d) and MeSH (Figure 2.12e) appeared to be correlated with bacteria composition (Adonis $P<0.001$), although clustering locations or associations were unique for each chemical species. This suggests that different bacterial populations are responsible for controlling the production of OSCs and their precursors (Figure 2.4a, b, Figure 2.13). Planctomycetes, Actinobacteria, and Vibrionales appeared to be more correlated with DMS while Bacteriodetes, Rhotobacterales, and Alteromonadales were more correlated with MeSH present in the system. (Figure 2.13h) While dissolved and particulate DMSP were not measured during these experiments, the distinct temporal shifts in measured OSCs (Figure 2.2a, c) and bacterial communities (Figure 2.2a, b) strongly suggest that catabolism of DMSP changed over the course of the bloom. The “bacterial switch” has been proposed as a regulatory system determining the fate of marine DMSP and thus the production of more or less DMS or MeSH. (Simo, 2001)

Bacteria will switch from the cleavage pathways to the demethylation pathways depending on their demand for carbon or sulfur from DMSP and the availability of other substrates in the water. Functional genes associated with DMSP cleavage and demethylation pathways were quantified over the course of blooms 1 and 3 (Figure 2.3c) to further assess the role of heterotrophic bacteria in OSCs production (DMS and MeSH respectively). DmdA genes represent the first step of the demethylation pathway that leads to the production of MeSH (Howard et al., 2006) whereas, dddP gene is one of the genes representing the cleavage pathway leading to the production of DMS (Todd et al., 2009). At the start of the experiments, the abundance of the dmdA genes was low or under the detection limit while dddP genes were more abundant (especially during bloom 3) suggesting that bacterial sulfur demand from DMSP was low at the time of sampling and DMSP was being used as a carbon source by bacteria. The abundance of dddP genes increased over the course of bloom 1 in correlation with DMS production (Figure 2.15). The initial high abundance of dddP in bloom 3 was also followed by an increase in concentration of DMS (Figure 2.3c). For both blooms, it appears that bacterial cleavage of DMSP was responsible for a major portion of the observed production of DMS in the system. Later in the blooms, the increase in MeSH concentration coupled with bacterial growth rates suggest that the increase in bacterial sulfur demand is routed towards DMSP demethylation (Pinhassi et al., 2005). The increase of Rhodobacterales over the course of the blooms and their potential capacities for demethylation (Curson et al., 2011; Varaljay et al., 2015), as well as dmdA genes increasing in correlation to MeSH, suggest that bacterial demethylation was responsible for a portion of the MeSH produced. However, the higher number of dddP genes but low concentration of DMS while MeSH concentration increased towards the end of bloom 1 (Figure 2.15), suggest a rapid turnover of DMS used as a source of sulfur. The increase of Methylophaga spp. towards the end of bloom 1

(Figure 2.15) also suggests bacterial oxidation of DMS, as described for Methylophaga thiooxidans (Boden et al., 2010) and potential release of MeSH as a byproduct. Through quantitative gene measurements of dddP and dmdA, a significant lack of dmdA was observed, indicating the traditionally understood route for MeSH production though DMSP was either not active, or occurring though genes not measured. Alternatively, MeSH production may have proceeded either through the breakdown of S-amino acids or consumption of DMS itself. The latter case represents an interesting prospect as the consumption of DMS by marine bacteria is normally considered a one-way process whereby the available sulfur pool is rendered unavailable for emission. Establishing a boundary on the quantity of MeSH available for flux generated from DMS consumption represents an important next step in understanding total ocean sulfur flux.

From these analyses, we found that the production of MeSH and DMDS in mesocosms 1, 2, and 3 was particularly enhanced versus measurements performed in the field. Through 16S amplicon sequencing, we found a diverse array of bacterioplankton positively correlated with the production of DMS and MeSH (Figure 2.4a, b), however we are unable to directly ascribe the production of either gas to any specific organism. These findings advance a particular line of questions regarding the formation of MeSH: Are cases where high MeSH is observed due to the presence of a particular set of bacterioplankton acting in a highly influential manner, or does the bulk physiochemical state of the mesocosm and seawater exert top-down over the entirety of the bacterioplankton population which switch to MeSH production? Given that the turnover of DMSP is thought to be mostly through the demethiolation pathway (Figure 2.1), even during periods of low-sulfur demand by bacterioplankton, are periods of MeSH buildup more controlled by variations in MeSH uptake than production? As discussed above, the low concentrations of functional gene dmdA despite high MeSH concentrations suggest that either other enzymes for

MeSH formation from DMSP were active, or the formation of MeSH could have originated from another sulfur source such as DMS or methionine consumption. Given the distinct decrease in DMS production during the death phase of each mesocosm which coincided with the formation of MeSH and DMDS, it is tempting to suggest the latter hypothesis. Furthermore, as DMS consumption by marine bacterioplankton is common and well distributed across the ocean, it would further appear that a deficiency in the MeSH uptake rate may be more responsible for periods of relatively high dissolved MeSH concentrations in seawater as opposed to large enhancements in production. Given the speculative nature of these hypotheses, further research into factors that affect MeSH uptake and lifetime should be undertaken.

2.4.4 Production of Atmospheric Sulfate by OSCs

To assess the potential contribution of DMDS and MeSH to sulfate aerosol production, we calculate the fraction of particulate sulfate formed from DMS, MeSH, and DMDS as a function of the emission ratios of MeSH+DMDS relative to DMS. Estimates of the emission ratios of (MeSH+DMDS)/DMS for ocean conditions (< 0.1) were calculated from the simultaneous measurements of DMS, MeSH, and DMDS aqueous concentrations measured in the North Atlantic (Leck & Rodhe, 1991), using a two-film air-sea transfer model (Johnson, 2010). The (MeSH+DMDS)/DMS emission ratios for this study were reported for both peak chl. a (0.2 – 0.8) and peak bacteria concentrations. By assuming that the aerosol sulfate yield for DMS and MeSH oxidation is 1 and the sulfate yield of DMDS oxidation is 2, we calculate the fraction of OSC-derived particulate sulfate that is formed from MeSH + DMDS. As shown in Figure 2.5, for conditions relevant to the North Atlantic, MeSH and DMDS may account for as much as 10% of the non-sea salt sulfate produced from OSC emissions. For the conditions discussed in this study, MeSH and DMDS emissions would account for over 40% of the non-sea salt sulfate produced

from OSC emissions. This represents a potentially significant unappreciated source of OSC and by extension sulfate aerosols in marine environments. More studies are needed to understand the factors controlling the ratios of non-DMS OSC species.

2.5 Conclusions

The results discussed herein establish that non-DMS OSC species, especially MeSH, can be produced by natural phytoplankton and microbial assemblages in higher amounts relative to DMS than previously reported. The production of MeSH spikes over short timescales which would account for the lack of field observations. Additionally, the high reactivity of these species leads to significantly lower steady-state atmospheric concentrations, further limiting their detection. We also observed DMDS at unexpectedly high concentrations; no field observations exist yet for comparison. We attribute some (up to 35%) of the DMDS detected in the MART experiments to dimerization of MeSH on the instrument inlet. However multiple periods of high DMDS significantly exceeded values (>50%) predicted by MeSH conversion indicating production occurred through natural processes in seawater. Based on the observation of DMDS in these blooms, we believe that further investigations of MeSH dimerization in natural seawater should be investigated as an additional pathway for formation of OCS species. Lastly though modeling we contrast our mesocosm OSC production ratios with measurements from the field. Particularly in coastal regions where heterotrophic bacteria can be highly active, non-DMS OSCs may represent a significant fraction of reactive sulfur species which has significant implications for clouds, climate, and air quality in coastal marine environments

2.6 Acknowledgements

The authors gratefully acknowledge the support of the National Science Foundation through the Centers of Chemical Innovation Program via the Center for Aerosol Impacts on

Chemistry of the Environment (CHE-1801971). The CI-TOFMS and biological data showed in this work can be found at the CAICE digital collection. The authors thank Meinrat Andreae for his constructive comments on this study. The authors declare no financial interests or conflicts of interest pertaining to this work.

Chapter 2, in full, is currently being prepared for resubmission to Journal of Geophysical Research: Biogeosciences. Sauer, J.S., Minich, J.J., Dinasquet, J., Malfatti, F., Mayer, K.J., Santander, M.V., Pendergraft, M.A., Mitts, B., Lee, C., Wang, X., Rico, B., Knight, R., Bertram, T.H, Prather, K.A. (2020). "Production of Dimethyl Sulfide, Methanethiol, and Dimethyl Disulfide During Controlled Phytoplankton-Bacterial Mesocosm Experiments." Journal of Geophysical Research: Biogeosciences (2020) The dissertation author is the primary investigator and author of this manuscript.

2.7 Figures

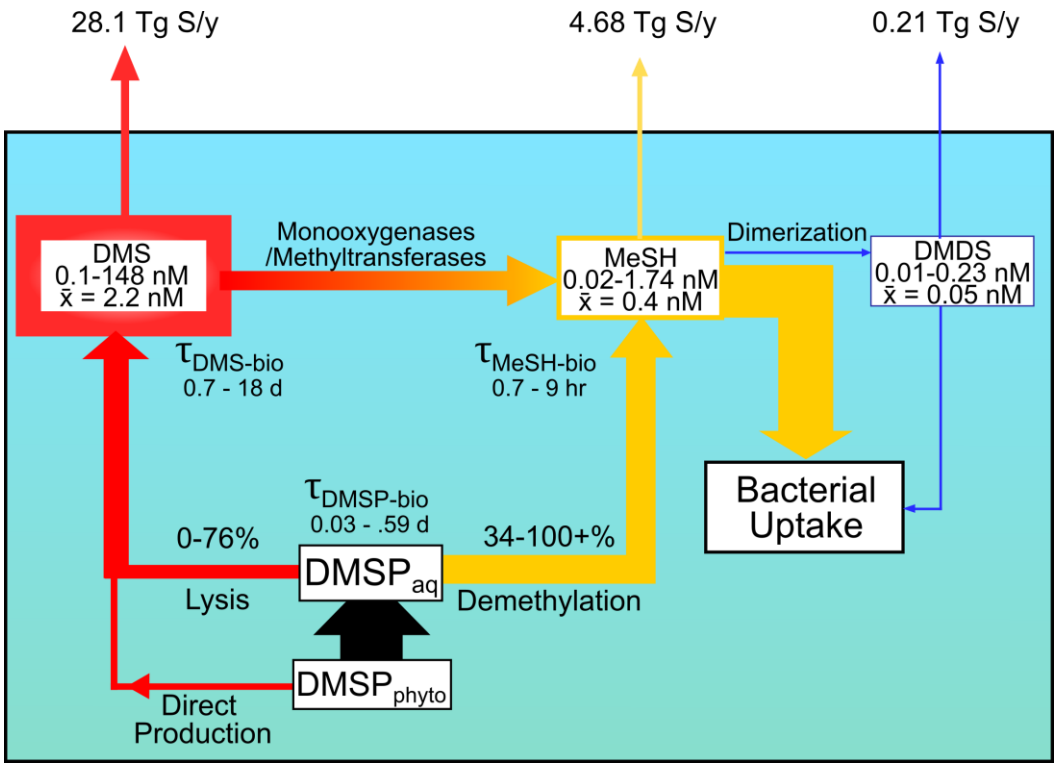

Figure 2.1 Known routing of dissolved organosulfur species in marine surface waters: (Kettle et al., 2001; Kieber et al., 2011; R. Kiene, 1996; R. Kiene et al., 2017; R. P. Kiene et al., 2000; Lana et al., 2011; Lee & Brimblecombe, 2016; Tanzer & Heumann, 1992; Zubkov et al., 2001)

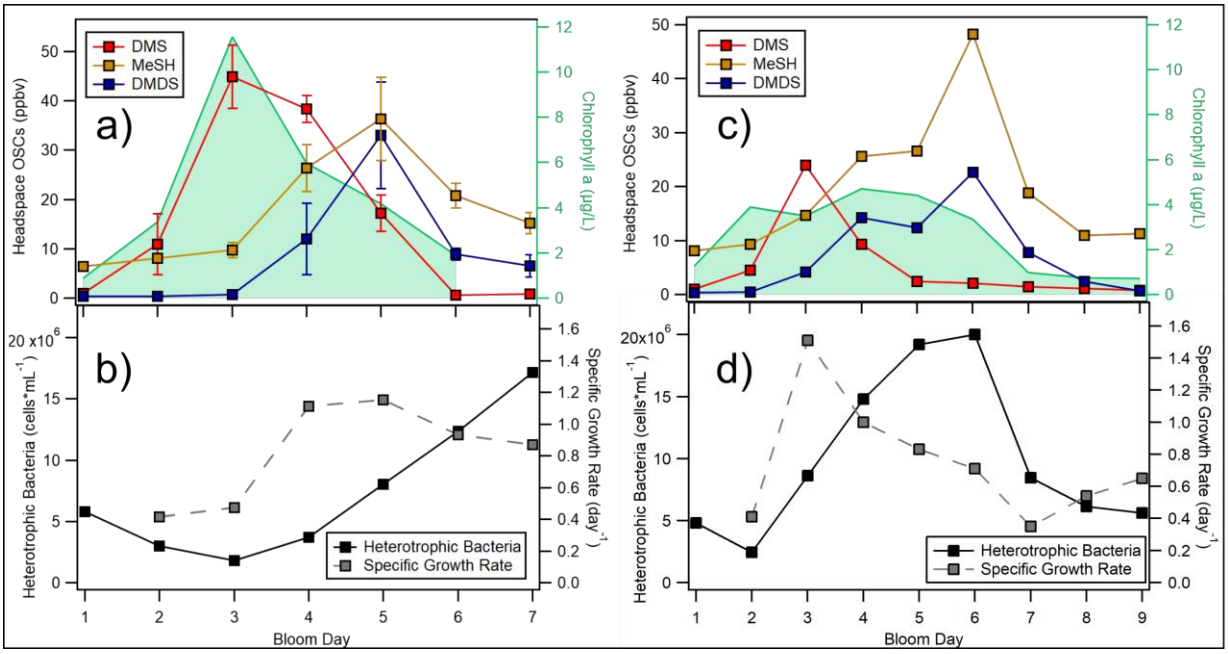

Figure 2.2 Mesocosm 1 (left panel a) and 3 (right panel c) headspace organosulfur compounds coplotted with bulk water chlorophyll-a. Heterotrophic bacteria count, and bacterial growth rate for mesocosms 1 and 3 shown in b) and d) respectively. Error bars on organosulfur concentrations in a) reflect ±1σ obtained from averaging MARTs 1-3, bloom 3 c) only possessed one MART for which σ could not be obtained.

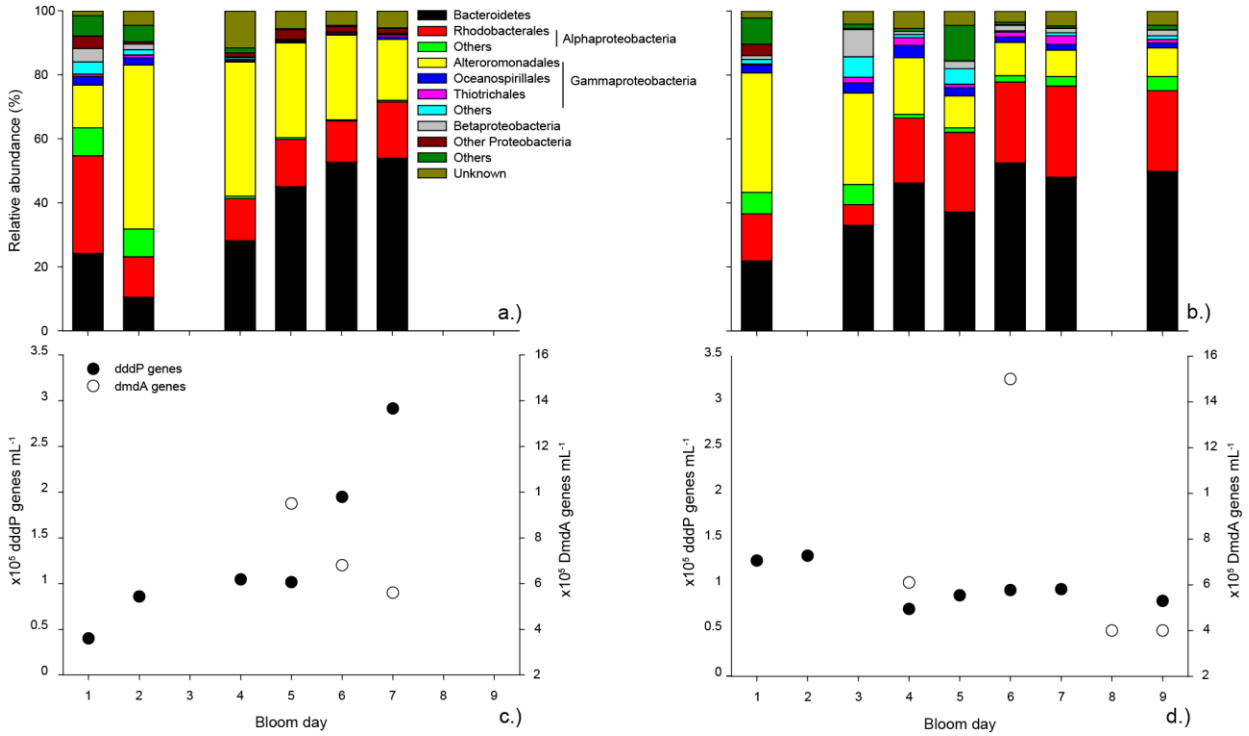

Figure 2.3 Microbial ecology of three independent bloom progressions in mesocosms a) bloom 1, b) bloom 3, qPCR measurements of dddP (white) and DmdA (black) in mesocosms c) bloom 1, d) bloom 3

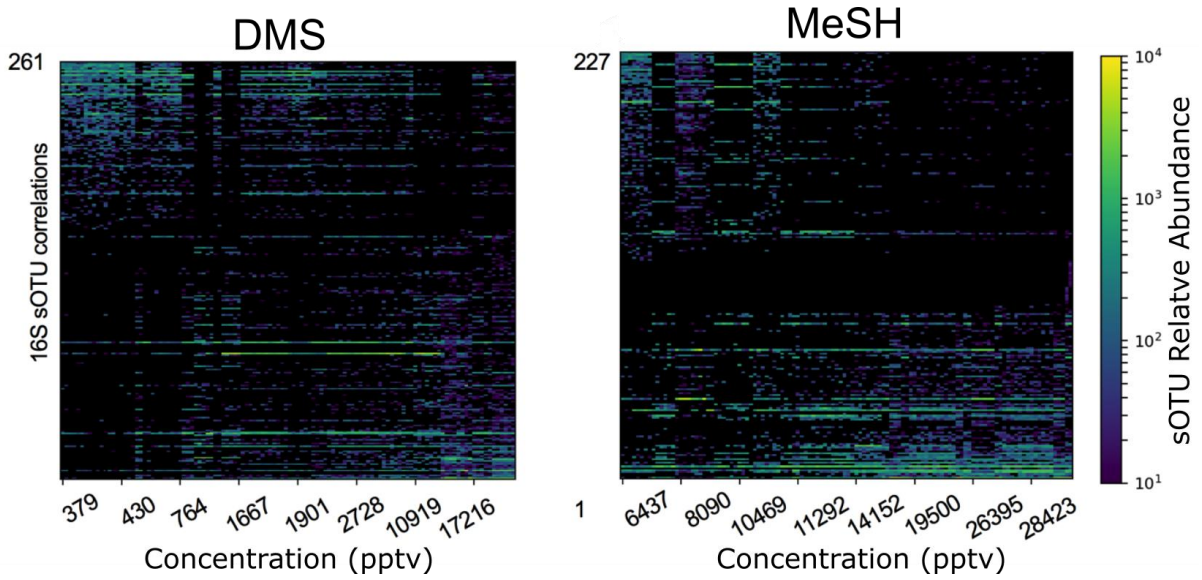

Figure 2.4 Microbial ecology of three independent bloom progressions in mesocosms a) bloom 1, b) bloom 3, qPCR measurements of dddP (white) and DmdA (black) in mesocosms c) bloom 1, d) bloom 3

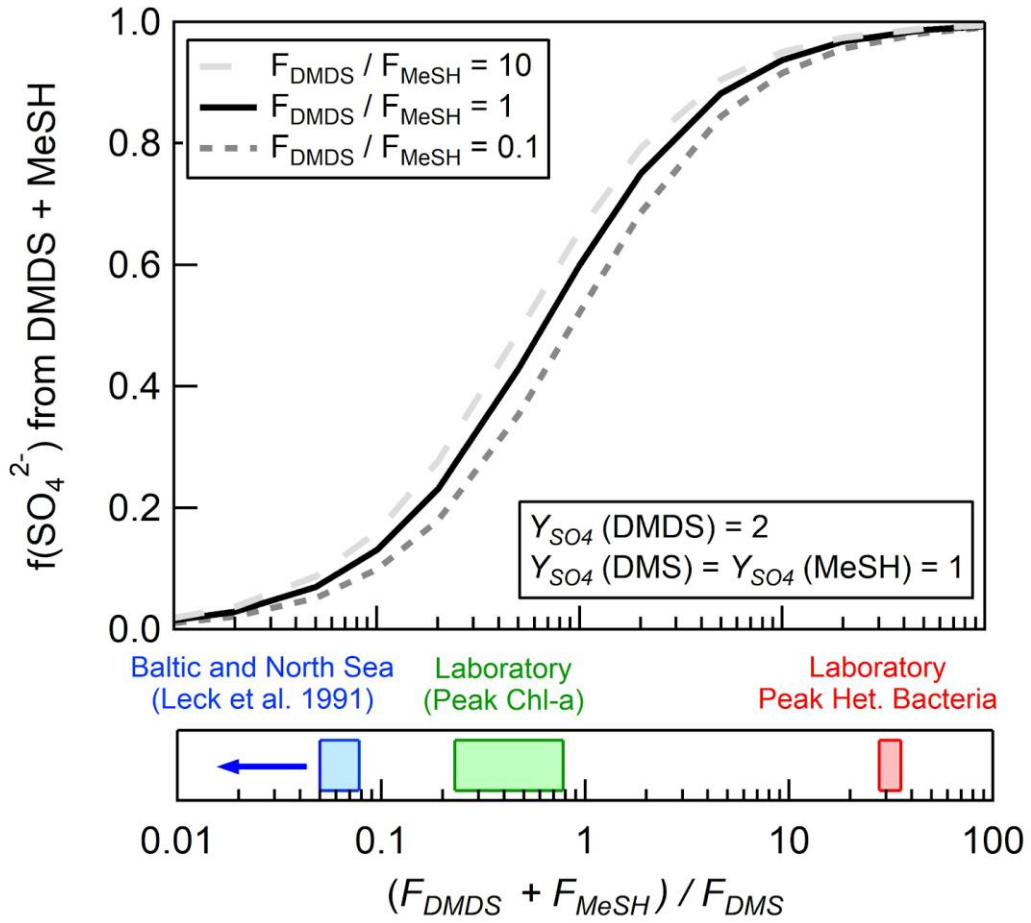

Figure 2.5 Fraction of sulfate produced from combined DMDS and MeSH compared to DMS compared between laboratory mesocosm peak chl a and peak HB with the only known field measurement of DMDS, MeSH, and DMS.

2.8 Supplementary methods

2.8.1 Methanethiol Conversion Controls

Controls were performed to assess the quantitative conversion of MeSH to DMDS on the CI-TOFMS inlet. First, 1 parts per billion mass MeSH in N_2 was diluted by zero air either at 0-5% RH or ~17.0 $g*kg^{-1}$ water vapor mixing ratio. The resultant air flowed through the same length of tubing used for sampling during BEAST 2018 and was measured for gas composition by the CI-TOFMS. Shown in Figure 2.8, the concentration of DMDS increased as more MeSH was added in a highly linear fashion until added [MeSH] > 60 ppbv.

Here we define the "actual" MeSH concentration detected by the CI-TOFMS using Equation 1:

$$[MeSH_a] = [MeSH_i] - 2 * [DMDS] \quad (1)$$

Where [MeSHi] is the expected concentration introduced from the calibrated MeSH gas cylinder to the CI-TOFMS and [DMDS] is the measured DMDS concentration calculated from the ion signal and humidity-dependent calibration factors (19.2ncps/pptv @ low humidity, 21.2ncps/pptv @ high humidity). Through obtaining MeSHa, calibration factors were calculated for MeSH and found to be 0.3 ncps/pptv at a mixing ratio of ~17.0 g/kg.

Lastly, in Equation 2, the MeSH conversion ratio (CR_{MeSH}) is defined as:

$$CR_{MeSH} = 1 - [MeSH_a]/[MeSH_i] \quad (2)$$

Shown in Figure 2.9, the conversion ratios for 4 separate inlet and humidity conditions were obtained across a range of introduced MeSH concentrations. It was found that the presence of the 20 cm stainless steel inlet significantly enhanced conversion of MeSH to DMDS before analysis by the CI-TOFMS. Despite a fairly high flow rate through the SS inlet (1.8 SLPM), conversion ratios of 0.3-0.4 were observed throughout the concentration range of MeSH measured during the bloom experiments. In both the PFA and SS inlets, the influence of humidity did not seem to

affect the conversion ratio significantly. Notably, at lower introduced MeSH concentrations (<1ppb) for the wet SS condition, the MeSH conversion rate was 1, which could be an artifact of the low MeSH flow rate from the gas cylinder. Nevertheless, the MeSH concentrations encountered in bloom experiments for this work remained above 1ppbv

2.9 Supplementary figures

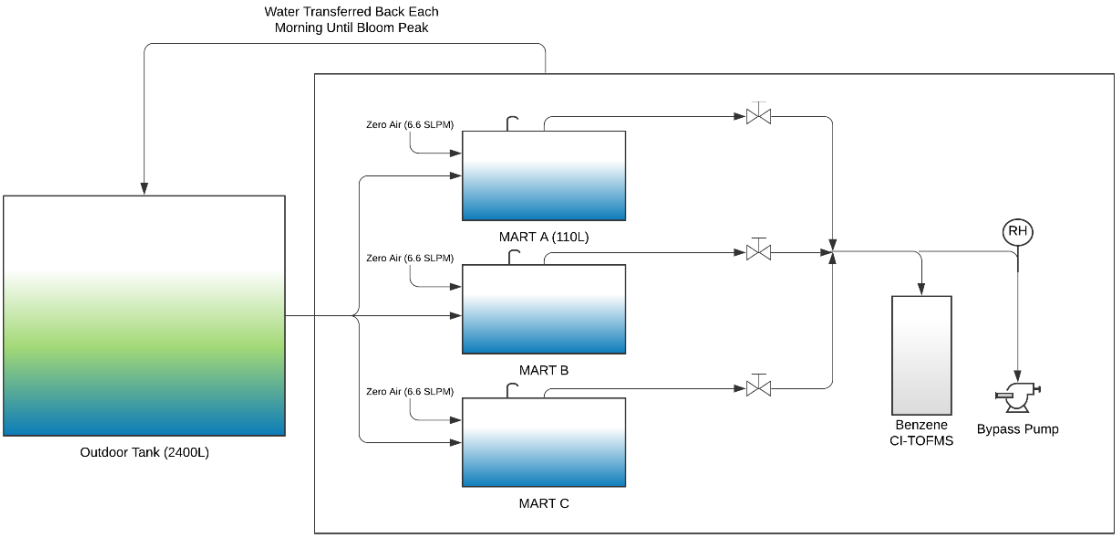

Figure 2.6. Management of daily sampled seawater for BEAST 2018

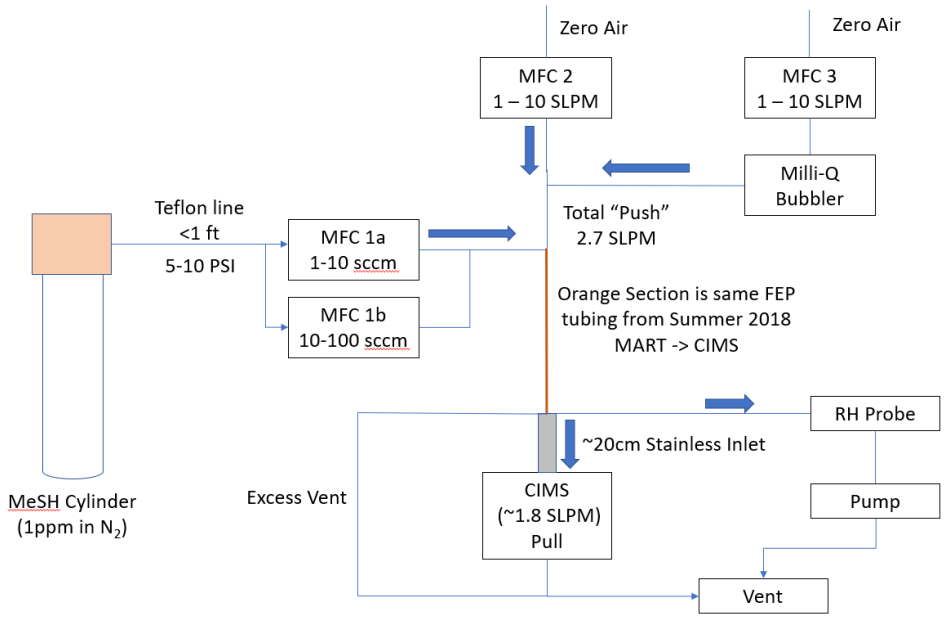

Figure 2.7. Methanethiol dimerization controls: arrangement of CI-TOFMS sampling apparatus

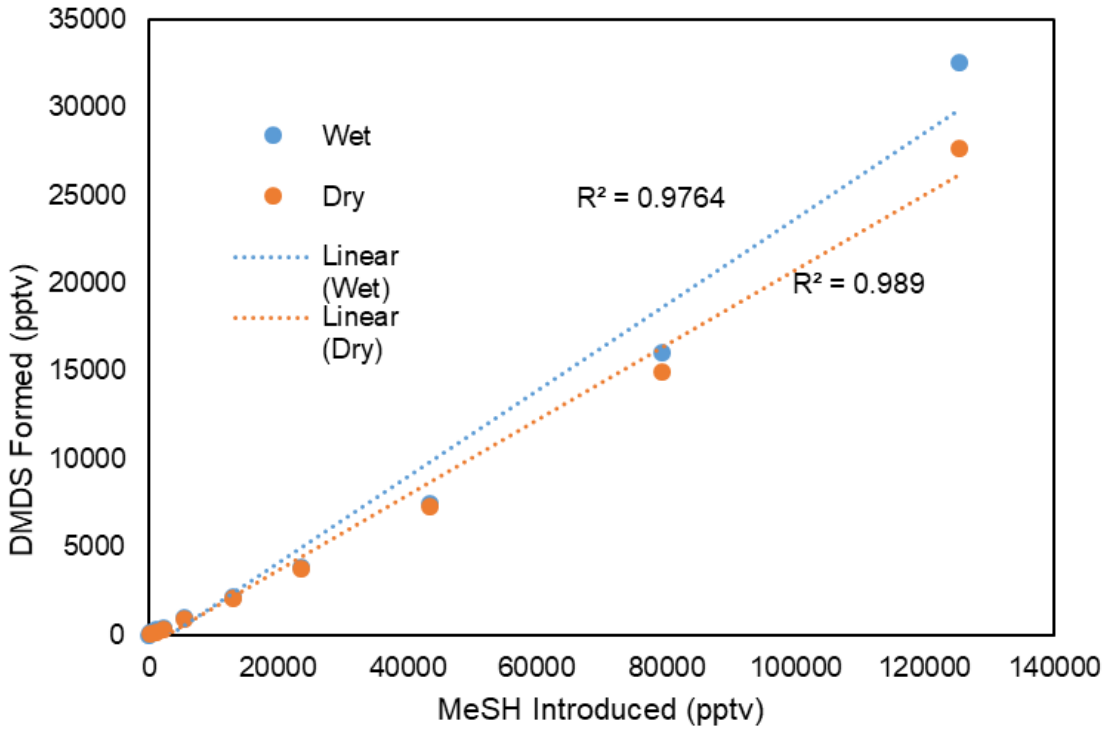

Figure 2.8 Formation of DMDS on the CI-TOFMS inlet from introduced MeSH

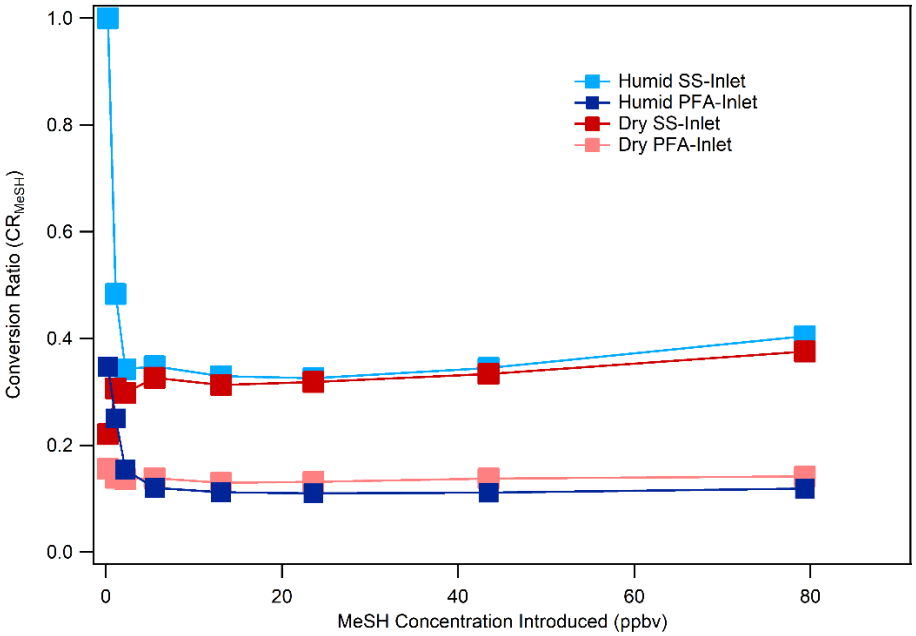

Figure 2.9 Variation of MeSH conversion ratio with introduced concentration of methanethiol directed to instrument inlet at different tubing inlet humidities and material compositions

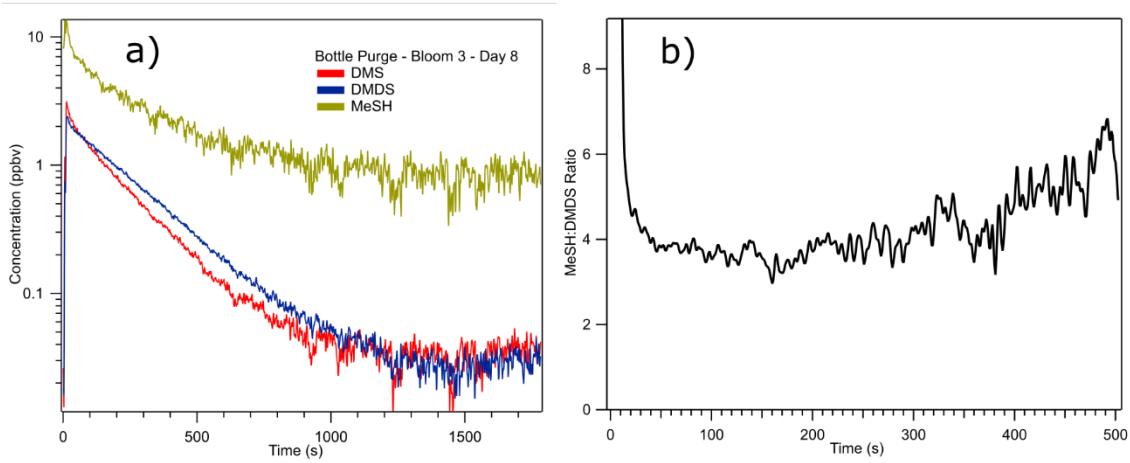

Figure 2.10 a) Purging of organosulfur gases from seawater directly sampled from the outdoor tank, b) MeSH:DMDS concentration ratio obtained from seawater purged with zero air

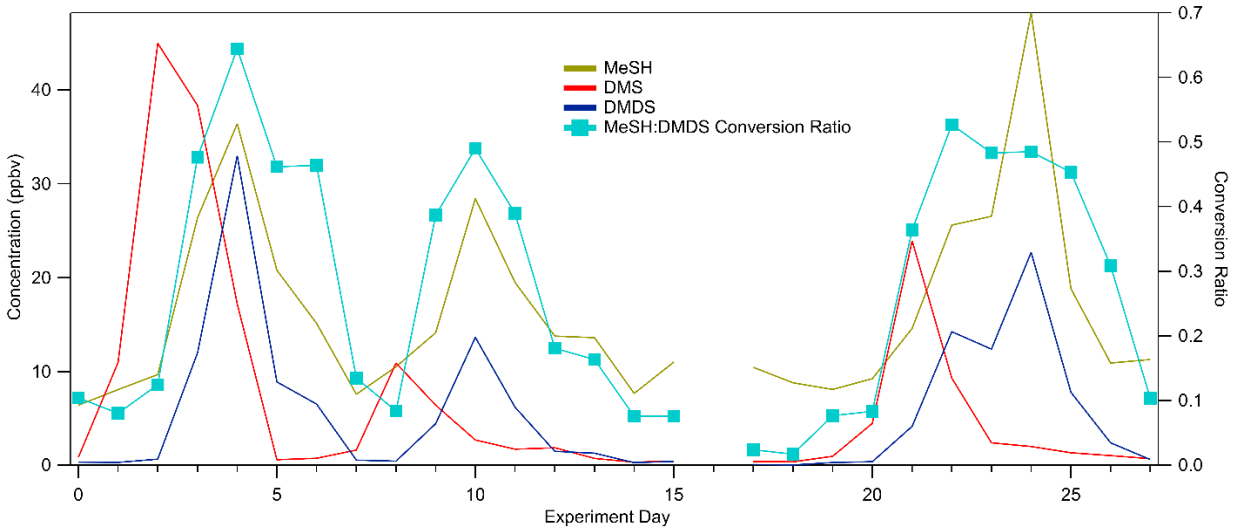

Figure 2.11 Time series gas concentrations of DMS, MeSH, and DMDS for mesocosms 1, 2, and 3 with the calculated conversion ratio assuming all DMDS was formed from MeSH observed

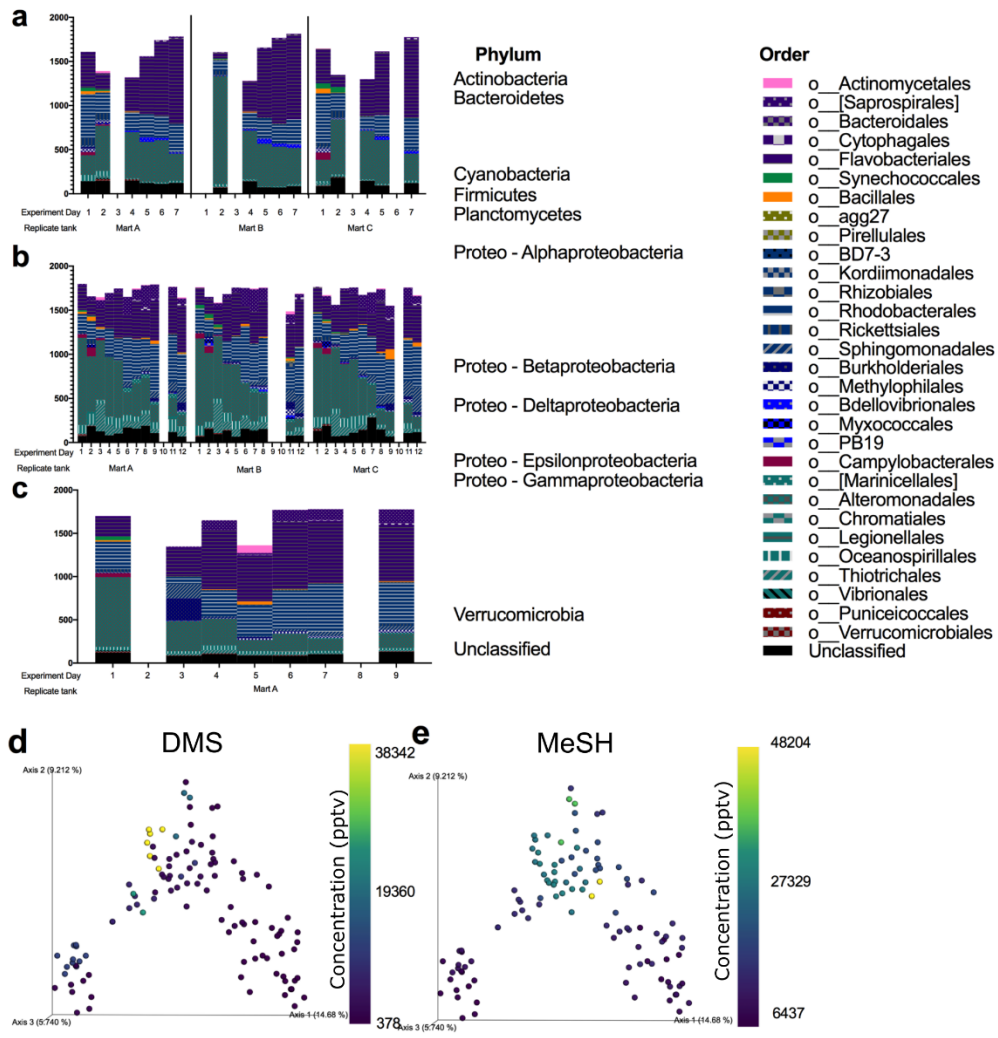

Figure 2.12 Microbial ecology of 3 mesocosm experiments: Relative abundance of sOTUs grouped at the order-level a) Mesocosm 1 represented by 3 MART vessels, b) Mesocosm 2 represented by 3 MART vessels, c) Mesocosm 3 represented by 1 MART vessel. (Eukaryotic and chloroplast sOTUs remove d),e) Principal coordinate analysis of unweighted Unifrac distances visualized by DMS and MeSH.

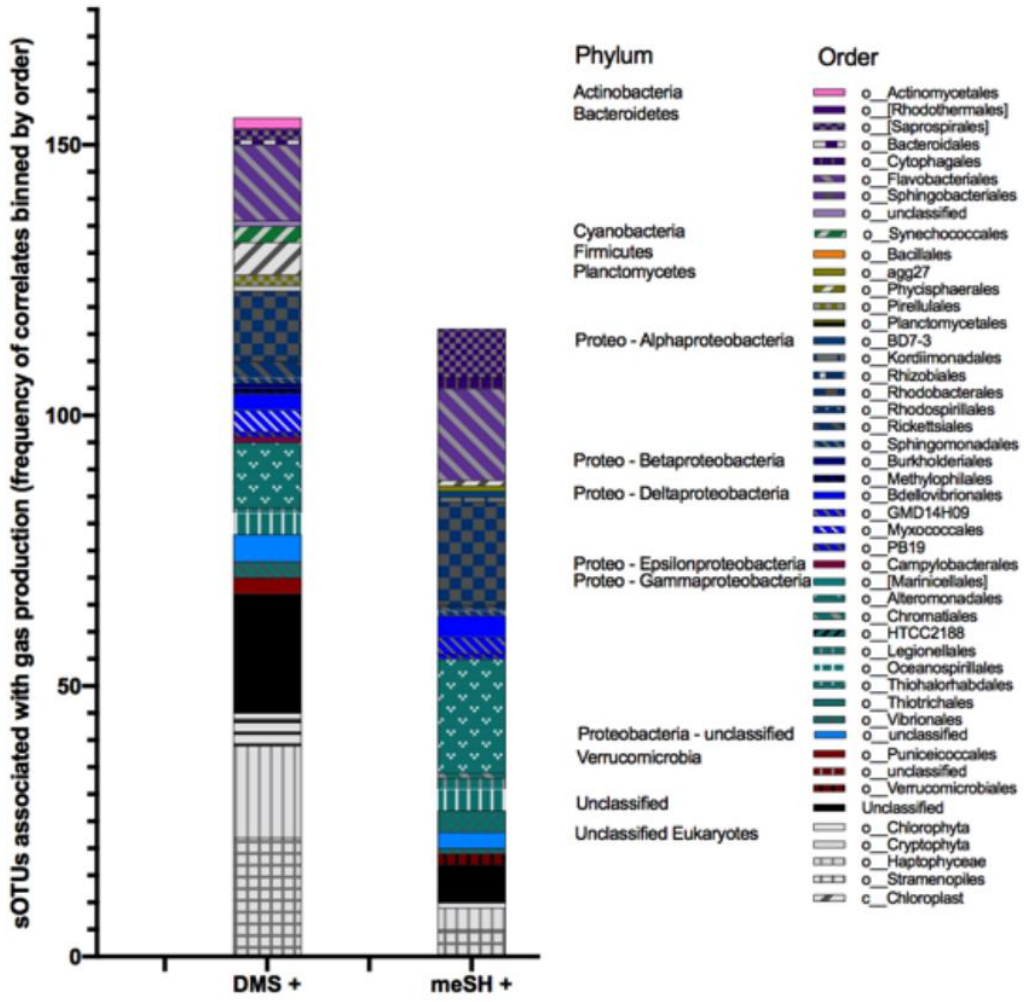

Figure 2.13 DMS and MeSH positively correlated sOTUs grouped by order for all three mesocosm experiments pooled together

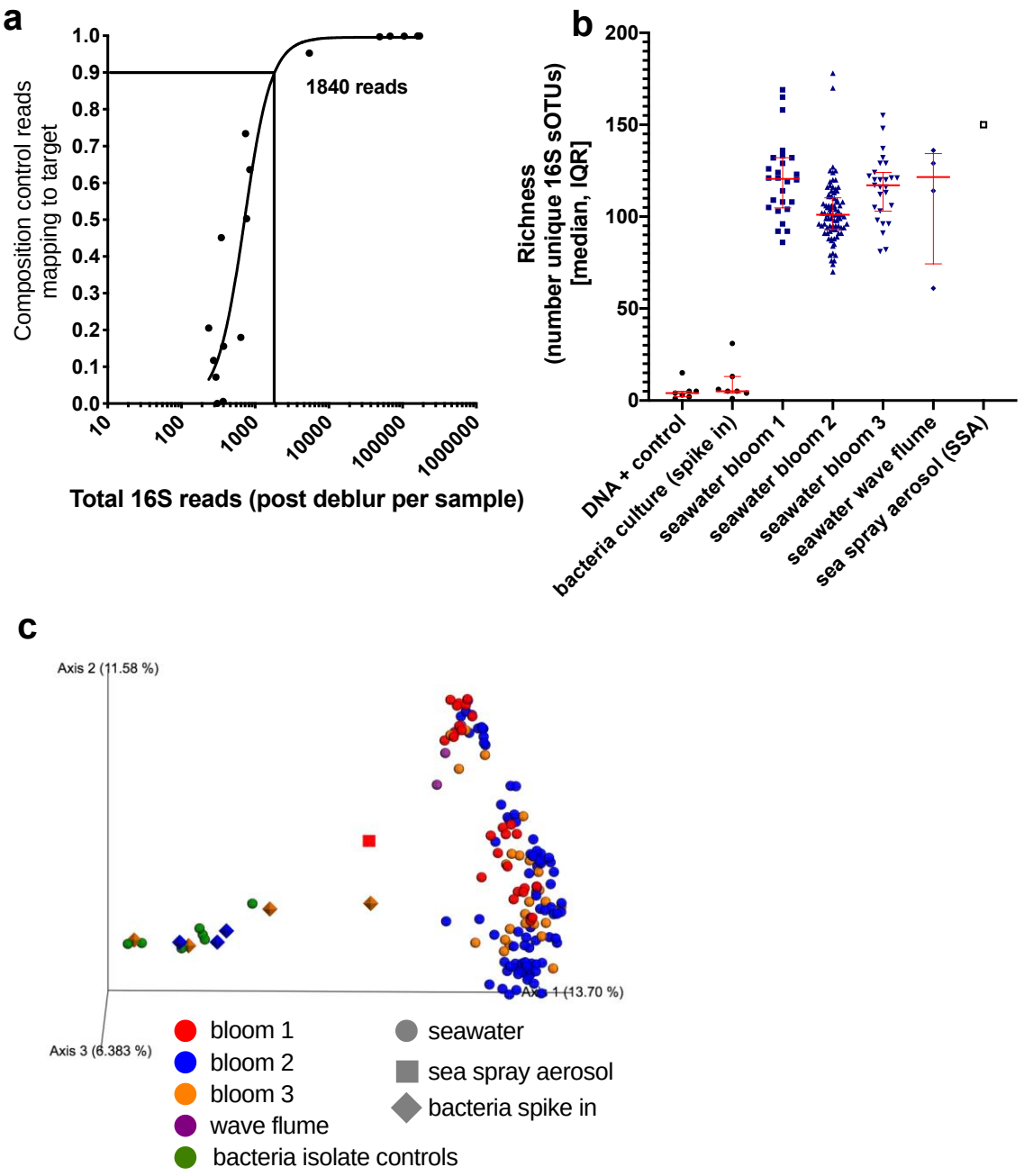

Figure 2.14 Success rate across sample types used in the experiment. a) Sample exclusion criteria calculated at 1840 reads based on KatharoSeq controls and procedure. b) Richness across bloom replicates along with comparison to controls. c.) Principal coordinate analysis of all samples from BEAST 2018 pooled

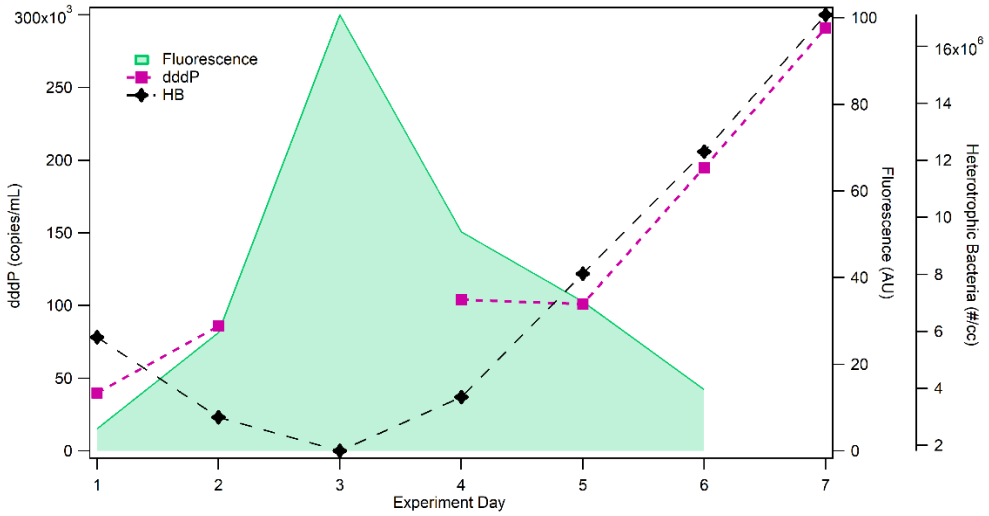

Figure 2.15 Time series dddP concentration over Mesocosm 1 time series with bulk fluorescence and heterotrophic bacteria concentration

2.10 References

Amir, A., Daniel, M., Navas-Molina, J., Kopylova, E., Morton, J., Xu, Z. Z., et al. (2017). Deblur Rapidly Resolves Single Nucleotide Community Sequence Patterns. American Society for Microbiology, 2(2), 1–7. https://doi.org/10.1128/mSystems.00191-16

Bashkova, S., Bagreev, A., & Bandosz, T. J. (2002). Effect of surface characteristics on adsorption of methyl mercaptan on activated carbons. Industrial and Engineering Chemistry Research, 41(17), 4346–4352. https://doi.org/10.1021/ie020137t

Boden, R., Kelly, D. P., Murrell, J. C., & Schäfer, H. (2010). Oxidation of dimethylsulfide to tetrathionate by Methylophaga thiooxidans sp. nov.: A new link in the sulfur cycle. Environmental Microbiology, 12(10), 2688–2699. https://doi.org/10.1111/j.1462-2920.2010.02238.x

Bolyen, E., Rideout, J. R., Dillon, M. R., Bokulich, N. A., Abnet, C. C., Al-Ghalith, G. A., et al. (2019). Reproducible, interactive, scalable and extensible microbiome data science using QIIME 2. Nature Biotechnology, 37(8), 852–857. https://doi.org/10.1038/s41587-019-0209-9

Buchshtav, T., Amrani, A., Said-Ahmad, W., & Kamyshny, A. (2019). Kinetics and mechanism of the abiotic decomposition of dimethyl disulfide under dark, oxic conditions. Environmental Chemistry, 16(7), 495–504. https://doi.org/10.1071/EN19076

Caporaso, J. G., Lauber, C. L., Walters, W. A., Berg-Lyons, D., Huntley, J., Fierer, N., et al. (2012). Ultra-high-throughput microbial community analysis on the Illumina HiSeq and MiSeq platforms. ISME Journal, 6(8), 1621–1624. https://doi.org/10.1038/ismej.2012.8

Chin, H. W., & Lindsay, R. C. (1994a). Ascorbate and transition-metal mediation of methanethiol oxidation to dimethyl disulfide and dimethyl trisulfide. Food Chemistry, 49(4), 387–392. https://doi.org/10.1016/0308-8146(94)90009-4

Chin, H. W., & Lindsay, R. C. (1994b). Mechanisms of Formation of Volatile Sulfur Compounds following the Action of Cysteine Sulfoxide Lyases. Journal of Agricultural and Food Chemistry, 42(7), 1529–1536. https://doi.org/10.1021/jf00043a026

Curson, A. R. J., Todd, J. D., Sullivan, M. J., & Johnston, A. W. B. (2011). Catabolism of dimethylsulphoniopropionate: Microorganisms, enzymes and genes. Nature Reviews Microbiology, 9(12), 849–859. https://doi.org/10.1038/nrmicro2653

Davis, D., Chen, G., Kasibhatla, P., Jefferson, A., Tanner, D., Eisele, F., et al. (1998). DMS Oxidation in the Antarctic marine boundary layer: Comparison of model simulations and field observations of DMS, DMSO, DMSO, H2SO4(g), MSA(g), and MSA(p). J. Geophys. Res., 103, 1657–1678. https://doi.org/10.1029/97JD03452

Van Duyl, F. C., Gieskes, W. W. C., Kop, A. J., & Lewis, W. E. (1998). Biological control of short-term variations in the concentration of DMSP and DMS during a Phaeocystis spring bloom. Journal of Sea Research, 40(3–4), 221–231. https://doi.org/10.1016/S1385-1101(98)00024-0

France, O. B., France, C. G., Germany, C. H., & Uk, A. J. (2013). Clouds and aerosols. Climate Change 2013 the Physical Science Basis: Working Group I Contribution to the Fifth Assessment Report of the Intergovernmental Panel on Climate Change, 9781107057, 571–658. https://doi.org/10.1017/CBO9781107415324.016

Fuhrman, J., & Azam, F. (1980). Bacterioplankton Secondary Production Estimates for Coastal Waters of British Columbia, Antarctica, and California, 39(6), 1085–1095. https://doi.org/10.1128/aem.39.6.1085-1095.1980

Gasol, J. M., & Del Giorgio, P. A. (2000). Using flow cytometry for counting natural planktonic bacteria and understanding the structure of planktonic bacterial communities. Scientia Marina, 64(2), 197–224. https://doi.org/10.3989/scimar.2000.64n2197

Gonzalez, A., Navas-Molina, J. A., Kosciolek, T., McDonald, D., Vázquez-Baeza, Y., Ackermann, G., et al. (2018). Qiita: rapid, web-enabled microbiome meta-analysis. Nature Methods, 15(10), 796–798. https://doi.org/10.1038/s41592-018-0141-9

Grenfell, J. L., Harrison, R. M., Allen, A. G., Shi, J. P., Penkett, S. A., Dowd, O., et al. (1999). An analysis of rapid increases in condensation nuclei concentrations at a remote coastal site in western Ireland, 104(Dll), 771–780. https://doi.org/10.1029/1999JD900096

Higgins, M. J., Yarosz, D. P., Chen, Y.-C., Murthy, S. N., Mass, N. A., & Cooney, J. R. (2012). Mechanisms of Volatile Sulfur Compound and Odor Production in Digested Biosolids. Proceedings of the Water Environment Federation, 2003(1), 993–805. https://doi.org/10.2175/193864703784292926

Howard, E. C., Henriksen, J. R., Buchan, A., Reisch, C. R., Bürgmann, H., Welsh, R., et al. (2006). Bacterial taxa that limit sulfur flux from the ocean. Science, 314(5799), 649–652. https://doi.org/10.1126/science.1130657

Kercher, J. P., Riedel, T. P., & Thornton, J. A. (2009). Chlorine activation by N 2 O 5 : simultaneous , in situ detection of ClNO 2 and N 2 O 5 by chemical ionization mass spectrometry, (2), 193–204.

Kettle, A. J., Rhee, T. S., Von Hobe, M., Poulton, A., Aiken, J., & Andreae, M. O. (2001). Assessing the flux of different volatile sulfur gases from the ocean to the atmosphere. Journal of Geophysical Research Atmospheres, 106(D11), 12193–12209. https://doi.org/10.1029/2000JD900630

Kieber, D. J., Kienea, R. P., Toole, D. A., Valle, D. A. del, & Brinkley, J. (2011). Biological consumption of dimethylsulfide (DMS) and its importance in DMS dynamics in the Ross

Sea, Antarctica. Limnology and Oceanography, 54(3), 785–798. https://doi.org/10.4319/lo.2009.54.3.0785

Kiene, R. (1996). Production of methanethiol from dimethylsulfoniopropionate in marine surface waters. Marine Chemistry, 54(1–2), 69–83. https://doi.org/10.1016/0304-4203(96)00006-0

Kiene, R., Williams, T., Esson, K., Tortell, P., & Dacey, J. (2017). Methanethiol Concentrations and Sea-Air Fluxes in the Subarctic NE Pacific Ocean. In AGU Fall Meeting Abstracts (Vol. 2017, pp. OS21A-1356).

Kiene, R. P., Linn, L. J., & Bruton, J. A. (2000). New and important roles for DMSP in marine microbial communities. Journal of Sea Research, 43(3–4), 209–224. https://doi.org/10.1016/S1385-1101(00)00023-X

Kiene, Ronald P., & Linn, L. J. (2000). Distribution and turnover of dissolved DMSP and its relationship with bacterial production and dimethylsulfide in the Gulf of Mexico. Limnology and Oceanography, 45(4), 849–861. https://doi.org/10.4319/lo.2000.45.4.0849

Kiene, Ronald P., Linn, L. J., González, J., Moran, M. A., & Bruton, J. A. (1999). Dimethylsulfoniopropionate and methanethiol are important precursors of methionine and protein-sulfur in marine bacterioplankton. Applied and Environmental Microbiology, 65(10), 4549–4558. https://doi.org/10.1016/j.entcs.2015.06.005

Kim, M. J., Zoerb, M. C., Campbell, N. R., Zimmermann, K. J., Blomquist, B. W., Huebert, B. J., & Bertram, T. H. (2016). Revisiting benzene cluster cations for the chemical ionization of dimethyl sulfide and select volatile organic compounds. Atmospheric Measurement Techniques, 9(4), 1473–1484. https://doi.org/10.5194/amt-9-1473-2016

Kwint, R. L. J., Kramer, K. J. M., Baart, A. C., & Verhagen, H. L. M. (1993). The production of DMS by a plankton community: a mesocosm experiment. Dimethylsulphide: Oceans, Atmosphere and Climate. Proc. International Symposium, Belgirate, 1992, 62, 63–81. https://doi.org/10.1007/978-94-017-1261-3_7

Lana, A., Bell, T. G., Simó, R., Vallina, S. M., Ballabrera-Poy, J., Kettle, A. J., et al. (2011). An updated climatology of surface dimethlysulfide concentrations and emission fluxes in the global ocean. Global Biogeochemical Cycles, 25(1), 1–17. https://doi.org/10.1029/2010GB003850

Lawson, S. J., Law, C. S., Harvey, M. J., Bell, T. G., Walker, C. F., De Bruyn, W. J., & Saltzman, E. S. (2020). Methanethiol, dimethyl sulfide and acetone over biologically productive waters in the southwest Pacific Ocean. Atmospheric Chemistry and Physics, 20(5), 3061–3078. https://doi.org/10.5194/acp-20-3061-2020

Leck, C., & Rodhe, H. (1991). Emissions of marine biogenic sulfur to the atmosphere of northern Europe. Journal of Atmospheric Chemistry, 12(1), 63–86. https://doi.org/10.1007/BF00053934

Lee, C. L., & Brimblecombe, P. (2016). Anthropogenic contributions to global carbonyl sulfide, carbon disulfide and organosulfides fluxes. Earth-Science Reviews, 160, 1–18. https://doi.org/10.1016/j.earscirev.2016.06.005

Levine, N. M., Varaljay, V. A., Toole, D. A., Dacey, J. W. H., Doney, S. C., & Moran, M. A. (2012). Environmental, biochemical and genetic drivers of DMSP degradation and DMS production in the Sargasso Sea. Environmental Microbiology, 14(5), 1210–1223. https://doi.org/10.1111/j.1462-2920.2012.02700.x

Lizotte, M., Levasseur, M., Scarratt, M. G., Michaud, S., Merzouk, A., Gosselin, M., & Pommier, J. (2008). Fate of dimethylsulfoniopropionate (DMSP) during the decline of the northwest Atlantic Ocean spring diatom bloom. Aquatic Microbial Ecology, 52(2), 159–173. https://doi.org/10.3354/ame01232

Lozupone, C., & Knight, R. (2005). UniFrac: A new phylogenetic method for comparing microbial communities. Applied and Environmental Microbiology, 71(12), 8228–8235. https://doi.org/10.1128/AEM.71.12.8228-8235.2005

McGowan, J. A., Deyle, E. R., Ye, H., Carter, M. L., Perretti, C. T., Seger, K. D., et al. (2017). Predicting coastal algal blooms in southern California. Ecology, 98(5), 1419–1433. https://doi.org/10.1002/ecy.1804

Minich, J. J., Humphrey, G., Benitez, R. A. S., Sanders, J., Swafford, A., Allen, E. E., & Knight, R. (2018). High-Throughput Miniaturized 16S rRNA Amplicon Library Preparation Reduces Costs while Preserving Microbiome Integrity, 3(6), 1–8. https://doi.org/10.1128/mSystems.00166-18

Minich, J. J., Zhu, Q., Janssen, S., Hendrickson, R., Amir, A., Vetter, R., et al. (2018). KatharoSeq Enables High-Throughput Microbiome Analysis from Low-Biomass Samples. MSystems, 3(3), 1–16. https://doi.org/10.1128/msystems.00218-17

Minich, J. J., Sanders, J. G., Amir, A., Humphrey, G., Gilbert, J. A., & Knight, R. (2019). Quantifying and Understanding Well-to-Well Contamination in Microbiome Research. MSystems, 4(4), 1–13. https://doi.org/10.1128/msystems.00186-19

Moran, M. A., & Durham, B. P. (2019). Sulfur metabolites in the pelagic ocean. Nature Reviews Microbiology, 17(11), 665–678. https://doi.org/10.1038/s41579-019-0250-1

Noble, R. T., & Fuhrman, J. A. (1998). Use of SYBR Green I for rapid epifluorescence counts of marine viruses and bacteria. Aquatic Microbial Ecology, 14(2), 113–118. https://doi.org/10.3354/ame014113

O'Dowd, C. D., & De Leeuw, G. (2007). Marine aerosol production: A review of the current knowledge. Philosophical Transactions of the Royal Society A: Mathematical, Physical and Engineering Sciences, 365(1856), 1753–1774. https://doi.org/10.1098/rsta.2007.2043

Perraud, V., Meinardi, S., Blake, D. R., & Finlayson-Pitts, B. J. (2016). Challenges associated with the sampling and analysis of organosulfur compounds in air using real-time PTR-ToF-MS and offline GC-FID. Atmospheric Measurement Techniques, 9(3), 1325–1340. https://doi.org/10.5194/amt-9-1325-2016

Persson, C., & Leck, C. (1994). Determination of Reduced Sulfur Compounds in the Atmosphere Using a Cotton Scrubber for Oxidant Removal and Gas Chromatography with Flame Photometric Detection. Analytical Chemistry, 66(7), 983–987. https://doi.org/10.1021/ac00079a009

Pinhassi, J., Simó, R., González, J. M., Vila, M., Alonso-Sáez, L., Kiene, R. P., et al. (2005). Dimethylsulfoniopropionate turnover is linked to the composition and dynamics of the bacterioplankton assemblage during a microcosm phytoplankton bloom. Applied and Environmental Microbiology, 71(12), 7650–7660. https://doi.org/10.1128/AEM.71.12.7650-7660.2005

Reisch, C. R., Moran, M. A., & Whitman, W. B. (2011). Bacterial catabolism of dimethylsulfoniopropionate (DMSP). Frontiers in Microbiology, 2(AUG), 1–12. https://doi.org/10.3389/fmicb.2011.00172

Sander, R. (2015). Compilation of Henry's law constants (version 4.0) for water as solvent. Atmospheric Chemistry and Physics, 15(8), 4399–4981. https://doi.org/10.5194/acp-15-4399-2015

Simo, R. (2001). Production of atmospheric sulfur by oceanic plankton: Biogeochemical, ecological and evolutionary links. Trends in Ecology and Evolution, 16(6), 287–294. https://doi.org/10.1016/S0169-5347(01)02152-8

Song, S. J., Amir, A., Metcalf, J. L., Amato, K. R., Xu, Z. Z., Humphrey, G., & Knight, R. (2016). Preservation Methods Differ in Fecal Microbiome Stability. MSystems, 1(3), e00021-16. https://doi.org/10.1128/mSystems.00021-16.Editor

Sorensen, J. (1988). Dimethylsulfide and Methane Thiol in Sediment Porewater of a Danish Estuary. Biogeochemistry, 6(3), 201–210. https://doi.org/10.1007/BF02182996

Stokes, M. D., Deane, G. B., Prather, K., Bertram, T. H., Ruppel, M. J., Ryder, O. S., et al. (2013). A Marine Aerosol Reference Tank system as a breaking wave analogue for the production of foam and sea-spray aerosols. Atmospheric Measurement Techniques, 6(4), 1085–1094. https://doi.org/10.5194/amt-6-1085-2013

Tanzer, D., & Heumann, K. G. (1992). Gas chromatographic trace-level determination of volatile organic sulfides and selenides and of methyl iodide in atlantic surface water. International

Journal of Environmental Analytical Chemistry, 48(1), 17–31. https://doi.org/10.1080/03067319208027039

Todd, J. D., Curson, A. R. J., Dupont, C. L., Nicholson, P., & Johnston, A. W. B. (2009). The dddP gene, encoding a novel enzyme that converts dimethylsulfoniopropionate into dimethyl sulfide, is widespread in ocean metagenomes and marine bacteria and also occurs in some Ascomycete fungi. Environmental Microbiology, 11(6), 1376–1385. https://doi.org/10.1111/j.1462-2920.2009.01864.x

Varaljay, V. A., Robidart, J., Preston, C. M., Gifford, S. M., Durham, B. P., Burns, A. S., et al. (2015). Single-taxon field measurements of bacterial gene regulation controlling DMSP fate. ISME Journal, 9(7), 1677–1686. https://doi.org/10.1038/ismej.2015.23

Vázquez-Baeza, Y., Pirrung, M., Gonzalez, A., & Knight, R. (2013). EMPeror: A tool for visualizing high-throughput microbial community data. GigaScience, 2(1), 2–5. https://doi.org/10.1186/2047-217X-2-16

Veres, P., Roberts, J. M., Warneke, C., Welsh-Bon, D., Zahniser, M., Herndon, S., et al. (2008). Development of negative-ion proton-transfer chemical-ionization mass spectrometry (NI-PT-CIMS) for the measurement of gas-phase organic acids in the atmosphere. International Journal of Mass Spectrometry, 274(1–3), 48–55. https://doi.org/10.1016/j.ijms.2008.04.032

Visscher, P. T., Quist, P., & Vangemerden, H. (1991). Methylated Sulfur-Compounds in Microbial Mats - Insitu Concentrations and Metabolism By a Colorless Sulfur Bacterium. Applied and Environmental Microbiology, 57(6), 1758–1763. https://doi.org/10.1128/AEM.57.6.1758-1763.1991

Wine, P. H., Kreutter, N. M., Gump, C. a, & Ravishankara, a. R. (1981). Kinetics of hydroxyl radical reactions with the atmospheric sulfur compounds hydrogen sulfide, methanethiol, ethanethiol, and dimethyl disulfide. The Journal of Physical Chemistry, 85(18), 2660–2665. https://doi.org/10.1021/j150618a019

Wolfe, G. V., & Kiene, R. P. (1993). Effects of methylated, organic, and inorganic substrates on microbial consumption of dimethyl sulfide in estuarine waters. Applied and Environmental Microbiology, 59(8), 2723–2726.

Wolfe, Gordon V., Strom, S. L., Holmes, J. L., Radzio, T., & BradyOlson, M. (2002). Dimethylsulfoniopropionate cleavage by marine phytoplankton in response to mechanical, chemical, or dark stress. Journal of Phycology, 38(5), 948–960. https://doi.org/10.1046/j.1529-8817.2002.t01-1-01100.x

Xu, Z., Amir, A., Sanders, J., Zhu, Q., Morton, J., Bletz, M., et al. (2019). Calour: an Interactive, Microbe-Centric Analysis Tool, 4(1), 1–12. https://doi.org/10.1128/mSystems.00269-18

Zeng, Y. X., Qiao, Z. Y., Yu, Y., Li, H. R., & Luo, W. (2016). Diversity of bacterial dimethylsulfoniopropionate degradation genes in surface seawater of Arctic Kongsfjorden. Scientific Reports, 6(August), 1–9. https://doi.org/10.1038/srep33031

Zubkov, M. V., Fuchs, B. M., Archer, S. D., Kiene, R. P., Amann, R., & Burkill, P. H. (2001). Linking the composition of bacterioplankton to rapid turnover of dissolved dimethylsulphoniopropionate in an algal bloom in the North Sea. Environmental Microbiology, 3(5), 304–311. https://doi.org/10.1046/j.1462-2920.2001.00196.x

Chapter 3. Multi-scale Examination of Grazer-Induced Changes in Molecular Signatures of Cyanobacteria

3.1 Abstract

Algal biomass production is a growing renewable source of fuels, nutrients, manufacturing materials, and pharmaceuticals. To make algal and cyanobacterial growth systems economically competitive, they are grown at large scale in open raceway ponds that are inexpensive to build, operate, and maintain as compared to closed bioreactors. However, open ponds suffer from increased opportunities for biological contamination from predators, pathogens, and competitors that result in, at minimum, reduced yields and, at maximum, whole scale disruptions in production upon destruction of the entire pond's crop population in a short period of time. Early detection of contaminants is a necessary step for triggering and informing an integrated past management-based intervention to prevent these crop losses. To develop a sensitive method of detection utilizing mass spectrometry (MS), we used three MS methods, imaging mass spectrometry (IMS), liquid chromatography MS/MS (LC-MS/MS) combined with molecular networking, and gas chromatography MS/MS (GC-MS/MS), to observe and identify molecular signatures from a model predator-prey system of the heterolobosean amoeba HGG1 predating on a cyanobacterial prey, the filamentous Anabaena sp. PCC 7120. IMS enabled association of molecules with the crop, the predator, or the activity of protozoan grazing, while LC-MS/MS-based molecular networking identified a subset of the grazing-specific signals as the chlorophyll breakdown products pyropheophytin, pheophorbide A, and pyropheophorbide. Volatile organic compounds (VOCs) predicted to be released through chlorophyll breakdown by IMS analysis were measured in the headspace over algal cultures under predation, however their intensities were diminished compared to other VOCs which responded more intensely to grazing. These results demonstrate

the versatility of using multiple MS technologies to identify molecular signatures for informing crop protection technologies.

3.2 Introduction

As the world's population and energy demands continue to increase, sustainable food and fuel sources must be developed to compensate for limited fossil fuel resources and to positively impact environmental and economic concerns, including accumulation of greenhouse gas emissions, climate change, increasing gas prices, and energy security (BP, 2016; Review and June, 2015). Algal biofuels and high-value co-products are a promising renewable and carbon-neutral alternative derived from the biomass of photosynthetic microorganisms that convert sunlight and carbon dioxide into usable organic molecules (Burkart and Mayfield, 2013; Jones and Mayfield, 2012). Natural and engineered strains of algae have been grown to produce lipid-based products such as plastics, surfactants, and pigments, high value co-products like protein therapeutics, nutraceuticals, and high value small molecules, as well as fuels such as bioethanol, biohydrogen, and drop-in fuel replacements for cars and airplanes (Ghadiryanfar et al., 2016; Hoh et al., 2016; Schoepp et al., 2015; Scranton et al., 2015).

While the technology exists to grow and process green algae and cyanobacteria on an agricultural scale, there are many challenges to making algal biofuels market-competitive and sustainable. Photobioreactors offer lower risks of contamination, increased crop yields, and better control of culture conditions such as light exposure, nutrient delivery, and temperature, but carry large economic and energetic costs (Gupta et al., 2015). The most common alternative for mass growth of photosynthetic organisms are open pond production systems. Open systems bypass the economic and energetic costs associated with closed systems due to their simple construction and low operational costs. Most open ponds are shallow, circular or rectangular loops that are mixed

by a paddle wheel for continuous water flow. However, open ponds are susceptible to predatory and pathogenic contaminants (Gupta et al., 2015; Kumar et al., 2015). Predatory, pathogenic, and parasitic contaminations are the primary biotic impediments to large-scale cyanobacterial or algal biomass production. Protozoan grazing occurs in natural environments and has been shown to cause marked decreases in populations of cyanobacteria (Dryden and Wright, 1987; Van Wichelen et al., 2010). In a review analysis, biomass losses due to predation on microalgae in open raceway ponds ranged from 10-30% (Richardson et al., 2014).

Recently, a large volume of research has been conducted to develop technologies for the detection of grazers which has been reviewed in detail (Achyuthan et al., 2017; Di Caprio, 2020; Deore et al., 2020). As of now, the predominant method of grazer detection has been optical methods, especially visible light microscopy or various methods of flow cytometry. These methods usually involve gathering a small liquid sample (μL-mL scale) and enumerating the quantity of unwanted species. While quite sensitive, sometimes detecting <1 contaminant cell*mL^{-1}, both techniques struggle to detect biological contaminants across all size ranges and each requires method-specific attention towards the detection of different types of grazers, such as usage of staining and pre-separation techniques like centrifugation. These shortfalls extend the time between sample collection and identification of grazers, which is a crucial factor to pond protection as some grazer infections can erode 1% of pond biomass per hour (Montagna, 1995). Analyses using DNA as a biomarker are also being pursued for grazer detection. These methods possess superior sensitivity in the theoretical sense (1 DNA molecule, pre-amplification), and can ideally identify all biological species present in a sample from one analysis. Unfortunately, these methods are often time consuming, require specific reagents and protocol development, and may be

insensitive depending on the number of DNA sequences per contaminant cell as discussed in detail by Di Caprio 2020.

Towards a method of diagnosing grazer contamination of algal ponds, attention has turned towards analysis of small molecule metabolites and volatile organic compounds (VOCs), produced from algal cultures (Achyuthan et al., 2017; Stasulli and Shank, 2016). Algae express a large variety of organic chemicals necessary for their metabolic functions, which are produced naturally during healthy growth but can be modulated in response to numerous external factors such as temperature or grazing (Tillmann and John, 2002; Willette et al., 2018). In addition, the metabolic processes of the grazers themselves also contribute to the assemblage of organic species present. The collection of these organic compounds within each organism and the extracellular space exist as distinct molecular signatures that are observable with detailed chemical composition measurements (Goulitquer et al., 2012; You et al., 2020). Utilization of these molecular signatures as tracers for identifying the algal state of health or infection is a promising opportunity for cultivation improvements in open raceway ponds. Mass spectrometry is an invaluable tool for chemical analysis due to its sensitivity, high throughput, and ability to analyze complex mixtures.

To examine molecules produced from algae and grazers in solid or liquid culture, imaging mass spectrometry (IMS) in combination with liquid chromatography tandem mass spectrometry (LC-MS/MS) and molecular networking can be used to identify organism specific signals as well as gain insight to those signals' molecular structures (Nguyen et al., 2013). IMS samples across a predefined region to generate MS ion images, which can be co-localized with visible phenotypes to allow for direct visualization of molecular spatial distributions (Yang et al., 2012, 2009) (Figure 3.7). Structural information is gained by subjecting samples and molecules of interest to LC-MS/MS followed by molecular networking analysis. Molecular networking visualizes observed

molecules as groups of molecular families; molecules that are structurally related and therefore give similar fragmentation patterns in an MS (Watrous et al., 2012). Studies up to date on the production of grazing-induced VOCs measured by gas chromatography mass spectrometry (GC/MS) have revealed consistent production of compounds such as β-ionone and β-cyclocitral derived from the breakdown of algal carotenoids during senescence and metabolic processing by grazers (Fisher et al., 2020; Reese et al., 2019). Approaches seeking to identify downstream algal metabolic and VOC targets using analyses of upstream larger metabolic moieties are not known to the authors and represent possible opportunities to pinpoint molecules which could be produced in significant quantities or targeted for detection.

Using a model predator-prey combination comprised of the heterolobosean amoeba, HGG1, and the filamentous nitrogen-fixing cyanobacteria *Anabaena* sp. PCC 7120, we use MALDI-IMS and LC-MS/MS molecular networking to identify grazing-specific molecular signatures (Simkovsky et al., 2012). Using this two-pronged MS approach, we have identified chlorophyll breakdown products that are only present during amoebal grazing. Extending these findings further, we sought to determine whether decomposition products identified by IMS and LC-MS/MS could be used to predict VOCs produced by the same cyanobacteria-grazer pair. By identifying and structurally characterizing these molecular signatures, we believe early detection of these molecules can allow for appropriate interventive actions (e.g. chemical protectants or pesticides) to take place, thereby avoiding the loss of high yield biomass.

3.3 Materials and methods

3.3.1 Cyanobacteria and amoeba culture conditions

Unless noted otherwise, cyanobacterial cultures were grown at 30°C in liquid or on solid BG-11 (Allen, 1968) with 1.5% (wt/vol) agar under constant illumination from fluorescent cool

white bulbs producing light levels ranging from 75 to 250 µmol photons m^{-2} s^{-1}. *Anabaena* sp. PCC 7120, hereafter referred to as PCC 7120, was maintained similarly, though in BG-11 media lacking sodium nitrate (BG-11 N-). *Synechocystis* sp. strain WHSyn (Taton et al., 2014), hereafter referred to as WHSyn, and *Hartmanella* amoeba LPG1 (Ma et al., 2016) were obtained from B. Palenik and B. Brahamsha (Scripps Institute of Oceanography). Amoebae LPG1 and the heterolobosean amoeba HGG1 were regularly maintained on lawn plates of *S. elongatus* PCC 7942, hereafter referred to as PCC 7942, as previously described (Ma et al., 2016; Simkovsky et al., 2012). Prior to *Anabaena* sp. PCC 7120 solid and liquid experiments, HGG1 was transferred from *S. elongatus* lawn plates and then regularly maintained on lawns of PCC 7120 by transferring material from the plaque to the center of a 7-day old lawn on BG-11 plates. For all IMS experiments, cyanobacterial cultures were grown on thin BG-11 agar plates, made with 11 ml of BG-11 agar in 10 cm petri dishes, in humidified plastic containers, as previously described (Yang et al., 2012).

3.3.2 Culture Conditions for 7120-HGG1 Interactions on Solid Media

For IMS experiments involving only PCC 7120 and amoeba HGG1, three 5 µl aliquots of a PCC 7120 culture grown to late-exponential phase were spotted in a horizontal line approximately 0.5 cm - 1 cm away from each other on thin BG-11 N- agar plates. These plates were housed in a plastic container with damp paper towels and incubated at continuous low light (75 µmol photons m^{-2} s^{-1}) and 30 °C for 5 days. For plates containing interactions of PCC 7120 and HGG1, HGG1 was collected from a maintenance plate and resuspended in 200 µL of BG-11 liquid media. Three 5 µl aliquots of this HGG1 resuspension, each containing approximately 2.5 × 10^4 amoebae, were spotted in a row 0.5 cm - 1 cm moving away from the PCC 7120 cultures. The first spot of HGG1 was placed so as to partially overlap an outer spot of PCC 7120. All plates,

whether containing amoebae or not, were returned to the humidified container, moved to a lower light shelf (10 μmol photons m^{-2} s^{-1}) at 30°C, and incubated for an additional 6 days.

For IMS experiments involving multiple cyanobacteria with either HGG1 or LPG1, single 5 μl aliquots of late-exponential phase cultures of PCC 7942, PCC 7120, *Leptolyngbya* sp. BL0902 (hereafter referred to as BL0902), *Synechocystis* sp. PCC 6803 (hereafter referred to as PCC 6803), and WHSyn were spotted individually on thin BG-11 agar plates and grown in humidified plastic containers at 30°C under continuous light (75 μmol photons m^{-2} s^{-1} for PCC 7120 and 200 μmol photons m^{-2} s^{-1} for all others) for 5 days. For those plates challenged with amoeba, HGG1 and LPG1 resuspension samples were collected as described above from PCC 7942-amoeba maintenance plates. Single 5 μl aliquots of the amoeba resuspension, each containing approximately 2.5×10^4 amoebae, were spotted to partially overlap the cyanobacterial culture grown on the plate. All plates with or without amoebae were returned to the humidified container and incubated for an additional 5 days at 30°C and 10 μmol photons m^{-2} s^{-1} light.

3.3.3 MALDI-IMS of 7120-HGG1 Interactions on Solid Media

After appropriate incubation, interaction plates of cyanobacteria with amoebae and cyanobacteria without amoebae controls were excised from the agar and transferred to a Bruker MSP 96 stainless steel target plate as previously described (Yang et al., 2012). A film of Universal MALDI Matrix (Sigma-Aldrich) was applied to the surface of the excised agar using a 53 μm sieve (Hogentogler & Co., Inc.). The target plate was dried at 37 °C until the agar pieces had dried completely and adhered to the target plate. The samples were subjected to MALDI-IMS using reflectron positive mode on a Bruker Autoflex with Compass 1.2 software suite containing flexImaging 2.0, flexControl 3.0, and flexAnalysis 3.0.

3.3.4 Culture Conditions for 7120-HGG1 Interactions in Liquid Media

5 mL of PCC 7120 from a late-exponential phase culture was inoculated into 100 mL of BG-11 or BG-11 N- media in an Erlenmeyer flask and incubated for 7 days at 30 °C, shaking at 150 rpm, and continuous light (75 μmol photons m^{-2} s^{-1}). After 7 days of incubation, HGG1 was collected from a maintenance plate as described above and 200 μL was inoculated into appropriate flasks for PCC 7120-HGG1 grazing studies. The flasks were incubated for an additional 7 days at room temperature and ambient light, at which point the samples were centrifuged, the cell pellet extracted 3 times with 20 mL of acetonitrile (Fisher Scientific), and the media supernatant was extracted with 3 times with 20 mL of n-butanol (Fisher Scientific). All extracts were dried *in vacuo*. Appropriate media controls and PCC 7120 controls were cultured, incubated, and extracted in the same process.

3.3.5 LC-MS/MS Analysis

Dried samples from the liquid grazing assays were dissolved in 1 mL of dimethyl sulfoxide (DMSO, Alfa Aesar), diluted 10x in MeOH containing glycocholic acid (Calbiochem, sodium salt) at a final concentration of 100 μM in 2.0 mL LC-MS vials (Thermo Fisher Scientific). Glycocholic acid served as an injection standard and quality control for the chromatography. MS analysis was performed on a micrOTOF-Q II (Bruker Daltonics) mass spectrometer with ESI source, controlled by OTOF control and Hystar. An external calibration with ESI-L Low Concentration Tuning Mix (Agilent Technologies) was performed prior to data acquisition and hexakis (1H,1H,3H-tetrafluoropropoxy)phosphazene (Synquest Laboratories) *m/z* 922.009798 was used as a lock mass internal calibrant during data acquisition. Two separate modes for MS acquisition were used. For the "wide" method for larger m/z values: MS Spectra were acquired in positive ion mode over a mass range of 100-2000 *m/z*. The following instrument settings were used for data acquisition: capillary voltage of 4500 V, nebulizer gas (nitrogen) pressure of 3 bar, ion source temperature of

200°C, dry gas flow of 9 L min^{-1}, source temperature, and spectra acquisition rate of 2 Hz for MS1 and MS2. Minutes 0-15 were recorded with Auto MS/MS turned on where the 10 most intense ions per MS1 scan were selected and subjected to collision induced dissociation according to the following fragmentation and isolation list (values are *m/z*, isolation width, and collision energy, respectively): 100, 4, 30; 300, 5, 40; 500, 6, 50; 1000, 8, 60; 1500, 10, 70; 2000, 12, 80. In addition, the basic stepping function was used to fragment ions at 100% and 160% of the CID calculated for each *m/z* from the above fragmentation and isolation list with a timing of 50% for each step.

Similarly, basic stepping of collision RF of 198 and 480 Vp-p with a timing of 50% for each step and transfer time stepping of 75 and 92 µs with a timing of 50% for each step. MS/MS active exclusion parameter was set to 5, released after 0.5 min, and Reconsider Precursor was set to 2.0. For the "low" method for smaller m/z's: MS spectra were acquired in positive ion mode over a mass range of 50-1500 m/z. The following instrument settings were used for data acquisition: capillary voltage of 4000 V, nebulizer gas (nitrogen) pressure of 2 bar, ion source temperature of 200 °C, dry gas flow of 9 L min^{-1}, source temperature, and spectra acquisition rate of 2 Hz for MS1 and MS2. Minutes 0-15 were recorded with Auto MS/MS turned on where the 5 most intense ions per MS1 scan were selected and subjected to collision induced dissociation according to the following fragmentation and isolation list (values are *m/z*, isolation width, and collision energy, respectively): 100, 4, 25; 300, 5, 30; 500, 6, 35; 1000, 8, 50, 2000, 10, 70. Advanced stepping was turned on. The values for time, Collision RF, Transfer Time, and Collision, respectively are as follows: 0, 100, 60, 50; 15, 100, 60, 100; 50, 150, 70, 50; and 65, 150, 70, 100. MS/MS active exclusion parameter was set to 2, released after 0.5 min, and Reconsider Precursor was set to 2.0. The injected samples were chromatographically separated using an Agilent 1290 Infinity Binary LC System (Agilent Technologies) controlled by Hystar software (Bruker

Daltonics), using a 50 x 2.1 mm Kinetex 1.7 μM, C18, 100 Å chromatography column (Phenomenex), 30 °C column temperature, 0.5 mL/min flow rate, mobile phase A 99.9% water (Fisher Scientific, LC-MS grade) 0.1% formic acid (Fisher Scientific, Optima LC/MS), mobile phase B 99.9% acetonitrile (Fisher Scientific, LC-MS grade) 0.1% formic acid (Fisher Scientific, Optima LC/MS), with the following gradient: 0-0.5 min 10% B, 0.5-8 min 100% B, 8-13 min 100% B, 13-13.1 min 10% B, 13.1-15 min 10% B. 0 μL (blank) injections, methanol injections containing 10x dilution of DMSO and glycocholic acid, and liquid media treated and extracted under the same conditions as the culture conditions, were used as controls.

3.3.6 Molecular networking

All LC-MS/MS data was converted to mzXML format using Compass Data Analysis (Bruker Daltonics) and uploaded to the Global Natural Products Social Molecular Networking (GNPS) webserver (Wang et al., 2016) (http://gnps.ucsd.edu). The data is publicly accessible at http://gnps.ucsd.edu under the MassIVE Accession number: MSV000086470 and the networking results and parameters can be found at the following link: https://gnps.ucsd.edu/ProteoSAFe/status.jsp?task=8dfc4d60dd644e4a8b1060877fba3687.

A molecular network was created using the online workflow at GNPS. The data was then clustered with MS-Cluster with a precursor mass tolerance of 2.0 Da and a MS/MS fragment ion tolerance of 0.5 Da to create consensus spectra. Further, consensus spectra that contained less than 2 spectra were discarded. A network was then created where edges were filtered to have a cosine score above .65 and more than 6 matched peaks. Further edges between two nodes were kept in the network if and only if each of the nodes appeared in each other's respective top 10 most similar nodes. The spectra in the network were then searched against GNPS' spectral libraries. All matches kept between network spectra and library spectra were required to have a score above 0.7 and at

least 6 matched peaks. All other settings were left default. The molecular network was visualized using Cytoscape version 2.8.3 and displayed using an unweighted force directed layout with the blanks (media controls and blank injections removed from the network).

3.3.7 SPME-GC/MS algae-grazer headspace analysis

Autoclaved 10 mL crimp cap vials were filled with 4 mL of BG-11 media with 1.5% (wt/vol) agar to produce a solid substrate for cyanobacterial growth. 200 µl aliquots of PCC 7120 or PCC 7942 from dense late-exponential phase cultures were spread over the entire surface of the agar substrate, after which the vial was sealed with an autoclaved cotton ball to allow gas exchange while maintaining sterility, and grown for 7 days at 30°C and 75 µmol photons m^{-2} $s^{-1}$for PCC 7120 or 250 µmol photons m^{-2} s^{-1} for PCC 7942. For each cyanobacteria-grazer experiment, 21 vials were prepared. After the growth of the cultures, 7 had a 5 µl aliquot of BG-11 media added to the center of the cyanobacterial lawn to generate uninfected controls of cyanobacteria, 7 were infected with a 5 µl aliquot of a HGG1 resuspension prepared as described above that was added to the center of the cyanobacterial lawn, and 7 were infected with a 5 µl aliquot of a LPG1 resuspension prepared as described above that was added to the center of the cyanobacterial lawn,.

For each day following infection with amoebae, an untested vial from each group was sampled by solid phase microextraction (SPME) fibers possessing a 50 µm stationary phase of divinylbenzene/Carboxen/polydimethylsiloxane (solid gray, Supelco) equilibrated in the vial headspace for 24 hours. Samples were analyzed on an Agilent Technologies 7820A/5975 gas chromatograph mass spectrometer (GC/MS) using an Agilent BP5 column. The following GC/MS parameters were utilized for analysis of SPME fibers: Inlet temperature: 250 °C, splitless injection, carrier flow: 2 mL min^{-1}, GC temperature program: 35 °C for 3 minutes then +7 C min^{-1} to 230 °C which was held for 2 minutes, MS transfer line temperature: 260 °C, MS scan range: m/z 32.5 –

m/z 300 over 1 second. MS data were baselined using the statistics-sensitive non-linear iterative peak-clipping (SNIP) algorithm (Ryan et al., 1988) and analyzed in OpenChrom (Wenig and Odermatt, 2010) (http://openchrom.net). MS spectra were identified using the NIST14 EI mass spectral database. Results were subsequently exported to Igor Pro 7 (Wavemetrics) for plotting.

3.3.8 Chemical ionization mass spectrometry analysis of algae-grazer headspace

250 mL borosilicate media bottles were filled with 150 mL of BG-11 media with 1.5% (wt/vol) agar to produce a solid substrate of growth media. 1 ml aliquots of PCC 7120 from dense late-exponential phase cultures were spread over the entire surface of the agar substrate, after which the vial was sealed with an autoclaved foam plug to allow gas exchange while maintaining sterility, and grown for 7 days at 30°C and 75 μmol photons m^{-2} s^{-1}, after which time a 5 μl resuspension of HGG1, prepared as described above, was added to each appropriate culture at the center of the cyanobacterial lawn as described above. Each borosilicate bottle was then sealed with a custom PTFE sealed cap to which two 1/8" ball valves were attached for gas sampling. Each day, both ball valves were opened and 100 standard cubic centimeters per minute (sccm) of zero air (Sabio 1001) was flushed through the bottle headspace to sample the bottle headspace. Bottle headspaces were then diluted in 2.0 SLPM zero air and sampled by a chemical ionization time of flight mass spectrometer (CI-TOFMS) which has been detailed before, and will be described here briefly (Bertram et al., 2011). Protonated water clusters, $H_3O(H_2O)_n^+$, where n = 1,2,3..., were generated by passing 2.2 standard liters per minute (SLPM) of humidified N_2 through a 30 mCi source of Po-210 (NRD) (Aljawhary et al., 2013). This ion stream was then sampled through an inline critical orifice at 1.8 SLPM into an ion molecule reaction chamber (IMR) which also sampled the analyte gas stream at 1.8 SLPM. The IMR pressure was maintained at 65 torr and 50 °C for all samples.

Product ions generated through proton transfer reactions with protonated water clusters (Reaction scheme 1).

$$(H_2O)_nH_3O^+ + A \rightarrow (H_2O)_{n+1} + AH \qquad (1)$$

Where A is the analyte. Ions were subsequently focused and declustered by a custom-fabricated electrodynamic ion funnel, and further transmitted through the instrument by an RF-only quadrupole (TOFWERK). Lastly, time of flight mass spectrometry was performed on the transmitted ion bundles at a frequency of 60 MHz, from 5-521 m/z, which were co-summed to 1 Hz. Mass spectral data were analyzed in the TofWare graphic user interface for Igor Pro 7. Ion intensities were normalized to the summed intensity of the water cluster reagent ions similar to other chemical ionization methodologies (Kim et al., 2016; Lavi et al., 2017).

3.4 Results and Discussion

3.4.1 MALDI-IMS analysis of the 7120-HGG interaction

Anabaena sp. PCC 7120 is a filamentous, heterocyst-forming cyanobacteria capable of fixing nitrogen in oxygen-containing environments. Under nitrogen deficient conditions, heterocysts form at semi-regular intervals along the filaments (Kaneko et al., 2001). The heterolobosean amoeba HGG1, isolated from a freshwater pond, has been shown to form plaques on lawns and can reduce the turbidity of liquid cultures of PCC 7120 (Figure 3.6 a-c) (Simkovsky et al., 2012). To examine the metabolic signatures associated with the cyanobacterial prey, the amoebal predator, and the act of grazing when these two organisms mix, 3 spots of PCC 7120 cultured on solid media were challenged with three spots of HGG1, where only the far right spot of PCC 7120 overlapping with the far left spot of HGG1 (Figure 3.1). After 6 days of grazing, the solid cultures were transferred to a MALDI target plate for IMS analysis (Figure 3.1). IMS analysis shows PCC 7120-specific ions that are colony associated (e.g. m/z 519, 527, 566), ions that are

found at the periphery of the colony (e.g. m/z 486), ions that are secreted into the agar outside of the colony (e.g. m/z 560), as well as ions that are both colony-associated and secreted into the agar (e.g. m/z 447, 459, 545, 547, 554). Similarly, ions were observed that were associated specifically with HGG1. The majority of these ions are only found during active amoeba grazing (m/z's 505, 533, 535, 539, 569, 575, 591, 593, 609, 617, 645, 702, 711, and m/z 813), however m/z's 533 and 813 show faint signals at the second and third amoeba spots where inactive or prey-depleted HGG1 reside. We did, however, observe one signal, m/z 1266 found distributed only over the two inactive amoeba spots (Figure 3.1). Interestingly, most of the active HGG1 signals correlate with a loss in signal from the corresponding 7120 spot demonstrating grazing of 7120.

3.4.2 LC-MS/MS and Molecular Networking of 7120-HGG1 Liquid Cultures

While MALDI-IMS allows high-resolution mapping of ion distributions between the interaction of 7120 and HGG1, there is an inherent lack of structural information of the observed metabolites. We used an orthogonal MS approach known as molecular networking housed on Global Natural Products Social Molecular Networking (GNPS) to aid in molecular annotation of the observed signals from IMS analysis (Wang et al., 2016). Molecular networking utilizes tandem mass spectrometry (MS/MS) as a proxy for molecular structure to enable efficient molecular annotation against the GNPS libraries, visualization of molecular space as a network of related compounds, and enables propagation of known chemical features to previously unidentified molecules (Nguyen et al., 2013; Wang et al., 2016; Watrous et al., 2012). Liquid cultures of 7120 were grown in BG-11 and BG-11 N- media for 7 days at 30 °C, shaking at 150 RPM, and continuous low light (75 μE m^{-2} s^{-1}). After 7 days of incubation, HGG1 was inoculated into flasks of 7120 for liquid culture interactions, and the flasks were moved to room temperature and ambient light. After an additional 7 days at ambient temperature and light, cultures of 7120-HGG1 began

to show discoloration and decreased turbidity (Figure 3.6c). The samples were centrifuged, the cell pellet extracted with acetonitrile, and the supernatant extracted with n-butanol for LC-MS/MS and molecular networking analysis. Characteristics of the samples such molecular weight (by way of mass-to-charge ratio), molecules produced under specific media conditions, and organism-specific molecule production were visualized in the network (Figure 3.2a-c). The majority of molecules in this experiment are found from samples of the 7120-HGG1 interaction and with only one molecular family specific to 7120 only (Figure 3.2a). We should note, however, that because HGG1 cannot be cultured in isolation from molecular networking analysis, we cannot distinguish whether molecules that overlap between 7120 samples and 7120-HGG1 samples are produced specifically by solely 7120 or if HGG1 also contributes to the production of these molecules. Additionally, two different molecular networks can be compared to in order to correlate molecules produced in the 7120-HGG1 interaction under standard BG-11 media only (Figure 3.2 a,c).

3.4.3 Identification of the chlorophyll molecular family and grazing specific molecular signatures

We took advantage of the dereplication feature of GNPS, where experimentally derived MS/MS are matched to spectra of annotated and curated MS/MS spectra within the GNPS database. A node of m/z 593 matched to a compound in the GNPS libraries—pheophytin A (chlorophyll A without the Mg^{2+} ion that is commonly lost under acidic conditions)—suggesting that the molecules in this cluster are chlorophyll-like compounds (Figures 3.2a, 3.3). As we investigated this molecular family further, we used pheophytin A as a starting point to propagate its known chemical features to *m/z* 813 and verified that this molecule was pyropheophytin A (pheophytin A having lost its methyl ester). Based on accurate mass measurements, comparison of MS/MS spectra between pheophytin A and pheophorbide A, as well as comparison to reported

chlorophyll breakdown products, we verified that this was indeed the chlorophyll molecular family. (Hortensteiner, 1999; Hörtensteiner et al., 1998; Hörtensteiner and Kräutler, 2011)

Simultaneously, we cross referenced signals observed in IMS to signals observed in molecular network analysis. Several ions specific to HGG1 grazing (*m/z* 535, 593, and 813) were structurally related to members of the chlorophyll molecular family (Figure 3.3). *m/z* 813 showed strong similarity scores to pheophytin A (*m/z* 871). By comparing the MS/MS spectra of pheophytin A to m/z 813, we were able to propose a structure, where the methyl ester has been removed from pheophytin A to give m/z 813 (Figure 3.3). Upon searching this structure in literature and databases, we annotated this molecule as pyropheophytin, however, from MS data alone, we cannot distinguish between the keto- or enol- form of this molecule (Hortensteiner, 1999; Hörtensteiner et al., 1998; Hörtensteiner and Kräutler, 2011). Similarly, pheophorbide A showed a direct connection to m/z 535. Here, we were able to again infer a structure based on comparison of MS/MS spectra between pheophytin A, pyropheophytin (m/z 813), pheophorbide A, and m/z 535. m/z 535 is an HGG1 grazing specific molecule that shows loss of both the methyl ester and lipid chain from pheophytin A, which matches to the structure of pyropheophorbide (Figures 3.2a, 3.3). (Van Boekel, 2008; Hörtensteiner and Kräutler, 2011; Wei et al., 2013) Again, pheophoride A, pyropheophorbide A, and pyropheophytin A are only observed with active HGG1, suggesting that the amoeba breaks down chlorophyll substrates during the grazing process. Lastly, we observed two additional chlorophyll analogs, m/z 829 and 865, that are specific to 7120 and do not appear to be degraded by HGG1. At this time, we have not been able to annotate these m/z's because no structure we have predicted correctly matches the observed mass.

Figure 3.4 shows chlorophyll and its associated breakdown products which are connected through the losses of Mg^{2+}, phytol, and methyl formate moieties. Of these products, pyropheophytin,

pheophorbide, and pyropheophorbide were IMS and LC-MS/MS observed metabolites associated with HGG1 grazing. While grazing-induced dephytlation of chlorophyll, pheophytin, and pyropheophytin have been studied in plants, algae, insects, and marine zooplankton (Badgaa et al., 2014; Guyer et al., 2018; Harradine et al., 1996; Schelbert et al., 2009; Shioi et al., 1996), the observations of these metabolites produced through amoebal grazing on algae is new and shows how these chemicals are processed similarly. Breakdown of chlorophyll by eukaryotes such as amoeba is expected as chlorophyll ingestion risks dietary phototoxicity through singlet oxygen production and must be mitigated (Kashiyama et al., 2019). For breakdown of pheophorbide, pheophytin, and chlorophyll, enzymatic cleavage of the CO_2CH_3 group is less well studied where questions remain as to whether the methyl formate group is cleaved at once, or in multiple steps which lead with demethylation producing methanol followed by decarboxylation (Shioi et al., 1996).

3.4.4 Detection of volatile organic compounds indicative of grazing

The breakdown of chlorophyll to pyropheophorbide through either the pheophytin or pheophorbide pathways predicts the production of phytol and methyl formate as byproducts.Both molecules are known to be volatile at standard room temperature and pressure. We hypothesized that these molecules would be produced and released into the headspace over a solid or liquid culture when under attack by amoeba.

To test this hypothesis, we grew cyanobacteria as either lawns on agar distributed to sealed vials or in media bottles. Over a time course of 7 days for the lawns, samples with or without added amoeba were investigated using SPME-MS for the presence of phytol or methyl formate, as well any other detectable volatile molecular signatures. Methyl formate was not detected by GC/MS in any samples investigated by SPME-GC/MS. We hypothesized a number of possible explanations;

The amoeba may use this molecule as an energy source for its metabolism, the high volatility of methyl formate precluded detection by the SPME-GC/MS method utilized, or methyl formate decomposed to methanol and formic acid. To address the latter 2 hypotheses, an alternative method of headspace analysis using chemical ionization time of flight mass spectrometry (CI-TOFMS) was performed. Protonated water cluster CI-TOFMS, highly similar to H_3O^+-only chemical ionization which can detect methyl formate (Warneke et al., 1996) and methanol, should also be reasonably sensitive and does not require chromatographic separation for analysis. 250mL bottles of agar lawn grown 7942 and 7120, both controls and infected were analyzed daily for the presence of methyl formate. In neither control or grazer-infected samples were changes in the intensity m/z 61, methyl formate detected. In addition, one of the primary hydrolysis product of methyl formate, methanol, was also not observed to change in any significant quantity (Figure 3.9). It cannot be ruled out that the production of either gas was below the detection limits of the CI-TOFMS or microbial consumption of either chemical occurred during grazing. Further work to assess the consumption of methanol and methyl formate by HGG1 is warranted. CI-TOFMS however did detect other molecules, such as an ion at m/z 137, likely a monoterpene species which was found to decrease during the late infection period of 7942 compared to control (Figure 3.9). In contrast to the absence of methyl formate and methanol, changing levels of a phytol-derived metabolite, 2-pentadecanone, 4,6,10 trimethyl- also known as phytol ketone (Moldoveanu, 2019; Rontani and Volkman, 2003) were observed using SPME-GC/MS from grazer-infected 7942. Shown in Figure 3.5, the intensity of phytol ketone released from 7942 lawns was elevated for HGG1 infected cultures at the outset of the experiment on day 1. Over the remainder of the experiment, phytol ketone intensities decreased for grazer-infected S. Elongatus, and by day 7, the uninfected control possessed the highest concentration of phytol ketone. We interpret the gradual increase in phytol

ketone from experiment beginning to end in the control vials as a sign of gradual senescence caused by the sealed nature of the vials which prevents gas exchange necessary for sustained algal growth.

In the HGG1 infected vial on day 1, the accelerated senescence rate caused by grazing temporarily increased the concentration of phytol ketone, however, consumption of this molecule by the grazer in the following days led to lower levels of observed phytol ketone versus the control. Low signal (<1000 counts) of phytol ketone were also observed in 7120 control and grazer infected 7120 vials, however these intensities were not adequate to extract time series information. We observed several other molecular signatures which displayed changes correlated with grazing in both cultures. Shown in Table S5, these molecules reflect multiple classes of organic compounds produced through different metabolic pathways and are potential targets for the identification of grazers using VOCs. Some VOCs were observed to decrease in intensity in response to grazing while others increased, sometimes in cases where none of the same VOC was measurable in the control vials (Table S5). Similar to work by others, we found carotenoid breakdown products, specifically β-ionone and β-cyclocitral, to be distinctly elevated in grazer-infected 7942, but not 7120 (Figure 3.8)(Reese et al., 2019). Notably, these gases were still observed to increase in uninfected 7942 controls, likely due to natural senescence. Given these VOCs seem to be produced from multiple processes, further research into their ability to specifically indicate state of health from grazing should be further investigated.

3.5 Conclusion

Investigations of spatially resolved metabolites specifically associated with healthy cyanobacteria and grazer-infected cyanobacteria by IMS yielded the ability to connect production of metabolites with presence of grazing. By leveraging molecular networking of matching liquid samples run on LC-MS/MS, chemical identities and relationships between the IMS-observed

chemicals were determined to show how chlorophyll breakdown products can be used as chemical indicators of grazing. A challenge of solid-phase IMS is the lack of time resolution where analysis captures a snapshot of metabolites produced during the grazing process. Variations in concentration of these metabolites is influenced by the metabolic activity of the algae and grazers, as well as natural degradation and oxidation processes of the metabolites. This is further complicated by aspects of the IMS analysis which obtains chemical information both from intra and extracellular matrices simultaneously. These limitations make it challenging to assess whether metabolites indicative of grazing are robust indicators throughout the grazing process. Further study of algae-grazer interactions by IMS with particular attention to the timescale of the process is warranted.

Molecular networking information was utilized to build a chemical breakdown pathway for algal chlorophyll a caused by grazing. Informed by this pathway, an investigation of gas phase species produced by grazer-infected cyanobacteria was undertaken to look for methyl formate and phytol. While neither species was observed in their intact forms, intensities of phytol ketone were observed to change for LPG and HGG infected 7942. Changes in phytol ketone intensity over the experiment duration were not especially straightforward and reflect the complexities of metabolic processing by grazers as algae cells are being simultaneously distressed and damaged. Failure to detect VOCs predicted by IMS and LC-MS/MS is not necessarily surprising considering that grazers are likely interested in consuming the chemical moieties clipped from the chlorophyll a scaffold. Subsequently, this combined analysis infers that IMS, LC-MS/MS, and GC/MS may also be useful tools to explore the chemical targets that grazers seek for energy and are capable of metabolizing effectively. Lastly, the dynamics of β-cyclocitral and β-ionone (Figure 3.8) show that the production of these chemicals by 7942 under healthy conditions can be further enhanced by

natural senescence. While addition of grazers did produce higher intensities of both VOCs, it should be noted that the usage of these chemicals may be somewhat nonspecific to grazing and the thresholds used for detection of grazing will require further refinement.

As energy demands increase and the world's oil reserves diminish, and the negative impact of burning fossil fuels results in accumulation of greenhouse gasses and climate change, new energy sources need to be developed. Solar, wind, and hydroelectric energy production are all promising sources of alternative energy and are continually being developed, but each form is not without drawbacks Green alternatives of electricity production will hopefully replace fossil fuel electricity production someday, but there may always be a need for high energy density fuels for transportation. Algae biofuels can serve as a renewable and carbon-neutral drop-in alternative to current transportation fuels without major changes in infrastructure, but still encounter many challenges such as contamination of open pond production systems. Here we demonstrate MS methods are capable of detecting and identifying grazing specific signals from both solid, liquid, and gas phases of interactions of cyanobacteria and protozoan grazers. Currently, it is not uncommon for MS equipment to analyze the quality and composition of fuel mixtures. We foresee that existing MS instrumentation could also be adapted for the detection of biological contaminants. Additionally, with a properly curated reference library, MS could be used to type contaminants based on the detection of specific metabolites thereby allowing tailored interventive measures. Even now, MS instrumentation and methods are being developed and large equipment is being miniaturized which could aid open pond live monitoring or remote site sampling.

Ultimately, we believe that the methodology presented here can already be applied for use in algae biofuels and with further refinement can be shaped into a simple, quick, and routine assay. Such developments will help overcome the pitfalls currently faced by contamination of large-scale

open pond algae production and will ultimately aid in making algae biofuels a more economically viable alternative energy.

3.6 Acknowledgements

This material is based upon work supported by the Department of Energy, Grant No: DE-EE0007094. The University of California San Diego Frontiers of Innovation Scholars Program (UC-FISP) is also acknowledged for the funding contributions to Don Nguyen.

Chapter 3, in full, is currently being prepared for submission for publication of the material. Nguyen, D.D., Sauer, J.S., Camarda, L.P., Sherman, S., Prather, K.A., Golden, S.S., Pomeroy, R., Dorrestein, P.C., Simkovsky, R. (2020), "Multi-scale Examination of Grazer-Induced Changes in Molecular Signatures of Cyanobacteria" Dr. Don G. Nguyen and the dissertation author are co-first authors of this manuscript.

3.7 Figures

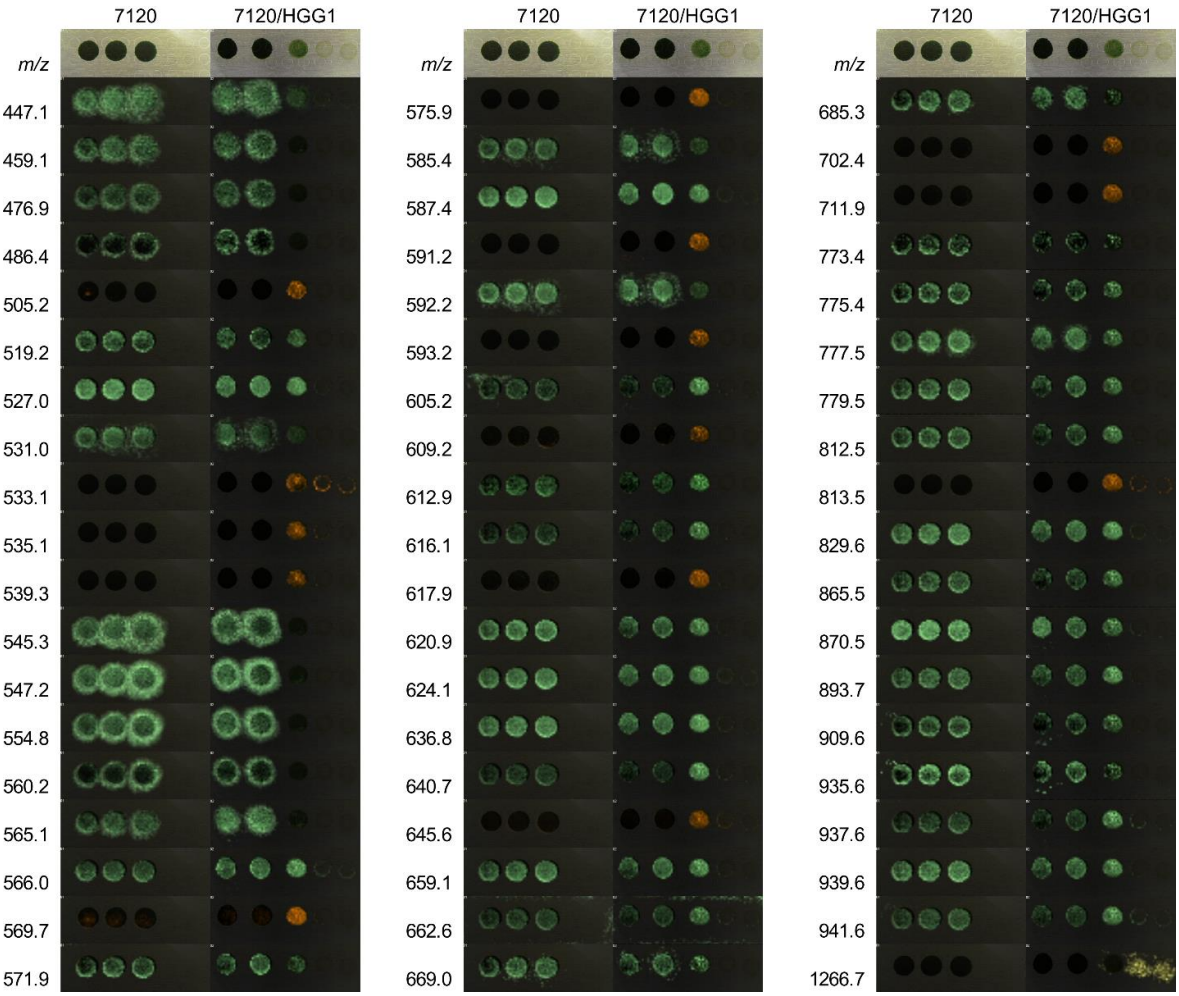

Figure 3.1 MALDI-IMS of 7120-HGG1 interaction. In each column, from left to right, we have the observed m/z, 7120 control, and 7120-HGG1 interaction. Green ions show 7120 specific signals. Orange ions show HGG1 specific signals primarily from actively grazing amoeba. The yellow ion is the only observed HGG1 from inactive amoeba.

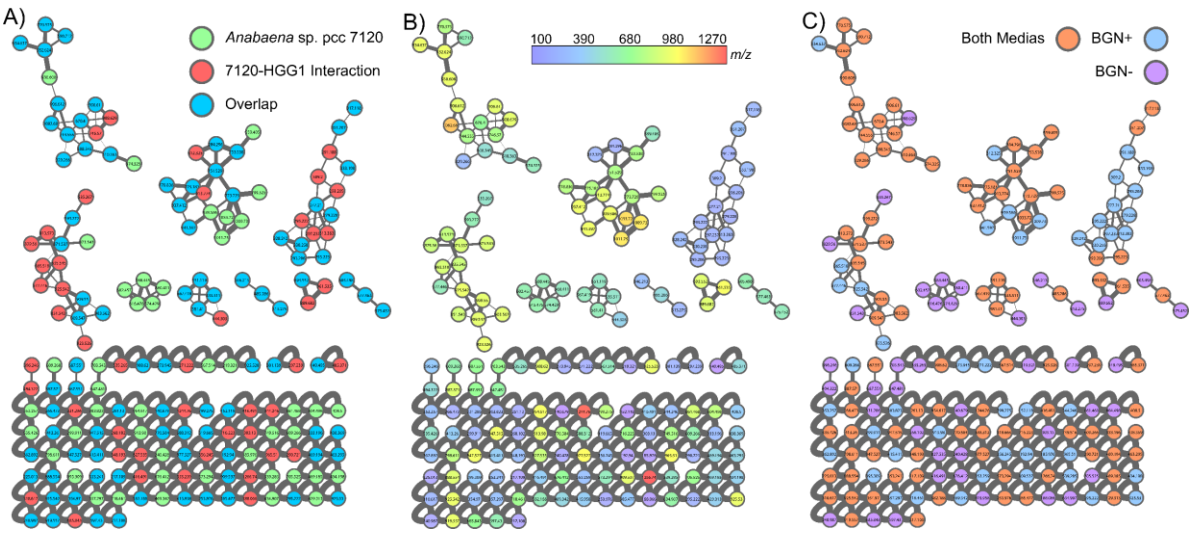

Figure 3.2 Molecular networks of a) 7120-HGG1 liquid culture interactions. Node colors represent molecules from the 7120 control (green nodes), the 7120-HGG1 interaction (red nodes), or molecules that overlap between both cultures (blue nodes). Grey highlight signifies the location of the chlorophyll molecular family. b) Molecular network of 7120-HGG1 liquid culture interactions by mass, node colors represent the mass range of the observed molecules. c) Molecular network of 7120-HGG1 liquid culture interactions by media condition Blue; molecules produced under normal BG-11 media, Purple; molecules produced under BG-11 N- media, Orange; molecules produced under both media conditions.

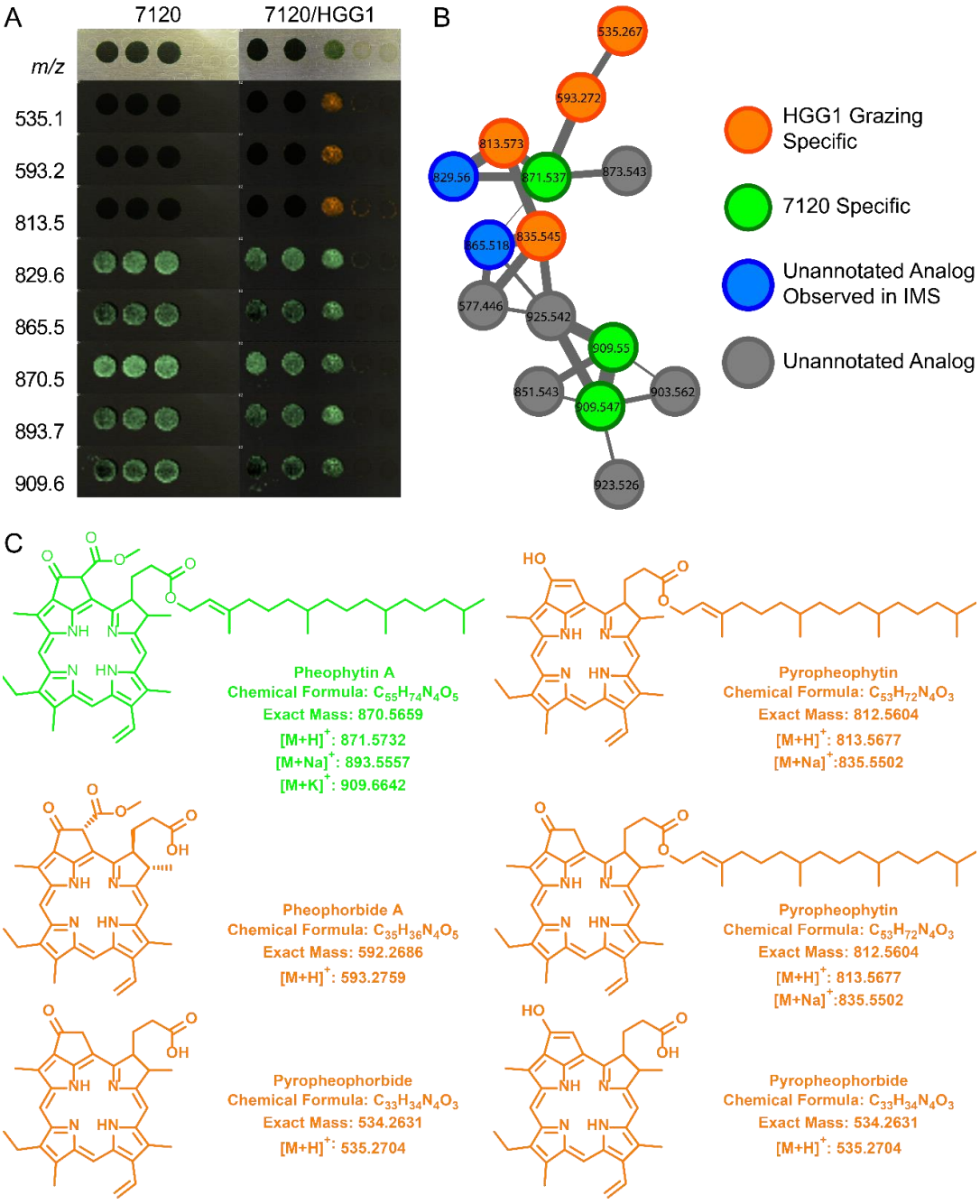

Figure 3.3 Annotation of chlorophyll molecular family by IMS and molecular networking. A) IMS of chlorophyll molecular family. B) Chlorophyll molecular families observed by molecular networking. Orange nodes; HGG1 grazing specific signals. Green nodes; 7120 specific signals. Blue; unannotated analogs within the chlorophyll molecular family observed in IMS. Grey; unannotated analogs within the chlorophyll molecular family.

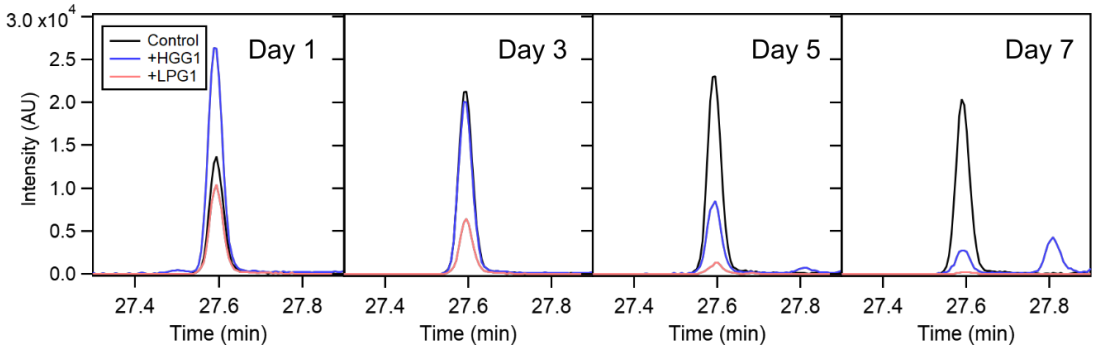

Figure 3.4 GC/MS extracted ion chromatograms of m/z 109 for SPME analyzed cultures of 7942 control (Black), 7942 with HGG1 grazer (Blue), and 7942 with LPG1 infected (Red). m/z 109 intensity at 27.6 minutes corresponds to the molecular assignment of 2-pentadecanone, 4,6,10 trimethyl- (phytol ketone)

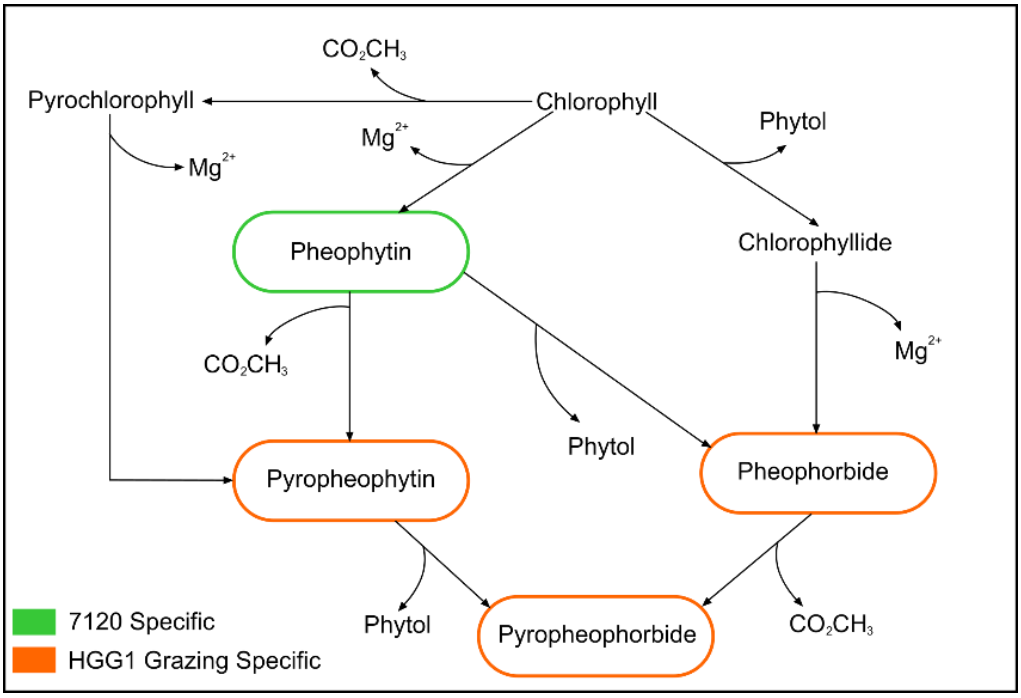

Figure 3.5 Chlorophyll and associated breakdown products connected by loss of molecular moieties. Compounds outlined in color are associated with species observed by LC-MS and IMS analyses.

3.8 Supplementary figures

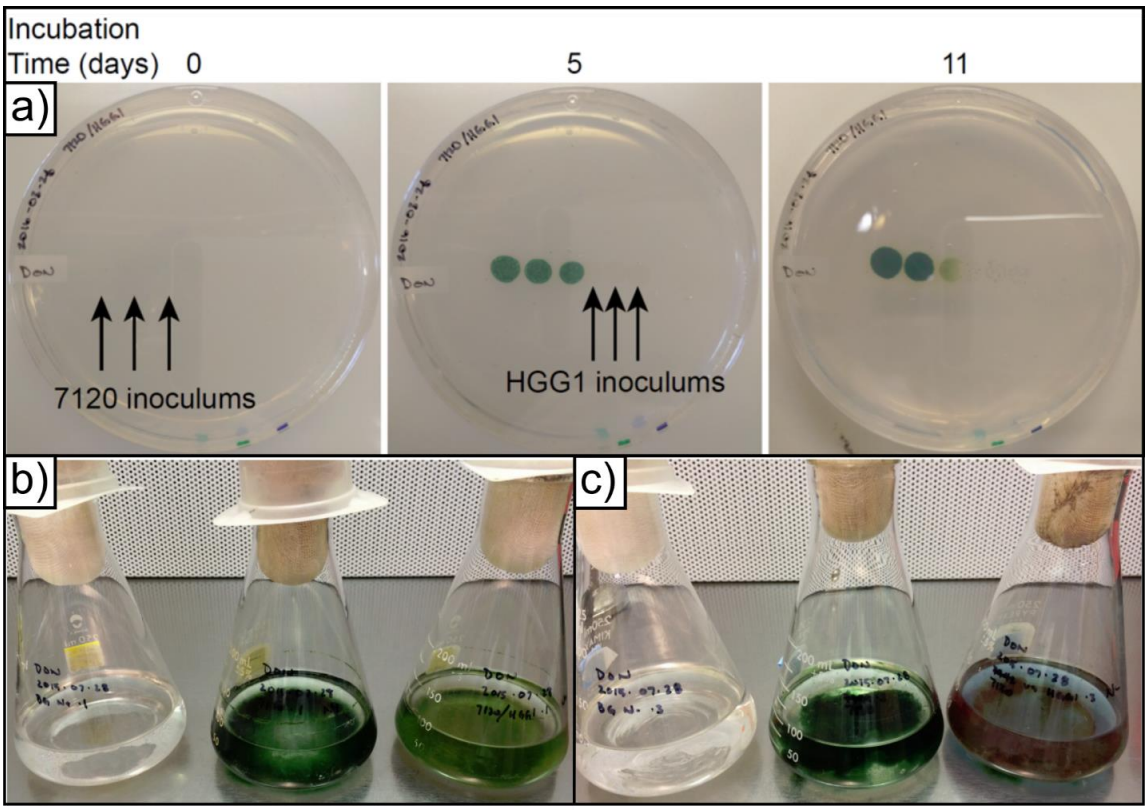

Figure 3.6 a) Time course photos of 7120 and HGG1 interaction over 11 days total. 7120 was inoculated at timepoint 0 and allowed to grow. After 5 days of incubation, 3 spots of HGG1 were spotted adjacent to 7120. At time point 11, the first spot of 7120 is almost entirely consumed. Photos of liquid cultures of 7120 and HGG1 after 14 days. b) Interaction of 7120 and HGG1 in BG-11 liquid media. Left: BG-11 liquid media control. Middle: culture. Right: 7120-HGG1 interaction. HGG1 was inoculated at day 7. With enough time the 7120-HGG1 interaction in standard BG-11 media also begins to show a blue hue in the media supernatant as is demonstrated in BG-11 N- media. c) Interaction of 7120 and HGG1 in BG-11 N- liquid media. Left: BG-11 N- media control. Middle: 7120 culture. Right 7120-HGG1 interaction. HGG1 was inoculated at day 7.

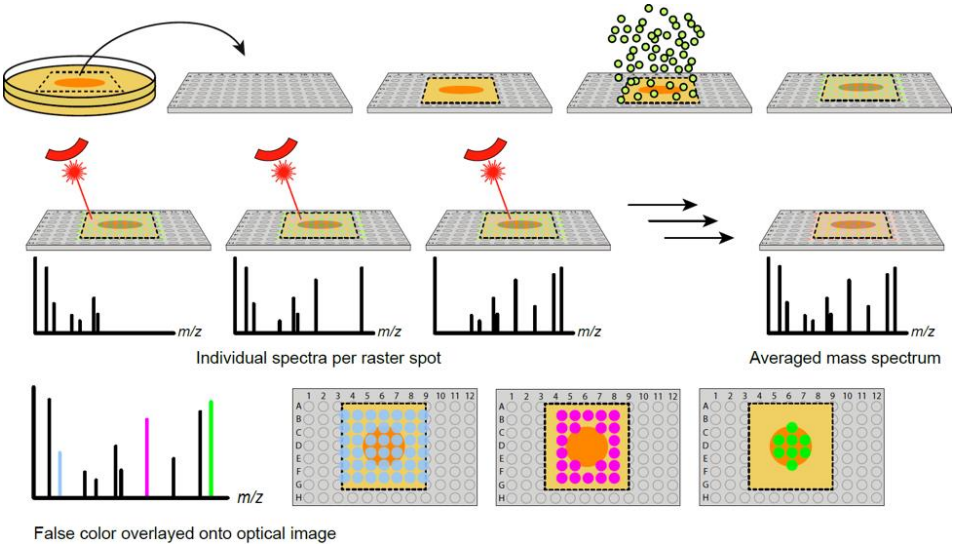

Figure 3.7 MALDI-IMS workflow. A sample grown on agar is transferred to a MALDI target plate, coated with matrix, dehydrated, and measured over a predefined raster region. Individual mass spectra are collected at each pixel and are then averaged together. Ions are given a false color which is then overlaid on top of an optical image of the sample and target plate, showing the distribution of that particular ion.

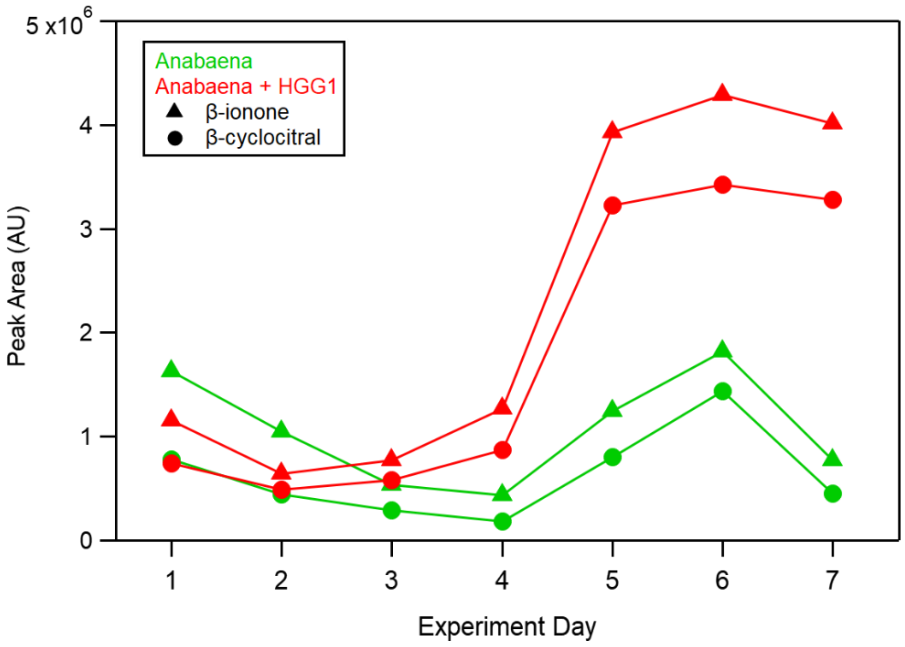

Figure 3.8 GC/MS integrated peak areas for β-cyclocitral and β-ionone across the vial experiment for control anabaena (Green) and HGG1 infected anabaena (Red)

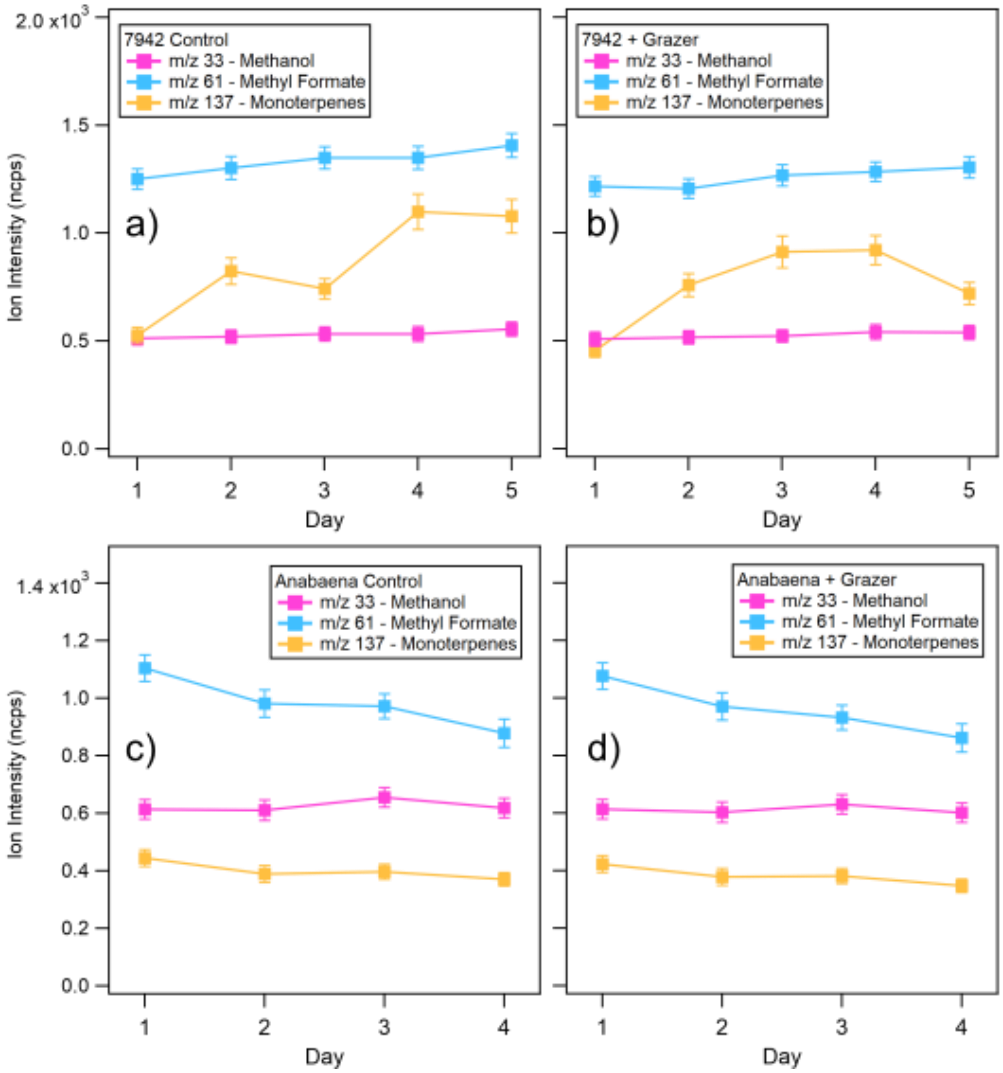

Figure 3.9 CI-TOFMS daily averaged intensities for select VOCs in a) S. Elongatus controls, b) S. Elongatus infected with LPG1 c) Anabaena control, d) Anabaena infected with LPG1. Error bars reflect +/- 1σ of ion signal acquired over 5 minutes during each day of sampling.

3.9 Supplementary tables

Table 3.1 NIST 14 Library matched ions detected from SPME-GC/MS analyses of HGG1 infected anabaena and S. Elongatus. Match % values were calculated by averaging forward and reverse NIST scores for IDs. Area ratios were determined by dividing the peak area obtained from the control by the same peak in the HGG1 infected vial on day 5 of the experiment. Values of UDF indicate periods when the intensity of a peak was below detection limit in the control, but present in the HGG1 infected vial. The value in parentheses indicates the intensity of the peak in the infected vial to illustrate the intensity of response.

Compound	Name	Area Ratio	m/z	NIST Match %	Compound Class
1	3,4 Dimethylcyclohexanol	0.302795	128	80	Cyclohexanol
2	Neophytadiene	0.699937	267	70	Alkene
3	β-cyclocitral	UDF (8E5)	152	80	Carotenoid
4	Butylated Hydroxytoluene	2.84291	220	86	Phenol Derivative
5	Z-1,9-Hexadecadiene	0.7193	180	78	Alkene
6	Trans β-ionone	UDF (3E6)	192	91	Carotenoid
7	Nonadecane	UDF (8E5)	268	94	Alkane
8	1-Pentadecene	0.124273	210	94	Alkene
9	Pentadecane	0.584325	212	94	Alkane
10	z-6-Pentadecen-1-ol	UDF (4E6)	212	80	Aliphatic Alcohol
11	8-Heptadecene	UDF (5E6)	238	91	Alkene
12	5-Octadecene, (E)	UDF (3E7)	252	91	Alkene
13	Icosane	0.567099	282	91	Alkane
14	2-Pentadecanone, 4,6,10 trimethyl-	2.86466	268	76	Aliphatic Ketone

3.10 References

Achyuthan, K. E., Harper, J. C., Manginell, R. P. and Moorman, M. W.: Volatile metabolites emission by in vivo microalgae—an overlooked opportunity?, Metabolites, 7(3), doi:10.3390/metabo7030039, 2017.

Aljawhary, D., Lee, A. K. Y. and Abbatt, J. P. D.: High-resolution chemical ionization mass spectrometry (ToF-CIMS): Application to study SOA composition and processing, Atmos. Meas. Tech., 6(11), 3211–3224, doi:10.5194/amt-6-3211-2013, 2013.

Allen, M. M.: Simple conditions for growth of unicellular blue-green algae on plates, J. Phycol., doi:10.1111/j.1529-8817.1968.tb04667.x, 1968.

Badgaa, A., Jia, A., Ploss, K. and Boland, W.: Chlorophyll Degradation in the Gut of Generalist and Specialist Lepidopteran Caterpillars, J. Chem. Ecol., 40(11–12), 1232–1240, doi:10.1007/s10886-014-0523-0, 2014.

Bertram, T. H., Kimmel, J. R., Crisp, T. A., Ryder, O. S., Yatavelli, R. L. N., Thornton, J. A., Cubison, M. J., Gonin, M. and Worsnop, D. R.: A field-deployable, chemical ionization time-of-flight mass spectrometer, Atmos. Meas. Tech., 4(7), 1471–1479, doi:10.5194/amt-4-1471-2011, 2011.

Van Boekel, M. A. J. S.: Kinetic modeling of food quality: A critical review, Compr. Rev. Food Sci. Food Saf., 7(1), 144–158, doi:10.1111/j.1541-4337.2007.00036.x, 2008.

BP: BP Energy Outlook - 2016 edition - Focus on North America, [online] Available from: www.bp.com/energyoutlook., 2016.

Burkart, M. D. and Mayfield, S. P.: Biofuels for the 21st century, Curr. Opin. Chem. Biol., 17(3), 436–438, doi:10.1016/j.cbpa.2013.05.003, 2013.

Di Caprio, F.: Methods to quantify biological contaminants in microalgae cultures, Algal Res., 49(March), 101943, doi:10.1016/j.algal.2020.101943, 2020.

Deore, P., Beardall, J. and Noronha, S.: A perspective on the current status of approaches for early detection of microalgal grazing, J. Appl. Phycol., doi:10.1007/s10811-020-02241-x, 2020.

Dryden, R. C. and Wright, S. J. L.: Predation of cyanobacteria by protozoa, Can. J. Microbiol., 33(6), 471–482, doi:10.1139/m87-080, 1987.

Fisher, C. L., Lane, P. D., Russell, M., Maddalena, R. and Lane, T. W.: Low molecular weight volatile organic compounds indicate grazing by the marine rotifer brachionus plicatilis on the microalgae microchloropsis salina, Metabolites, 10(9), 1–20, doi:10.3390/metabo10090361, 2020.

Ghadiryanfar, M., Rosentrater, K. A., Keyhani, A. and Omid, M.: A review of macroalgae production, with potential applications in biofuels and bioenergy, Renew. Sustain. Energy Rev., 54, 473–481, doi:10.1016/j.rser.2015.10.022, 2016.

Goulitquer, S., Potin, P. and Tonon, T.: Mass spectrometry-based metabolomics to elucidate functions in marine organisms and ecosystems., 2012.

Gupta, P. L., Lee, S. M. and Choi, H. J.: A mini review: photobioreactors for large scale algal cultivation, World J. Microbiol. Biotechnol., 31(9), 1409–1417, doi:10.1007/s11274-015-1892-4, 2015.

Guyer, L., Salinger, K., Krügel, U. and Hörtensteiner, S.: Catalytic and structural properties of pheophytinase, the phytol esterase involved in chlorophyll breakdown, J. Exp. Bot., 69(4), 879–889, doi:10.1093/jxb/erx326, 2018.

Harradine, P. J., Harris, P. G., Head, R. N., Harris, R. P. and Maxwell, J. R.: Steryl chlorin esters are formed by zooplankton herbivory, Geochim. Cosmochim. Acta, 60(12), 2265–2270, doi:10.1016/0016-7037(96)00132-9, 1996.

Hoh, D., Watson, S. and Kan, E.: Algal biofilm reactors for integrated wastewater treatment and biofuel production: A review, Chem. Eng. J., 287, 466–473, doi:10.1016/j.cej.2015.11.062, 2016.

Hortensteiner, S.: Chlorophyll breakdown in higher plants and algae, Cell. Mol. Life Sci., 56, 330–347, doi:https://doi.org/10.1007/s000180050434, 1999.

Hörtensteiner, S. and Kräutler, B.: Chlorophyll breakdown in higher plants, Biochim. Biophys. Acta - Bioenerg., 1807(8), 977–988, doi:10.1016/j.bbabio.2010.12.007, 2011.

Hörtensteiner, S., Wüthrich, K. L., Matile, P., Ongania, K. H. and Kräutler, B.: The key step in chlorophyll breakdown in higher plants. Cleavage of pheophorbide a macrocycle by a monooxygenase, J. Biol. Chem., 273(25), 15335–15339, doi:10.1074/jbc.273.25.15335, 1998.

Jones, C. S. and Mayfield, S. P.: Algae biofuels: Versatility for the future of bioenergy, Curr. Opin. Biotechnol., 23(3), 346–351, doi:10.1016/j.copbio.2011.10.013, 2012.

Kaneko, T., Nakamura, Y., Wolk, C. P., Kuritz, T., Sasamoto, S., Watanabe, A., Iriguchi, M., Ishikawa, A., Kawashima, K., Kimura, T., Kishida, Y., Kohara, M., Matsumoto, M., Matsuno, A., Muraki, A., Nakazaki, N., Shimpo, S., Sugimoto, M., Takazawa, M., Yamada, M., Yasuda, M. and Tabata, S.: Complete genomic sequence of the filamentous nitrogen-fixing cyanobacterium Anabaena sp. Strain PCC 7120, DNA Res., 8(5), 205–213, doi:10.1093/dnares/8.5.205, 2001.

Kashiyama, Y., Yokoyama, A., Shiratori, T., Hess, S., Not, F., Bachy, C., Gutierrez-Rodriguez, A., Kawahara, J., Suzaki, T., Nakazawa, M., Ishikawa, T., Maruyama, M., Wang, M.,

Chen, M., Gong, Y., Seto, K., Kagami, M., Hamamoto, Y., Honda, D., Umetani, T., Shihongi, A., Kayama, M., Matsuda, T., Taira, J., Yabuki, A., Tsuchiya, M., Hirakawa, Y., Kawaguchi, A., Nomura, M., Nakamura, A., Namba, N., Matsumoto, M., Tanaka, T., Yoshino, T., Higuchi, R., Yamamoto, A., Maruyama, T., Yamaguchi, A., Uzuka, A., Miyagishima, S., Tanifuji, G., Kawachi, M., Kinoshita, Y. and Tamiaki, H.: Taming chlorophylls by early eukaryotes underpinned algal interactions and the diversification of the eukaryotes on the oxygenated Earth, ISME J., 13(8), 1899–1910, doi:10.1038/s41396-019-0377-0, 2019.

Kim, M. J., Zoerb, M. C., Campbell, N. R., Zimmermann, K. J., Blomquist, B. W., Huebert, B. J. and Bertram, T. H.: Revisiting benzene cluster cations for the chemical ionization of dimethyl sulfide and select volatile organic compounds, Atmos. Meas. Tech., 9(4), 1473–1484, doi:10.5194/amt-9-1473-2016, 2016.

Kumar, K., Mishra, S. K., Shrivastav, A., Park, M. S. and Yang, J. W.: Recent trends in the mass cultivation of algae in raceway ponds, Renew. Sustain. Energy Rev., 51, 875–885, doi:10.1016/j.rser.2015.06.033, 2015.

Lavi, A., Vermeuel, M. P., Novak, G. A. and Bertram, T. H.: The sensitivity of benzene cluster cation chemical ionization mass spectrometry to select biogenic terpenes, Atmos. Meas. Tech. Discuss., 3251–3262, doi:10.5194/amt-2017-408, 2017.

Ma, A. T., Daniels, E. F., Gulizia, N. and Brahamsha, B.: Isolation of diverse amoebal grazers of freshwater cyanobacteria for the development of model systems to study predator-prey interactions, Algal Res., 13(1), 85–93, doi:10.1016/j.algal.2015.11.010, 2016.

Moldoveanu, S. C.: Pyrolysis of Alcohols and Phenols., 2019.

Montagna, P. A.: Rates of metazoan meiofaunal microbivory: a review, Vie Milieu, 45(1), 1–9, 1995.

Nguyen, D. D., Wu, C. H., Moree, W. J., Lamsa, A., Medema, M. H., Zhao, X., Gavilan, R. G., Aparicio, M., Atencio, L., Jackson, C., Ballesteros, J., Sanchez, J., Watrous, J. D., Phelan, V. V., Van De Wiel, C., Kersten, R. D., Mehnaz, S., De Mot, R., Shank, E. A., Charusanti, P., Nagarajan, H., Duggan, B. M., Moore, B. S., Bandeira, N., Palsson, B., Pogliano, K., Gutieŕrez, M. and Dorrestein, P. C.: MS/MS networking guided analysis of molecule and gene cluster families, Proc. Natl. Acad. Sci. U. S. A., 110(28), doi:10.1073/pnas.1303471110, 2013.

Reese, K. L., Fisher, C. L., Lane, P. D., Jaryenneh, J. D., Moorman, M. W., Jones, A. D., Frank, M. and Lane, T. W.: Chemical Profiling of Volatile Organic Compounds in the Headspace of Algal Cultures as Early Biomarkers of Algal Pond Crashes, Sci. Rep., 9(1), 1–10, doi:10.1038/s41598-019-50125-z, 2019.

Review, B. P. S. and June, W. E.: BP Statistical Review of World Energy, , (June), 2015.

Richardson, J. W., Johnson, M. D., Zhang, X., Zemke, P., Chen, W. and Hu, Q.: A financial assessment of two alternative cultivation systems and their contributions to algae biofuel economic viability, Algal Res., 4(1), 96–104, doi:10.1016/j.algal.2013.12.003, 2014.

Rontani, J.-F. and Volkman, J. K.: Phytol degredation products as biogeochemical tracers in aquatic environments, , 34, 1–35, 2003.

Ryan, C. G., Clayton, E., Griffin, W. L., Sie, S. H. and Cousens, D. R.: SNIP, a statistics-sensitive background treatment for the quantitative analysis of PIXE spectra in geoscience applications, Nucl. Inst. Methods Phys. Res. B, 34(3), 396–402, doi:10.1016/0168-583X(88)90063-8, 1988.

Schelbert, S., Aubry, S., Burla, B., Agne, B., Kessler, F., Krupinska, K. and Hörtensteiner, S.: Pheophytin pheophorbide hydrolase (pheophytinase) is involved in chlorophyll breakdown during Leaf senescence in Arabidopsis, Plant Cell, 21(3), 767–785, doi:10.1105/tpc.108.064089, 2009.

Schoepp, N. G., Wong, W., Mayfield, S. P. and Burkart, M. D.: Bulk solvent extraction of biomass slurries using a lipid trap, RSC Adv., 5(70), 57038–57044, doi:10.1039/c5ra11444f, 2015.

Scranton, M. A., Ostrand, J. T., Fields, F. J. and Mayfield, S. P.: Chlamydomonas as a model for biofuels and bio-products production, , 82(3), 523–531, doi:10.1111/tpj.12780, 2015.

Shioi, Y., Watanabe, K. and Takamiya, K. I.: Enzymatic conversion of pheophorbide a to the precursor of pyropheophorbide a in leaves of Chenopodium album, Plant Cell Physiol., 37(8), 1143–1149, doi:10.1093/oxfordjournals.pcp.a029065, 1996.

Simkovsky, R., Daniels, E. F., Tang, K., Huynh, S. C., Golden, S. S. and Brahamsha, B.: Impairment of O-antigen production confers resistance to grazing in a model amoeba-cyanobacterium predator-prey system, Proc. Natl. Acad. Sci. U. S. A., 109(41), 16678–16683, doi:10.1073/pnas.1214904109, 2012.

Stasulli, N. M. and Shank, E. A.: Profiling the metabolic signals involved in chemical communication between microbes using imaging mass spectrometry, FEMS Microbiol. Rev., 40(6), 807–813, doi:10.1093/femsre/fuw032, 2016.

Taton, A., Unglaub, F., Wright, N. E., Zeng, W. Y., Paz-Yepes, J., Brahamsha, B., Palenik, B., Peterson, T. C., Haerizadeh, F., Golden, S. S. and Golden, J. W.: Broad-host-range vector system for synthetic biology and biotechnology in cyanobacteria, Nucleic Acids Res., doi:10.1093/nar/gku673, 2014.

Tillmann, U. and John, U.: Toxic effects of Alexandrium spp. on heterotrophic dinoflagellates: An allelochemical defence mechanism independent of PSP-toxin content, Mar. Ecol. Prog. Ser., 230(1999), 47–58, doi:10.3354/meps230047, 2002.

Wang, M., Carver, J. J., Phelan, V. V., Sanchez, L. M., Garg, N., Peng, Y., Nguyen, D. D., Watrous, J., Kapono, C. A., Luzzatto-Knaan, T., Porto, C., Bouslimani, A., Melnik, A. V., Meehan, M. J., Liu, W. T., Crüsemann, M., Boudreau, P. D., Esquenazi, E., Sandoval-Calderón, M., Kersten, R. D., Pace, L. A., Quinn, R. A., Duncan, K. R., Hsu, C. C., Floros, D. J., Gavilan, R. G., Kleigrewe, K., Northen, T., Dutton, R. J., Parrot, D., Carlson, E. E., Aigle, B., Michelsen, C. F., Jelsbak, L., Sohlenkamp, C., Pevzner, P., Edlund, A., McLean, J., Piel, J., Murphy, B. T., Gerwick, L., Liaw, C. C., Yang, Y. L., Humpf, H. U., Maansson, M., Keyzers, R. A., Sims, A. C., Johnson, A. R., Sidebottom, A. M., Sedio, B. E., Klitgaard, A., Larson, C. B., Boya, C. A. P., Torres-Mendoza, D., Gonzalez, D. J., Silva, D. B., Marques, L. M., Demarque, D. P., Pociute, E., O'Neill, E. C., Briand, E., Helfrich, E. J. N., Granatosky, E. A., Glukhov, E., Ryffel, F., Houson, H., Mohimani, H., Kharbush, J. J., Zeng, Y., Vorholt, J. A., Kurita, K. L., Charusanti, P., McPhail, K. L., Nielsen, K. F., Vuong, L., Elfeki, M., Traxler, M. F., Engene, N., Koyama, N., Vining, O. B., Baric, R., Silva, R. R., Mascuch, S. J., Tomasi, S., Jenkins, S., Macherla, V., Hoffman, T., Agarwal, V., Williams, P. G., Dai, J., Neupane, R., Gurr, J., Rodríguez, A. M. C., Lamsa, A., Zhang, C., Dorrestein, K., Duggan, B. M., Almaliti, J., Allard, P. M., et al.: Sharing and community curation of mass spectrometry data with Global Natural Products Social Molecular Networking, Nat. Biotechnol., 34(8), 828–837, doi:10.1038/nbt.3597, 2016.

Warneke, C., Kuczynski, J., Hansel, A., Jordan, A., Vogel, W. and Lindinger, W.: Proton transfer reaction mass spectrometry (PTR-MS): Propanol in human breath, Int. J. Mass Spectrom. Ion Process., 154(1–2), 61–70, doi:10.1016/0168-1176(96)04369-8, 1996.

Watrous, J., Roach, P., Alexandrov, T., Heath, B. S., Yang, J. Y., Kersten, R. D., Van Der Voort, M., Pogliano, K., Gross, H., Raaijmakers, J. M., Moore, B. S., Laskin, J., Bandeira, N. and Dorrestein, P. C.: Mass spectral molecular networking of living microbial colonies, Proc. Natl. Acad. Sci. U. S. A., 109(26), 1743–1752, doi:10.1073/pnas.1203689109, 2012.

Wei, J., Li, H., Barrow, M. P. and O'Connor, P. B.: Structural characterization of chlorophyll-a by high resolution tandem mass spectrometry, J. Am. Soc. Mass Spectrom., 24(5), 753–760, doi:10.1007/s13361-013-0577-1, 2013.

Wenig, P. and Odermatt, J.: OpenChrom: A cross-platform open source software for the mass spectrometric analysis of chromatographic data, BMC Bioinformatics, 11, doi:10.1186/1471-2105-11-405, 2010.

Van Wichelen, J., van Gremberghe, I., Vanormelingen, P., Debeer, A. E., Leporcq, B., Menzel, D., Codd, G. A., Descy, J. P. and Vyverman, W.: Strong effects of amoebae grazing on the biomass and genetic structure of a Microcystis bloom (Cyanobacteria), Environ. Microbiol., 12(10), 2797–2813, doi:10.1111/j.1462-2920.2010.02249.x, 2010.

Willette, S., Gill, S. S., Dungan, B., Schaub, T. M., Jarvis, J. M., St. Hilaire, R. and Omar Holguin, F.: Alterations in lipidome and metabolome profiles of Nannochloropsis salina in response to reduced culture temperature during sinusoidal temperature and light, Algal Res., 32(March), 79–92, doi:10.1016/j.algal.2018.03.001, 2018.

Yang, J. Y., Phelan, V. V., Simkovsky, R., Watrous, J. D., Trial, R. M., Fleming, T. C., Wenter, R., Moore, B. S., Golden, S. S., Pogliano, K. and Dorrestein, P. C.: Primer on Agar-Based Microbial Imaging Mass Spectrometry, J. Bacteriol., 194(22), 6023–6028, doi:10.1128/JB.00823-12, 2012.

Yang, Y.-L., Xu, Y., Straight, P., Dorrestein, P. C., Chem, N. and Author, B.: Translating metabolic exchange with imaging mass spectrometry HHS Public Access Author manuscript, Nat Chem Biol, 5(12), 885–887, doi:10.1038/nchembio.252, 2009.

You, J., Mallery, K., Mashek, D. G., Sanders, M., Hong, J. and Hondzo, M.: Microalgal swimming signatures and neutral lipids production across growth phases, Biotechnol. Bioeng., 117(4), 970–980, doi:10.1002/bit.27271, 2020.

Chapter 4. Early Detection of Algal Grazing with Rapid, Continuous Measurements of Volatile Gases

4.1 Abstract

Algae cultivation in outdoor open raceway ponds is considered the most economically viable method for photosynthetically producing high yields of biomass for biofuels, chemical feedstocks, and other high value products. Unfortunately, one of the primary challenges for open ponds is the loss of biomass due to grazers, competitors, and infectious organisms. Grazer infections can rapidly eliminate biomass in short timescales (~48 hours) where higher frequency observations than typically employed in the field would be well suited for the detection of such catastrophic contamination. We applied chemical ionization mass spectrometry (CIMS) for the simultaneous real-time monitoring of multiple cyanobacterial cultures before and after grazer infections. Numerous volatile gases were produced from freshwater *Synechococcus elongatus* PCC 7942 during healthy growth periods. After the introduction of a field-isolated ciliate grazer, a *Tetrahymena*, changes in multiple volatile species were identified from the infected media after a latent period, with definitive diagnoses within 18 hours at grazer concentrations below the detection limits of microscopy (1 mL^{-1}). Grazing detection by CI-TOFMS was significantly faster than both microscopy and continuous fluorescence, which detected significant changes 37-76 hours later. CIMS analysis of PCC 7942 VOCs identified biomass-dependent rates of VOC loss and production, which adds new biological complexity towards the goal of using VOC analysis as a diagnostic for grazer detection.

4.2 Introduction

Microalgae are prokaryotic or eukaryotic photosynthetic organisms that can grow rapidly in varied conditions at large scales. Their efficiency in producing large amounts of biomass in

small areas with few added resources, as compared to terrestrial crops such as corn or soybeans, makes them a promising, sustainable platform for bioproduction of fuels or industrial products. In addition to most sought-after product, biodiesel, microalgae can also be utilized for production of other valuable fine chemicals such as dyes, cosmetics, pharmaceuticals, and food additives (Carney and Lane, 2014; Christaki et al., 2013; Schoepp et al., 2015). Alternatively, microalgae can also be use in tandem with other industrial processes such as removal of dissolved nutrients from wastewater and CO_2 removal from flue gases or the atmosphere (Kroumov et al., 2016; Molazadeh et al., 2019). Algal research to date has focused extensively on improvements in crop productivity, including strain selection, nutrient control, and management of physiochemical parameters (pH, temperature, etc.). Towards this goal, many cultivators use high volume open raceway ponds (ORPs) as opposed to more expensive laboratory-style photobioreactors (PBRs) (Klein-Marcuschamer et al., 2013). While the cost of algal biomass from ORPs is approximately an order of magnitude lower than PBRs, a key disadvantage is the elevated risk from contamination by unwanted grazers, such as ciliates and rotifers (Mata et al., 2010). Recent estimates of commercial monocultures in ORPs have found grazer-initiated crop failures reduce 10-30% of produced biomass resulting in losses in the tens of millions of dollars (Richardson et al., 2014). Part of the challenge posed by grazer contamination involves their ability to rapidly eradicate a microalgae culture, sometimes within 48 hours of contamination (Moreno-Garrido and Cañavate, 2000). A component of proper integrated pest management is the utilization of technologies that can rapidly detect grazers at the earliest time or lowest pest concentration possible (McBride et al., 2014). Once the grower is informed of an infection, they can choose to treat the culture to kill or slow the growth of the contaminant, if complementary grazer identity information is available, or prematurely harvest to salvage the crop (Carney and Lane, 2014).

The detection of grazers has been approached from many analytical directions (Di Caprio, 2020; Carney and Lane, 2014; Deore et al., 2020). Microscopy and automated optical techniques, such as flow cytometry, have made progress in detecting grazers at low concentrations (<10 units/mL) (Day et al., 2012; Forehead and O'Kelly, 2013). These techniques, while simple and cost-effective, are offline, can be slow to operate, and require specific protocols or knowledge of the grazer's appearance. Alternatively, technologies from molecular biology such as qPCR have showed promise in definitively identifying grazers, with theoretical detection limits of a single molecule, however challenges associated with producing a library of primers specific to harmful grazers and cost are significant factors (Di Caprio, 2020; Letcher et al., 2013). Notably, both methods are highly vulnerable to sampling biases, where the preference of some grazers to localize on surfaces or on biofilms preclude identification as most samples are taken from the liquid bulk.

Recently, attention has been directed to the suite of volatile organic compounds (VOCs) emitted from microalgae as they progress through their life cycle (Achyuthan et al., 2017; Fisher et al., 2020; Reese et al., 2019). For algae, VOC emissions can be mediated by their environmental conditions or biological state such as exponential growth, nutrient availability, photooxidative stress, and senescence (Achyuthan et al., 2017). Collectively the microalgae "volatilome" represents a reflection of the organism's state of health (SoH) and, due to the significant effect of grazing on microalgae health, a reflection of the infection state of the bloom. Development of techniques and instrumentation to measure the microalgae volatilome therefore represents an opportunity to identify grazer infections in a highly sensitive and descriptive manner (Achyuthan et al., 2017). Currently, the predominant technique for analysis of the algae volatilome has been gas chromatography mass spectrometry (GC/MS). While extremely sensitive and effective for identification of VOCs, common GC/MS systems are not particularly well suited for continuous,

in-situ measurements without significant modifications (Miller et al., 2008). In addition, the dominant sampling technique for microalgae VOCs, solid phase microextraction (SPME), often requires long equilibration times of up to 24 hours to obtain sufficient signal (Achyuthan et al., 2017). Unfortunately, such long sampling times not only delay detection but can average out transient, but important, VOC emissions. Given the fast timescales that grazer infections occur, the need for a headspace monitoring technique with higher time resolution and multi-vessel capacity is warranted.

Chemical ionization mass spectrometry (CIMS) is a chemically selective method frequently utilized in the atmospheric sciences for the online detection of various species that are spatiotemporally heterogenous in concentration (Laskin et al., 2018). In CIMS, a preformed ionized reagent gas is mixed with a continuously sampled stream of analyte from the sample headspace. Favorable chemical energetics between the reagent gas and analytes in the sample headspace result in a soft ionization of the analytes, which then are detected by various types of mass spectrometry. Notably, this method can bypass the need for a gas chromatography column as the selection of a particular reagent ion (e.g. H_3O^+, $C_6H_6^+$, or I^-) precludes the detection of unwanted molecules, such as the inorganic gases (N_2, O_2, CO_2, and CH_4) that are normally ionized by electron impact in GC/MS (Harrison, 1992). The removal of gas chromatography enables the measurement of ambient VOCs in a highly continuous (1 Hz or better) manner, while the soft nature of chemical ionization prevents significant ion fragmentation, which would overcomplicate the mass spectrum of unseparated VOCs. Studies of VOC emissions from natural marine and freshwater systems have indicated the ability of CIMS to identify distinct states of biogenic activity from phytoplankton and bacteria (Carpenter et al., 2012; Halsey et al., 2017; Kim et al., 2015,

2017). These findings suggest that CIMS may possess the ability to monitor highly concentrated algal monocultures and benefit from the far greater throughput over modern GC/MS technology. In this work we discuss the utilization of CIMS to monitor freshwater cyanobacterial monocultures of *Synechococcus elongatus* PCC 7942 before and after the addition of a field-isolated ciliate grazer, *Tetrahymena*. Over a 28-day experiment, three 40 L carboys were monitored continuously by CIMS with commensurate biological measurements as they proceeded through healthy growth and were sequentially infected with *Tetrahymena*. Switching between sampling vessels on a 15-minute interval allowed the probing of algal VOC production at time resolutions not usually investigated, enabling true comparisons of the ability of VOC analysis to detect grazer infections faster than traditional techniques. Analysis of the CIMS data revealed novel features regarding the timescales of VOC production that highlight the potential implications of high temporal resolution VOC analysis on monitoring SoH and grazer infections in microalgae cultivation.

4.3 Results

4.3.1 Experimental setup

To demonstrate the capabilities of CIMS analysis on SoH and grazer infections of cyanobacteria, we simultaneously monitored three 20-L carboy cultures of *S. elongatus* PCC 7942, hereafter referred to as PCC 7942, through axenic exponential growth and subsequent planned infections with a field-isolated *Tetrahymena* that rapidly grazes on PCC 7942. Liquid samples were collected from each carboy at least once daily for microscopy, absorbance spectroscopy, and fluorescence spectroscopy. Upon addition of the predator, the infected carboy was also monitored using a continuous fluorescence spectroscopy system. Cultures were continuously bubbled with sterile zero air, which pushed headspace gases above the culture to a custom-built solenoid valve array that was programmed to switch every fifteen minutes between each of the three carboys and

a direct zero air input (Figure 4.1b). The headspace or zero air sample source made available by the solenoid valve array was pushed directly into the ion-molecule region (IMR) of a chemical ionization time of flight mass spectrometer (CI-TOFMS), where the continuous flow of air from the carboys or zero air was ionized by charged water clusters and directly introduced into the CI-TOFMS without any column chromatography (Figure 4.1a). Mass spectra were accumulated as an average of 65,000 spectra over a one second time period and were organized for analysis based on the solenoid array's sampling schedule (Figure 4.1c).

4.3.2 General MS characteristics

The mass spectra collected from the headspace over the PCC 7942 cultures were distinct from that of clean zero air and displayed numerous peaks indicative of VOCs. Figure 4.2a shows a comparison of average mass spectra obtained from both the headspace of Carboy 1 and clean zero air during a period of axenic algal growth on the fourth day after PCC 7942 inoculation. The mass spectrum for both sample types is dominated in intensity by the water cluster reagent ion at m/z's 19, 37, 55, 73, and 91, which is typical for chemical ionization. In Carboy 1, the remainder of the mass spectrum is composed of numerous ions which fall between m/z 40-200, consistent with the molecular weights of VOCs. At this timepoint, the fraction of ion intensity occupied by non-water cluster ions was 7% for zero air and 11% for the headspace of Carboy 1, where total ion count (TIC) was approximately 2.5×10^6 counts per second. The ratio of ion intensity for non-water cluster ions between Carboy 1 and zero air was 1.51. Of this ion intensity, Carboy 1 possessed 75 unique m/z's that were 25% greater in average intensity than zero air, suggesting their origin from either cyanobacterial production, the BG-11 growth medium, or the carboy assembly. Of these 75 unique m/z's, 49 ions were found to exhibit distinct time-variant behavior over the course of Carboy 1's experimental lifetime, where time-variant behavior is defined operationally as a >10%

increase or decrease in normalized intensity over the timescale of the experiment. Time series that showed exponential decay from the outset of the experiment or spikes caused by pressure instabilities were excluded from this analysis, indicating that the 49 ions that changed intensity over the course of the culture's lifespan were most likely due to active biogenic processes and not off-gassing from the media or experimental arrangement. These results together give an initial demonstration that water cluster CI-TOFMS can detect numerous unique volatile gases related to the activity of the cyanobacterial culture.

Of the ions detected by the CI-TOFMS, direct assignments of some species were made utilizing complementary MS methods such as solid phase microextraction gas chromatography mass spectrometry (SPME-GC/MS) and modified atmospheric pressure chemical ionization high resolution mass spectrometry (APCI-Orbitrap) incorporating recent innovations for direct analysis of gas phase species (Roveretto et al., 2019) (Supplementary Information). These identifications are listed in Table 4.2. Overall, molecular formulae or putative identifications were made for a small fraction <15% of the total number of ions observed by CI-TOFMS during the experiment duration. While many of these species were observed to be aliphatic ketones and aldehydes similar to investigations of algae by others (Reese et al., 2019), nitrogen containing gases, including ammonia and C_4H_7N were an important constituent that has been generally overlooked by previous analyses of commercial algal VOCs, despite some evidence of the production of methylated amines from phytoplankton in natural seawater (Facchini et al., 2008; Steiner and Hartmann, 1968).

4.3.3 Evaluation of tubing sticking delays

While CI-TOFMS possesses a relatively low-mass resolution (~1200 full width at half maximum) and does not induce significant ion fragmentation that can be used for molecular

identification, valuable analyte information can be obtained through monitoring the rise or decay time of an ion as the CI-TOFMS switches between sampling vessels. This rise or decay time (see Figure 4.6 for an example), can be modeled using a double exponential fit and the resultant time for the ion to reach $1/e^2$ (86.5%) of its final value can be calculated (Liu et al., 2019; Pagonis et al., 2017). $1/e^2$ decay times are reflected as the sum of multiple physical processes as VOCs travel down the length of the tubing from the sample source to the instrument IMR inlet. Molecules with a high saturation concentration (volatility) remain in the gas phase, which results in short equilibration times between samples. Conversely, low volatility molecules tend to stick to tubing and result in longer equilibration times (Pagonis et al., 2017). In addition to saturation concentration, smaller molecules with high dipole moments, such as NH_3 or HCl, may partition into water microlayers on tubing walls, thus increasing their equilibration times significantly (Liu et al., 2019). Together, an analysis of tubing VOC rise or decay times, in combination with their corresponding m/z's, provides valuable information as to the general chemical characteristics of observed ions. This analysis also enables calculation of the minimum time the CI-TOFMS must monitor a sampling vessel before it can switch to the next vessel. We applied this analysis to a set of 42 unique m/z's using rise or decay times as the CI-TOFMS switched between sample carboys and zero air. The results of such an analysis performed on data acquired on the fourth day after inoculation of Carboy 1 with PCC 7942 are shown in Figure 4.2b, with the single omission of the $1/e^2$ value of ammonia (NH_3). Notably, the majority of $1/e^2$ decay times fall under 12 seconds, comparable with equilibration times necessary for high-speed environmental measurements (Yu and Lee, 2012). In contrast, ammonia and other even mass VOCs at m/z's 70 and 76, whose even m/z values suggest an odd number of nitrogen atoms if ionized by proton transfer, displayed longer equilibration times, with ammonia's $1/e^2$ being approximately 335 s. The assignment of nitrogen

in the molecular formulas of these species is consistent with their longer equilibration times, as their pronounced basicity enables effective dissolution into water coated on tubing walls. These data also inform the minimum sampling time the CI-TOFMS must reach before moving on to the next sample. Based on the longest equilibration time of ammonia of 5.6 min, this key operational parameter means that the CI-TOFMS, with an appropriate sample switching device, is capable of sampling 10 vessels in under an hour. Furthermore, these equilibration times are not fixed, and can be further improved through higher flow rates, tubing diameters, heating, and coating of the tubing or the CI-TOFMS inlet. Finally, this analysis demonstrates that the 15-min sampling schedule used in this experiment was more than sufficient to accurately determine ion intensities for a diverse suite of VOCs present in the culture headspace samples.

4.3.4 Time Series Analysis

VOCs from Carboys 1, 2, and 3 were monitored over a total period of 28 days. All carboys were inoculated with PCC 7942 at the same time and each carboy was sequentially infected on days 8, 13, and 23, respectively, with *Tetrahymena* at a concentration of 0.1 cells/mL (Figure 4.3, solid vertical lines). This infection density was chosen for being well below the typical limit of detection of microscopy at $1x10^4$ to $1x10^5$ cells/mL and the theoretical limit of blank for the technique used of 20 cells/mL (Bedrossian et al., 2017; Cadena-Herrera et al., 2015; Morono et al., 2009). Twice daily after infection, liquid samples were taken manually from the infected carboy and analyzed by microscopy for the presence of *Tetrahymena*. Grazers were observed first from each carboy on days 12, 16, and 27 (Figure 4.3, dashed vertical lines), with further information on the specific duration until detection summarized in Table 4.1. To observe changes in algal biomass associated with grazing at faster timescales, each grazer inoculated carboy was monitored by continuous fluorescence (Figure 4.3b) until the complete loss of biomass as indicated

by the daily fluorescence measurements and visible color change and culture collapse (Figure 4.3a). Continuous fluorescence, while providing a higher temporal resolution in showing biomass loss during the grazer-induced crash, did not confer any significant advantage to grazer detection over manual daily fluorescence sampling. In addition, during the infection of carboy 3, the continuous fluorescence signal began to gradually diminish before changes in the manual daily sampling, likely due to observed biofouling of the sensor at high algal biomass.

For headspace sampling by the CI-TOFMS, numerous VOCs showed drastic changes in intensity in response to grazer infection, however only the time series of the fastest responding and most intense species will be primarily discussed here. The most significant change in ion intensity was dominated by NH_3 at a m/z 18 (Figure 4.3c) and its associated water cluster ions at m/z's 36 and 54. Initial NH_3 ion intensities were observed to be elevated at the outset of the experiment, and are indicative of volatized NH_3 off-gassing from the BG-11 medium, which contains 6 mg/L ferric ammonium citrate, as observed by monitoring sterile BG-11 (data not shown). After the first two days of algal growth, this NH_3 ion signal decreased by nearly two orders of magnitude and remained below $2x10^4$ counts*s^{-1} until after *Tetrahymena* addition. This decrease was likely caused by uptake of ammonium by PCC 7942 as well as gradual ventilation of NH_3 by the bubbled zero air. After grazer addition to each carboy, an initial intensity spike of NH_3 was observed for each carboy on days 11, 15, and 25. Notably, some NH_3 signal carryover from Carboy 1 to Carboys 2 and 3 occurred during Carboy 1's ammonia spike, as well as carryover from Carboy 2 to Carboy 3 during Carboy 2's ammonia spike. These carryover events were caused by excess ammonia in the sampling lines and CI-TOFMS inlet that did not sufficiently evaporate before the CI-TOFMS switched to the next sampling vessel, consistent with the slow equilibration rate observed for ammonia. After the first intensity spike, the NH_3 signal decreased before spiking a second time for

each infected carboy in concert with the culture crash and decrease in fluorescence signals. Notably, the magnitude of the first ammonia spike increased in intensity as the experiment duration continued in concert with the increase in algal biomass in later carboys (Figure 4.3a,c). We tentatively suggest that the first ammonia spike appears to be biomass dependent and may be an algal stress-related response. Although ammonia release has been described for some strains of *Anabaena* (Subramanian and Shanmugasundaram, 1986), though not as a stress or predation response, algal growers have used free ammonia addition as a method to control pests (Thomas et al., 2017). We hypothesize that this initial ammonia spike represents a possible defense mechanism. In contrast to the first spike, the magnitude of the second ammonia spike is relatively consistent for all three carboys, suggesting that its production is a function of biomass degradation caused by the predation of the grazer on the cyanobacteria.

While ammonia signals increased after predator addition, the intensity of m/z 137, an unidentified monoterpene, showed a clear decrease in Carboys 1 and 2 multiple days before detection of *Tetrahymena* by microscopy (Figure 4.3d). For Carboy 3, the intense NH_3 signal from the first spike disrupted the ion chemistry of the CI-TOFMS preventing reliable observations of m/z 137 (Figure 4.7). For this reason, in cases where m/z 18 intensity exceeded 2500 counts per second, m/z 137 intensity was discarded. In Figure 4.3e, the intensity of m/z 70, which was determined to have the molecular formula C_4H_7N, and is likely 1- or 3-pyrroline, showed strong positive changes in intensity for infected Carboys 2 and 3, but only decreased in intensity in Carboy 1 (Figure 4.3e inset). Unlike m/z 137, m/z 70 was unaffected by periods of high NH_3, likely due to a high gas phase proton affinity. Similar to the double spike phenomenon observed for NH_3, it appears that the amount of algal biomass present at infection time is an important effector of m/z 70 production in response to grazing. These results are further supported by measurements of m/z

32, methylamine, which only appeared in response to grazing in Carboy 3, the highest biomass vessel (Figure 4.8).

4.3.5 VOCs as indicators of grazing

Having observed VOC signatures that change consistently across cultures after the introduction of predators, we compared the timing of VOC intensity changes as detected by CIMS to indicate the presence of grazers relative to the timing of grazer detection by microscopy and continuous fluorescence. By applying an empirically-derived detection threshold based on the ion signal changing by 10σ over a 4-hour window, we find that the CI-TOFMS detects grazers 25-76 hours faster than microscopy, depending on the VOC used for detection and the specific experiment (Table 4.1). C_4H_7N in all cases was the fastest VOC to respond to grazing, and was effective for use in all three carboys, while monoterpenes are more effective at lower biomass where complications from high ammonia was less problematic. Notably, the duration at which grazer detection was achieved by VOC analysis decreased over the experimental duration, indicating that the increased biomass in Carboys 2 and 3 seems to have shortened the algal response to infection. For microscopy, detection of grazers after inoculation was quite similar for Carboys 1 and 3, however occurred earlier for Carboy 2. High variance in detection time by microscopy is reflective of challenges inherent in the technique at low cell densities, where statistical fluctuation and heterogeneous localization of the predator may be prominent factors. For example a 1 mL sample screened for grazers at a detection limit of 1 cell/mL may not contain a grazer, even if the bulk grazer concentration is ~1 cell/mL. While continuous fluorescence cannot not detect grazers until after cyanobacteria biomass began to diminish, the remarkably similar times reflect a grazing consistency between the three carboy inoculations which help validate chemical comparisons between the three systems.

4.3.6 Temporal changes in ion intensity

To better understand if the apparent correlation for some ions between increased cyanobacterial biomass and increased changes in VOC intensity is a more generalized phenomenon, we calculated the derivative of ion signals which changed in response to grazing and evaluated these signal changes by separate carboy. From an analysis of the maximum raw ion intensity derivative of VOCs in each carboy (Figure 4.4a), it is apparent that denser algal cultures produce larger total quantities of VOC change in response to grazing, suggesting that the utilization of algal VOCs as a diagnostic will be more effective for denser, mature ponds. In addition, the maximum derivative of each VOC was normalized to their respective intensities at the time of *Tetrahymena* addition, and then the time for the VOC to double in intensity at this rate of change was calculated (Figure 4.4b). This calculation allows the investigation of how much, by fraction, each VOC changed in time as a response to grazer addition between the three carboys. The results in Figure 4.4b show that the doubling time for VOCs significantly decreased from Carboy 1 to Carboy 3, indicating that the quantity of initial algal biomass at time of infection accelerates the production or loss of VOCs in response to grazing. Furthermore, this observation demonstrates that as the doubling time decreases, the need for higher time resolution analytical methods, such as CIMS, become necessary to capture these signal changes for effective grazer detection in a manner that current GC/MS-based VOC analysis techniques simply cannot.

4.4 Discussion

The utilization of chemical ionization mass spectrometry identified several promising molecular species as diagnostic tracers to identify *Tetrahymena* grazing in 7942. We found that nitrogen-containing gases represent a previously overlooked molecular type in commercial algae and may serve as highly reliable tracers of algal grazing. While the putative identification of all

ions was not possible, complementary analyses with GC/MS and APCI-HRMS assisted in increasing clarity. However, ascertaining the identity of all VOCs measured by CI-TOFMS is not mandatory towards the goal of identifying predation or infection in algal cultures. Provided the m/z's measured by the CI-TOFMS consistently respond to destructive contamination, knowledge of their identity and biochemical purpose only play a supporting role to better understanding the biochemistry of the system overall. This perspective can be thought as analogous to medical measurements of temperature or blood pressure, which are linked to pathogenesis in often unknown and highly complicated ways but nevertheless indicate a change in the SoH of the patient.

Furthermore, this study is the first to compare volatile gas measurements with microscopy, the current gold standard, in how quickly after grazer inoculation can a diagnostic signal be produced. We find that VOC analysis of 7942 infected with grazers is at minimum 24 hours faster than microscopy and can be up to 3 days faster for the experimental conditions discussed herein. We further identify fascinating new features regarding the timescale and intensity with which VOCs are produced in response to grazing that appear linked to algal biomass. The ability of algae to respond to stressful stimuli in a population-dependent manner informs that gas analysis as a diagnostic method will likely require multiple data types to contextualize the overall state of health of the algal crop. We furthermore leveraged our high-temporal resolution measurements to show that changes in gas composition due to grazing occur on a <24 hr basis, with some VOC intensities changing by a factor of two or more in less than an hour. This timescale indicates that the sampling frequency of a VOC diagnostic measurement for algae needs to occur more than once daily and perhaps as frequently as once hourly or more, which would be difficult for the most prevalent form of gas analysis, GCMS. Given the constraints imposed by adhesion of VOCs to sampling tubing, we find that CI-TOFMS could monitor ~10 carboys per hour, which could be improved through

modifications of sampling arrangement for field application, greatly offsetting the cost of this higher-complexity instrumentation. Future applications of this approach to algal monitoring will significantly benefit from higher complexity numerical analyses, possibly AI, that can draw connections between algal VOC production and various other indicators of health, ultimately towards the goal of giving the power for a MS to automatedly "decide" a pond is infected and either inform a grower immediately or initiate a predetermined intervention in an automated fashion to minimize biomass losses prior to the rapid losses observed in these experiments and in the field. Given the reports of regular losses in the field of 30% or greater in biomass production and the one to three days of prior notice to any significant biomass loss that is capable with the CIMS system, we believe that the CIMS monitoring system could effectively allow a grower time to recover nearly all of the biomass lost, even through the most drastic intervention of harvesting the entire system. While the analysis depicted herein has been focused on microalgae, we stress that chemical ionization mass spectrometry's ability to monitor many samples in an automated manner could be applied to other systems similar to algal cultivation such as beer, monoclonal antibody production, and lab-grown meats which all must maintain stringent cleanliness.

4.5 Materials and methods

4.5.1 Culture condition

Synechococcus elongatus PCC 7942 was grown for maintaining *Tetrahymena* or for inoculations for larger cultures in BG-11 medium (Allen, 1968) in 250 ml or 2 L flasks with continuous shaking (125 rpm) at 30 °C under continuous illumination of 200 μmol photons m^{-2} s^{-1} from fluorescent cool white bulbs.

4.5.2 Tetrahymena Isolation and Culturing

A 30-L BG-11 culture of *S. elongatus* PCC 7942 grown in a 100-L polybag at the UCSD Greenhouse Biology Field Station, as described by Schoepp, et al. (Schoepp et al., 2014), had crashed due to an unknown contaminant. A sample of this crashed culture was brought into the lab and analyzed by light microscopy, where it was observed that the predominant organism was a free-swimming ciliate. This culture sample was serially diluted or manually isolated under microscopic visualization into flask cultures of PCC 7942 or into wells of a flat bottom multiwell cell culture dish (Costar, Corning) containing dense *S. elongatus* cultures as diluents to first isolate the grazer and subsequently to culture the grazer. Grazer cultures were incubated at 30°C under low light conditions (10 μmol photons $m^{-2}s^{-1}$) or more routinely at room temperature under ambient light conditions. In contrast to healthy PCC 7942 cultures, grazed cultures were yellow, resulted in visible clumping of the few remaining *S. elongatus* cells, and were predominantly composed of ciliates when viewed by light microscopy on a dissecting microscope. A 1 μl sample of a grazed culture was used as a template for Q5 (NEB) PCR amplification of the ITS2 region using the ITS1 (5'- AGGAGAAGTCGTAACAAGGT-3') and ITS4 (5'- TCCTCCGCTTATTGATATGC-3') primers (ref), producing an approximately 600 bp band. PCR was performed according to the Q5 standard protocol with an annealing temperature of 55°C and an elongation time of 3 min and 45 sec. The PCR product was purified using the Zymo DNA Clean & Concentrator-5 kit and sequenced by Sanger sequencing with the ITS1 primer. The resulting sequence was analyzed by BLAST to determine the closest identified species as *Tetrahymena tropicalis, Tetrahymena thermophila,* or *Tetrahymena rostrata.*

4.5.3 Carboy cultures and chemical ionization mass spectrometry

Three 20-L transparent polycarbonate carboys (Nalgene) fitted with a custom inlet/outlet polypropylene cap with stainless steel bulkhead compression fittings sealed with Viton O-rings for

gastight liquid and gas sampling designed to prevent the unwanted introduction of organisms from the ambient environment were filled with 18 L of BG-11 and autoclaved (Figure 4.5). Once cooled, the carboys were inoculated with 2 L of *Synechococcus elongatus* PCC 7942 cultures previously grown in 2-L flasks to an OD at 750 nm of 0.08 – 0.1 so that the carboys were inoculated to an OD at 750 nm of approximately 0.01. Carboys were connected to sampling devices as shown in Figure. 4.1 and 4.5. Cultures were grown continuously under cool (4100 K) fluorescent light, starting at 135 μE incident radiation at the front face of each carboy and increased to 190 μE after 24 hours of growth, at which time self-shading lowered the risk of photobleaching. *Tetrahymena* were added at a calculated concentration of 0.1 cells/mL separately to Carboy 1, 2, and 3 after 8-, 13-, and 23-days following culture inoculation, respectively.

Clean zero air, obtained from a generator (Sabio 1001), and regulated by a mass flow controller (Alicat) to 3 standard liters per minute (SLPM) was directed through a 47 mm 0.2 μm PTFE filter into each carboy where the air input line was terminated at a submerged circular length of perforated ¼”-OD perfluoroalkyl (PFA) tubing so that all input air was released as bubbles directly into the culture. This construction distributed bubbles throughout the carboy to adequately mix and supply air to enable culture growth. Liquid samples were collected from the carboy using a manifold of three-way and 1-way check valves connected by Tygon tubing to the compression fittings on the cap, all of which were autoclaved attached to the carboy at the time of media preparation. The valve manifold allowed sanitation of liquid sample lines by 70% ethanol with significantly reduced backflow risk of ethanol or microorganisms into the carboy. The output headspace gas from each carboy flowed through 3.175 mm ID PFA tubing into a custom Labview controlled 4-channel solenoid valve array which switched between each carboy and clean zero air on a 15-minute sampling cycle (Scheme 1c). Sample air from the solenoid array was drawn in by

the CI-TOFMS at a flow fixed flow rate of 1.8 SLPM, with excess sample gas overflowing to a downward pointing exhaust port for condensed water droplets to drain (Figure 4.1).

Ultra-high purity N_2 gas, produced by boil-off from a liquid nitrogen dewar, was bubbled through a 250 mL Pyrex bottle filled with LCMS purity H_2O at 2.2 standard liters per minute (SLPM). Humidified N_2 exiting the bottle was passed into a Po-210 α-particle source (20 mCi) to produce protonated water clusters, $(H_2O)_nH^+$ where n = 1,2,3,…, that were mixed with sample air in the ion-molecule region (IMR) of the instrument. (P_{IMR} = 23 Torr). Input flow of sample and reagent gas into the IMR was controlled by inline critical orifices (O'Keefe) at 1.8 SLPM for both flows. Chemical ionization of analytes in the IMR by protonated water clusters proceeds through several possible reaction mechanisms which are controlled by the chemical energetics of the analytes and reagent ion. These reactions are detailed in equations 1 – 4 (Aljawhary et al., 2013).

$$M + X^+ \rightarrow M^+ + X \qquad \text{Charge Transfer} \qquad (1)$$

$$M + HX^+ \rightarrow MH^+ + X \qquad \text{Proton Transfer} \qquad (2)$$

$$MH + X^+ \rightarrow M^+ + HX \qquad \text{Hydride Abstraction} \qquad (3)$$

$$X^+ + M + Z \rightarrow MX^+ + Z \qquad \text{Adduct Formation} \qquad (4)$$

Where M is the analyte, X is the reagent, and Z is a third body required to carry away excess energy. For $(H_2O)_nH^+$, it is assumed that the predominant reaction channel is through proton transfer which occurs when the proton affinity of the analyte exceeds that of the water cluster. For $(H_2O)_nH^+$, the range of proton affinities for n = 0,1,2,3 water clusters is 691, 694, 730, and 769 kJ mol^{-1} respectively, however it is difficult to predict the true distribution of water clusters in the IMR as the observed mass spectrum may not reflect this directly (Aljawhary et al., 2013). Given the relatively high pressure of the IMR, water clusters are expected to reach the equilibrium cluster distribution far faster than their residence time (~100 ms) in the IMR.

After ionization, reagent and product ions are passed further into the instrument, starting with an electrodynamic ion funnel (P_{IF} = 0.3 Torr), which radially confines ions using a radio frequency pseudopotential applied across 30+ concentric brass plates of decreasing diameter. Ions transmitted through the funnel are passed into a RF-only transfer quadrupole ($P_{Quad} = 5*10^{-5}$ Torr) which directs the ions into the final chamber: a commercial orthogonal extraction time of flight mass spectrometer ($P_{ToF} = 4.0*10^{-7}$ Torr) with chevron microchannel plate (MCP) detector (Tofwerk AG) (Figure 4.1c). Approximately 60,000 mass spectra are averaged per second on an analog-to-digital converter and transferred to computer storage for later analysis. For the analyses in this work, the mass spectral window was limited between 10-400 m/z as there was a dearth of ions observed above this mass range. Mass resolution was ~1200 full width at half maximum for the spectra obtained in this experiment. MS data was baselined, calibrated, and analyzed in Tofware, a GUI plugin for Igor Pro 7. Time series data of unit-mass m/z's were averaged into ~15-minute bins to reduce data density and were separated by the carboy sampled using a complementary mask file generated by the solenoid valve array. ~5 minutes of MS data acquired at the beginning of each time bin was discarded to remove signal that was equilibrating between samples.

4.5.4 Biological measurements

Tetrahymena cell counts were obtained by manual counting of ciliates present in 1 to 10 µl droplets of culture on a microscope slide under a dissecting microscope with 25x objective and 10x eyepiece. Alternatively, for low density grazer cultures, 200 µl of culture in a 96 well plate could be rapidly scanned using the same dissecting microscope set up. For all cell counts, at least five individual sample counts were collected and averaged to calculate the cell density of the culture or inoculum.

Manually collected cyanobacterial culture samples were analyzed by optical density at 750 nm in a clear, plastic cuvette, or by absorbance and fluorescence spectroscopy of a 200 µl sample in a 96-well plate using a TECAN Infinite M200 plate reader to collect OD_{750} values and autofluorescence values at an excitation of 590 nm and emission of 670 nm.

Culture samples were checked for bacterial and fungal contamination by spotting 5 µl of sample on BG-11 Omni plates (BG-11 with 0.04% glucose, 5% LB, and 1.5% agar) and incubating the plate in the dark at 30 °C overnight (Taton et al., 2012). All *S. elongatus* flask and carboy cultures were demonstrated to be free of contaminants prior to *Tetrahymena* addition.

4.5.5 Continuous Fluorescence

After each carboy was inoculated with *Tetrahymena* grazer, a low flow (~1 mL/min) peristaltic pump was connected and withdrew carboy liquid through 1/8" OD Tygon tubing to a quartz 1 cm^2 flow-through cuvette before returning the liquid back to the carboy in a closed loop. The cuvette was placed in a custom fabricated fluorescence spectrometer which irradiated the cell with 420 nm light produced by a photodiode laser (Thorlabs). An orthogonally oriented photodiode detector (Thorlabs) with a 650 nm high pass filter measured fluorescence which was logged at a rate of 1 Hz by a custom written Labview MyDAQ interface. Continuous fluorescence data was background subtracted, normalized, and averaged into 10-minute intervals after experiment completion.

4.5.6 Gas chromatography mass spectrometry of grazer infected 7942

10 mL crimp cap vials were filled with 4 mL of BG-11 growth media, 4 mL of a previously grown culture of PCC 7942 at an OD of ~0.25, or 4 mL of PCC 7942 culture with approximately 370 *Tetrahymena* cells added. Vials were crimp sealed and held under fluorescent light for the experiment duration. For each microalgae-grazer experiment, 10 vials were prepared, where 5

were controls of algae only, 5 were infected at the experiment start with *Tetrahymena* ciliate. Each day of the experiment, an untested vial from each group was sampled by solid phase microextraction (SPME) fibers possessing a 50 μm stationary phase of divinylbenzene/Carboxen/polydimethylsiloxane (solid gray, Supelco) equilibrated in the vial headspace for 24 hours. Samples were analyzed on an Agilent Technologies 7820A/5975 gas chromatograph mass spectrometer (GC/MS) using an Agilent BP5 column. The following GC/MS parameters were utilized for analysis of SPME fibers: Inlet temperature: 250° C, splitless injection, carrier flow: 2 mL min^{-1}, GC temperature program: 35° C for 3 minutes then +7 C min^{-1} to 230° C which was held for 2 minutes, MS transfer line temperature: 260° C, MS scan range: m/z 32.5 – m/z 300 over 1 second. MS data were baselined using the statistics-sensitive non-linear iterative peak-clipping (SNIP) algorithm (Ryan et al., 1988) and analyzed in OpenChrom (Wenig and Odermatt, 2010) (http://openchrom.net). MS spectra were identified using the NIST14 EI mass spectral database. Results were subsequently exported to Igor Pro 7 (Wavemetrics) for plotting.

4.6 Acknowledgements

The authors would like to thank Kerry Kizer, Laura Lowe, and Paul Kasrazadeh for their helpful assistance in preparing cultures for the experiments herein. This material is based upon work supported by the Department of Energy, Grant No: DE-EE0007094.

Chapter 4, in full, is currently being prepared for submission for publication of the material. Sauer, J.S., Simkovsky, R.S., Moore, A., Prather, K.A., Pomeroy, R. “Early Detection of Algal Grazing with Rapid, Continuous Measurements of Volatile Gases” The dissertation author is the primary investigator and author of this manuscript.

4.7 Figures

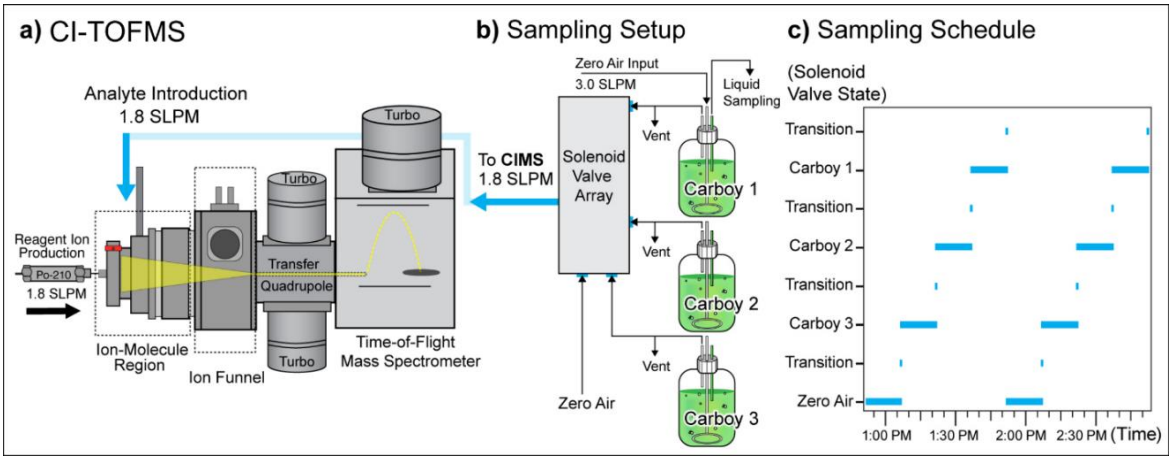

Figure 4.1 Experimental arrangement of carboy infection experiments. a) Diagram of CI-TOFMS instrument, b) Carboy sampling setup with solenoid valve array, c) Example sampling schedule of solenoid valve array for switching between carboys for CI-TOFMS headspace sampling.

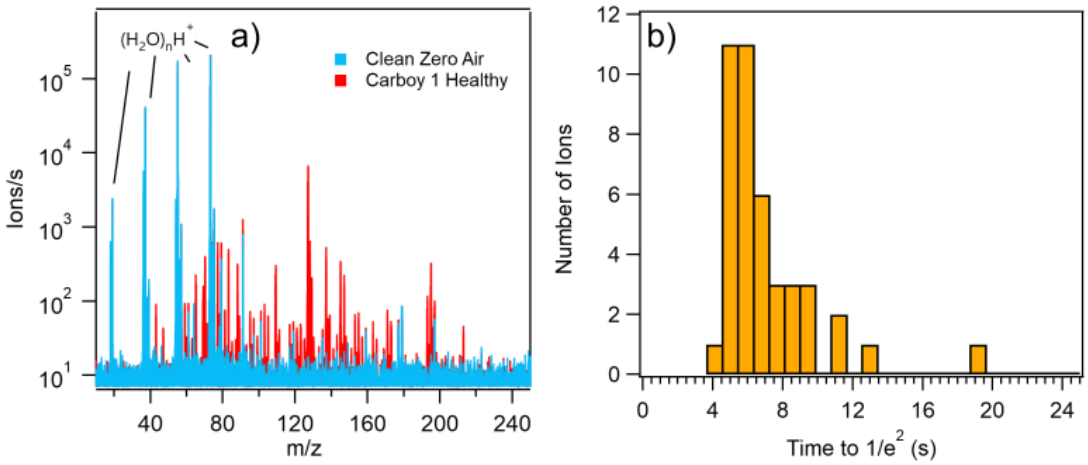

Figure 4.2 a) Average CI-TOFMS mass spectrum for zero air and Carboy 1 headspace, b) $1/e^2$ histogram of ion equilibration times obtained from switching between sampling zero air and Carboy 1

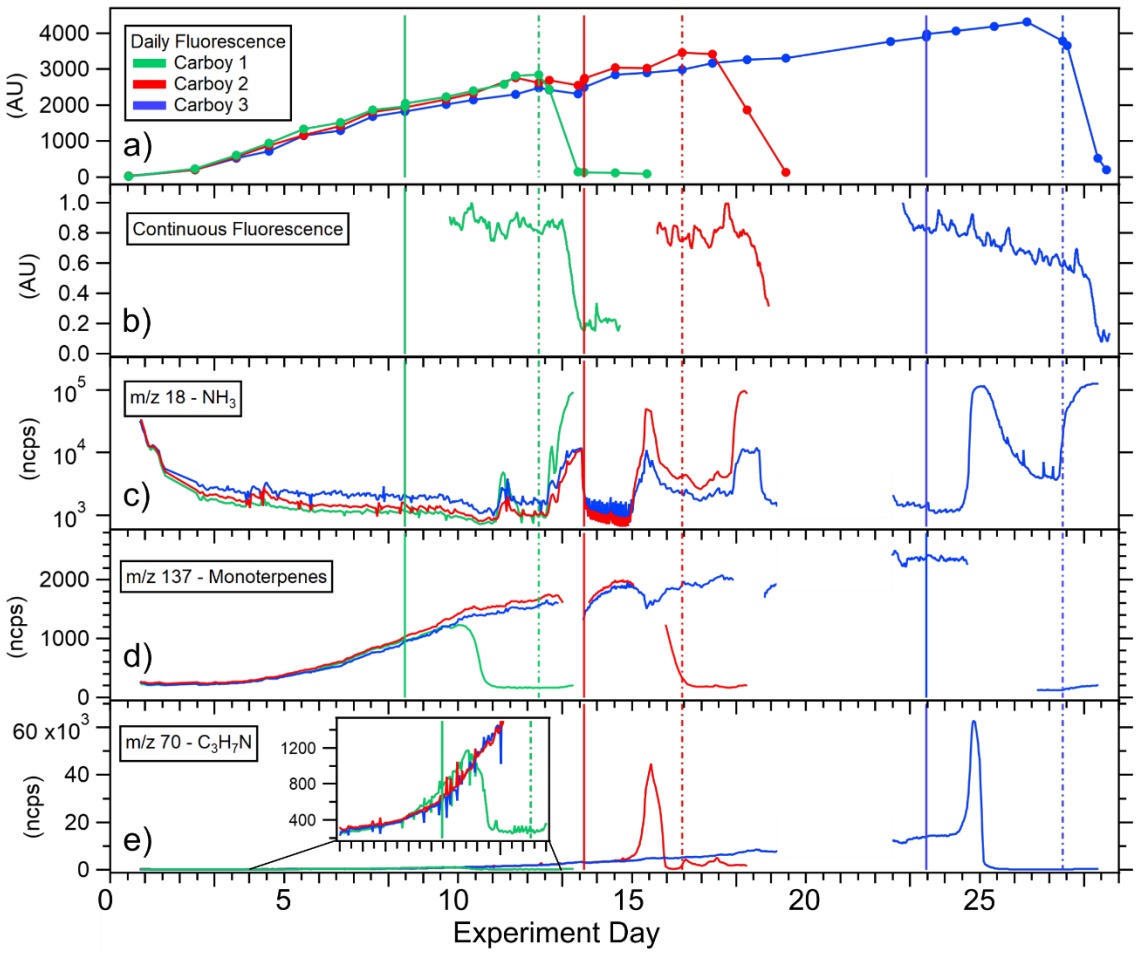

Figure 4.3 Time-series data of carboy experiment colored by carboy (Carboy 1: Green, Carboy 2: Red, Carboy 3: Blue): a) Daily fluorescence 590 nm excitation/670 nm emission, b) Continuous flow-through cuvette fluorescence 420 nm excitation/670 nm emission, c) CI-TOFMS m/z 18 (NH3) intensity, d) CI-TOFMS m/z 137 (monoterpenes) intensity, e) CI-TOFMS m/z 70 (C3H7N) intensity. Solid vertical lines denote time of Tetrahymena addition for each carboy, dashed vertical lines denote first time of Tetrahymena detection via microscopy

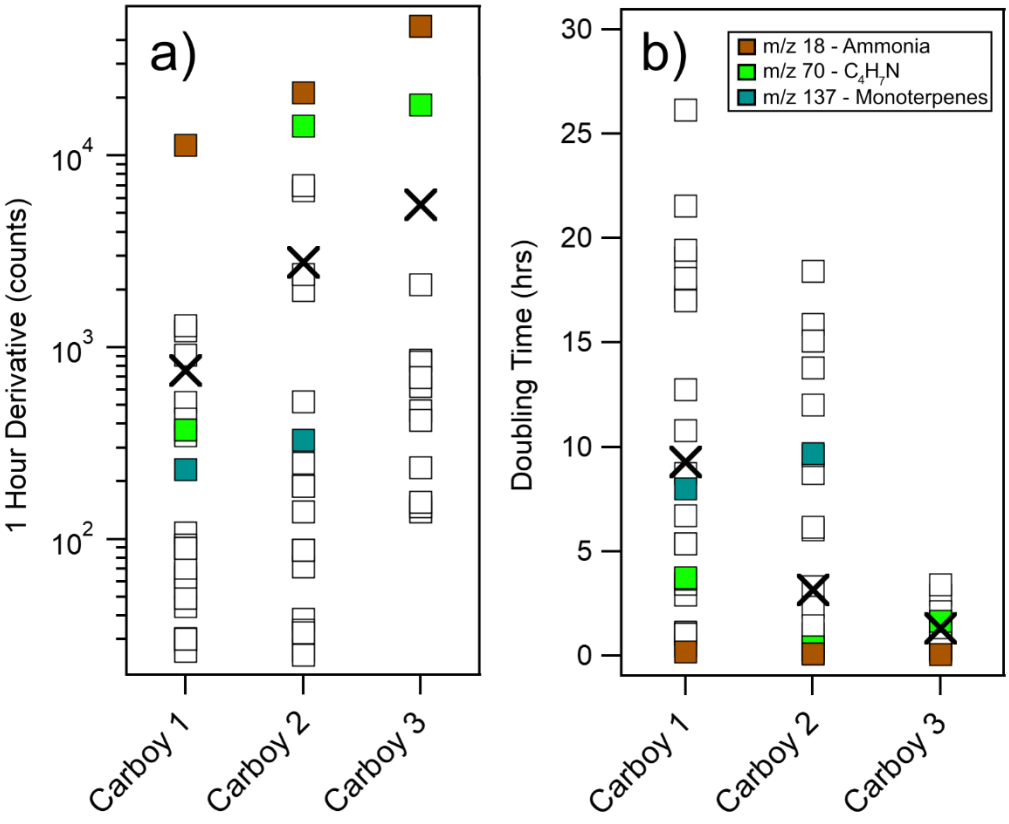

Figure 4.4 Derivative analysis of grazer-affected VOC production from 7942. a) Maximum derivative of raw ion signal change b) Normalized derivative doubling time for the same VOC set

4.8 Tables

Table 4.1 Time after grazer addition before detection technique flags presence of Tetrahymena grazer. For CI-TOFMS measured species, grazer detection was based on a signal intensity change of 10σ over a duration of 4 hours. Microscopy identification was at the first date of visible grazers observed during liquid grab sampling. Continuous fluorescence detection was based on a 10σ over a duration of 4 hours.

Carboy	**NH_3** (hrs after grazer addition)	**Monoterpenes** (hrs after grazer addition)	**C_4H_7N** (hrs after grazer addition)	**Microscopy** (hrs after grazer addition)	**Continuous Fluorescence** (hrs after grazer addition)
1	67	46.5	44	92	119
2	36	38.5	32	68	114
3	30	-	17	94	112

4.9 Supplementary information

The molecular assignment of m/z 70 was particularly challenging as the measurment of a matching ion from the SPME-GC/MS analysis, nor APCI-HRMS was not found. At unit mass 70, assuming the ionization by the CI-TOFMS occurred by proton transfer, 3 likely molecular formulae were proposed C_3H_3NO, C_4H_7N, and $C_2H_3N_3$, which corresponded to 7 molecular species. From the mass calibration of the CI-TOFMS which possessed a mean residual error of 150 ppm ($m*10^6/\Delta m$), formulae C_3H_3NO, and $C_2H_3N_3$ were eliminated as potential species, leaving C_4H_7N as the expected molecular formula which corresponded to butanenitrile, 1-isocyanopropane, or the pyrroline isomers as likely species. To further eliminate other potential factors, a time-series correlation analysis was performed to assess whether other ions covaried in intensity with m/z 70. Surprisingly, apart from the ^{13}C isotope of m/z 70, no ions of greater or lesser m/z were found to be correlated $>r^2=0.7$, where for other observed species, water cluster adducts or fragments normally correlated $>r^2=0.9$. This result suggests that m/z 70 did not fragment, which is consistent with proton transfer ionization of nitriles and nitrogenous heterocycles such as pyrroline, but not 1-isocyanopropane.

To generate molecular formulae for other ions observed by CI-TOFMS, high resolution mass spectrometry analysis was performed using a commercial atmospheric pressure chemical ionization (APCI) source interfaced with an Orbitrap Mass Spectrometer (Thermo Scientific). The APCI source was operated by applying a charge of 4kV and a current of 5 μA to the corona discharge needle. A 100 ml algal culture in a 250 ml media bottle, bubbled with 1.5 lpm of nitrogen, was measured by continuously flowing the headspace to the inlet using 1/4" Teflon tubing. A high-resolution mass spectrum of the algal culture was collected for at least 2 mins with a mass range set to 50 – 150 m/z.

4.10 Supplementary figures

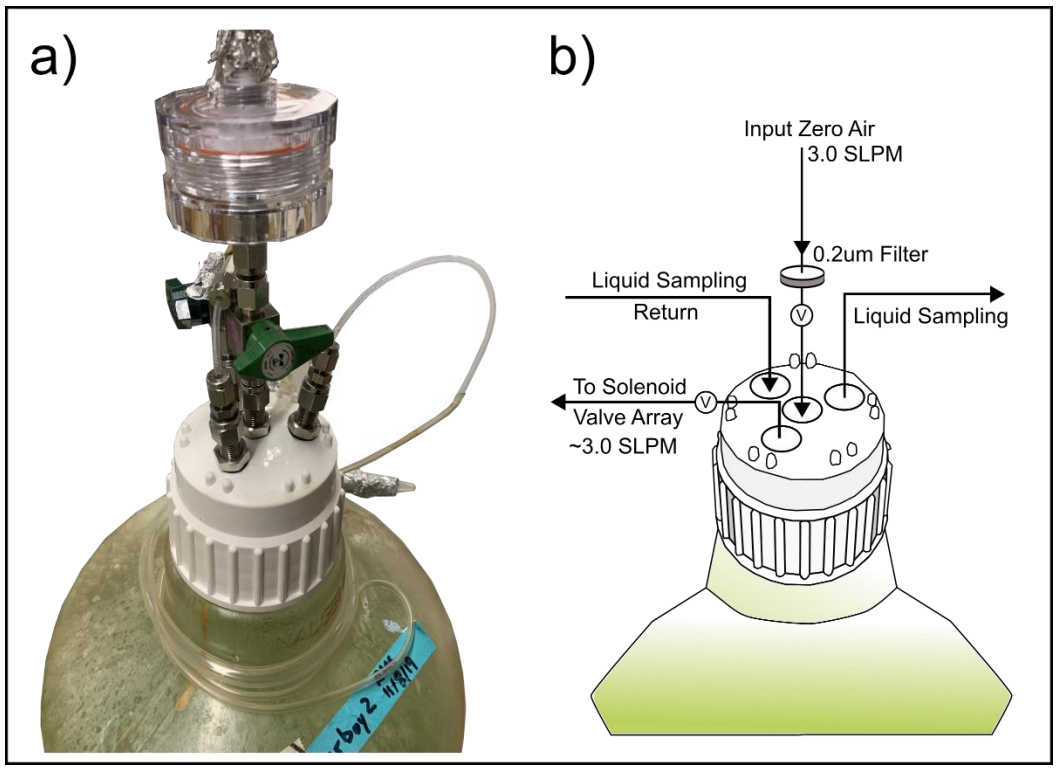

Figure 4.5 Carboy cap arrangement for experiments. a) photograph of assembled carboy cap, b) Illustration of carboy cap with annotations of sampling ports. Circles with the letter V indicate positions of needle valves used to control flow and maintain seals.

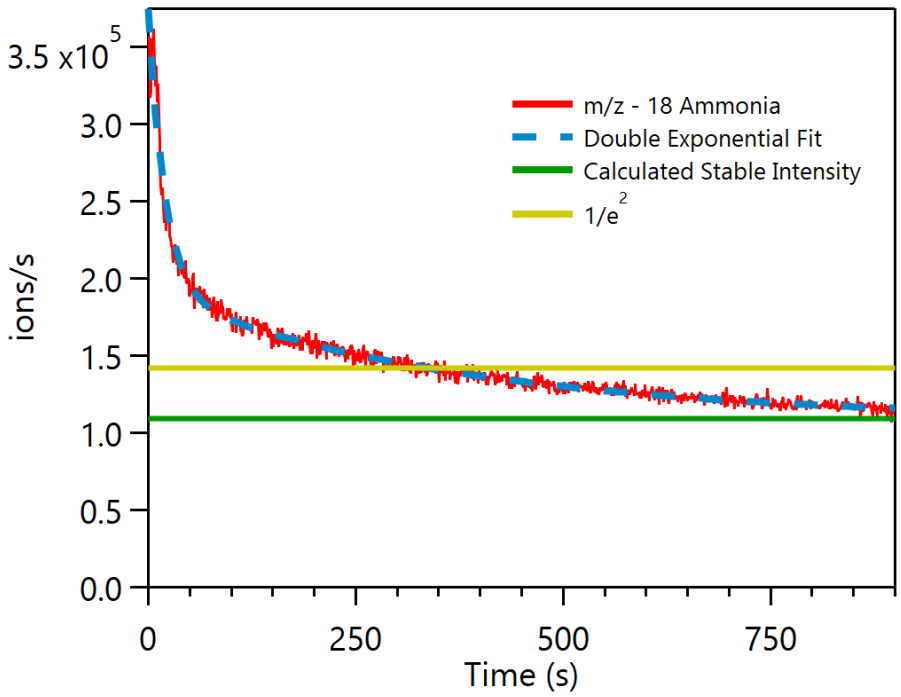

Figure 4.6 Decay curve for m/z 18, NH3, as the vessel sampled by the CI-TOFMS was switched from Carboy 1 to clean zero air.

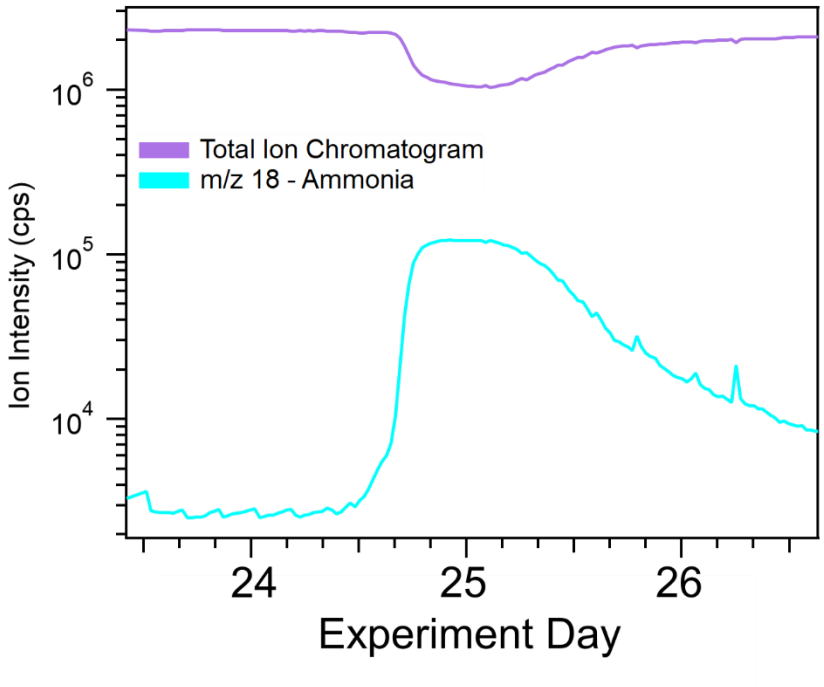

Figure 4.7 Impact of high NH3 concentration on total ion count.

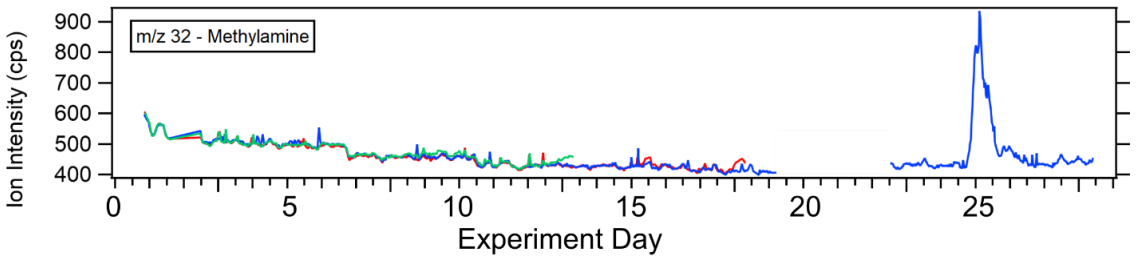

Figure 4.8 Time series ion intensity of m/z 32, methylamine, for carboys 1 (Green), 2 (Red), and 3 (Blue).

4.11 Supplementary tables

Table 4.2 Identifications of ions observed by CI-TOFMS using complementary MS methods: GC/MS and APCI-HRMS. Ammonia and methylamine were identified by process of elimination based on their low mass which limited the number of possible formulae significantly.

CI-TOFMS Unit Mass	Compound Name	GC/MS NIST Match Score	HRMS Mass	Exact Formula Mass	Mass Error (ppm)
18	Ammonia	-	-	-	-
32	Methylamine	-	-	-	-
69	Isoprene	-	69.0698	69.0704	-8.7
70	C_4H_7N	-	-	-	-
87	Isoprenol/Prenol	90/87	87.0802	87.0809	-8.0
109	C_8H_{12}	-	109.1007	109.1017	-9.2
127	Sulcatone	91.5	127.1113	127.1122	-7.1
129	Sulcatol	85.2	129.1272	129.1279	-5.4
137	$C_{10}H_{16}$	-	137.1320	137.1330	-7.3
139	Isophorone	70.8	-	-	-
153	β-Cyclocitral	89.8	-	-	-
193	β-Ionone	86.7	-	-	-

4.12 References

Achyuthan, K. E., Harper, J. C., Manginell, R. P. and Moorman, M. W.: Volatile metabolites emission by in vivo microalgae—an overlooked opportunity?, Metabolites, 7(3), doi:10.3390/metabo7030039, 2017.

Aljawhary, D., Lee, A. K. Y. and Abbatt, J. P. D.: High-resolution chemical ionization mass spectrometry (ToF-CIMS): Application to study SOA composition and processing, Atmos. Meas. Tech., 6(11), 3211–3224, doi:10.5194/amt-6-3211-2013, 2013.

Allen, M. M.: Simple conditions for growth of unicellular blue-green algae on plates, J. Phycol., 4, 1–4, 1968.

Bedrossian, M., Barr, C., Lindensmith, C. A., Nealson, K. and Nadeau, J. L.: Quantifying microorganisms at low concentrations using digital holographic microscopy (DHM), J. Vis. Exp., 2017(129), 1–11, doi:10.3791/56343, 2017.

Cadena-Herrera, D., Esparza-De Lara, J. E., Ramírez-Ibañez, N. D., López-Morales, C. A., Pérez, N. O., Flores-Ortiz, L. F. and Medina-Rivero, E.: Validation of three viable-cell counting methods: Manual, semi-automated, and automated, Biotechnol. Reports, 7, 9–16, doi:10.1016/j.btre.2015.04.004, 2015.

Di Caprio, F.: Methods to quantify biological contaminants in microalgae cultures, Algal Res., 49(March), 101943, doi:10.1016/j.algal.2020.101943, 2020.

Carney, L. T. and Lane, T. W.: Parasites in algae mass culture, Front. Microbiol., 5(JUN), 1–8, doi:10.3389/fmicb.2014.00278, 2014.

Carpenter, L. J., Archer, S. D. and Beale, R.: Ocean-atmosphere trace gas exchange, Chem. Soc. Rev., 41(19), 6473–6506, doi:10.1039/c2cs35121h, 2012.

Christaki, E., Bonos, E., Giannenasa, I. and Florou-Paneria, P.: Functional properties of carotenoids originating from algae, J. Sci. Food Agric., 93(1), 5–11, doi:10.1002/jsfa.5902, 2013.

Day, J. G., Thomas, N. J., Achilles-Day, U. E. M. and Leakey, R. J. G.: Early detection of protozoan grazers in algal biofuel cultures, Bioresour. Technol., 114, 715–719, doi:10.1016/j.biortech.2012.03.015, 2012.

Deore, P., Beardall, J. and Noronha, S.: A perspective on the current status of approaches for early detection of microalgal grazing, J. Appl. Phycol., doi:10.1007/s10811-020-02241-x, 2020.

Facchini, M. C., Decesari, S., Rinaldi, M., Carbone, C., Finessi, E., Mircea, M., Fuzzi, S., Moretti, F., Tagliavini, E., Ceburnis, D. and O'Dowd, C. D.: Important source of marine secondary

organic aerosol from biogenic amines, Environ. Sci. Technol., 42(24), 9116–9121, doi:10.1021/es8018385, 2008.

Fisher, C. L., Lane, P. D., Russell, M., Maddalena, R. and Lane, T. W.: Low molecular weight volatile organic compounds indicate grazing by the marine rotifer brachionus plicatilis on the microalgae microchloropsis salina, Metabolites, 10(9), 1–20, doi:10.3390/metabo10090361, 2020.

Forehead, H. I. and O'Kelly, C. J.: Small doses, big troubles: Modeling growth dynamics of organisms affecting microalgal production cultures in closed photobioreactors, Bioresour. Technol., 129, 329–334, doi:10.1016/j.biortech.2012.11.082, 2013.

Halsey, K. H., Giovannoni, S. J., Graus, M., Zhao, Y., Landry, Z., Thrash, J. C., Vergin, K. L. and de Gouw, J.: Biological cycling of volatile organic carbon by phytoplankton and bacterioplankton, Limnol. Oceanogr., 62(6), 2650–2661, doi:10.1002/lno.10596, 2017.

Harrison, A. G.: Chemical ionization mass spectrometry, 2nd ed., Taylor & Francis, Toronto., 1992.

Kim, M. J., Michaud, J. M., Williams, R., Sherwood, B. P., Pomeroy, R., Azam, F., Burkart, M. and Bertram, T. H.: Bacterial-driven production of nitrates in seawater, Geophys. Res. Lett., 42(2), 1–8, doi:10.1002/2014GL062865., 2015.

Kim, M. J., Novak, G. A., Zoerb, M. C., Yang, M., Blomquist, B. W., Huebert, B. J., Cappa, C. D. and Bertram, T. H.: Air-Sea exchange of biogenic volatile organic compounds and the impact on aerosol particle size distributions, Geophys. Res. Lett., 44(8), 3887–3896, doi:10.1002/2017GL072975, 2017.

Klein-Marcuschamer, D., Chisti, Y., Benemann, J. R. and Lewis, D.: A matter of detail: Assessing the true potential of microalgal biofuels, Biotechnol. Bioeng., 110(9), 2317–2322, doi:10.1002/bit.24967, 2013.

Kroumov, A. D., Módenes, A. N., Trigueros, D. E. G., Espinoza-Quiñones, F. R., Borba, C. E., Scheufele, F. B. and Hinterholz, C. L.: A systems approach for CO2 fixation from flue gas by microalgae—Theory review, Process Biochem., 51(11), 1817–1832, doi:10.1016/j.procbio.2016.05.019, 2016.

Laskin, J., Laskin, A. and Nizkorodov, S. A.: Mass Spectrometry Analysis in Atmospheric Chemistry, Anal. Chem., 90(1), 166–189, doi:10.1021/acs.analchem.7b04249, 2018.

Letcher, P. M., Lopez, S., Schmieder, R., Lee, P. A., Behnke, C., Powell, M. J. and McBride, R. C.: Characterization of Amoeboaphelidium protococcarum, an Algal Parasite New to the Cryptomycota Isolated from an Outdoor Algal Pond Used for the Production of Biofuel, PLoS One, 8(2), doi:10.1371/journal.pone.0056232, 2013.

Liu, X., Deming, B., Pagonis, D., Day, D. A., Palm, B. B., Talukdar, R., Roberts, J. M., Veres, P. R., Krechmer, J. E., Thornton, J. A., De Gouw, J. A., Ziemann, P. J. and Jimenez, J. L.: Effects of gas-wall interactions on measurements of semivolatile compounds and small polar molecules, Atmos. Meas. Tech., 12(6), 3137–3149, doi:10.5194/amt-12-3137-2019, 2019.

Mata, T. M., Martins, A. A. and Caetano, N. S.: Microalgae for biodiesel production and other applications: A review, Renew. Sustain. Energy Rev., 14(1), 217–232, doi:10.1016/j.rser.2009.07.020, 2010.

McBride, R. C., Lopez, S., Meenach, C., Burnett, M., Lee, P. A., Nohilly, F. and Behnke, C.: Contamination Management in Low Cost Open Algae Ponds for Biofuels Production, Ind. Biotechnol., 10(3), 221–227, doi:10.1089/ind.2013.0036, 2014.

Miller, B. R., Weiss, R. F., Salameh, P. K., Tanhua, T., Greally, B. R., Mühle, J. and Simmonds, P. G.: Medusa: A sample preconcentration and GC/MS detector system for in situ measurements of atmospheric trace halocarbons, hydrocarbons, and sulfur compounds, Anal. Chem., 80(5), 1536–1545, doi:10.1021/ac702084k, 2008.

Molazadeh, M., Ahmadzadeh, H., Pourianfar, H. R., Lyon, S. and Rampelotto, P. H.: The use of microalgae for coupling wastewater treatment with CO2 biofixation, Front. Bioeng. Biotechnol., 7, doi:10.3389/fbioe.2019.00042, 2019.

Moreno-Garrido, I. and Cañavate, J. P.: Assessing chemical compounds for controlling predator ciliates in outdoor mass cultures of the green algae Dunaliella salina, Aquac. Eng., 24(2), 107–114, doi:10.1016/S0144-8609(00)00067-4, 2000.

Morono, Y., Terada, T., Masui, N. and Inagaki, F.: Discriminative detection and enumeration of microbial life in marine subsurface sediments, ISME J., 3(5), 503–511, doi:10.1038/ismej.2009.1, 2009.

Pagonis, D., Krechmer, J. E., De Gouw, J., Jimenez, J. L. and Ziemann, P. J.: Effects of gas-wall partitioning in Teflon tubing and instrumentation on time-resolved measurements of gas-phase organic compounds, Atmos. Meas. Tech., 10(12), 4687–4696, doi:10.5194/amt-10-4687-2017, 2017.

Reese, K. L., Fisher, C. L., Lane, P. D., Jaryenneh, J. D., Moorman, M. W., Jones, A. D., Frank, M. and Lane, T. W.: Chemical Profiling of Volatile Organic Compounds in the Headspace of Algal Cultures as Early Biomarkers of Algal Pond Crashes, Sci. Rep., 9(1), 1–10, doi:10.1038/s41598-019-50125-z, 2019.

Richardson, J. W., Johnson, M. D., Zhang, X., Zemke, P., Chen, W. and Hu, Q.: A financial assessment of two alternative cultivation systems and their contributions to algae biofuel economic viability, Algal Res., 4(1), 96–104, doi:10.1016/j.algal.2013.12.003, 2014.

Roveretto, M., Li, M., Hayeck, N., Brüggemann, M., Emmelin, C., Perrier, S. and George, C.: Real-Time Detection of Gas-Phase Organohalogens from Aqueous Photochemistry Using Orbitrap Mass Spectrometry, ACS Earth Sp. Chem., 3(3), 329–334, doi:10.1021/acsearthspacechem.8b00209, 2019.

Ryan, C. G., Clayton, E., Griffin, W. L., Sie, S. H. and Cousens, D. R.: SNIP, a statistics-sensitive background treatment for the quantitative analysis of PIXE spectra in geoscience applications, Nucl. Inst. Methods Phys. Res. B, 34(3), 396–402, doi:10.1016/0168-583X(88)90063-8, 1988.

Schoepp, N. G., Stewart, R. L., Sun, V., Quigley, A. J., Mendola, D., Mayfield, S. P. and Burkart, M. D.: System and method for research-scale outdoor production of microalgae and cyanobacteria, Bioresour. Technol., 166, 273–281, doi:10.1016/j.biortech.2014.05.046, 2014.

Schoepp, N. G., Wong, W., Mayfield, S. P. and Burkart, M. D.: Bulk solvent extraction of biomass slurries using a lipid trap, RSC Adv., 5(70), 57038–57044, doi:10.1039/c5ra11444f, 2015.

Steiner, M. and Hartmann, T.: Über Vorkommen und Verbreitung flüchtiger Amine bei Meeresalgen, Planta, 79(2), 113–121, doi:10.1007/BF00390154, 1968.

Subramanian, G. and Shanmugasundaram, S.: Uninduced ammonia release by the nitrogen-fixing cyanobacterium Anabaena, FEMS Microbiol. Lett., 37(2), 151–154, doi:10.1111/j.1574-6968.1986.tb01784.x, 1986.

Taton, A., Lis, E., Adin, D. M., Dong, G., Cookson, S., Kay, S. A., Golden, S. S. and Golden, J. W.: Gene transfer in Leptolyngbya sp. strain BL0902, a cyanobacterium suitable for production of biomass and bioproducts, PLoS One, 7(1), doi:10.1371/journal.pone.0030901, 2012.

Thomas, P. K., Dunn, G. P., Passero, M. and Feris, K. P.: Free ammonia offers algal crop protection from predators in dairy wastewater and ammonium-rich media, Bioresour. Technol., 243, 724–730, doi:10.1016/j.biortech.2017.07.008, 2017.

Wenig, P. and Odermatt, J.: OpenChrom: A cross-platform open source software for the mass spectrometric analysis of chromatographic data, BMC Bioinformatics, 11, doi:10.1186/1471-2105-11-405, 2010.

Yu, H. and Lee, S. H.: Chemical ionisation mass spectrometry for the measurement of atmospheric amines, Environ. Chem., 9(3), 190–201, doi:10.1071/EN12020, 2012.

Chapter 5. Liquid Sampling-Atmospheric Pressure Glow Discharge Ionization as a Technique for the Characterization of Salt-Containing Organic Samples

5.1 Abstract

Typical ionization techniques used for mass spectrometry (MS) analysis face challenges when trying to analyze organic species in a high salt environment. Here, we present results using a recently developed ionization source, liquid sampling-atmospheric pressure glow discharge (LS-APGD), for marine-relevant salt-containing organic samples. Using two representative sample types, a triglyceride mixture and dissolved organic matter, this method is compared to traditional electrospray ionization (ESI) under saline and neat conditions. LS-APGD produced equal or higher (15%+) ion intensities than ESI for both salt-containing and neat samples, although important differences linked with adduct formation in high salt conditions explain the molecular species observed. For all sample types, LS-APGD observed a higher diversity of molecules under optimized settings (0.25 mm electrode spacing at 20 mA) compared to traditional ESI. Furthermore, because the LS-APGD source ionizes molecular species in a ~1 mm3 volume plasma using a low-power source, there is the potential for this method to be applied in field studies, eliminating de-salting procedures which can be time-consuming and non-ideal for low concentration species.

5.2 Introduction

Analysis of complex environmental samples using mass spectrometry represents a challenging problem due to low concentrations of target analyte(s), chemical lability, and the presence of matrix materials such as salts.(Nebbioso and Piccolo, 2013) Despite these challenges, numerous improvements which utilize unique methods for sample preparation, introduction, and data analysis have been made over the past several decades.(Artifon et al., 2019) Samples

containing dissolved organic matter (DOM), an abundant component in terrestrial and marine environments and operationally defined as molecular species that passes through a 0.45 um filter (Thurman, 1985), can contain over 10,000 different molecular signatures (Nebbioso and Piccolo, 2013), most of which are not fully characterized. Even selectively filtered samples from field studies aiming to look at specific classes of molecules, fatty acids or lipids at the ocean-air interface for example, can contain hundreds of unique structures as well as salts.(Kennicutt and Jeffrey, 1981) Besides the complex organic nature of environmental samples, the interfering presence of salt is a limitation for in-depth mass spectrometry analysis of samples such as marine-DOM.

Electrospray ionization (ESI) is the predominant ionization method used in high resolution mass spectrometry for environmental samples because it can ionize a wide range of molecules with respect to polarity and molecular weight (Banerjee and Mazumdar, 2012). However, sea salts nominally at ~0.6M NaCl, can greatly affect signal intensity even with concentrations below 0.1 mM (Constantopoulos et al., 1999). There are a few modified ESI methods that can deal with elevated salt concentrations - however, these modified methods are specific to protein relevant systems and often result in either low ion signal or high sample consumption rates (Chang et al., 2002; Karki et al., 2018; Mandal et al., 2010). Other methods exist to circumvent this salt issue entirely, such as using solid phase extraction (SPE) to collect marine-dissolved organic matter (m-DOM or sometimes known as SPE-DOM), described in detail by Dittmar and coworkers in 2008 (Dittmar et al., 2008). However, concentrating and removing salt from natural organic matter samples (via ultrafiltration, SPE, reverse osmosis, etc.) can result in recovery issues depending on the type of sample (Guo and Santschi, 1996; Simjouw et al., 2005) and possibly alter the chemical nature of the sample (Kruger et al., 2011). Thus, there is a need to analyze complex salt-containing environmental samples in both the field and lab without extensive pre-processing. Herein we have

applied a new ionization method for the analysis of complex marine samples containing high concentrations of salts, liquid sampling-atmospheric pressure glow discharge (LS-APGD). This method shows high sensitivity, is field-ready, and leads to reasonably low levels of molecular fragmentation.

The LS-APGD ion source used in this study was purchased from Clemson University and has been described previously by Marcus and coworkers, (Marcus et al., 2011) and briefly, the source operates similarly to a traditional atmospheric pressure chemical ionization (APCI) source using a corona discharge. However, in this case, a ~1 mm^3 helium-based plasma is formed at the end of the capillary where the liquid sample would normally be vaporized before contact with the APCI corona. This plasma assists in the vaporization of the liquid samples into ionized gas phase molecules. The relatively low power (maximum of 60 mA and 500 V) of the plasma-forming electrode, compared to common 3-6 kV corona or glow discharge sources, enables practical requirements for field deployment.

Initially, LS-APGD was developed for elemental and isotopic analysis, where it produces ng/L detection limits of select metals such as Cs and U, and μg/L detection for Fe, Ni, Cu, In, Cd, and Pb (Hoegg et al., 2016; Marcus et al., 2011; Quarles et al., 2012). The simple and field-ready LS-APGD has detection limits that are semi-competitive with ICP-MS. Because the source is optimized for aqueous salts and metals, samples with ocean salinity levels would not be a large issue as it is with other ionization sources. With such a low power plasma, it has already been shown that LS-APGD can analyze intact organic species, therefore the analysis of organics in seawater is possible (Zhang and Kenneth Marcus, 2016). Thus, we show here the capabilities of LS-APGD for the analysis of samples that are expected in a marine environment, with and without salt, are demonstrated through investigations of three distinct sample types, a simple well-

characterized triglyceride mixture (C8-C16), and highly complex samples of Suwannee river fulvic acid (SRFA) and m-DOM. LS-APGD and ESI are contrasted to identify the spectral features acquired for each sample type.

5.3 Materials and methods

An initial model sample was prepared for this study. A certified triglyceride reference mixture was purchased from Sigma Aldrich (Supelco). This reference mixture is composed of five saturated triglycerides of chain length C8-16 at approximately equal mass fractions. The mixture was dissolved in acetonitrile and all analyzed samples were run at a concentration of 9 mg/L. Samples of triglyceride mixture and environmental mimics were prepared in saltless or 0.20 M NaCl in 1:2 H_2O/MeOH and teed at 15 μL/min into an isocratic stream of 1:2 H_2O/MeOH + 0.1% Formic Acid with 1:200 Ultramark calibration mix also flowing at 15 μL/min using the pump, gas controller, and high voltage assembly (Fusion 100T, Chemyx, Stafford TX). The LS-APGD spectra were collected at a range of probe conditions from 20-30 mA and an electrode spacing 0.25-1.5 mm past the plasma ignition point (SI Scheme 1). Sample flow rates were chosen to maximize stability of the plasma and reduce deposition of involatile material on the inlet. Mass spectral data were extracted using Thermo XCalibur data analysis software and imported into R-Studio or Igor (Wavemetrics) for further analysis.

5.3.1 Ultra-High Resolution Mass Spectrometry

To compare the LS-APGD source to a universal ionization method, a heated electrospray ionization-linear ion trap Orbitrap high-resolution mass spectrometer (HESI-LIT-Orbitrap, Thermo Fisher Scientific) was used for this study. Samples were directly injected into the electrospray source at 5-15 μL/min. Peaks were detected and analyzed in positive mode at a capillary voltage set to 2.8 kV, where the capillary was maintained at a temperature of 325 °C.

HESI gases (arbitrary units) were set to: sheath at 30, auxiliary at 10, and sweep at 0. The HESI-LIT-Orbitrap was always calibrated before both HESI and LS-APGD configurations using a calibration mix (Pierce ESI Ion Calibration Solutions, Thermo Fisher Scientific) to maintain mass accuracy below 2 ppm. During data acquisition, the Orbitrap mass range is set to m/z 50-2000 with the mass resolution set at 120,000. All solutions in this study contained 0.1% formic acid. Mass error drift was prevented by mass locking the data acquisition to persistent signals from the calibration solutions, giving a range from m/z 195 to 1250.

Using the Orbitrap, in both HESI and LS-APGD modes, masses of thousands to tens of thousands of unique molecular signatures were observed for the complex mixtures. Molecular formula assignments were acquired using the Xcalibur Thermo Fisher Scientific software. The following element ranges were used: ^{12}C, 0−100; ^{1}H, 0−200; ^{16}O, 0− 50; ^{14}N, 0−5; ^{32}S, 0−2; and ^{23}Na, 0−1. These element ranges were chosen based on past studies attempts on mass spectral characterization of highly complex organic samples (Koch et al., 2005; Stenson et al., 2003). Formulae with an O/C ratio below 0 or greater than 2.5, as well as a relative double bond equivalence values above 25 or below zero, were excluded. In addition, formulas were required to be below a mass error of 2 ppm and have a relative intensity greater than 0.1% of the base peak. Based on these strict heuristic filtering rules and depending on the sample, only between ~30-60% of the ions detected during data acquisition were assigned a molecular formula.

Two environmentally complex samples were used in this study to test the LS-APGD ability to ionize complex systems: Suwannee River fulvic acid (Standard III, International Humic Substances Society) and m-DOM (collected from Scripps Pier, La Jolla). The collection and purification of m-DOM in this study is described by Dittmar and coworkers.(Dittmar et al., 2008) Briefly, coastal ocean water was passed through a 50 micron mesh is collected from the pier.

Nutrients, f/2 algae growth medium (Proline, Aquatic Eco-Systems) as well as solutions of sodium metasilicate, were added to the water. The m-DOM was collected after the subsequent bloom and senescent-phase of phytoplankton over 1-3 weeks. The water was then passed through a series of filters: 10, 0.7, and 0.2 micron pore sizes. The samples to be extracted were acidified to a pH value at or close to 2.0 using 1 M HCl (Sigma Aldrich). The acidified solution was gravity filtered through a solid phase extraction column (Bond Elut PPL, Agilent) at no more than 5 mL/min or about 2 drops per second. The column was then washed and eluted using methanol and the resulting yellow/orange solution was quickly (under an hour) dried using a rotary evaporator. All glassware used was combusted at 500℃ for 8 hours to remove trace organics before use. The solid sample was stored at -21°C under nitrogen.

5.4 Results and discussion

For the majority of measurements shown in this work, salt concentrations were kept at 0.2 M or lower. For marine samples, this was done by simply diluting with methanol. A few measurements on samples containing up to 0.6 M salt (seawater salinity) were performed, however significant deposition of material on the MS inlet capillary prevented extended operation before cleaning was required. Further improvements of the LS-APGD source to reduce salt buildup, such as positioning the LS-APGD capillary orthogonal to the MS inlet or the introduction of an auxiliary sweep gas are warranted. Furthermore, it is recommended that upstream instrument orifices and ion optics such as transfer capillaries and S-lenses be cleaned more frequently after sustained periods of analysis of salt-containing samples.

5.4.1 Analysis of a Triglyceride Reference Material Mixture

Normalized averaged mass spectra of the triglyceride mixture by electrospray and LS-APGD are shown in Figure 5.1 at 100 mM NaCl. Further analysis conditions of non-saline

triglyceride mixtures by LS-APGD and ESI are shown in 5.6. Both the neat ESI and LS-APGD analysis preferentially formed cationized triglyceride ions adducted with NH_4^+ (Figure 5.6a,b). However, at 0.1 M NaCl for the LS-APGD (Figure 5.6c), the prevalence of sodium adducted species was significantly higher in proportion to the ammoniated ion. This effect is driven by the preferential binding of sodium over ammonium to triglycerides previously observed in ESI mass spectrometric studies in lipidomics (Adams and Gross, 1986; Hsu and Turk, 2010). For ESI at 0.1 M NaCl, the production of NaCl ion clusters completely eclipses the production of the sodiated triglyceride cations (Figure 5.1a) and is not effective at ionizing triglycerides above 1 mM (Figure 5.6c) (Hao et al., 2001). Triglyceride precursor ion counts for LS-APGD were equal to or 10-20% greater than those produced by ESI, suggesting that the ionization technique is comparably sensitive for the sample type. (Figure 5.1a, b; Figure 5.6 a, b, c) Furthermore, LS-APGD was more capable of ionizing higher-mass triglycerides in greater proportion to the total ion count than ESI (Figure 5.1b). Notably, significant differences in the ratio of quasi-molecular ions to their primary decomposition products (M-RCOO-) between neat and saline conditions stimulated an investigation to understand the influence of salinity and LS-APGD conditions (current and electrode distance) on the production and fragmentation of triglyceride species.

Here we define the fragmentation ratio from the measured ion intensity of triglyceride precursor and product species in Equation 1:

$$F_{Triglyceride} = \frac{[TAG+Na]_I+[TAG+NH_4]_I}{[TAG-RCOO^-]_I} \qquad (1)$$

Where I is the average raw ion intensity of each species and the selection of the diglyceride fragment of the ammoniated and sodiated species is based on the observation that very little other fragmentation products are observed in the mass spectrum. Observations of diglyceride fragments from both collisionally activated $-Na^+$, $-NH_4^+$, and protonated triglycerides in the literature have

also been commonly identified (Asbury et al., 2000; Kalo et al., 2006; Rezanka and Sigler, 2007). A list of the selected ions can be found in Table 5.1 of the supplementary information.

Figures 5.7 a-e explore the influence of discharge current and electrode distance under saline conditions. Various tradeoffs were observed in the production of precursor cations, with higher ratios of precursor to product ion at further electrode distances (Figure 5.8). However, for the current parameters studied, higher electrode currents favored the production of precursor cations and decreased fragmentation (Figure 5.7). Differences in fragmentation ratio with triglyceride carbon tail chain length (Figure 5.8a) are likely due to general reduced stability with increased length, a common feature in organic species. These results contrast recent investigations of LS-APGD parameters for analysis of caffeine, where electrode distance showed little effect on fragmentation conditions (Zhang and Kenneth Marcus, 2016). In addition, for the present investigations with triglycerides there is a general increase in fragmentation ratio with discharge current observed. In conclusion, it is further suggested that ionization behavior, especially fragmentation, in LS-APGD requires a compound-class dependent investigation to optimize analysis conditions.

Interestingly, LS-APGD fragmentation ratios between the neat and saline samples were significantly different at the same LS-APGD conditions, with reduced fragmentation in the saline samples. To explore this behavior further, triglyceride mixture samples were analyzed over 5 orders of magnitude of [NaCl]. The resultant fragmentation ratios are shown in Figure 5.2. Fragmentation ratios at 0.01 mM NaCl are below 1, indicating the majority of all triglycerides under these conditions are fragmented to diglyceride or other fragments, barring differences in ion transfer efficiency. In contrast, at 1 mM, the fragmentation ratio favors the production of the sodiated cations over fragmentation. This observation is attributed to the altered adduct distribution

in the saline analysis, which is supported by studies of collisionally induced dissociation of triglyceride species (Duffin et al., 1991).

It has been observed that the generation of products via collisionally induced dissociation requires significantly larger collisional energies for sodiated triglycerides over ammoniated triglycerides, likely due to strong coordination between the Na^+ cation and the electron donating groups on the triglycerides (Adams and Gross, 1986). Thus, it is proposed that in-source adduct assisted stabilization of the ionized triglyceride significantly enhanced the persistence of the psuedomolecular ion from thermal decomposition in the LS-APGD source. In support of this hypothesis, Figure 5.9 shows the ratio of sodiated to ammoniated cations over varying NaCl concentrations, indicating a significant shift in adduct distribution towards sodium with increasing [NaCl]. This trend is driven primarily by increases in the production of sodiated molecular ions as opposed to a decrease in ammoniated precursor species, as evidenced in Figure 5.10 a,b where sodiated species increase with added [NaCl] and ammoniated species remain relatively constant. Curiously, the trends in both the fragmentation and adduct ratios reflect different dependencies on salt concentration. It is further hypothesized that this effect is caused by the reduction of excited, but unionized triglyceride species at increasing salt concentrations as they are preferentially sodiated. Unfortunately, production of protonated triglyceride species was not particularly effective and cannot be used to verify this hypothesis further. This result adds interesting detail to the aspects of salt-containing analysis as the alteration of the overall adduct state may enhance, or possibly hinder the observation of intended species through changes in fragmentation. Although changes in adduct state with varying salinity add interesting features and detail to LS-APGD that must be considered, the source successfully analyzes triglycerides in the presence of high salt concentration in comparison to ESI where salts render the spectra unusable.

5.4.2 Complex Environmental Samples

DOM in the Earth's oceans is the single largest pool of reduced carbon.(Hansell, 2013) Complex DOM samples are notoriously difficult to characterize and therefore a suite of instrumental techniques has been developed (Nebbioso and Piccolo, 2013). This study aims to provide a possible alternative to the current approaches used historically for DOM collection, extraction, and analysis. Since m-DOM is particularly understudied due to its relatively low concentration in the ocean (~ 1 mg/L) and high concentration of salts, it was selected as a model system to be tested by this new approach in this study.

Since the composition of DOM and humic like substances can change significantly based on location and/or time (D'Andrilli et al., 2015), SRFA was used as a standard in this study. SRFA and Suwannee River DOM have been extensively studied over the past two decades (Stenson et al., 2003). Though much of the identity of species in terrestrial DOM remains elusive, this system provided a reasonable benchmark for LS-APGD for comparison to other ionization techniques.

The electrode distance and plasma current in the LS-APGD have a significant impact on the ability to ionize species in the SRFA sample. Figure 5.3 shows that the lowest current and shortest electrode distances result in the most similar spectral characteristics between neat and saline samples. This is largely attributed to the fact that the smaller and weaker plasma results in softer ionization. Comparisons between salt-containing and salt-free samples in LS-APGD indicate that the incidence of Na^+ adducts increases by 15% or more depending on the LS-APGD source parameters such as electrode distance and current, indicating that these effects must be accounted for in data analyses of salt-containing samples. Notably, fragmentation of organic species (most commonly $C_9H_7^+$ and $C_{10}H_8^+$) was prevalent in both salt-containing and salt-free samples, a drawback to the technique when the composition of the sample is mostly unknown.

In Figures 5.3a and 5.3b, the LS-APGD ionization of the SRFA, both with and without salt, shows good agreement when compared to ESI. However, in Figure 5.3c, a notable difference in the O/C ratio is observed, where LS-APGD analysis of the SRFA sample consistently measures a lower O/C value (between 0.20 and 0.33). In this study, ESI of SRFA produced an O/C ratio of about 0.38, which is within the range of literature values of 0.3 to 0.6 (Kovács et al., 2010; Stenson et al., 2003). The observations of a lower O/C ratio in the LS-APGD experiment is attributed to the source more efficiently ionizing non-polar or low-polarity organics compared to ESI, comparable to a corona-based ionization source such as APCI. This finding makes LS-APGD an attractive option for studying complex organic samples due to its apparently wide range of potential species, polar and nonpolar, to be ionized. A more detailed comparison of SRFA molecular composition by LS-APGD and ESI is planned for a future study.

A sample of m-DOM was extracted from seawater collected off Scripps Pier in La Jolla, California. The m-DOM was analyzed with both heated-ESI and the LS-APGD ion sources with direct infusion at 5 μL/min and 15 μl/min respectively. Sample collection was relatively fast, in part due to the high throughput of the Orbitrap, resulting in sample consumption less than 60 uL for the LS-APGD.

The ESI and LS-APGD mass spectra of non-salt containing m-DOM were similar in overall spectral range from 150-600 m/z (Figure 5.11), with the LS-APGD spectra differing due to the appearance of aforementioned ion fragmentation signatures as well as a factor of ten increase in total ion intensity. Adding 50 mM of NaCl to the m-DOM sample, the ESI shows a vastly different spectrum compared to the no-salt spectra, with multiple groups of peaks separated by 23 m/z units due to the formation of a large number of sodium adducts. Figure 5.4a shows the small overlap in the no-salt and salt-containing m-DOM (less than 20%) analyzed by ESI in a Van Krevelen

diagram (Kim et al., 2003). Conversely, Figure 5.4b shows significant overlap between the no-salt and salt containing m-DOM when ionizing with the LS-APGD (above 80%). There is also a significant increase in identified features (such as condensed aromatics, shown below 0.25 O/C ratio and below 1.25 H/C ratio) in the LS-APGD mass spectra compared to the ESI, possibly in part due to fragmentation, but more likely a result of: 1) LS-APGD being able to ionize non-polar compounds more efficiently than ESI and 2) an increase in total ion signal, thus increasing sensitivity for a wider range of low concentration compounds. Comparisons of unique molecular signatures detected using traditional ESI and LS-APGD show that around 33% of exact masses (including adducts) found in ESI were also detected using the LS-APGD (Figure 5.12).

The ability of LS-APGD to analyze organics in complex matrices was further demonstrated by directly measuring seawater acquired during a phytoplankton bloom with no pre-concentration or extraction step (Figure 5.5). This experiment cannot be compared to traditional ESI mass spectrometry due to the high amount of salt clogging the ESI probe tip and rendering it unusable. The spectrum is composed of many spectral envelopes, similar to those observed in ESI Fourier Transform ion cyclotron resonance mass spectra using the PPL SPE method and contains over 7,000 unique masses (Koch et al., 2005; Kovács et al., 2010). To our knowledge, this is the first full-mass spectrum of DOM in pure seawater without any sample preparation required.

5.5 Conclusions

In this study, liquid sampling-atmospheric pressure glow discharge ionization has been shown to ionize complex organic samples successfully in the presence of environmentally relevant salt concentrations. Optimization of the ionization source, using a triglyceride mixture, SRFA, and mDOM led to the conclusion that the operational conditions for the analysis of marine relevant organics depend on sample type and need to be optimized on a case-by-case basis. Mass spectra

of environmentally complex compounds (humics, triglycerides, etc), in the presence of salt, produced more informative ion signals via LS-APGD in comparison to ESI. Such characterization was based on the comparison of the diglyceride:triglyceride fragmentation ratios as well as the ensemble metrics concerning the spectra of SRFA. Notably, the presence of salts can significantly alter the fraction of adducts which may hinder, or possibly assist fragmentation depending on the stability of the coordinated ion complex. For LS-APGD, which has been shown to fragment some organic species, high salinity analysis may enhance sensitivity to the molecular ion. Additionally, changes in the fragmentation patterns due to adducts forming in LS-APGD indicate the need for salinity-dependent calibrations when quantitatively analyzing and comparing samples that have varying salt concentrations.

Preliminary analysis of coastal seawater and m-DOM using LS-APGD points to interesting possibilities for compositional analysis, providing an avenue for field analysis of these complex systems. More work on identifying these species is planned for a future study. Besides being able to analyze discrete complex environmental samples, the LS-APGD has the potential to be used for real-time measurements of aqueous systems in the presence of salts to capture temporal changes in chemistry. Future work using LS-APGD and salt-containing samples will aim to investigate its potential for ionizing sea spray aerosol - where organic fractions can reach up to 80% by mass and salt concentrations can exceed 10 M depending on the size of the aerosol particle (Bertram et al., 2018). The ability of LS-APGD Orbitrap mass spectrometry to successfully ionize m-DOM in seawater without any sample preparation has far-reaching implications for analyzing m-DOM in the future – where using direct analysis techniques, without inadvertent sample modification, will lead to a more complete characterization of a complex and important component in the marine environment.

5.6 Acknowledgements

The authors gratefully acknowledge the Marcus Research Group from Clemson University for their support and assistance with the installation of the ionization source and pump assembly. We acknowledge the support of the National Science Foundation through the Centers of Chemical Innovation Program via the Center for Aerosol Impacts on Chemistry of the Environment (CHE-1801971) and the National Science Foundation Graduate Research Fellowship Program (DGE1650112). We also appreciate the support from Dr. Neal Arakawa at the Environmental Complex Analysis Laboratory (ECAL) during this study.

Chapter 5, in full, is a reprint of material that has been published in Analytical Chemistry. Alves, M.R., Sauer, J.S., Prather, K.A., Grassian, V.H., Wilkins, C.L. (2020). "Liquid Sampling-Atmospheric Pressure Glow Discharge Ionization as a Technique for the Characterization of Salt-Containing Organic Samples." Analytical Chemistry (2020) Michael Alves and the dissertation author are the primary investigators and author of this work.

5.7 Figures

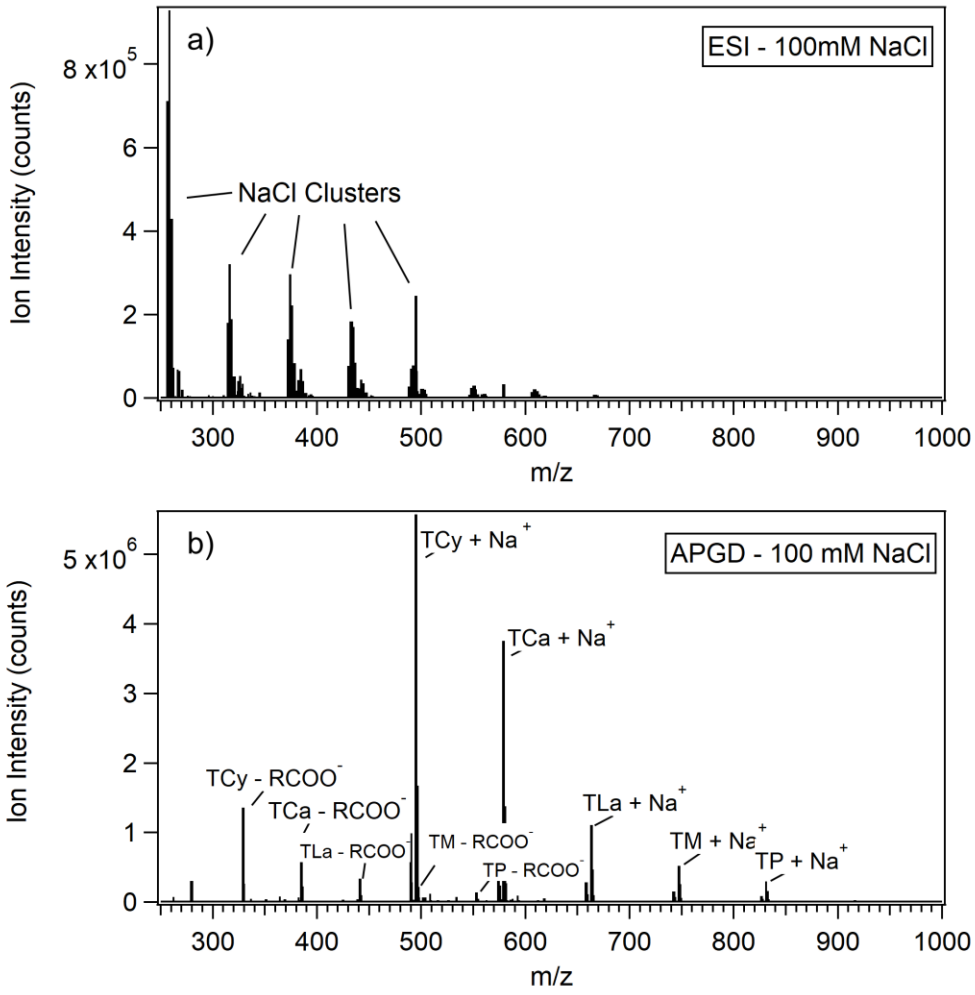

Figure 5.1. Averaged mass spectra obtained from HRMS analysis of triglyceride mixture in 100 mM NaCl by ESI (a) and LS-APGD (b).

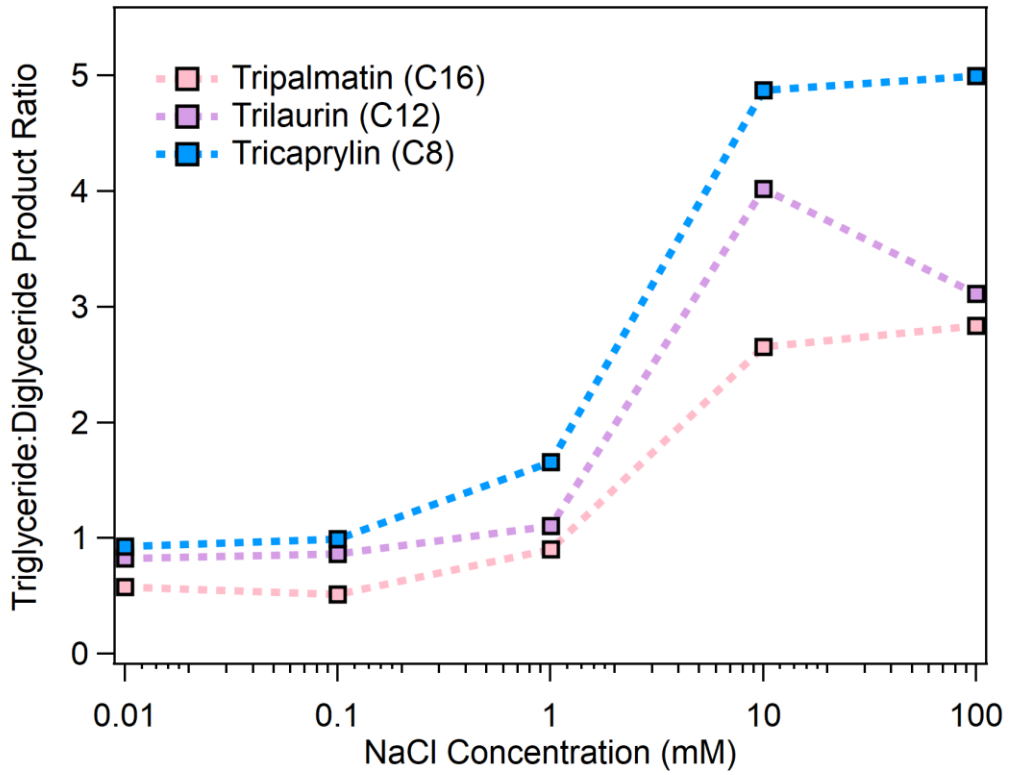

Figure 5.2. LS-APGD Triglyceride:diglyceride fragmentation ratios from 0.01-100mM for triglyceride mixture samples at constant electrode distance (0.5 mm) and discharge current (30 mA).

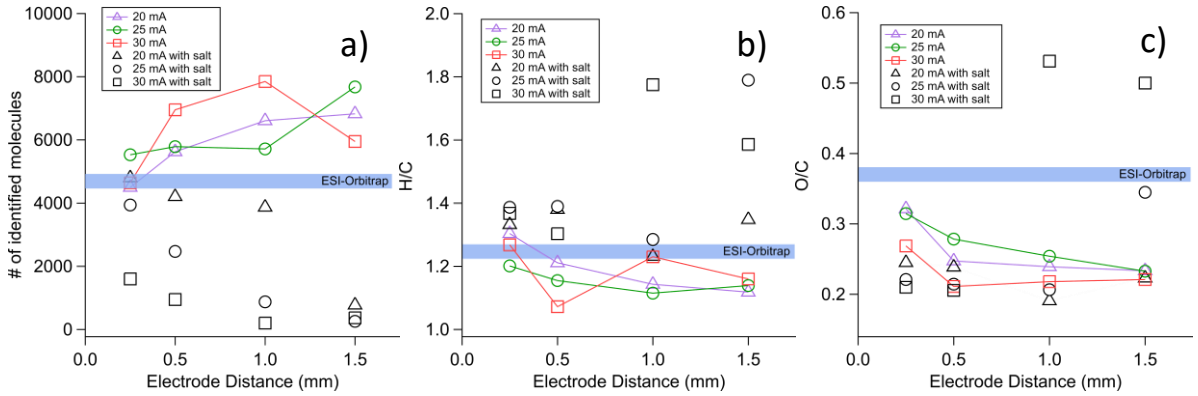

Figure 5.3. HRMS analysis of SRFA, with (black) and without salt (colored), at various electrode currents and positions with corresponding ESI values analyzed using SRFA (no salt) at the same concentration. Relationships shown between: (a) Number of identified molecules averaged mass spectra; (b) hydrogen:carbon ratios and; (c) oxygen:carbon ratios.

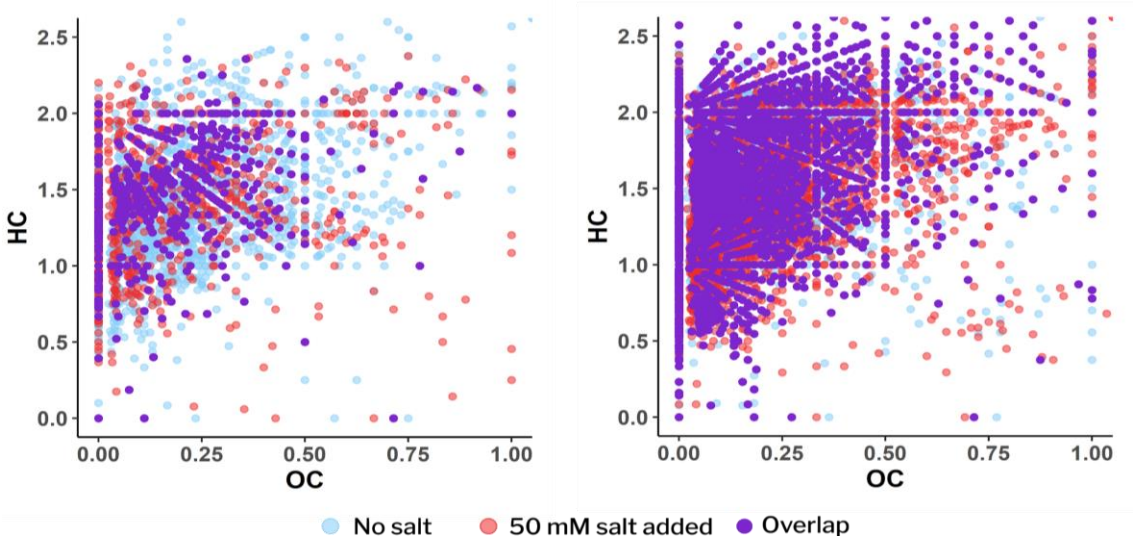

Figure 5.4. Van Krevelen diagrams of m-DOM spectra showing oxygen:carbon (OC) and hydrogen:carbon (HC) ratios, measured by (a) traditional ESI and (b) LS-APGD. A comparison is shown for spectra obtained with (50 mM added NaCl) salt (red circles) and without salt (light blue circles), where the overlap of elemental compositions is also shown (purple circles).

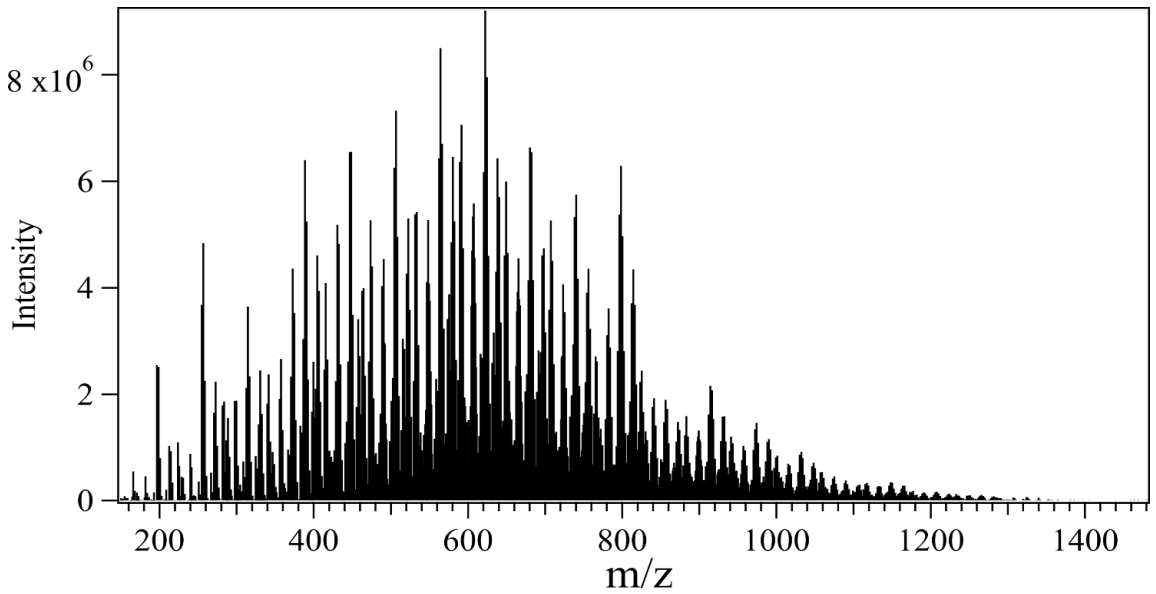

Figure 5.5. High resolution mass spectra of pure bloom coastal seawater obtained by LS-APGD Orbitrap mass spectrometry.

5.8 Supplementary figures and tables

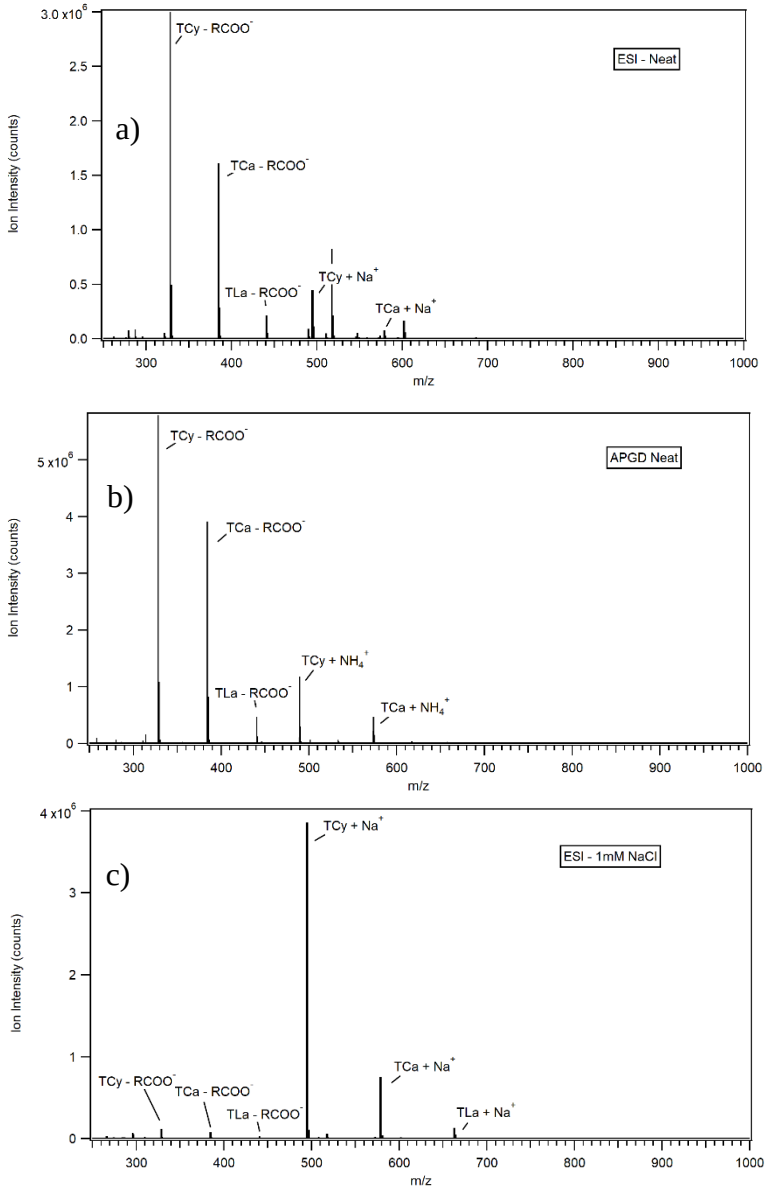

Figure 5.6. Triglyceride mixture analysis for neat ESI (a), APGD (b), and ESI at 1mM NaCl (c)

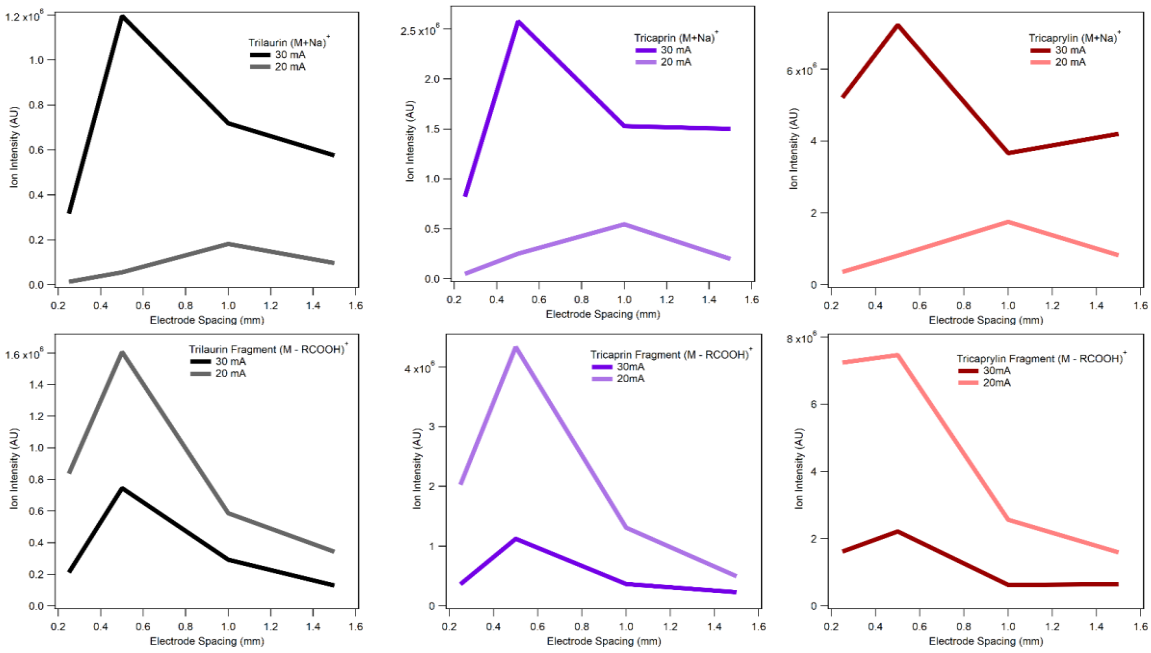

Figure 5.7. Ion intensities for select triglyceride species and primary diglyceride fragments for varying APGD electrode current and electrode spacing conditions (Saline 0.1 M NaCl)

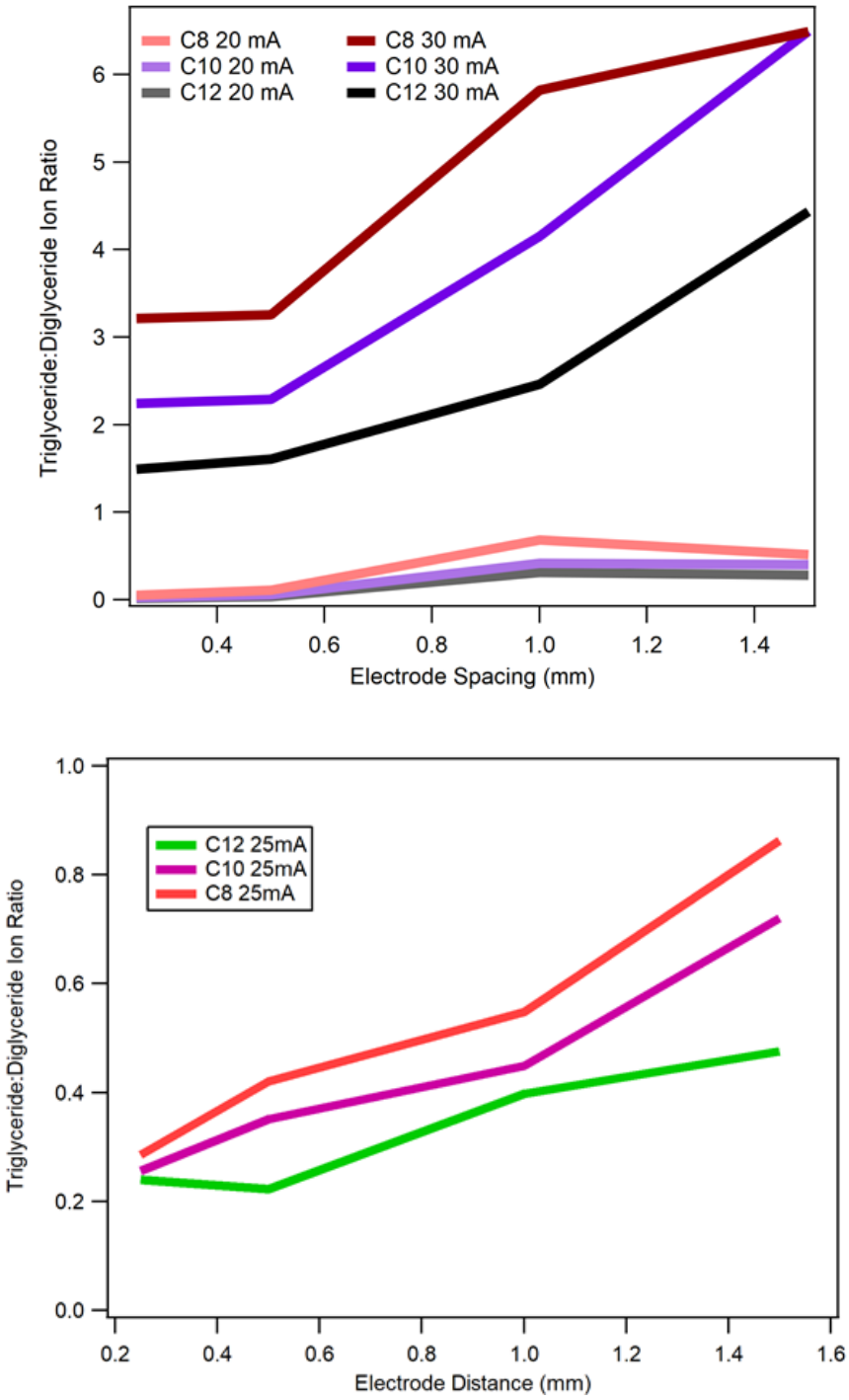

Figure 5.8. Triglyceride:Diglyceride fragmentation ratios obtained by LS-APGD for saline (0.1M NaCl) (top) and neat (bottom) analysis conditions

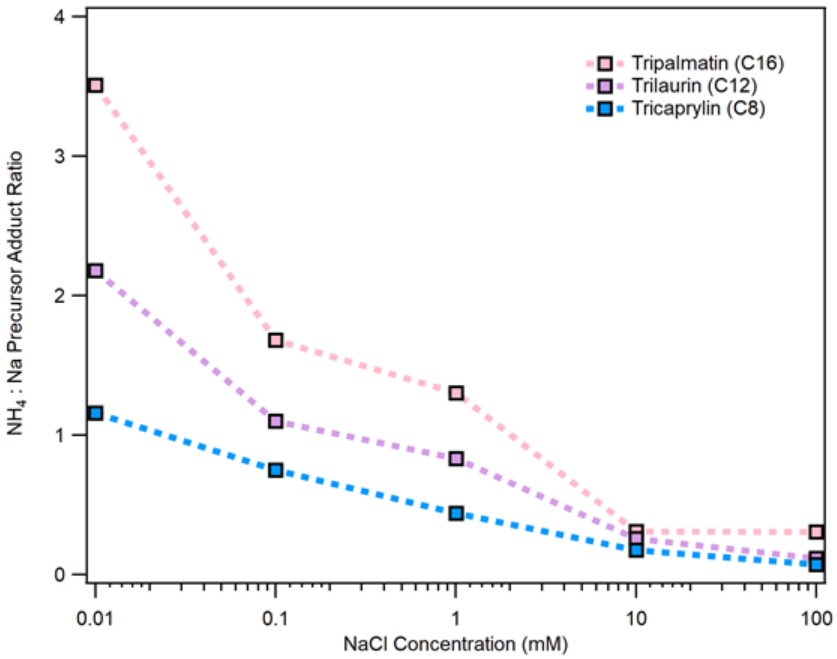

Figure 5.9. Ammoniated to sodiated triglyceride ratio over varying NaCl concentrations (30mA, 0.5mm electrode spacing)

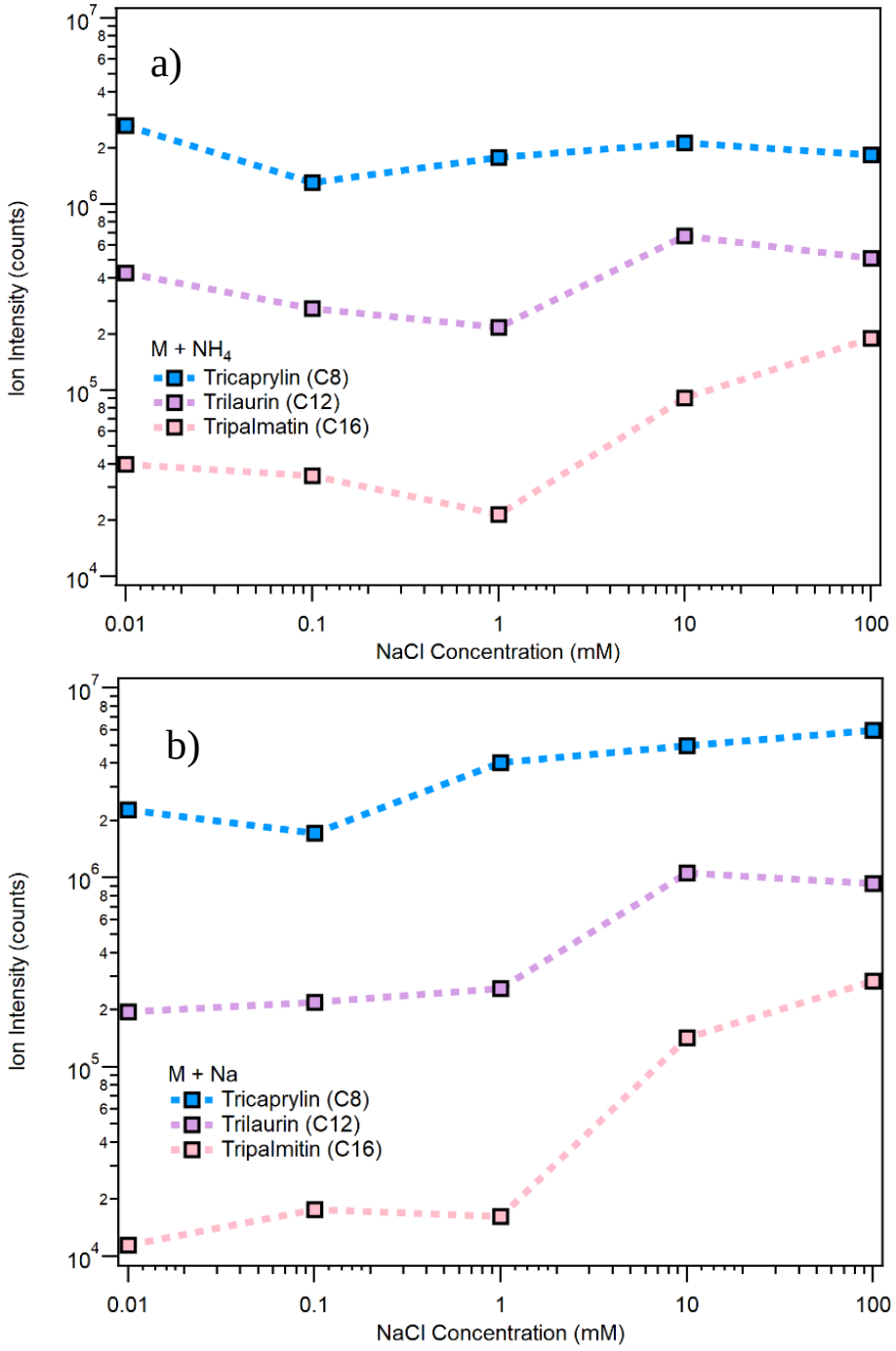

Figure 5.10. Pseudomolecular ion intensities across NaCl concentration range for sodiated (a) and ammoniated (b) triglycerides

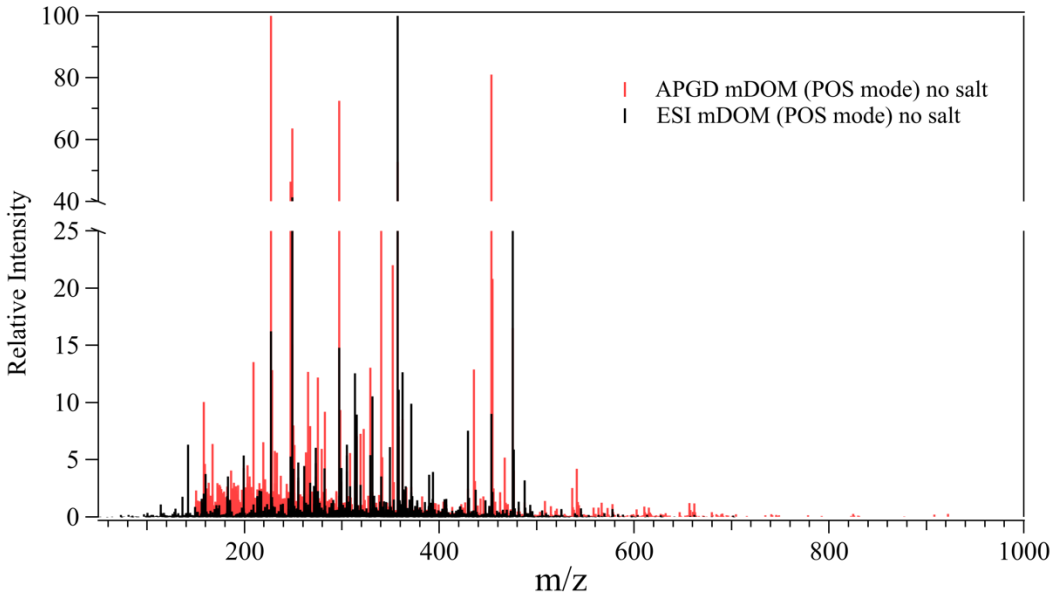

Figure 5.11. High resolution mass spectral data, in positive mode, comparing data collected from ionized marine dissolved organic matter using APGD (red) and traditional ESI (black).

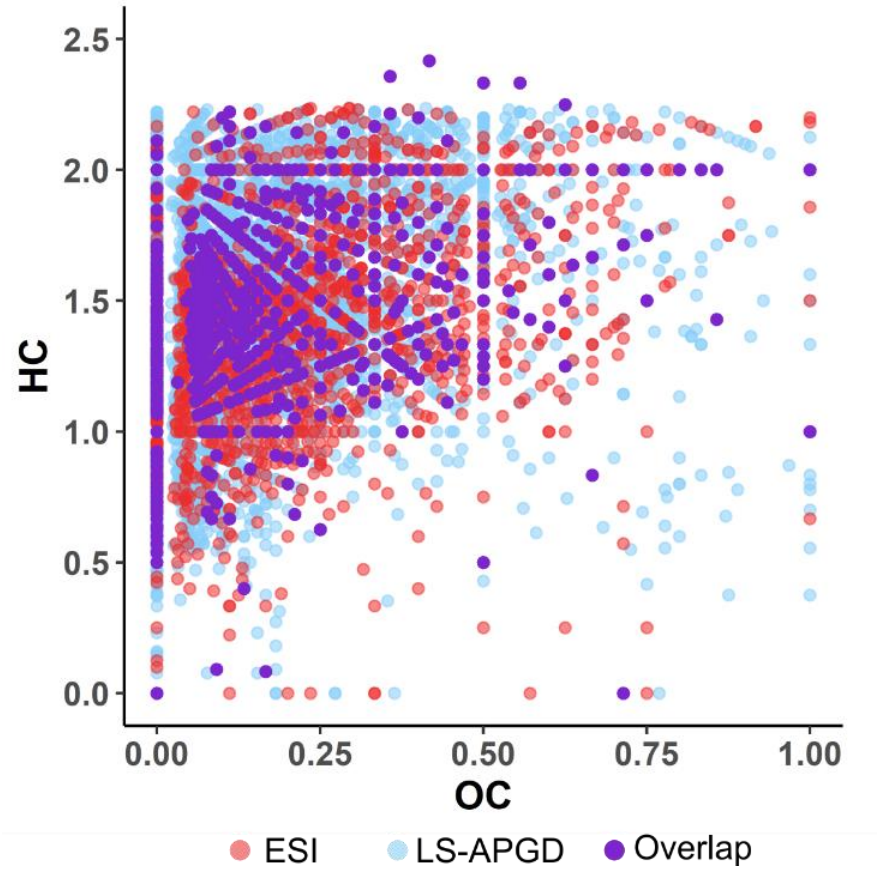

Figure 5.12. Van Krevelen analysis of high resolution Orbitrap mass spectra of an mDOM sample being ionized by traditional ESI (red) and LS-APGD (blue), where matching detected compounds (~33%) between the two techniques are shown in purple.

5.9 Supplementary tables

Table 5.1. Table of Triglyceride Precursors + Fragments Observed by LS-APGD.

Triglyceride	Abbreviation	M + Na (m/z)	M + Na Detected	Error (ppm)	M + NH4 (m/z)	M + NH4 Detected	Error (ppm)	M - RCOOH (m/z)	M - RCOOH Detected	Error (ppm)
Tripalmitin	TP	829.72607	829.72633	0.313356	824.77067	824.77129	0.751724	551.50392	551.50423	0.571165
Trimyristin	TM	745.63217	745.63236	0.254817	740.67677	740.67721	0.594051	495.44131	495.44103	-0.575245
Trilaurin	TLa	661.53827	661.53835	0.12093	656.58287	656.58336	0.746288	439.37871	439.37889	0.39829
Tricaprin	TCa	577.44437	577.44440	0.0519531	572.48897	572.48972	1.31007	383.31612	383.31621	0.247837
Tricaprylin	TCy	493.35047	493.35062	0.304043	488.39507	488.39599	1.88372	327.25351	327.25358	0.198623

5.10 References

Adams, J. and Gross, M. L.: Energy Requirements for Remote Charge Site Ion Decompositions and Structural Information from Collisional Activation of Alkali Metal Cationized Fatty Alcohols, J. Am. Chem. Soc., 108(22), 6915–6921, doi:10.1021/ja00282a014, 1986.

Artifon, V., Zanardi-Lamardo, E. and Fillmann, G.: Aquatic organic matter: Classification and interaction with organic microcontaminants, Sci. Total Environ., 649, 1620–1635, doi:10.1016/j.scitotenv.2018.08.385, 2019.

Asbury, G. R., Al-saad, K., Siems, W. F., Hannan, R. M. and Hill, H. H.: Analysis of Triacylglycerols and Whole Oils by Matrix-Assisted Laser Desorption/Ionization Time of Flight Mass Spectrometry, , 0305(99), 2000.

Banerjee, S. and Mazumdar, S.: Electrospray Ionization Mass Spectrometry: A Technique to Access the Information beyond the Molecular Weight of the Analyte, Int. J. Anal. Chem., 2012, 1–40, doi:10.1155/2012/282574, 2012.

Bertram, T. H., Cochran, R. E., Grassian, V. H. and Stone, E. A.: Sea spray aerosol chemical composition: Elemental and molecular mimics for laboratory studies of heterogeneous and multiphase reactions, Chem. Soc. Rev., 47(7), 2374–2400, doi:10.1039/c7cs00008a, 2018.

Chang, D. Y., Lee, C. C. and Shiea, J.: Detecting large biomolecules from high-salt solutions by fused-droplet electrospray ionization mass spectrometry, Anal. Chem., 74(11), 2465–2469, doi:10.1021/ac010788j, 2002.

Constantopoulos, T. L., Jackson, G. S. and Enke, C. G.: Effects of salt concentration on analyte response using electrospray ionization mass spectrometry, J. Am. Soc. Mass Spectrom., 10(7), 625–634, doi:10.1016/S1044-0305(99)00031-8, 1999.

D'Andrilli, J., Cooper, W. T., Foreman, C. M. and Marshall, A. G.: An ultrahigh-resolution mass spectrometry index to estimate natural organic matter lability, Rapid Commun. Mass Spectrom., 29(24), 2385–2401, doi:10.1002/rcm.7400, 2015.

Dittmar, T., Koch, B., Hertkorn, N. and Kattner, G.: A simple and efficient method for the solid-phase extraction of dissolved organic matter (SPE-DOM) from seawater, Limnol. Oceanogr. Methods, 6(6), 230–235, doi:10.4319/lom.2008.6.230, 2008.

Duffin, K. L., Henion, J. D. and Shieh, J. J.: Electrospray and Tandem Mass Spectrometry Characterization of Acylglycerol Mixtures That Are Dissolved in Nonpolar Solvents, Anal. Chem., 63(17), 1781–1788, doi:10.1021/ac00017a023, 1991.

Guo, L. and Santschi, P. H.: A critical evaluation of the cross-flow ultrafiltration technique for sampling colloidal organic carbon in seawater, Mar. Chem., 55(1–2), 113–127, doi:10.1016/S0304-4203(96)00051-5, 1996.

Hansell, D. A.: Recalcitrant Dissolved Organic Carbon Fractions, Ann. Rev. Mar. Sci., 5(1), 421–445, doi:10.1146/annurev-marine-120710-100757, 2013.

Hao, C., March, R. E., Croley, T. R., Smith, J. C. and Rafferty, S. P.: Electrospray ionization tandem mass spectrometric study of salt cluster ions. Part 1 - Investigations of alkali metal chloride and sodium salt cluster ions, J. Mass Spectrom., 36(1), 79–96, doi:10.1002/jms.107, 2001.

Hoegg, E. D., Barinaga, C. J., Hager, G. J., Hart, G. L., Koppenaal, D. W. and Marcus, R. K.: Preliminary Figures of Merit for Isotope Ratio Measurements: The Liquid Sampling-Atmospheric Pressure Glow Discharge Microplasma Ionization Source Coupled to an Orbitrap Mass Analyzer, J. Am. Soc. Mass Spectrom., 27(8), 1393–1403, doi:10.1007/s13361-016-1402-4, 2016.

Hsu, F. F. and Turk, J.: Electrospray ionization multiple-stage linear ion-trap mass spectrometry for structural elucidation of triacylglycerols: Assignment of fatty acyl groups on the glycerol backbone and location of double bonds, J. Am. Soc. Mass Spectrom., 21(4), 657–669, doi:10.1016/j.jasms.2010.01.007, 2010.

Kalo, P. J., Ollilainen, V., Rocha, J. M. and Malcata, F. X.: Identification of molecular species of simple lipids by normal phase liquid chromatography–positive electrospray tandem mass spectrometry, and application of developed methods in comprehensive analysis of low erucic acid rapeseed oil lipids, Int. J. Mass Spectrom., 254(1–2), 106–121, doi:10.1016/j.ijms.2006.05.022, 2006.

Karki, S., Shi, F., Archer, J. J., Sistani, H. and Levis, R. J.: Direct Analysis of Proteins from Solutions with High Salt Concentration Using Laser Electrospray Mass Spectrometry, J. Am. Soc. Mass Spectrom., 29(5), 1002–1011, doi:10.1007/s13361-018-1893-2, 2018.

Kennicutt, M. C. and Jeffrey, L. M.: Chemical and GC-MS characterization of marine dissolved lipids, Mar. Chem., 10(5), 367–387, doi:10.1016/0304-4203(81)90016-5, 1981.

Kim, S., Kramer, R. W. and Hatcher, P. G.: Graphical Method for Analysis of Ultrahigh-Resolution Broadband Mass Spectra of Natural Organic Matter, the Van Krevelen Diagram, Anal. Chem., 75(20), 5336–5344, doi:10.1021/ac034415p, 2003.

Koch, B. P., Witt, M., Engbrodt, R., Dittmar, T. and Kattner, G.: Molecular formulae of marine and terrigenous dissolved organic matter detected by electrospray ionization Fourier transform ion cyclotron resonance mass spectrometry, Geochim. Cosmochim. Acta, 69(13), 3299–3308, doi:10.1016/j.gca.2005.02.027, 2005.

Kovács, K., Gáspár, A., Sajgó, C., Schmitt-Kopplin, P. and Tombácz, E.: Comparison of humic substances isolated from thermal water and surface water by electrospray ionization Fourier transform ion cyclotron resonance mass spectrometry, Eur. J. Mass Spectrom., 16(5), 625–630, doi:10.1255/ejms.1087, 2010.

Kruger, B. R., Dalzell, B. J. and Minor, E. C.: Effect of organic matter source and salinity on dissolved organic matter isolation via ultrafiltration and solid phase extraction, Aquat. Sci., 73(3), 405–417, doi:10.1007/s00027-011-0189-4, 2011.

Mandal, M. K., Chen, L. C., Hashimoto, Y., Yu, Z. and Hiraoka, K.: Detection of biomolecules from solutions with high concentration of salts using probe electrospray and nano-electrospray ionization mass spectrometry, Anal. Methods, 2(12), 1905–1912, doi:10.1039/c0ay00530d, 2010.

Marcus, R. K., Quarles, C. D., Barinaga, C. J., Carado, A. J. and Koppenaal, D. W.: Liquid sampling-atmospheric pressure glow discharge ionization source for elemental mass spectrometry, Anal. Chem., 83(7), 2425–2429, doi:10.1021/ac200098h, 2011.

Nebbioso, A. and Piccolo, A.: Molecular characterization of dissolved organic matter (DOM): A critical review, Anal. Bioanal. Chem., 405(1), 109–124, doi:10.1007/s00216-012-6363-2, 2013.

Quarles, C. D., Carado, A. J., Barinaga, C. J., Koppenaal, D. W. and Marcus, R. K.: Liquid sampling-atmospheric pressure glow discharge (LS-APGD) ionization source for elemental mass spectrometry: Preliminary parametric evaluation and figures of merit, Anal. Bioanal. Chem., 402(1), 261–268, doi:10.1007/s00216-011-5359-7, 2012.

Rezanka, T. and Sigler, K.: The Use of Atmospheric Pressure Chemical Ionization Mass Spectrometry with High Performance Liquid Chromatography and Other Separation Techniques for Identification of Triacylglycerols, Curr. Anal. Chem., 3(4), 252–271, doi:10.2174/157341107782109644, 2007.

Simjouw, J. P., Minor, E. C. and Mopper, K.: Isolation and characterization of estuarine dissolved organic matter: Comparison of ultrafiltration and C18 solid-phase extraction techniques, Mar. Chem., 96(3–4), 219–235, doi:10.1016/j.marchem.2005.01.003, 2005.

Stenson, A. C., Marshall, A. G. and Cooper, W. T.: Exact masses and chemical formulas of individual Suwannee River fulvic acids from ultrahigh resolution electrospray ionization Fourier transform ion cyclotron resonance mass spectra, Anal. Chem., 75(6), 1275–1284, doi:10.1021/ac026106p, 2003.

Thurman, E. M.: Organic geochemistry of natural waters., 1985.

Zhang, L. X. and Kenneth Marcus, R.: Mass spectra of diverse organic species utilizing the liquid sampling-atmospheric pressure glow discharge (LS-APGD) microplasma ionization source, J. Anal. At. Spectrom., 31(1), 145–151, doi:10.1039/c5ja00376h, 2016.

Chapter 6. The Sea Spray Chemistry and Particle Evolution Study (SeaSCAPE): Overview and Experimental Methods

6.1 Abstract

Wave channels have traditionally been used for studies of physical oceanography; however, they have recently been adapted to study marine aerosols and atmospheric chemistry. Here, we discuss the modifications and methods used to facilitate ocean-atmosphere experiments in a wave channel and select results from the 2019 Sea Spray Chemistry and Particle Evolution (SeaSCAPE) study. Using a variety of analytical techniques, we investigated the cleanliness of a 11,800 L wave channel which was filled with real seawater and sealed for operation. We further investigated the channel's production and transport of sea spray aerosols by adjusting sampling location as well as parameters controlling the breaking waves. Lastly, we summarize the SeaSCAPE study which sought to understand the role of ocean biology in controlling the chemistry of marine aerosols and gases, as well as the impact of atmospheric aging on the composition and climate-relevant properties of primary and secondary marine aerosols was investigated.

6.2 Introduction

Oceans cover 71% of the Earth's surface and represent a major source of both aerosols and trace gases, which affect climate, air quality, and human health. Aerosols influence climate directly by absorbing and scattering solar radiation, and indirectly by serving as cloud condensation nuclei. The interactions between aerosols and clouds represent one of the largest sources of uncertainty in estimates of the Earth's radiative budget (Boucher et al., 2013). Understanding the sources and properties of marine aerosols is crucial to improve our ability to understand and predict future changes in the climate. Sea spray aerosol (SSA) is the largest source of atmospheric particles by mass, with a global emission flux of 10.1 $Tg \cdot yr^{-1}$, 98% of which is attributed to supermicron

particles (Gong et al., 2002). SSA is produced when breaking waves entrain air bubbles beneath the ocean surface, which rise to the surface and burst. This process produces two types of droplets: film drops from the bursting of the bubble cap and jet drops from the collapse of the bubble cavity. Measurements of authentic marine aerosols have been traditionally limited to studies performed on research cruises or at remote field stations. More recently, usage of ocean-atmosphere simulators such as wave channels and Marine Aerosol Reference Tanks (MARTs) have brought the complexity of the marine environment into the laboratory (Prather et al., 2013; Stokes et al., 2013, 2016). These devices use breaking waves or plunging waterfalls to produce bubble plumes which possess the correct size and surface residence time to match bubbles in the real ocean. Subsequent rupturing of these bubbles at the air-sea interface produce SSA which closely resemble the size distribution of SSA observed in the marine environment.

These simulators have been contrasted against other laboratory SSA production devices such as fritted bubblers. While simple in design and application, fritted bubblers tend to produce less accurate aerosol size distributions which can exhibit physiochemical discrepancies in morphology and composition versus authentic SSA (Collins et al., 2014). The utilization of ocean atmosphere simulators to generate realistic marine aerosols has revealed a large breadth of information across the disciplines of marine geosciences (Mayer et al., 2020). This includes the production of marine ice nucleating particles; the aerosolization of marine microorganisms; biochemical control of SSA composition by enzymes; biogenic volatile gas production; physical and chemical heterogeneity of SSA; and SSA surface reactivity and uptake properties (Ault et al., 2013; DeMott et al., 2015; Kim et al., 2015; Michaud et al., 2018; Patterson et al., 2016; Ryder et al., 2015; Wang et al., 2015). The further use of these simulators to disentangle the highly complex

mechanisms present in the marine environment is being advanced by improvements in their construction and understanding the factors which are relevant for ideal operation.

While many past CAICE studies have focused solely on the composition and properties of freshly emitted nascent SSA, atmospheric aging processes can transform SSA through reactions with trace gases, oxidants, and sunlight. For example, heterogenous reaction of SSA with HNO_3 has been shown to result in the displacement of HCl forming $NaNO_3$ (Ault et al., 2013). In addition to SSA, the oceans are a source of secondary marine aerosol (SMA), which is formed from the reactions of gas-phase compounds emitted from seawater. SMA can either form as new particles via nucleation or it can condense onto existing particles in the marine atmosphere, such as SSA, changing their size and chemical composition (O'Dowd and de Leeuw, 2007). Recently, oxidation flow reactors (OFRs) have been used to simulate both the heterogeneous oxidation of SSA (Trueblood et al., 2019b) and the formation of SMA (Mayer et al., 2020; Schneider et al., 2019) in laboratory studies of marine mesocosms.

Here we detail the features and usage of a newly constructed wave channel located at the Scripps Institution of Oceanography from June to August of 2019 with over 30 participants focused on the production and measurement of marine aerosols. The Sea Spray Chemistry and Particle Evolution (SeaSCAPE) experiment sought to provide an environment where SSA, marine biogenic volatile organic compounds (VOCs), marine microbiology, and seawater chemistry could be studied under clean, isolated conditions. The questions this experiment sought to address were:

- How does biological activity in seawater, namely the interactions of phytoplankton, bacteria, and viruses, affect the chemistry of marine aerosols and gases?
- What are the effects of atmospheric aging on the chemical composition and climate-relevant properties of SSA?

- How does the formation and cloud-forming potential of SMA change with respect to both marine biology and photochemical aging timescales?

To enable the SeaSCAPE experiment, the wave channel was thoroughly studied to optimize the production and collection of SSA and minimize anthropogenic contamination. These studies informed various modifications to wave channel construction and insights into best practices for operation while also giving context to future analyses of data collected using this platform. We further outline the scope and scale of the SeaSCAPE experiment, providing several vignettes which demonstrate the types of new discoveries enabled by the mesocosm experiments discussed herein, emphasizing the incorporation of atmospheric oxidation processes.

6.3 Methods and Materials

6.3.1 Description of Wave Channel

The Scripps Institution of Oceanography (SIO) wave channel is a 33 m x 0.5 m x 0.8 m (L x W x H) glass channel which is filled to a depth of 0.56 m with seawater, giving a total water volume of 11,800 L (Figure 6.1). The facility is located indoors in the Hydraulics Laboratory. An electromagnetically driven paddle (surface area = 9600 cm^2) operating at 0.3 Hz with a stroke length of 73 cm is used to generate waves which break on a fiberglass beach located midway down the channel. This beach (2.4 m in length) is positioned at an angle of approximately 16˚ relative to the bottom of the channel to generate a plume of entrained bubbles that closely match those in the ocean and previous campaigns (Prather et al., 2013; Wang et al., 2015b). Sampling ports are located both upstream and downstream from the breaking wave (Figure 6.1). A second beach, located at the far end of the channel, serves to dissipate residual wave energy. The top of the channel is sealed from the paddle area to approximately 30 m, well past the downstream sampling ports, with acrylic lids, backed by marine-grade plywood for support. A PTFE sheet was suspended

from the last lid section to the water surface to prevent backflow of room air into the channel. In addition, the unlidded sections of the channel were draped with lightweight polyethylene film to prevent dust and debris from settling into the channel.

The paddle assembly, including motors, is enclosed within a tent made of flexible PTFE film (TEKFILM, FEP2000E, 0.127 mm in thickness) to seal the system and prevent contamination from the room air while accommodating pressure fluctuations caused by the reciprocating paddle. Clean, particle-free air was delivered to the wave channel from the top of the tent (Figure 6.1) using a custom air handling system made with galvanized steel duct pipes and 314 grade stainless steel connectors to the PTFE tent and the channel. Ambient air pulled in using a custom fan-blade powered by an induction motor (Marathon Electric 5THW8) was filtered through a four-stage filter system (Hydrosil International), consisting of a pre-filter, activated charcoal pellets, potassium permanganate ($KMnO_4$), and a HEPA filter. The scrubbed air was then directed into the wave channel headspace. A condensation particle counter (CPC) positioned upstream of the wave break (Figure 6.1, position 1) was used to continuously monitor background particle counts in the headspace, which would indicate breakthrough from the filter system as well as leaks in the paddle tent. NO_x, SO_2, O_3, and air velocity, temperature, and relative humidity were also continuously monitored from the same upstream sampling location.

The wave channel was equipped with fluorescent lights to provide the light flux necessary for photosynthetic organisms to grow in the seawater. Four light fixtures, two on either side, were attached to the outside of each 2 m glass panel of the channel below the water surface. Each fixture was equipped with two 120 cm fluorescent bulbs (Spectra 5700K F32-T8, Full Spectrum Solutions, Inc), giving a total of 8 bulbs per panel. The lights extended the full length of the channel, except for the paddle tank at the front of the channel and the end tank, which are

constructed stainless steel and thus not transparent to light. The flux of photosynthetically active radiation (PAR) in the channel was measured to be ~80 μE/m^{2}s in the center of the channel, approximately ~30 cm below the water surface (Apogee Instruments, MQ-200). While this is significantly lower than typical daytime PAR levels, which often exceeds 1,000 μE/m^{2}s on clear days (Bouvet et al., 2002), it is comparable to PAR levels reported in other studies for the purpose of growing marine phytoplankton (Lee et al., 2015). To simulate day/night light cycles, the lights were turned on for 14 hours during the daytime and off for 10 hours at nighttime.

6.3.2 Description of Isolated Sampling Vessel

Due to challenges associated with removing all VOCs from both the air handler and off gassing from wave channel materials, a secondary isolated sampling vessel (ISV) was utilized for sampling of VOCs produced from seawater. The isolated headspace was constructed from a single cylindrical tube of borosilicate glass (Greatglas, Delaware U.S.A.). The dimensions of the glass tube were as follows: 400 mm outer diameter, 6 mm wall thickness, 74 cm long, resulting in a total volume (pre-water) of 87 L, and when filled with water halfway, giving a water volume of 44 L (Figure 6.11). Each end of the ISV was sealed by a PTFE disk, thickness 1.6 mm, braced against the face of the cylinder by a 9.5 mm acrylic disk and backed by an aluminum frame. Six 6.4 mm stainless steel Swagelok bulkhead ports in the headspace partition were used for the zero air inlet and gas sampling outlets (located on opposite ends), with one 13 mm bulkhead to continuously pump seawater and a, 25 mm bulkhead drain port located 13 mm above the center of a PTFE sealing plate opposite of the filling bulkhead (Figure 6.11). Seawater was delivered to the ISV via a plunging stream, located opposite the sampling ports. The seawater was delivered using a peristaltic pump equipped with Tygon tubing, which withdrew water from the wave channel, ~0.5 m beneath the water surface. For maintenance of consistent flow rates and prevention of leaks,

inlet tubing position within the peristaltic pump was adjusted every 6-8 hours and tubing replaced every 3 days. ISV water drained back into the channel through 25 mm tubing attached to the large central port opposite the plunging jet, with the end of the return flow tubing submerged beneath the water level. Zero air flow rate through ISV headspace varied from 8-10 LPM, leading to an average air residence time of 5 minutes. Water flow rate was fixed at 1.5 LPM, leading to a water residence time of 29 minutes.

6.3.3 OFR Operation

To study the effect of atmospheric aging processes on marine aerosols, potential aerosol mass oxidation flow reactors (PAM-OFR, Aerodyne Inc) were used to simulate both the heterogeneous oxidation of primary sea spray aerosol and the formation of secondary marine aerosol from the oxidation of VOCs. The PAM-OFR uses UV lamps to produce high concentrations of OH radical, simulating atmospheric aging from days to weeks, with a residence time of 1-3 minutes (Kang et al., 2007; Lambe et al., 2011). Two OFRs (OFR1 and OFR2) sampled from the wave channel headspace at sampling port #2, with the goal of producing heterogeneously aged SSA (hetSSA), although SMA is also produced from the oxidation of VOCs in the wave channel headspace. A third OFR (OFR3) sampled from the ISV (Figure 6.1), for the purpose of producing SMA under the cleanest possible conditions.

All OFRs were operated in OFR185 mode, meaning that UV light with wavelengths of both 185 nm and 254 nm was produced inside the reactors. The OH exposure was determined by introducing carbon monoxide to the OFR, then measuring the change in CO concentration versus the lamp intensity using a CO analyzer (APMA-370, Horiba Ltd). The OH exposure is determined using the rate coefficient of CO + OH ($k_{OH + CO, 298K} = 1.5\times10^{-13}$ cm^3 $molec^{-1}$ s^{-1}), assuming pseudo-first order kinetics (Chen and Marcus, 2006). The OH exposure can be converted to “days of

equivalent aging" using typical tropospheric OH concentrations ([OH] = 1.0×10^6 molec cm^{-3}) (Wolfe et al., 2019). O_3 concentrations were monitored after each of the OFRs using an O_3 analyzer (Model 202 and Model 106-L, 2B Technologies). Before aerosol measurements, the sample air was passed through a denuder to remove O_3 (Carulite-200, obtained from Ozone Solutions).

6.3.4 Control Experiments

Control experiments for characterizing the wave channel can be divided into two main types: 1) obtaining minimum background aerosol levels and 2) optimizing the sampling location and depth into the channel headspace. For the control experiments, the wave channel was filled with sand-filtered seawater. This seawater is automatically pumped, filtered, and plumbed directly into the research buildings at SIO including the wave channel from the Ellen Browning Scripps Memorial Pier (Scripps Pier, 32-52'00" N, 117-15'21" W). As sand-filtration removes most of the large marine microbiology (>1-2 μm) and differs from the seawater used in mesocosm experiments, the seawater used in the control experiments will be referred to as tap seawater.

Using the flexible PTFE film mentioned above, a box-shaped tent of 244 cm length x 117 cm height x 80 cm depth was fabricated where all edges were double heat-sealed and was housed in a stainless-steel cage over the paddle. The seam between tent and the wave channel metal body was sealed using polyester tape (3M 8403, 5 cm diameter).

Air velocity through the wave channel headspace was periodically measured using a hot-wire anemometer (TSI 9545-A), inserted at the upstream sampling location approximately 9 m before wave break and 5 cm below the channel lid to minimize the impact of water droplets affecting the measurements.

Total particle counts in the wave channel were measured before and after the wave break with condensation particle counters (Magic CPC, Aerosol Devices Inc). The purpose of the

upstream CPC was to detect particle leaks in the paddle tent and the air handling system. Counts were typically very low (< 5 #/cm^3). The downstream CPC measured the total number of particles after the breaking wave. Thus, it can be assumed that the difference between upstream and downstream particle counts is the total concentration of SSA generated by the breaking wave. During periods when the upstream counts are negligible, it can be assumed that all the particles measured are SSA generated by wave breaking.

Aerosol size distributions of SSA were measured using an Aerodynamic Particle Sizer (APS 3321, TSI Inc) and a Scanning Mobility Particle Sizer (SMPS 3938, TSI Inc) equipped with an X-ray neutralizer (Model 3088, TSI Inc) at various locations downwind of the wave break (5 locations, 60 cm intervals) at 0-10 cm below the channel lid. The induction motor was tuned between 1250 and 2500 rotations per minute (RPM) to optimize the airflow and the total particle number concentration. Particles were dried prior to measurement with a silica diffusion dryer. The electrical mobility diameters (d_m) measured by the SMPS are assumed to be the same as the physical diameter (d_p). The aerodynamic diameters (d_a) measured by the APS were converted to physical diameter using the effective density of sea spray aerosol (ρ_{eff} = 1.8 g·cm^{-3}) (Stokes et al., 2013).

6.3.5 SeaSCAPE – Water collection and Bloom Initiation

Seawater was collected from the Scripps Pier. Seawater was pumped up from the end of the pier and travelled through a gravity flume on the south side of the pier to the entrance. During the pumping process, the seawater passed through a rough aluminum screen to collect large marine detritus such as seaweed. A submersible pump (Grundfos UNILIFT AP12.40.04.A1) was placed into the gravity flume and water was pumped through a hose into 1,135 L plastic tanks and transported to the wave channel by truck immediately after filling at the Scripps Pier. The seawater

was further filtered to remove large particulates and zooplankton using an acid-clean 50-micron Nitex nylon mesh (Flystuff; Cat # 57-106) and pumped into the wave channel. Algae growth media was added to the seawater at the beginning of each bloom cycle to promote phytoplankton growth (Guillard and Ryther, 1962). The dates and concentrations of the nutrient additions are summarized in Table 1.

During the third bloom cycle, a separate phytoplankton bloom was grown in a 1,135 L plastic tank outside of the hydraulics laboratory. The purpose of this was to inoculate the wave channel with healthy phytoplankton biomass grown under natural sunlight to promote a larger bloom. Seawater was collected from Scripps Pier and filtered using 50 μm Nitex mesh, then it was transferred to the 1,135 L outdoor tank, covered with wire mesh to keep out debris, and placed in partial shade. Then, f/2 growth media and silicates were added immediately to stimulate the growth of a phytoplankton bloom. The seawater was bubbled gently to oxygenate and remained in the outdoor tank for 4 days until it reached the exponential growth phase as indicated by *in vivo* fluorescence measurements (AquaFluor, Turner Designs). Then, 1,135 L of water were drained from the wave channel and the contents of the tank were added to the wave channel. Water was transferred gently using sanitized buckets to avoid damaging the phytoplankton during the transfer. Additional nutrients were added to the wave channel immediately following the outdoor tank addition to bring the total concentration of growth media and silicates up to f/2 in the wave channel.

6.3.6 SeaSCAPE – Aerosol Measurements

A large suite of aerosol measurements was conducted during the SeaSCAPE experiment to study the properties of nascent SSA, hetSSA, and SMA. These include measurements of the size distributions, chemical composition, ice nucleating particle (INP) characteristics, cloud condensation nuclei (CCN) activity and water uptake, and phase state and morphology, among

other properties. All measurements conducted during the campaign are summarized in Tables 6.2 and 6.3.

6.3.7 Aerosol Number and Size Distributions

Total particle counts in the wave channel were measured before and after the wave break with condensation particle counters. The aerosol size distributions of nascent SSA after the wave break was measured using the APS and SMPS as described in the control experiment. Size distributions from OFR1 and OFR2, which includes both hetSSA and SMA, were measured using a Scanning Electrical Mobility Spectrometer (SEMS, Brechtel Manufacturing, Inc) and an APS (3321, TSI Inc). SMA size distributions from OFR3 were measured using an SMPS (Model 3938, TSI Inc) equipped with a Nano DMA (DMA 3085, TSI Inc) and a soft X-ray Neutralizer (Model 3088, TSI Inc).

6.3.8 Single Particle Atomic Force Microscopy (AFM) Measurements

For a preliminary investigation of SSA and aged SSA morphology, nascent and aged sea spray aerosols were collected on August 3rd which corresponded to the peak of the phytoplankton growth in Bloom 3 (Figure 6.2). The SSA were deposited onto hydrophobically treated silicon substrates (Ted Pella, Inc.) using a micro-orifice uniform deposit impactor (MOUDI, MSP, Inc., model 110) at ca. 80% RH (i.e. wet deposition). The aged SSA were deposited onto the hydrophobically treated silicon substrates using a separate MOUDI (MSP, Inc., model 125R) at ca. 20% RH (i.e. dry deposition) (Lee et al., 2019, 2020a). MOUDI stages 6, 7 and 8 were used, which corresponds to an aerosol aerodynamic diameter 50% cut off range of 0.18-1.0 μm. The aged SSA were generated using OFR2, with a UV lamp voltage of 2.0 V which corresponds to approximately 4-5 days of photochemical aging in the atmosphere. The substrate-deposited

nascent and aged SSA samples were stored in clean Petri dishes and kept inside a laminar flow hood (NuAire, Inc., NU-425-400) at ambient temperature (20−25°C) and pressure.

AFM height images of individual nascent and aged SSA particles were recorded using the molecular force probe 3D AFM (Asylum Research, Santa Barbara, CA), at ambient temperature (20−25°C) and pressure. Silicon nitride AFM tips (MikroMasch, Model NSC35, tip radius of curvature ~10 nm) were used to image individual particles. A custom-made humidity cell was used to control the RH at 50% for all imaging; the elevated RH was used due to expected lowering of the viscosity for the organic components relative to inorganic that facilitates differentiation of their spatial distribution using AFM. AC mode AFM was used to image individual particles and determine their morphology. A total of 50 individual particles were characterized for each sample type.

6.3.9 SeaSCAPE – Gas-phase Measurements

In addition to the gas phase measurements discussed below, Table 6.4 details the full collection of gas phase measurements made throughout the SeaSCAPE experiment to assess questions regarding the influence of biology on VOCs produced from seawater and the introduction of anthropogenic contaminants from the laboratory environment.

6.3.10 Trace Inorganic Gases

The concentrations of trace gases were monitored at several locations: the air handling system, room air, and the wave channel headspace upstream of the wave break. A custom-fabricated solenoid valve switching array was used to automatically switch between the different air sampling lines. The concentrations of the oxides of nitrogen (NOx) were continuously monitored using a Model 42C NO-NO_2-NOx analyzer (Thermo Electron Corporation). Ozone concentrations were measured using a UV photometric based O_3 analyzer (Model 49C, Thermo

Electron Corporation). The analyzer was calibrated using an ozone calibration source (Model 306, 2B Technologies). Sulfur dioxide concentrations were measured using a pulsed fluorescence SO_2 analyzer (Model 43iQ Trace Level SO_2 Analyzer, Thermo Electron Corporation).

6.3.11 Chemical Ionization Time of Flight Mass Spectrometry

Measurements of the wave channel air velocity were obtained using 50 uL of 45 mM dimethyl sulfide (DMS) headspace spikes sprayed onto a sanitary laboratory wipe suspended in the wave channel at the upstream sampling port. As DMS was carried along the length of the wave channel by the headspace flow, a custom fabricated chemical ionization time of flight mass spectrometer (CI-TOFMS) drew headspace at 2 LPM from the primary sampling port. CI-TOFMS has been previously described by others, briefly, ~300 ppm benzene vapor was generated by passing 10 standard cubic centimeters per second (sccm) of N_2 over a cylinder of liquid benzene and diluted to concentration with further N_2 (Kercher et al., 2009; Kim et al., 2016; Lavi et al., 2017). Benzene vapor was passed through a 20mCi Po-210 α-source, and further drawn through an inline critical orifice at 1.8 SLPM into the ion-molecule region (IMR) of the CI-TOFMS. Sample analyte was similarly drawn into the IMR at the same flow rate as analyte. The IMR pressures was maintained at 60 Torr and 60 V for all analyses. Analyte ions generated through charge transfer and ligand switch reactions with benzene cluster cations were further focused by a radio frequency ion funnel, and subsequently transferred by an RF-only quadrupole into an orthogonal-extraction time of flight analyzer (Tofwerk). Mass spectra from 5-500 m/z were obtained at a rate of 1 Hz, with generated data analyzed using the Tofware plugin for Igor Pro 7 software.

6.3.12 Proton Transfer Reaction Mass Spectrometry

A Vocus proton transfer reaction time-of-flight mass spectrometer (PTR-ToF-MS) (TOFWERK, Aerodyne Inc.) was deployed to measure gas-phase VOCs. The focusing ion-molecule reactor was operated at high reduced field strength (E/N = 143 Td) with a pressure of 1.5 mbar, electric field of 41.5 V cm^{-1}, and heated to 100 °C. The big segmented quadrupole voltage was set to 275 V, which reduced the transmission of low mass (<35 m/Q) ions. The Vocus mass spectra were saved at 1 Hz time resolution. The headspace of the air handling system and wave channel headspace was sampled at 100 sccm through a roughly 2.5 m, 6.35 mm O.D. PFA tube. Instrument background signals were determined about 8 times daily by overflowing the Vocus inlet with zero air from a zero-air generator (Sabio 1001) that provided air to the ISV headspace. Daily average background signals were used for background correction. Peak fitting and integration were completed in Tofware 3.1.2.

6.3.13 Offline Atmospheric Pressure Chemical Ionization for Irradiation Experiments

A high resolution Orbitrap Elite (ThermoFisher) mass spectrometer equipped with a modified gas-phase atmospheric pressure chemical ionization (APCI) source was used to detect VOCs from the surface of collected water during the SeaSCAPE campaign (Roveretto et al., 2019) upon irradiation using an LCS-100 solar simulator (94011A, Oriel). Data was collected solely in positive mode, where voltage was set to 4 kV, needle current at 5 mA, and vaporizer temperature at 150 °C. Sheath and auxiliary flow were set to zero. An AM1.5G and water filter were used to simulate the solar spectrum and block infrared radiation respectively. From the wave channel, 200 mL of surface water was collected and transferred into a 350 mL jacketed custom glass tube (Ace Glass Inc.) with quartz windows on each end. The surface area of the water sample in the tube was approximately 12 sq.in. With a headspace of 150 mL, pure nitrogen gas was used as a carrier at a

rate of 200 sccm. Temperature was regulated and measured constantly to ensure minimal thermal variation (± 1°C) during the experiment. The collected water settled for 2 hours before being irradiated to allow a stable surface layer to form. To verify whether the immediate spike in signal was abiotic or biotic in nature when under lighted conditions, a separate experiment using the same water, but filtered with a 0.2 μm GTTP filter (MilliporeSigma), was shown to not be able to remove the signal spike seen in Figure 6.9a.

6.3.14 SeaSCAPE – Water Measurements

A vast set of seawater and sea surface microlayer measurements made through the duration of SeaSCAPE. These measurements sought to understand various important aspects of the mesocosm experiments such as nutrient availability, organic chemical composition, biological speciation, biological productivity, dissolved gas turnover and other important factors.

6.3.15 Bulk Seawater Collection

16 L of Bulk seawater was sampled daily around 9:30 PST for the following analyses: dissolved organic carbon (DOC); inorganic nutrients; extracted chl-a; bacterial and viral abundances, and phytoplankton speciation-identification. Seawater was collected using a ~2 m long siphon, which consisted of 9.5 mm OD Teflon tubing that was left open on one end, and a double barbed valve installed on the other. Nalgene carboys were used to transport and dispense the collected seawater for analysis. Both the siphon and the carboys were rinsed with methanol, 70% ethanol, 0.1 M HCl solution, and ultra-purified water prior to water collection. The siphon was inserted near the end of the channel before the second beach (Figure 6.1) approximately 20 cm below the surface of the water. The volume of collected seawater was replenished by adding a corresponding volume of Milli-Q (Millipore) water (<18 μΩ) every other day.

6.3.16 Sea Surface Microlayer Collection

Sea surface microlayer (SSML) sample collection was conducted using a glass plate, a glass funnel and a Teflon scraper. During the day proceeding collection of SSML samples, the glass plate and funnel were cleaned of biological material using Millipore water, methanol, 70% ethanol, and 10% HCl. The collection glassware was placed in a combustion furnace for 5 hours at 500 ˚C to remove organic contaminants. The glass plate with a handle was lowered carefully by hand at a rate of 5-6 $cm \cdot s^{-1}$ and withdrawn at the same rate. This withdrawal rate corresponds to a sampled SSML thickness of around 50 µm (Carlson, 1982; Cunliffe and Wurl, 2015). After removal from the wave channel, the glass plate was suspended for 20 seconds to allow any bulk seawater to drain off the plate back into the channel, ensuring that the majority of what remained on the plate was SSML. The remaining liquid was scraped from the glass plate into a collection vessel using a Teflon scraper. This process was repeated until approximately 200 mL of sample was collected.

6.3.17 Phytoplankton Enumeration and Photography

In order to determine the taxonomic composition of the mesocosm, two methods were employed: 1) Whole seawater samples were collected and manually counted under confocal microscopy; 2) A dual version of the Scripps Plankton Camera System (SPCS: https://spc.ucsd.edu) was placed on the bottom of the wave channel before the dampening beach (Figure 6.1) to continuously image the developing plankton community for *in situ* observations. For the manual counting method, 400 mL of whole seawater was collected from approximately 30 cm depth at both ends of the wave channel. Samples were taken twice per day with Teflon tubing and poured gently into amber Nalgene bottles. Samples were immediately fixed with a 2% buffered formalin solution and kept cold to preserve samples for enumeration. 50 mL of seawater from these samples were poured into a settlement chamber and allowed to settle for 24 hrs. The cells

were prepared for enumeration using the Utermöhl method under an Olympus IX-71 inverted microscope (Utermöhl, 1931)). Two full rows of the settlement chamber were counted to calculate the cells/L for each distinct species. Then, the taxa cell counts were binned into functional phytoplankton types, including a microzooplankton group. These bins were used to calculate the relative abundance of the functional groups over time and were then compared to the *in-situ* camera data.

The *in-situ* camera enabled the research team to study the plankton community undisturbed in the mesocosm, monitor the presence of delicate taxa, and observe intra- and inter-species interactions that would be impossible to detect using other sampling techniques. The goal of the image analysis was to target detritus, aggregates, phytoplankton and zooplankton between 20-1000 µm in major axis length. For this reason, only images from the 5x magnification system were considered. Over the course of the 3-week experiment nearly 1.85 x 10^6 images of particles were collected within this size range. The system uses darkfield illumination to image free-floating particles in approximately 3 µL/frame sampling volume with a resolution of 3-5 µm (Orenstein et al., 2020). In order to train a neural net to classify this large amount of data, a subset of the images was manually labelled to serve as a training set.

6.3.18 Chlorophyll-a and Dissolved Oxygen Measurements

A continuous time series of i*n vivo* Chl-a and dissolved oxygen was measured throughout all three wave channel experiments using an Environmental Sample Processor (ESP). The ESP was located at the back of the wave channel just behind the seawater sampling section (Figure 6.1). The ESP is a homemade, continuous flow system that pumps seawater through tubing at a flow rate around 1 LPM using a peristaltic pump. The seawater first passed an SBE 37 MicroCAT that measures conductivity, followed by an SBE 63 optical dissolved oxygen sensor before being

deposited into a reservoir. In the reservoir, Chl-a is quantified through fluorescence measurements using a Sea Bird Scientific ECO-Triplet-BBFL2 sensor at excitation/emission wavelengths of 470/695 nm. After measurement of Chl-a, the seawater is circulated out of the ESP and back into the wave channel.

Each morning the ESP was rinsed by circulating Millipore water through the tubing for 20 minutes, and every fourth day, solutions of 0.1% bleach, 30% ethanol, and Millipore water were sequentially circulated through the tubing for 20 minutes to thoroughly clean the instrument. This helped prevent biological growth in the tubing and biofouling of the optics. Additionally, in between each experiment the reservoir was removed from the laser optics and both were carefully wiped with 70 % ethanol. Any ESP measurement periods that were affected by instrument maintenance or biofouling were corrected using *in vivo* Chl-a measurements made by a hand-held fluorometer (Aquafluor, Turner Designs). Aquafluor Chl-a measurements were made every few hours from the seawater sampling section of the wave channel.

To calibrate both the ESP and AquaFfluor Chl-a measurements, Chl-a was extracted from the bulk seawater and analyzed by fluorometric analysis in accordance with CALCOFI methods (Holm-Hansen et al., 1965). Bulk seawater was collected once daily from the seawater sampling section of the wave channel and filtered on 25 mm Whatman GF/F filters. The filters were then submerged in 8 mL of 90 % acetone for 24 hours at -20 ˚C to extract the Chl-a. Concentrations of the extracted Chl-a were determined by a calibrated fluorometer (10AU, Turner Designs). For calibration purposes, the extracted Chl-a data was separately plotted against both the ESP and Aquafluor data. Each plot was fit with a least squares regression, used to calibrate the ESP and Aquafluor Chl-a values. A continuous time series of the calibrated ESP Chl-a data for all three experiments is shown in Figure 6.2.

6.3.19 Bacteria, virus, nano- and picophytoplankton, and heterotrophic nanoflagellate enumeration

Seawater, SSML and aerosol samples were run with a BD FACSCanto II™ flow cytometer (FCM, bacteria, cyanobacteria and viruses). Samples were prepared according to the protocols for bacteria (heterotrophic and autotrophic) and viral enumeration (Brussaard, 2004; Gasol and Del Giorgio, 2000; Marie et al., 1997). All samples were preserved with glutaraldehyde at 5% final concentration and stored at -80°C after flash freezing (Noble and Fuhrman, 1998). For heterotrophic bacteria staining: water was diluted (1:10) in 1×TE buffer (pH 8), then stained with SYBRGreenI at RT for 10 min in the dark (Gasol and Del Giorgio, 2000). For viruses staining: water was diluted (1:50) in 1×TE buffer (pH 8) and stained with SYBRGreen I at 80°C for 10 min in the dark (Brussaard, 2004).For autotrophic bacteria, *Cyanobacteria* namely *Synechococcus*, water was run unstained (Olson et al., 1990). For SSA preparation, 0.9 mL of SSA, recovered in 4X PBS buffer via SPOT sampler (sampling for 6 hours at 1.8 L/min) were brought to 1 mL by adding 4X PGE and then were split into two 0.5 mL aliquots that were processed as described above for heterotrophic bacteria and viruses. SSA blank samples were also collected via SPOT sampler and processed accordingly. The values counted in the same SSA blank gates were subtracted from the SSA sample runs. For heterotrophic bacteria and viruses, the samples were analyzed at medium rate (60 µL min^{-1}) with a threshold set on green fluorescence. Side scatter versus green fluorescence plots were generated to identify and quantify heterotrophic bacterial and viral populations (Marie et al., 1997). *Synechococcus* population were identified on forward scatter versus orange fluorescence and red fluorescence (Olson et al., 1990). *Synechococcus* population were identified on forward scatter versus orange fluorescence and red fluorescence (Olson et al.,

1990). Samples for nano-, picophytoplankton and heterotrophic nanoflagellates were run on a BD Accuri flow cytometer following protocols by Marie et al and Christaki et al.

6.4 Results: Characterization and Optimization of the Wave Channel

6.4.1 Results of PTR-MS wave channel/room/air handling headspace composition

Volatile organic compounds (VOCs) were measured in the wave channel headspace, air handling system, ISV, and room air, with PTR-MS to determine the relative degree of cleanliness of the experiment (Figure 6.3). Dimethyl sulfide (DMS) and methanethiol (MeSH) were chosen as proxies for expected marine biogenic VOCs in comparison to benzene and toluene which are more closely associated with anthropogenic pollutants and are not expected to be produced biogenically in large quantities in the marine environment (Wakeham et al., 1986). Figure 6.3 shows that benzene and toluene were most elevated in room air, the air handling system, and the wave channel headspace, but were significantly diminished in the ISV. These results suggest that the primary source of benzene and toluene in the wave channel was not derived from the seawater, but likely as breakthrough of the air handling system and possible off-gassing of building materials in the wave channel. Conversely, the concentrations of DMS and MeSH in the ISV were significantly elevated compared to the wave channel, due to the relative ratio of water to headspace renewal in the ISV which was much higher than the wave channel. These results show that the ISV was effective in maintaining a clean headspace that better reflects the emissions of seawater without anthropogenic influences.

6.4.2 Wave channel headspace velocity

To assess the air velocity in the wave channel, momentary spikes of dimethyl sulfide were generated in the wave channel headspace by spraying a laboratory wipe suspended from the upstream sampling port with 50uL of 45mM dimethyl sulfide dissolved in methanol. The rapidly

evaporated gas was then carried along the air flow to the downstream sampling port after wave breaking. Shown in Figure 6.4 are DMS spikes measured by the CI-TOFMS. Mean arrival time was 200s, with a standard deviation of 35s (N=3) with the paddle running. Replicate experiments with the paddle stationary did not yield arrival times that significantly differed. Given the distance of the upstream sampling port from the downstream ports, the wave channel headspace velocity was calculated to be 4.9-7.0 cm/s. This contrasts measurements from the hot wire anemometer, which describe a velocity range from 32-35 $cm*s^{-1}$. The disagreement between these two measurement techniques may be due to the operation of the hot wire anemometer at the lower boundary of its analytical dynamic range, in combination with gas turbulence induced by the waves as they passed through the channel. In addition, while the CIMS measurement obtains a flow velocity that reflects an average of the velocity throughout the wave channel length between the upstream and downstream sampling ports, the velocity measurement by the hot wire anemometer was only performed at the upstream location. These results further suggest that significant variability in flow conditions occur along the length of the wave channel and merit further investigation.

6.4.3 Results of wave channel characterization on particle backgrounds and SSA production

Background particle concentrations were measured in the wave channel headspace at the upstream sampling port (Figure 6.1, Location 1) using a CPC to determine the contribution from non-marine particles from sources such as leaks in the paddle tent or breakthrough in the air handling system while the waves were being generated. Setting the RPM of the induction motor that supplied the clean air to wave channel to a speed less than 1500 RPM introduced ambient non-marine particles into the wave channel headspace (10-50x more), thus establishing a lower limit

of the air handling unit. While increasing the speed of the motor could increase the amount of clean air into the headspace of the wave channel, doing so dilutes the total number of SSA from wave break, thus our testing found that 1500 RPM was the optimal setting (Figure 6.5a).

With the optimized setting of the air handling unit, these background particle concentrations were generally extremely low (~3 #/cm^3, Figure 6.8), indicating that the wave channel headspace was quite clean, with respect to ambient particulate contamination (~10,000 #/ cm^3). In comparison, the average particle concentrations after the breaking wave were significantly higher (242 ± 91 #/ cm^3), indicating that the almost all of particles sampled downwind of breaking wave were sea spray aerosols produced from the channel.

With the air handling unit and the background optimized, next was to optimize the sampling location for SSA downwind of the breaking wave. Five locations at 0 cm, 60 cm, 120 cm, 180 cm, and 240 cm downwind of the breaking wave were tested. The APS and SMPS size distributions were used to calculate the total SSA number at each location. Figure 6.5b shows that position 4, which corresponds to 180 cm downwind of the breaking waves, had the highest SSA number concentrations. The continuous water and air flows pushed the entrained air bubbles and the generated SSA downwind of the breaking wave (Lewis and Schwartz, 2004; Prather et al., 2013). In addition to sampling location, the sampling port (1.27 cm i.d.) depth was tested from 0 cm to 10 cm into the headspace. While the specific relationship between port depth and SSA number concentration varied with sampling location, at position 4, a port depth of 5 cm yielded the highest values. However, this inconsistent relationship indicates that there may be heterogeneous mixing within the wave channel headspace. It was observed during testing that port depths of 10 cm or greater were prone to splashing by the breaking waves, resulting in excess water being pulled into the sampling lines. Similarly, a port depth of 0 cm (flush with the lid

surface) resulted in condensation from the lids being pulled into the sampling lines. Thus, from an operational standpoint, it is a sampling port depth of 2-8 cm is ideal to minimize the introduction of water droplets to the sampling lines.

6.5 Results: SeaSCAPE Experiment

6.5.1 Biological dynamics of the phytoplankton blooms

Shown in Figure 6.2a is the time series of seawater Chl-a, heterotrophic bacteria, and dissolved organic carbon measurements which provide an overview of the biological course of the 3rd mesocosm. The wave channel after the initial nutrient additions (Figure 6.2a first two asterisks) did not show indicators of significant phytoplankton growth (< 2 µg/L Chl-a), possibly due light limitation. To create a major step change biological perturbation, a phytoplankton bloom, an external mesocosm was initiated in an outdoor tank using natural seawater gathered from the same location and reached a Chl-a concentration of 25 µg/L. This 1,135L starter mesocosm was then added to the wave channel on 8/1, which continued to grow, peak, and then proceed through an extended senescent phase (Figure 6.2a). The senescent phase Chl-a concentration remained stable around 5 µg/l, suggesting an activated state compared to the pre-bloom state. Over the course of mesocosm 3, dissolved organic matter steadily increased in concentration, due to primary production and bacterial production of DOC, consistent with previous bloom incubation experiments (Wang et al., 2015). Notably, about 100 µM were added by the tank amendment over the background level of the first week. The dissolved inorganic gases, O_2 and CO_2, were monitored to assess the relative degrees of active autotrophy and heterotrophy by the phytoplankton and bacteria in the wave channel (Figure 6.2b). As expected, dissolved O_2 concentrations varied on a diurnal basis as the phytoplankton utilized light for photosynthesis and produced O_2 as a byproduct during the daytime. During periods of higher Chl-a (Figure 6.2a), after the tank amendment,

dissolved O_2 concentrations were generally more elevated, except for 8/2 when the heterotrophic bacteria reached a local maximum concentration, and again on 8/5 during the senescent phase of the algal bloom. These trends in dissolved O_2 are mirrored inversely by changes in dissolved CO_2, which decreased with respect to phytoplankton growth due to increased carbon fixation by phytoplankton. After reaching a minimum on 8/5 (Figure 6.2b), the CO_2 concentration slowly increased during the senescent phase of the mesocosm as bacterial respiration increased relative to phytoplankton carbon fixation. Lastly, the seawater temperature of the wave channel initially began at the temperature that it was gathered from the ocean but equilibrated quickly to resemble room conditions within ~24 hours (Figure 6.2b). Daily, temperature varied ~0.75 $C*day^{-1}$ with the ambient temperature of the laboratory. Longer term variation following changes in local weather but ranged between 24.5-27 °C for the duration of experiment after initial equilibration.

6.5.2 Phytoplankton enumeration

A preliminary inspection of the images revealed that they provide a more detailed taxonomic description of the wave channel's contents, including an assortment of interactions that were not detected via microscopy. ESP and microscopy paired with chlorophyll concentrations over time, both methods confirm a distinct natural bloom progression from a diatom dominated phytoplankton community structure at the onset of the bloom to one dominated by microzooplankton and mixed aggregates near the end of the experiment (Figure 6.6). Increased observation of potential grazing on phytoplankton by microzooplankton and aggregate formation towards the end of the bloom, provides insight on the physiological state of the phytoplankton bloom across the experiment (Figure 6.6). These types of stressors upon phytoplankton may lead to released exudate containing carbon and sulfur that will supply microbial metabolisms which in turn may influence the production of climate relevant trace gas production and biogenic aerosol

composition (Levine, 2016). Based on these initial results it seems that the high temporal resolution time series produced by this image data set will lead to an improved understanding of plankton bloom dynamics in mesocosms and the subsequent production of oceanic aerosols.

6.5.3 Impact of experimental approach on dissolved organic matter composition

While a complete discussion of the analysis of mDOM over the duration of SeaSCAPE is beyond the scope of this manuscript, two analyses are shown to illustrate various factors which describe the operation of the experiment. Shown in Figure 6.12 is a GCxGC ion chromatogram of seawater obtained before addition to the wave channel. Notable in the composition of this seawater is the vast chemical diversity of the sample in addition to a large quantity of anthropogenic contaminants. These species are ubiquitous in the coastal zone and are unavoidable in mesocosm experiments using coastal water.

To understand effect of perturbations on the chemical composition of SeaSCAPE seawater, TD-GC/GC-EI-HRToFMS was performed on the following samples: mDOM from seawater gathered at the SIO pier before transfer to the wave channel on 7/23, mDOM of the seawater after transfer to the wave channel on 7/23, and mDOM of the seawater after the addition of the outdoor phytoplankton culture on 8/1. Shown in Figure 6.7a is a spectral comparison plot in which the ion intensity chromatogram obtained after the water transfer was subtracted by the chromatogram obtained before the water was transfer. Very few ions were introduced by the transfer process, with 4% of the ion current for species classified as anthropogenic contaminants being added during the water transfer process. In contrast to the small perturbation made by water transfer, a much larger quantity of ion current was measured in mDOM after the addition of the outdoor phytoplankton tank to the wave channel, likely from biogenic organics (Figure 6.7b).

6.5.4 SSA Size Distributions and Stability

The shape of the SSA size distributions is largely consistent with previous studies of SSA generated by breaking waves (Prather et al., 2013). However, there was significant temporal variability in the total concentration of particles observed during the experiment. A strong diurnal trend was observed, with higher, more variable concentrations observed during the daytime (N_{day} = 272 ± 92 #/cm^3) and lower, yet more stable concentrations observed during the nighttime (N_{night} = 199 ± 70 #/cm^3) (Figure 6.8). While seawater temperature can affect the flux of SSA, the daily changes observed during the SeaSCAPE experiment were likely not large enough to explain the variability in SSA concentration (Lewis and Schwartz, 2004). Typical daily water temperature changes were 1-2°C (Figure 6.2), which should correspond to a change in SSA flux of only 2-8% (Forestieri et al., 2018), whereas the observed change from night to day is, on average, ~37%. The diurnal changes also do not appear to be linked to other changes such as the wave channel lights or the chemical composition of the seawater. Rather, we suspect that the changes in SSA production were driven by the opening and closing of the laboratory doors, which resulted in a pressure change in the air flow and mixing dynamics within the channel headspace. These findings, alongside the results of the sampling port location and depth testing (Figure 6.5), demonstrate the heterogeneous mixing within the wave channel headspace, resulting in variable SSA number concentrations. Further testing and modelling of the wave channel is necessary to fully understand these observations.

6.5.5 Evidence of abiotic volatile organic compounds from interfacial photochemistry

To test whether abiotic VOCs could be produced simply by irradiating the surface species with sunlight, surface water from the wave channel was taken into the UCSD environmental complex analysis laboratory (ECAL) facility nearby and exposed to light from a solar simulator.

Shown in Figure 6.9a, there were two unique molecular signatures that were immediately sensitive upon irradiation, as well as three others not shown here (isoprene, dimethyl sulfone, and decadienal only in some days during Bloom 3) analyzed using a modified gas-phase APCI Orbitrap MS. Several other species also increased during this time but exhibited a more gradual increase, indicating a diffusion limited, and therefore most likely a biogenic, process. Two of these abiotically-produced species were able to be structurally identified using tandem MS, showing fragmentation patterns that clearly indicated the presence of phenol, C_6H_6O, and (mostly) beta-cyclocitral, $C_{10}H_{16}O$. The signal enhancement of these molecules, immediately upon irradiation (within 3 minutes), compared to the background dark signal, are shown in Figures 6.9b and 6.9c respectively. There was evidence in the fragmentation data of $C_{10}H_{16}O$ to suggest that beta-cyclocitral was not the only species of the same mass-to-charge ratio. Without an in-depth experiment to constrain the many multiple variables in seawater such as the microbiology or surface tension, it is difficult to make any assumptions about mechanisms. Gas-phase APCI Orbitrap MS was shown to successfully ionize a variety of molecular signatures off-gassing from the sea sample surface as well as detect changes when the sample was exposed to solar light.

6.5.6 Relative distribution of morphologies for nascent and aged SSA

Nascent SSA displayed four unique morphologies including prism-like, core-shell, rounded and aggregates, while aged SSA had two main morphologies: core-shell and rounded (Figure 6.10a). The morphological categorization was performed qualitatively, analogous to previous studies (Lee et al., 2020b; Ray et al., 2019). Next, the relative distribution of morphologies for nascent and aged SSA samples were compared (Figure 6.10b). For the nascent SSA sample morphologies, the rounded (47%) was most common, followed by the core-shell (22%), while prism-like (17%) and aggregates (14%) showed similar abundancies. On the other

hand, for the aged SSA sample morphologies, core-shell (72%) was most common, followed by the rounded (28%) morphology, while no prism-like and aggregates were observed. Overall, SSA aging results in significant increase of the abundance for core-shell morphology, and concomitant decreases in the rounded and prism-like morphologies. Additionally, core-shell aged SSA particles showed a thicker coating compared with similar size nascent core-shell particles.

6.6 Discussion

A key challenge in ocean-atmosphere simulation experiments is maintaining the highest degree of experimental cleanliness while still capturing the complexity of the natural environment. This challenge is further pressed by the massive volumes of seawater that must be collected and transferred without significant perturbation of the biological assemblages and chemical contamination of the water. For the headspace, large airflows are necessary to offset the flow demand required by online instrumentation and filter sampling. Generating large volumes of high purity air is a significant challenge beyond the removal of particulates. Here we showed that the transfer of seawater from the ocean to the laboratory incurred little contamination, however the headspace of the wave channel was challenging to keep clean of anthropogenic VOCs with the air handling system. For sampling of VOCs produced from seawater, the incorporation of the ISV was a critical addition that enabled the measurement of secondary aerosol and gases by generating a clean headspace for seawater VOCs to flux into. In the future, advances in economically generating high volumes of particle free, low VOC air would be ideal to enable the measurements of seawater-produced VOCs without the incorporation of secondary chambers.

Systematic testing of the wave channel was conducted to determine the optimal sampling conditions for nascent SSA. This testing showed a clear relationship between the air flowrate in the channel headspace and the measured concentrations of SSA particles, with lower air speeds

resulting in higher particle concentrations. However, when the effect of both sampling port location and penetration depth into the channel headspace were evaluated, it was apparent that the SSA concentrations in the headspace were heterogeneous and highly variable, depending on sampling locations. Further observations during the SeaSCAPE experiment showed a strong diurnal trend in the SSA concentrations, which may have been caused by the opening and closing of the laboratory doors, creating a change in air pressure in the building. Based on these findings, future work is needed to model the fluid dynamics in the wave channel to understand the mixing and transport of aerosols and gases in the headspace. Additionally, it was observed that SSA concentrations were typically more stable at night, when the laboratory doors were closed, which could have caused higher air pressure in the room. This suggests that future modifications could be made to the wave channel to increase stability in the particle concentrations, such as replacing the open flap at the end of the channel with a sealed vent system. However, despite the variability in total number concentrations, the shape of the SSA size distributions remained consistent throughout the experiment and agrees well with previous wave channel experiments (Prather et al., 2013). This indicates that the heterogeneity in the number concentrations was driven by different degrees of dilution, due to uneven mixing in the headspace, as opposed to variations in the SSA production mechanism or bubble sizes generated by the breaking wave.

One of the most crucial elements of mesocosm experiments to study ocean-atmosphere processes is the stimulation of a phytoplankton bloom (Lee et al., 2015; Pomeroy et al., 2007) involving all the trophic interactions in the microbial loop (Azam et al., 1983; Buchan et al., 2014) between phytoplankton, protozoans, heterotrophic bacteria, and viruses (Lee et al., 2015; Pomeroy et al., 2007). Recent efforts have sought to better reproduce the complexity of marine biology while also accurately measure the turnover of assemblages to better ascribe changes in seawater,

SSA composition and properties, and VOC production. An ongoing challenge is the successful stimulation of rich mesocosms using natural seawater which varies in biological composition and may not respond immediately to nutrient amendments. For the 3rd bloom during SeaSCAPE, the addition of the outdoor tank grown in elevated nutrient conditions and natural sunlight provided a richer starter culture for further growth in the wave channel. In the future, enhanced lighting intensity, possibly the usage of actinic flux, will be implemented to allow bloom formation without this added intervention. Phytoplankton community showed a natural succession across the experiment from a diatom dominated community at the peak of the bloom during the growth phase towards a diatom aggregate and zooplankton populated senescent phase. Connection of these biological phases with the composition of gases, DOM, and aerosol composition will be the focus of ongoing work by CAICE. Further analysis of the functional (e.g. production, enzymes) and community adaptation (16S and 18S rDNA amplicon sequencing) of the marine microbes over the course of the bloom in the water, SML and aerosols will help address some of the chemical changes observed during SeaSCAPE.

The abiotic production of VOCs from seawater via reactions of surface-present organics with light and oxidants has been recently discussed as a possible source of atmospheric VOCs competitive in emission quantity with marine biology (Novak and Bertram, 2020). Currently, only laboratory measurements of abiotic VOC production have been undertaken, with most utilizing SSML or synthetic organic films doped with terrestrially relevant photosensitizers to enhance yields of irradiation-initiated VOC emission (Ciuraru et al., 2015; Trueblood et al., 2019a). Here, using unadulterated seawater from our mesocosm experiments, we show small quantities of abiotic VOC generation, including cyclic species, but do not maintain sustained emission compared to other laboratory investigations. Lack of sustained emission is likely due to the limited pool of

organic species in raw seawater which may have been lost through emission and chemical transformation. While the complex mechanisms that control photoinitiated VOC production are poorly understood, mesocosm experiments serve as a valuable bridge between field and laboratory work towards answering the relative contributions of biotic and abiotic VOC production in the marine environment and will be further pursued.

Heterogeneous aging of SSA by OH radical led to significant changes in its morphology, with the total loss of prism-like and aggregate type particles, and a large enhancement in core-shell particles. Increased oxidation of organic aerosol has been shown to increase its viscosity, potentially affecting its phase state (Athanasiadis et al., 2016; Saukko et al., 2012). This process may have contributed to the change in SSA morphologies observed here. An alternative explanation is that coating of secondary organic species onto the SSA altered its morphology. Future studies are necessary to understand how both of these processes influence SSA phase and morphology, and the potential influence on its climate relevant properties, such as ice nucleation, water uptake, and light scattering.

6.7 Conclusions

In summary, wave channels represent an important method for understanding the production and properties of marine aerosols and gases under controlled laboratory conditions. Optimization of the wave channel system has enabled even more detailed atmospheric measurements over previous experimental campaigns. In addition, major improvements have been made in the capability to simulate complex seawater biology. The incorporation of oxidation flow reactors has, for the first time, enabled the study of secondary aerosol formation and photochemical aging of SSA during a large-scale wave channel experiment. Preliminary findings from the SeaSCAPE campaign have shed light on the photochemical production of VOCs, impact of

atmospheric aging on SSA phase and morphology, and the chemical composition of SMA. Future analysis of the SeaSCAPE dataset is expected to give insight to, among other processes, the nature of marine INPs in both freshly-emitted and aged SSA; the potential for both SSA and SMA to serve as CCN in the marine atmosphere; the molecular composition of SSA and its links to biological activity; the identity of unique marine VOCs and possible SOA precursors; and the effect of photochemical aging on the chemical composition of marine aerosols. Oceanic emissions of both gases and particles have profound effects on the climate through their interactions with clouds and solar radiation. Laboratory ocean-atmosphere experiments have and will continue to expand our knowledge of marine aerosols and their influence on the climate system.

6.8 Acknowledgements

This material is based upon work supported by the National Science Foundation through the Center for Aerosol Impacts on the Chemistry of the Environment, an NSF Center for Chemical Innovation (CHE-1801971). The authors would like to acknowledge the extensive SeaSCAPE team who helped make the experiment possible.

Chapter 6, in full, is currently being prepared for submission for publication of the material. Sauer, J.S., Mayer, K.J., Lee, C., Crocker, D.R., A., Alves, M.R., Amiri, S., Barnes, E., Crocker, D.R., Dinasquet, J., Kaluarachchi, C.P., Dang, D., Glicker, H., Kilgour, D., Lawler, M.J., Mitts, B.A., Morris, C.K., Moore, A.N., Tumminello, P.R., Walker, J.L., Goldstein, A.H., Grassian, V.H., Jaffe, J.S., Malfatti, F., Martz, T.R., Tivanski, A.V.,Cappa, C.D., Bertram, T.H., Prather, K.A. "The Sea Spray Chemistry and Particle Evolution Study (SeaSCAPE): Overview and Experimental Methods", Kathryn J. Mayer, Christopher Lee, and the dissertation author are co-first authors of this manuscript.

6.9 Figures

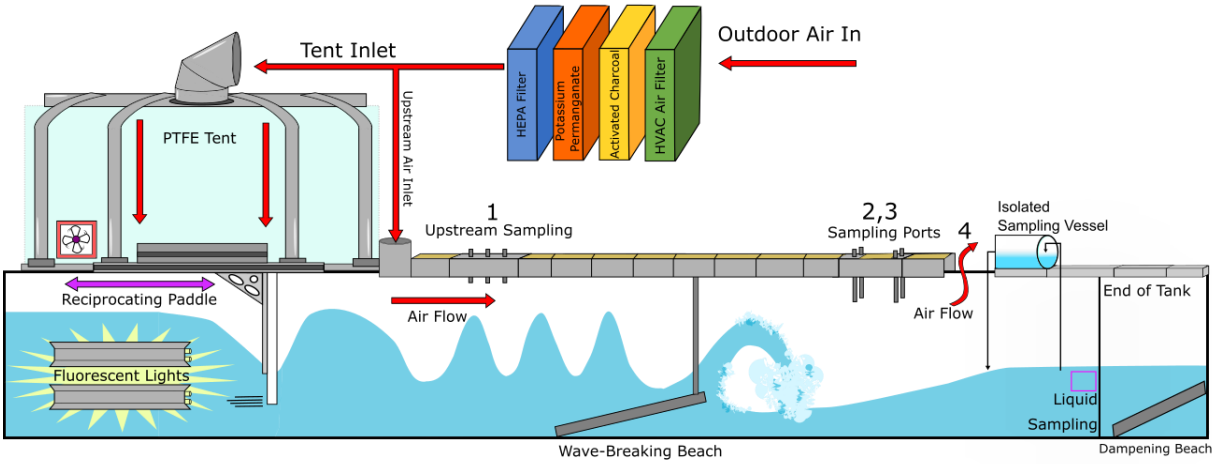

Figure 6.1 Schematic of the SIO Ocean Atmosphere Interaction Facility (OAIF) Wave Channel: Notable locations for sampling and air outflow are denoted by 1, 2, 3, 4 where the distances of each (from the front of the wave channel): 1 = 6 m , 2 = 16.0 m , 3 = 17.5 m , 4 = 20.6 m. Fluorescent lighting was strung across the entire length of the wave channel

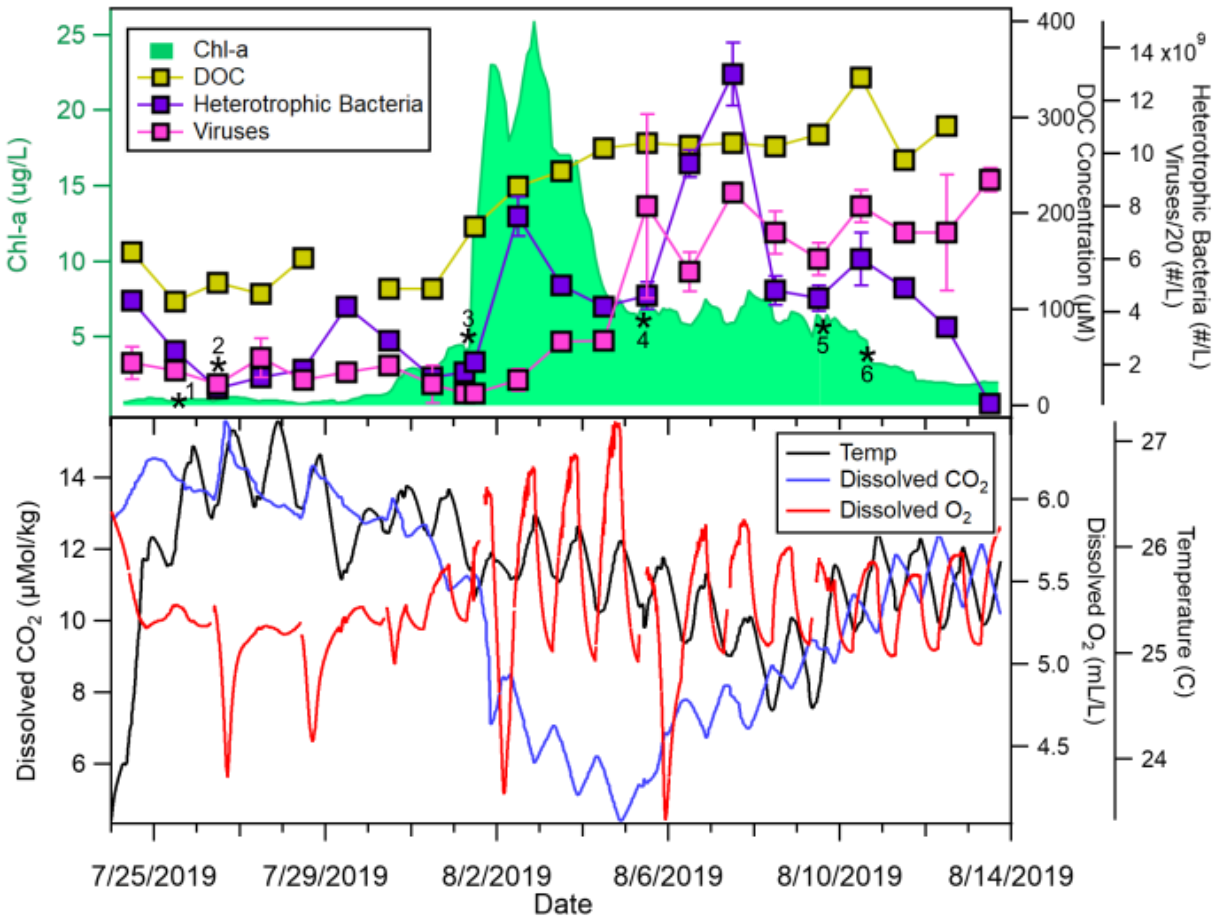

Figure 6.2 a) SeaSCAPE Bloom 3 Chl-a, DOC, and heterotrophic bacteria counts over the mesocosm duration. Asterisks indicate notable interventions in mesocosm. Asterisks 1 and 2 correspond to nutrient additions specified in Table 6.1. Asterisk 3 corresponds to the addition of the outdoor tank to the wave channel. Asterisk 4 corresponds to the scraping of wave channel walls to remove light-obstructive detritus. Asterisks 5 and 6 correspond to the addition of circulating pumps to resuspend cellular material aggregated on the wave channel bottom. b) SeaSCAPE Bloom 3 water temperature, dissolved CO_2, and dissolved O_2.

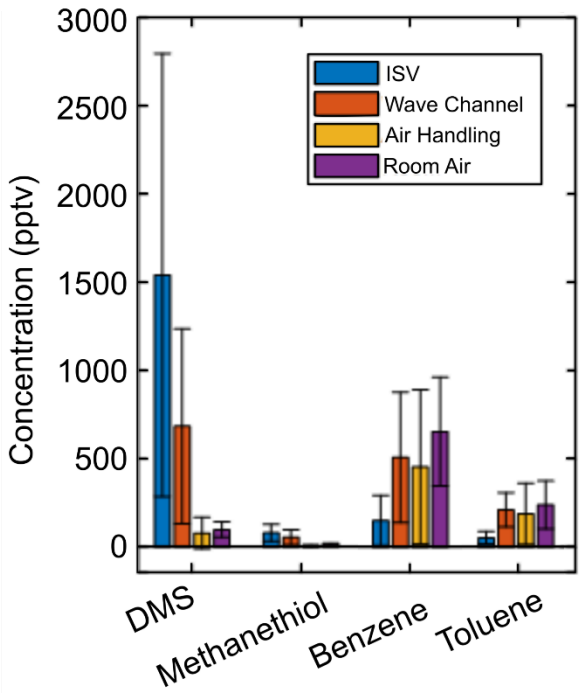

Figure 6.3 Histogram comparing mixing ratios of DMS, methanethiol, benzene, and toluene in the ISV, wave channel headspace downstream of wave-breaking, hydraulics laboratory room air, and air handling system. Bars represent the averages over the first eight days (7/24-8/1) of the third bloom, and error bars represent the standard deviation in the measurements.

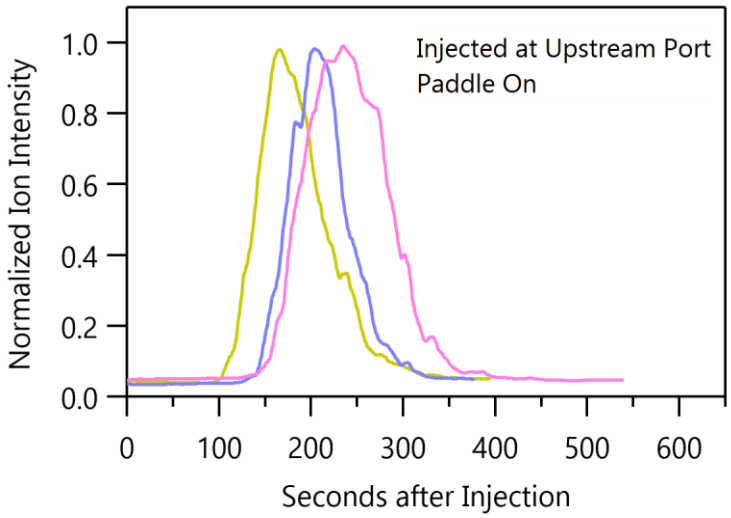

Figure 6.4 Replicate experiments of m/z 62 (dimethyl sulfide) arrival time at sampling port after injection into wave channel headspace at the upstream location. Instrument signal was boxcar smoothed into 10 second bins. Arrival times of DMS correspond to a wave channel headspace velocity between 4.9-7 $cm \cdot s^{-1}$

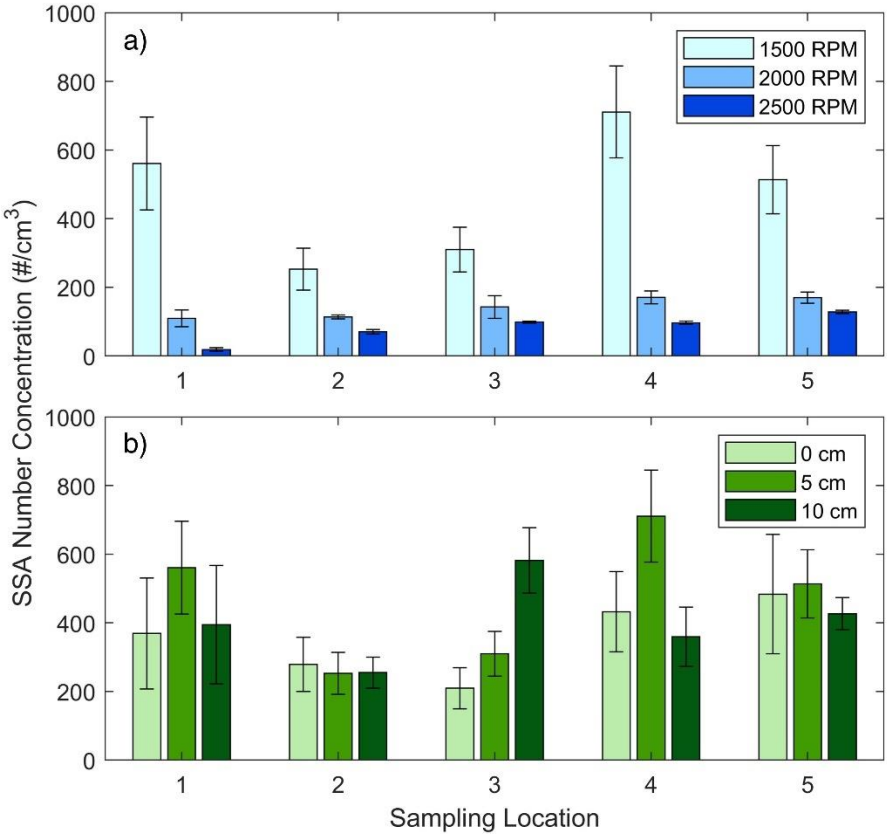

Figure 6.5 a) SSA number concentrations measured at 5 sampling locations with a 5 cm port depth, testing 3 different fan settings, which will control the air velocity in the wave channel headspace. The lowest setting (1500 RPM) was determined to yield the highest SSA concentrations at all sampling locations due to less dilution. b) SSA number concentrations at the different sampling locations with a fan speed of 1500 RPM, showing the effect of sampling port depth below the lids (0 cm, 5 cm, and 10 cm below the channel lids). There is no clear relationship between sampling port depth or location and number concentration, indicating heterogeneous particle concentrations in the channel headspace. The sampling port locations are evenly spaced and correspond to 0 cm, 60 cm, 120 cm, 180 cm, and 240 cm after the end of the wave breaking beach.

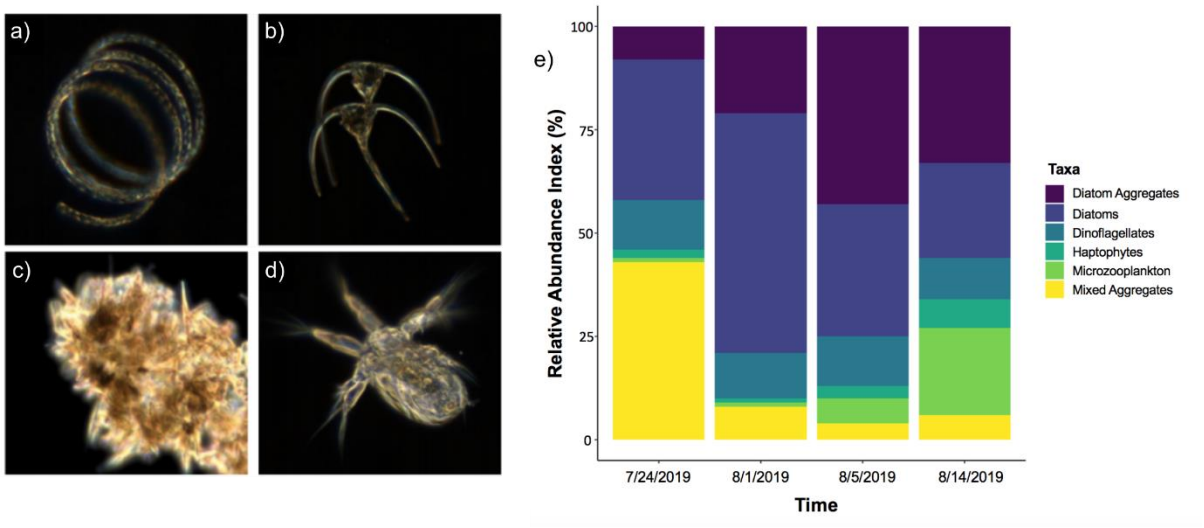

Figure 6.6 Micrographs of representative taxa across the duration of bloom 3, a-b) diatoms and dinoflagellates (beginning of bloom), c) mixed aggregates (dominated by diatoms and haptophytes mid bloom), d) microzooplankton (micro zooplankton and ciliates peak at the end of the bloom). e) Time series speciation of phytoplankton taxa across SeaSCAPE.

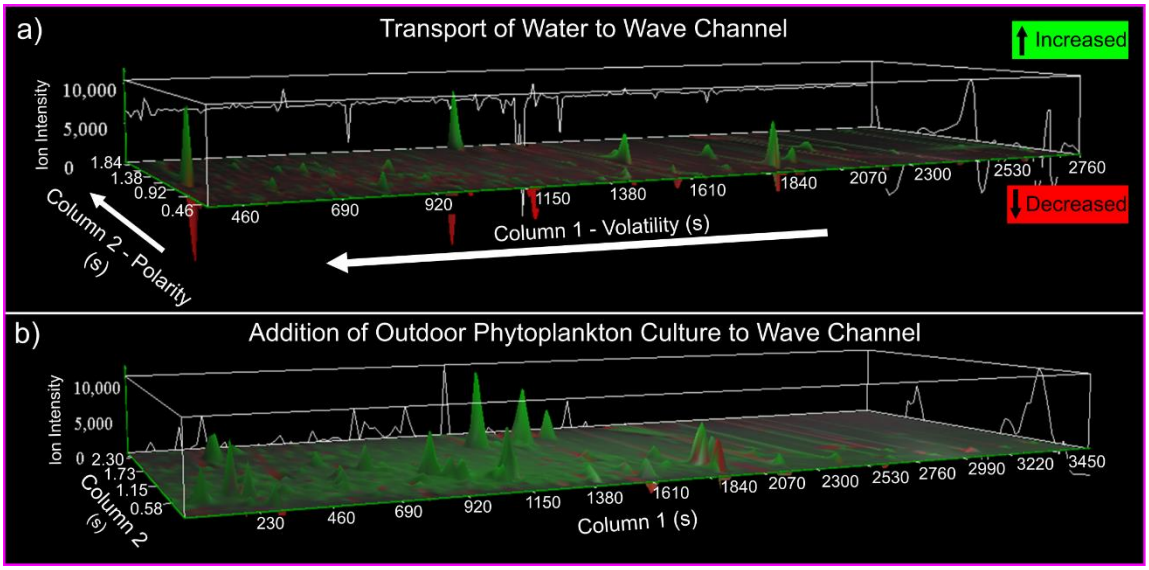

Figure 6.7 Three dimensional mDOM GCxGC comparison spectra: a) Comparison of organic signature pre and post water transport from pier b) Comparison of organic signature pre and post concentrated bloom addition (8/1/2019). Peaks of positive (upward facing) intensity reflect ions observed to increase in intensity following treatment. Very few ions increased in intensity after transfer from ocean to wave channel compared to the addition of the outdoor culture.

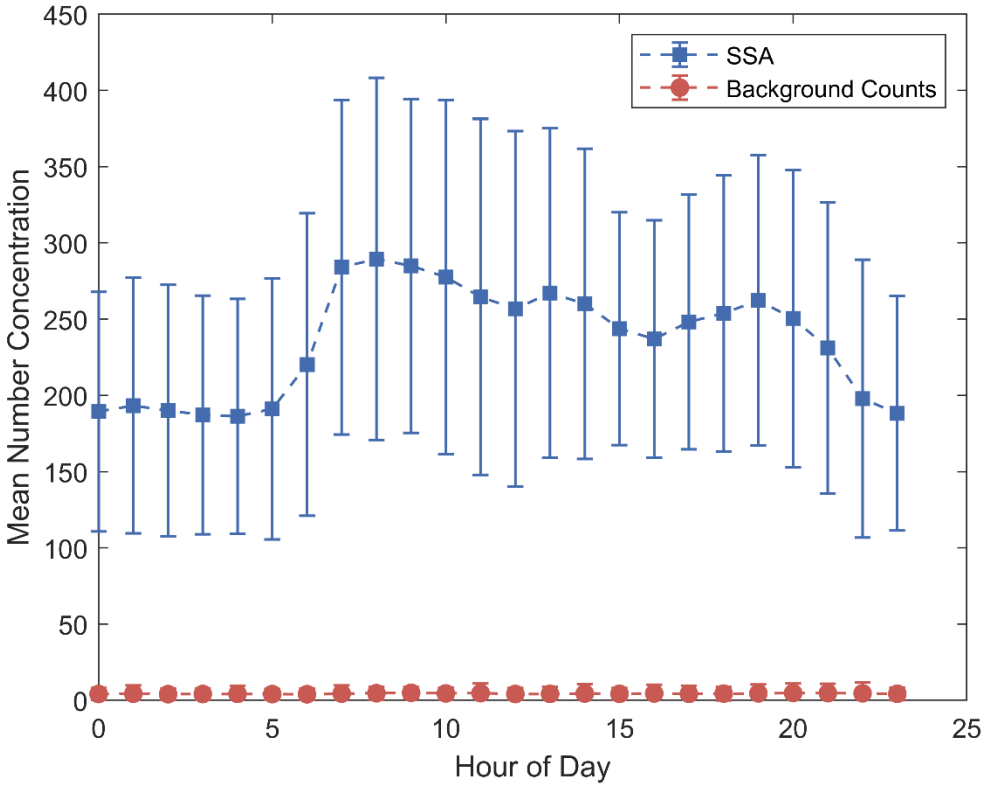

Figure 6.8 Hourly average SSA number concentrations for all blooms, demonstrating the large variability in aerosol production, as well differing diurnal behavior. In general, particle concentrations tended to be higher and more variable during the daytime, but lower and more stable overnight. The background particle counts, as measured by the upstream CPC, are also shown.

-

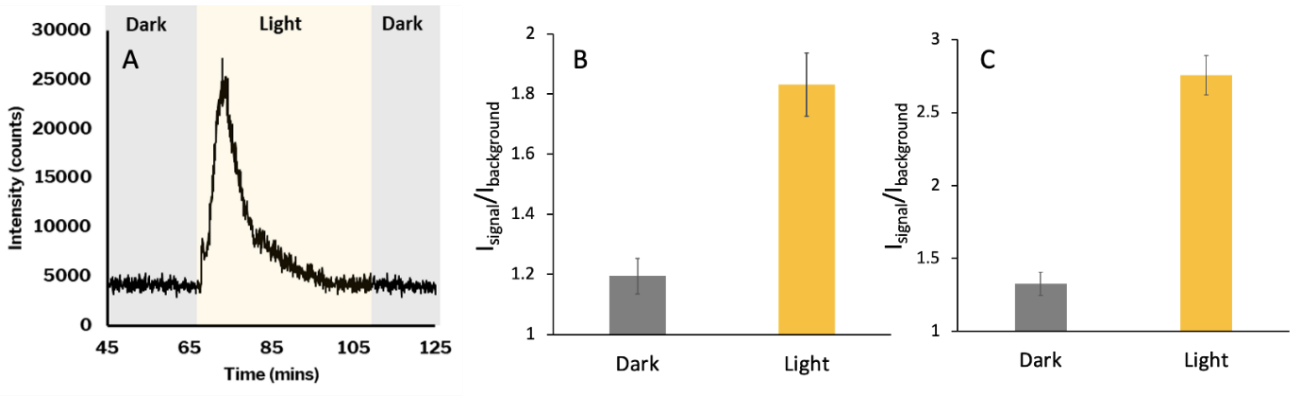

Figure 6.9 Data from gas-phase modified APCI high resolution mass spectrometry of Bloom 2 seawater collected on July 20th showing a) total ion current of summed volatile species found to be sensitive to irradiation, where gray indicates when the sample was kept dark and yellow when the sample was subjected to light; b) the signal enhancement of C_6H_6O, or phenol, immediately upon irradiation, and c) the signal enhancement of $C_{10}H_{16}O$, or beta-cyclocitral, immediately upon irradiation. Error bars represent one standard deviation of the signal averaged over its highest peak.

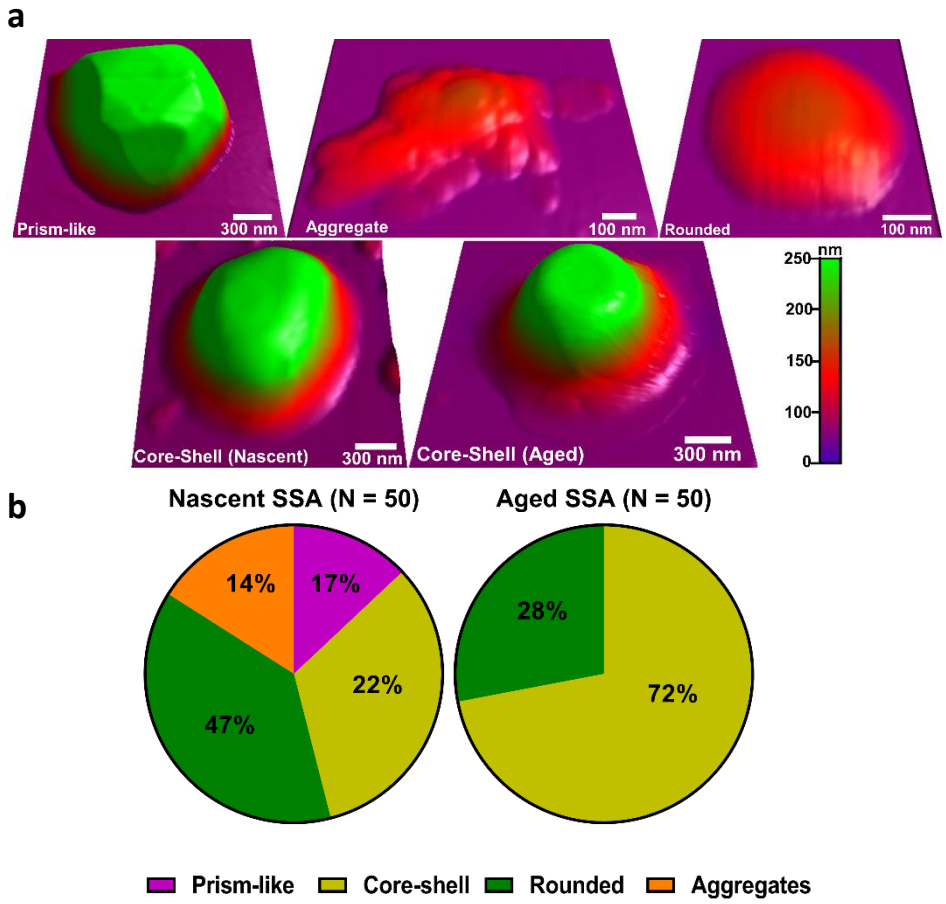

Figure 6.10 a) Representative AFM 3D-height images of individual SSA particles observed during the peak of the bloom (Aug 3rd). Color scale shows height difference between the particles b) Relative distribution of the morphologies in nascent and aged SSA samples. Prism-like, core-shell, rounded, and aggregates particles are represented by purple, yellow, green, and orange colors, respectively. Impacts of aging on SSA show a relative increase in the fraction of core-shell particles and the loss of prism-like particles.

6.10 Tables

Table 6.1: Summary of nutrient additions during the three SeaSCAPE bloom cycles.

Bloom Cycle	Water Fill Date	Nutrient Addition Date	Nutrient Concentration
Bloom 1	7/1/2019	7/4/2019	f/2 nutrients + silicates
Bloom 2	7/12/2019	7/14/2019	f/20 nutrients + silicates
Bloom 3	7/23/2019	7/25/2019	f/20 nutrients + f/40 silicates
		7/26/2019	Addition silicates, to f/20 total
		8/1/2019	Additional nutrients and silicates, to total concentration of f/2 for both

Table 6.2 Summary of all online aerosol measurement techniques employed during SeaSCAPE. The sample type is designated by a single letter (N = Nascent SSA, H = Heterogeneously-aged SSA, S = Secondary Marine Aerosol)

Measurement	**Technique**	**Sample type**	**Sampling Interval**	**Reference**
Dry (RH<20%) particle size distributions from 5 nm to 20 μm	Scanning Mobility Particle Sizer (SMPS, TSI Inc)	N,H,S	2-5 min	(Shen et al., 2002)
	Aerodynamic Particle Sizer (APS 3321, TSI Inc)	N,H	1 min	(Peters and Leith, 2003)
	Scanning Electrical Mobility Spectrometer (SEMS, Brechtel)	N,H	5 min	(Lopez-Yglesias et al., 2014)
Total particle number	Condensation Particle Counter (CPC)	N	1 s	(Hering et al., 2019)
Single particle composition and size	Aerosol Time-of-Flight Mass Spectrometer (ATOFMS)	N,H	1 min	(Gard et al., 1997)
Size-resolved submicron aerosol non-refractory composition	High Resolution Time-of-Flight Aerosol Mass Spectrometer (HR-ToF-AMS)	N,H,S	5 min	(DeCarlo et al., 2006)
Submicron aerosol chemical composition	Thermal Desorption Chemical Ionization Mass Spectrometer (TD-CIMS)	N,S	N: 1 h S: 30 min	(Smith et al., 2004; Voisin et al., 2003)
Submicron aerosol chemical composition	Extractive Electrospray Ionization Mass Spectrometry (EESI-MS)	N,H,S	1 s	(Lopez-Hilfiker et al., 2019)
Size-resolved cloud condensation nuclei activity	Continuous-flow streamwise thermal-gradient CCN counter	N,H,S	30-60 min	(Roberts and Nenes, 2005)
Relative humidity-dependent aerosol bounce	Electrical Low Pressure Impactor (ELPI)	N,H,S	1 min	(Jain and Petrucci, 2015)
INP concentration	Continuous-flow diffusion chamber (CFDC)	N,H	5-15 min	(Demott et al., 2015)
Size-resolved fluorescent biological particle number concentrations	Wideband Integrated Bioaerosol Sensor (WIBS)	N,H	1 s	(Gabey et al., 2011)

Table 6.3 Summary of all offline aerosol measurement techniques employed during SeaSCAPE. The sample type is designated by a single letter (N = Nascent SSA, H = Heterogeneously-Aged SSA, S = Secondary Marine Aerosol)

Measurement	Collection Technique	Analysis Technique	Sample type	Sampling Interval	Reference
INP concentration and characteristics	Polycarbonate filters	Ice Spectrometer	N,H	1-5.5 h	(Perkins et al., 2020)
Size-segregated organic aerosol composition	Sioutas Cascade Impactor	High resolution mass spectrometry	N,H	6-12 h	(Cochran et al., 2016; Hettiyadura et al., 2017)
Single particle morphology, phase state, organic volume fraction, and water uptake	MOUDI Impactor	Atomic force microscopy (AFM)	N,H	N: 5-6 h H: 1-2 h	(Lee et al., 2017, 2020a)
		AFM photothermal infrared spectroscopy (AFM-PTIR)	N,H	N: 5-6 h H: 1-2 h	(Or et al., 2018)
Immersion freezing of single particles	MOUDI Impactor	Micro-Raman spectroscopy	N,H	N: 5-6 h H: 1-2 h	(Mael et al., 2019)
Aerosol pH	MOUDI Impactor	pH paper	N	1-2 h	(Angle et al., 2020)
Chemical and microbial composition	Quarts fiber filters	High-resolution mass spectrometry	N	24 h	(Petras et al., 2017)
		16S/18S rDNA sequencing	N	24 h	Michaud
Viral and bacterial abundances	Spot sampler	Flow cytometry	N	6h	(Brussaard, 2004; Gasol and Del Giorgio, 2000)
Enzymes Activities	Spot sampler	Fluorogenic substrates	N	6 h	(Hoppe, 1983)
C_{13}-C_{36} n-alkane equivalents chemical speciation	Quartz Fiber Filters	GCxGC-HRTOF-MS	N	14 h /10 h (day/night)	(Jen et al., 2019)
Submicron and Supermicron Isotopic Analysis	Cyclone and Quartz Fiber Filters	MAT 253 Isotope-ratio mass spectrometry (IRMS)	N	48 h	(Crocker et al., 2020)

Table 6.4 Summary of all gas-phase measurement techniques employed during SeaSCAPE. The sample type is designated by a single letter (W = wave channel headspace, I = isolated sampling vessel headspace, D = dissolved gases, A = air handling system, O = OFR, B = bulk seawater, L = SSML)

Measurement	Technique	Sample type	Sampling Interval	Reference
O_3	UV absorption, Thermo Environmental Model 49C	W	1 s	N/A
	UV absorption, 2B Technologies Model 202	A,O	1 s	N/A
$NO\text{-}NO_2\text{-}NO_x$	Chemiluminescence, Thermo Environmental Model 42C	W,A	1 s	N/A
SO_2	Pulsed fluorescence, Thermo Environmental Model 43iQ	W,A	1 s	N/A
VOCs	Vocus Proton Transfer Reaction Mass Spectrometry (PTR-MS)	W,I,A	1 s	(Krechmer et al., 2018)
Sulfur-containing VOCs	Chemical Ionization Mass Spectrometry (Benzene reagent ion, B-CIMS)	I,D	1 s	(Kim et al., 2016)
C5-C18 n-alkane equivalents	TD-GCxGC-EI/VUV-HRTOF-MS	I	20 min collection, every 1-3 days	(Hatch et al., 2019)
Abiotic photo-enhanced surface products	Gas phase modified-atmospheric pressure chemical ionization Orbitrap mass spectrometry (APCI-MS)	B,L	24 h	(Roveretto et al., 2019)

6.11 Supplementary Figures

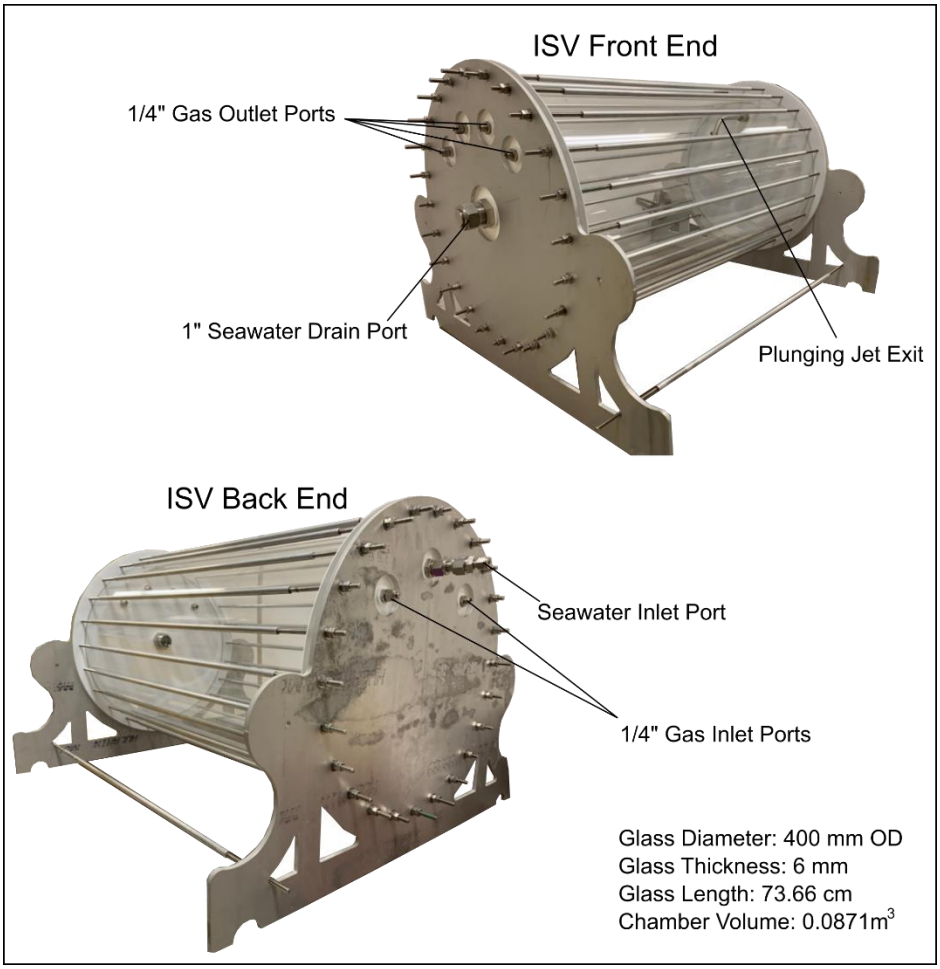

Figure 6.11 Photographs showing the design and dimensions of the isolate sampling vessel (ISV) used for gas-phase and OFR experiments during SeaSCAPE

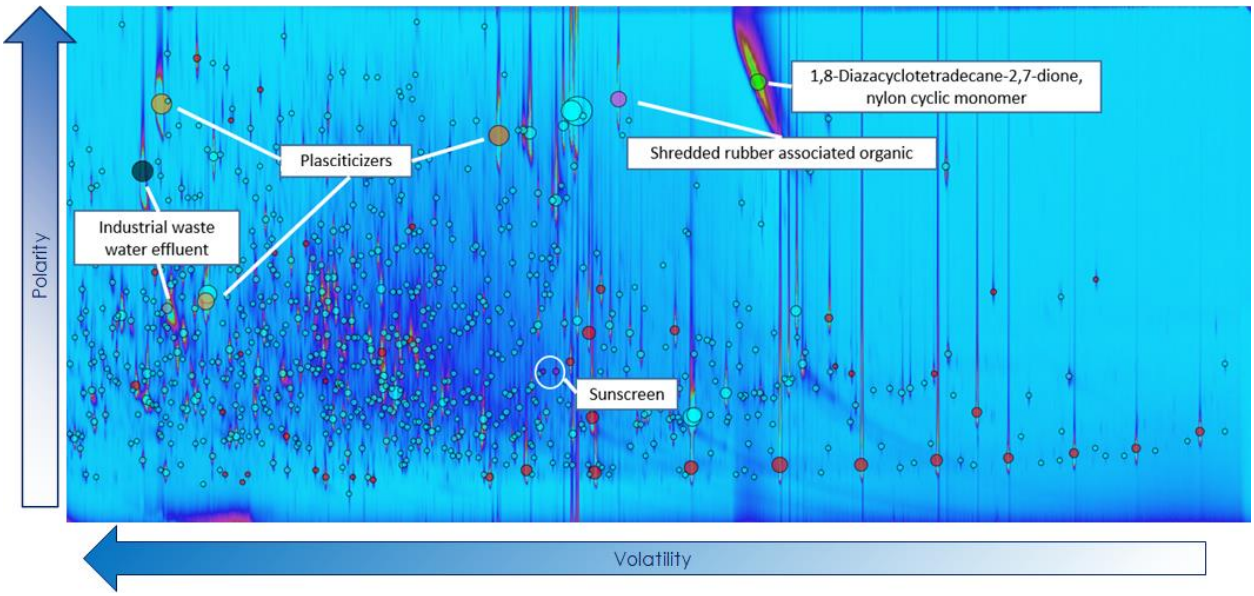

Figure 6.12 GCxGC spectrum of Scripps Pier mDOM prior to transport into the wave channel. Significant contributions of anthropogenic plasticizers, wastewater effluent products, and personal care products (identified by confident mass spectral match to NIST library complemented by literature review) highlighted.

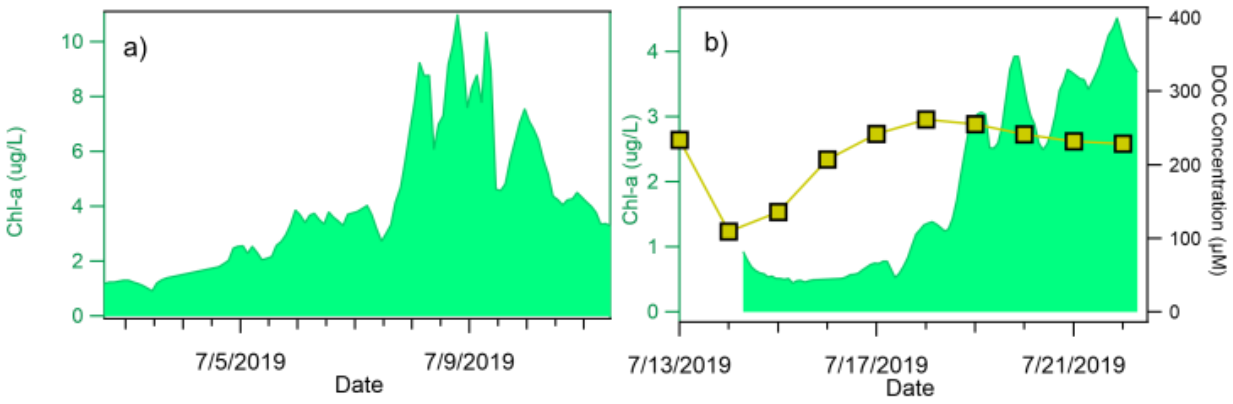

Figure 6.13 Time series chlorophyll-a and DOC for mesocosm blooms 1 (a) and 2 (b) during SeaSCAPE

6.12 References

Angle, K. J., Crocker, D. R., Simpson, R. M. C., Mayer, K. J., Garofalo, L. A., Moore, A. N., Garcia, S. L. M., Or, V. W., Srinivasan, S., Farhan, M., Sauer, J. S., Lee, C., Pothier, M. A., Farmer, D. K., Martz, T. R., Bertram, T. H., Cappa, C. D., Prather, K. A. and Grassian, V. H.: Acidity across the interface: from ocean waters to sea spray aerosol, Proc. Natl. Acad. Sci., Accepted, 2020.

Athanasiadis, A., Fitzgerald, C., Davidson, N. M., Giorio, C., Botchway, S. W., Ward, A. D., Kalberer, M., Pope, F. D. and Kuimova, M. K.: Dynamic viscosity mapping of the oxidation of squalene aerosol particles, , 30385–30393, doi:10.1039/c6cp05674a, 2016.

Ault, A. P., Guasco, T. L., Ryder, O. S., Baltrusaitis, J., Cuadra-Rodriguez, L. A., Collins, D. B., Ruppel, M. J., Bertram, T. H., Prather, K. A. and Grassian, V. H.: Inside versus outside: Ion redistribution in nitric acid reacted sea spray aerosol particles as determined by single particle analysis, J. Am. Chem. Soc., 135(39), 14528–14531, doi:10.1021/ja407117x, 2013.

Azam, F., Fenchel, T., Field, J., Gray, J., Meyer-Reil, L. and Thingstad, F.: The Ecological Role of Water-Column Microbes in the Sea, Mar. Ecol. Prog. Ser., 10, 257–263, doi:10.3354/meps010257, 1983.

Boucher, O., Randall, D., Artaxo, P., Bretherton, C., Feingold, G., Forster, P., Kerminen, V.-M. V.-M., Kondo, Y., Liao, H., Lohmann, U., Rasch, P., Satheesh, S. K., Sherwood, S., Stevens, B., Zhang, X. Y. and Zhan, X. Y.: Clouds and Aerosols, Clim. Chang. 2013 Phys. Sci. Basis. Contrib. Work. Gr. I to Fifth Assess. Rep. Intergov. Panel Clim. Chang., 571–657, doi:10.1017/CBO9781107415324.016, 2013.

Bouvet, M., Hoepffner, N. and Dowell, M. D.: Parameterization of a spectral solar irradiance model for the global ocean using multiple satellite sensors, J. Geophys. Res. Ocean., 107(C12), 8–18, doi:https://doi.org/10.1029/2001JC001126, 2002.

Brussaard, C. P. D.: Optimization of procedures for counting viruses by flow cytometry, , 70(3), 1506–1513, doi:10.1128/AEM.70.3.1506, 2004.

Buchan, A., LeCleir, G. R., Gulvik, C. A. and González, J. M.: Master recyclers: features and functions of bacteria associated with phytoplankton blooms., Nat. Rev. Microbiol., 12(10), 686–698, doi:10.1038/nrmicro3326, 2014.

Carlson, D. J.: Surface microlayer phenolic enrichments indicate sea surface slicks, Nature, 296, 426–429, doi:10.1038/296426a0, 1982.

Chen, W.-C. and Marcus, R. A.: On the theory of the reaction rate of vibrationally excited CO molecules with OH radicals, J. Chem. Phys., 124(2), 024306, doi:10.1063/1.2148408, 2006.

Ciuraru, R., Fine, L., Pinxteren, M. Van, D'Anna, B., Herrmann, H. and George, C.: Unravelling New Processes at Interfaces: Photochemical Isoprene Production at the Sea Surface, Environ. Sci. Technol., 49(22), 13199–13205, doi:10.1021/acs.est.5b02388, 2015.

Cochran, R. E., Laskina, O., Jayarathne, T., Laskin, A., Laskin, J., Lin, P., Sultana, C., Lee, C., Moore, K. A., Cappa, C. D., Bertram, T. H., Prather, K. A., Grassian, V. H. and Stone, E. A.: Analysis of Organic Anionic Surfactants in Fine and Coarse Fractions of Freshly Emitted Sea Spray Aerosol, Environ. Sci. Technol., 50(5), 2477–2486, doi:10.1021/acs.est.5b04053, 2016.

Collins, D. B., Zhao, D. F., Ruppel, M. J., Laskina, O., Grandquist, J. R., Modini, R. L., Stokes, M. D., Russell, L. M., Bertram, T. H., Grassian, V. H., Deane, G. B. and Prather, K. A.: Direct aerosol chemical composition measurements to evaluate the physicochemical differences between controlled sea spray aerosol generation schemes, Atmos. Meas. Tech., 7(11), 3667–3683, doi:10.5194/amt-7-3667-2014, 2014.

Crocker, D. R., Hernandez, R. E., Huang, H. D., Pendergraft, M. A., Cao, R., Dai, J., Morris, C. K., Deane, G. B., Prather, K. A. and Thiemens, M. H.: Biological Influence on 13C and Organic Composition of Nascent Sea Spray Aerosol, ACS Earth Sp. Chem., 4(9), 1686–1699, doi:10.1021/acsearthspacechem.0c00072, 2020.

Cunliffe, M. and Wurl, O.: Sampling the Sea Surface Microlayer., 2015.

DeCarlo, P. F., Kimmel, J. R., Trimborn, A., Northway, M. J., Jayne, J. T., Aiken, A. C., Gonin, M., Fuhrer, K., Horvath, T., Docherty, K. S., Worsnop, D. R. and Jimenez, J. L.: Field-deployable, high-resolution, time-of-flight aerosol mass spectrometer, Anal. Chem., 78(24), 8281–8289, doi:10.1021/ac061249n, 2006.

Demott, P. J., Prenni, A. J., McMeeking, G. R., Sullivan, R. C., Petters, M. D., Tobo, Y., Niemand, M., Möhler, O., Snider, J. R., Wang, Z. and Kreidenweis, S. M.: Integrating laboratory and field data to quantify the immersion freezing ice nucleation activity of mineral dust particles, Atmos. Chem. Phys., 15(1), 393–409, doi:10.5194/acp-15-393-2015, 2015.

DeMott, P. J., Hill, T. C. J., McCluskey, C. S., Prather, K. A., Collins, D. B., Sullivan, R. C., Ruppel, M. J., Mason, R. H., Irish, V. E., Lee, T., Hwang, C. Y., Rhee, T. S., Snider, J. R., McMeeking, G. R., Dhaniyala, S., Lewis, E. R., Wentzell, J. J. B., Abbatt, J., Lee, C., Sultana, C. M., Ault, A. P., Axson, J. L., Diaz Martinez, M., Venero, I., Santos-Figueroa, G., Stokes, M. D., Deane, G. B., Mayol-Bracero, O. L., Grassian, V. H., Bertram, T. H., Bertram, A. K., Moffett, B. F. and Franc, G. D.: Sea spray aerosol as a unique source of ice nucleating particles, Proc. Natl. Acad. Sci., 113(21), 201514034, doi:10.1073/pnas.1514034112, 2015.

Forestieri, S. D., Moore, K. A., Martinez Borrero, R., Wang, A., Stokes, M. D. and Cappa, C. D.: Temperature and Composition Dependence of Sea Spray Aerosol Production, Geophys. Res. Lett., 45(14), 7218–7225, doi:10.1029/2018GL078193, 2018.

Gabey, A. M., Stanley, W. R., Gallagher, M. W. and Kaye, P. H.: The fluorescence properties of aerosol larger than 0.8 μ in urban and tropical rainforest locations, Atmos. Chem. Phys., 11(11), 5491–5504, doi:10.5194/acp-11-5491-2011, 2011.

Gard, E., Mayer, J. E., Morrical, B. D., Dienes, T., Fergenson, D. P. and Prather, K. a: Real-time analysis of individual atmospheric aerosol particles: Design and performance of a portable ATOFMS, Anal. Chem., 69(20), 4083–4091, doi:10.1021/ac970540n, 1997.

Gasol, J. M. and Del Giorgio, P. A.: Using flow cytometry for counting natural planktonic bacteria and understanding the structure of planktonic bacterial communities, Sci. Mar., 64(2), 197–224, doi:10.3989/scimar.2000.64n2197, 2000.

Gong, S. L., Barrie, L. A. and Lazare, M.: Canadian Aerosol Module (CAM): A size-segregated simulation of atmospheric aerosol processes for climate and air quality models 2. Global sea-salt aerosol and its budgets, J. Geophys. Res. Atmos., 107(24), 1–14, doi:10.1029/2001JD002004, 2002.

Guillard, R. R. L. and Ryther, J. H.: Studies of Marine Planktonic Diatoms, Can. J. Microbiol., 8(2), 229–238, 1962.

Hatch, L. E., Jen, C. N., Kreisberg, N. M., Selimovic, V., Yokelson, R. J., Stamatis, C., York, R. A., Foster, D., Stephens, S. L., Goldstein, A. H. and Barsanti, K. C.: Highly Speciated Measurements of Terpenoids Emitted from Laboratory and Mixed-Conifer Forest Prescribed Fires, Environ. Sci. Technol., 53(16), 9418–9428, doi:10.1021/acs.est.9b02612, 2019.

Hering, S. V., Lewis, G. S., Spielman, S. R. and Eiguren-Fernandez, A.: A MAGIC concept for self-sustained, water-based, ultrafine particle counting, Aerosol Sci. Technol., 53(1), 63–72, doi:10.1080/02786826.2018.1538549, 2019.

Hettiyadura, A. P. S., Jayarathne, T., Baumann, K., Goldstein, A. H., De Gouw, J. A., Koss, A., Keutsch, F. N., Skog, K. and Stone, E. A.: Qualitative and quantitative analysis of atmospheric organosulfates in Centreville, Alabama, Atmos. Chem. Phys., 17(2), 1343–1359, doi:10.5194/acp-17-1343-2017, 2017.

Hoppe, H.-G.: Significance of exoenzymatic activities in the ecology of brackish water: measurements by means of methylumbelliferyl-substrates, Mar. Ecol. Prog. Ser., 11(3), 299–308, doi:10.3354/meps011299, 1983.

J. Mayer, K., S. Sauer, J., Dinasquet, J. and A. Prather, K.: CAICE Studies: Insights from a Decade of Ocean–Atmosphere Experiments in the Laboratory, Acc. Chem. Res., 53(11), 2510–2520, doi:10.1021/acs.accounts.0c00504, 2020.

Jain, S. and Petrucci, G. A.: A new method to measure aerosol particle bounce using a cascade electrical low pressure impactor, Aerosol Sci. Technol., 49(6), 390–399, doi:10.1080/02786826.2015.1036393, 2015.

Jen, C. N., Hatch, L. E., Selimovic, V., Yokelson, R. J., Weber, R., Fernandez, A. E., Kreisberg, N. M., Barsanti, K. C. and Goldstein, A. H.: Speciated and total emission factors of particulate organics from burning western US wildland fuels and their dependence on combustion efficiency, Atmos. Chem. Phys., 19(2), 1013–1026, doi:10.5194/acp-19-1013-2019, 2019.

Kang, E., Root, M. J. and Brune, W. H.: Introducing the concept of Potential Aerosol Mass (PAM), Atmos. Chem. Phys. Discuss., 7(4), 9925–9972, doi:10.5194/acpd-7-9925-2007, 2007.

Kercher, J. P., Riedel, T. P. and Thornton, J. A.: Chlorine activation by N2O5 : simultaneous , in situ detection of ClNO2 and N2O5 by chemical ionization mass spectrometry, , (2), 193–204, 2009.

Kim, M. J., Michaud, J. M., Williams, R., Sherwood, B. P., Pomeroy, R., Azam, F., Burkart, M. and Bertram, T. H.: Bacterial-driven production of nitrates in seawater, Geophys. Res. Lett., 42(2), 1–8, doi:10.1002/2014GL062865, 2015.

Kim, M. J., Zoerb, M. C., Campbell, N. R., Zimmermann, K. J., Blomquist, B. W., Huebert, B. J. and Bertram, T. H.: Revisiting benzene cluster cations for the chemical ionization of dimethyl sulfide and select volatile organic compounds, Atmos. Meas. Tech., 9(4), 1473–1484, doi:10.5194/amt-9-1473-2016, 2016.

Krechmer, J., Lopez-Hilfiker, F., Koss, A., Hutterli, M., Stoermer, C., Deming, B., Kimmel, J., Warneke, C., Holzinger, R., Jayne, J., Worsnop, D., Fuhrer, K., Gonin, M. and De Gouw, J.: Evaluation of a New Reagent-Ion Source and Focusing Ion-Molecule Reactor for Use in Proton-Transfer-Reaction Mass Spectrometry, Anal. Chem., 90(20), 12011–12018, doi:10.1021/acs.analchem.8b02641, 2018.

Lambe, A. T., Ahern, A. T., Williams, L. R., Slowik, J. G., Wong, J. P. S., Abbatt, J. P. D., Brune, W. H., Ng, N. L., Wright, J. P., Croasdale, D. R., Worsnop, D. R., Davidovits, P. and Onasch, T. B.: Characterization of aerosol photooxidation flow reactors: Heterogeneous oxidation, secondary organic aerosol formation and cloud condensation nuclei activity measurements, Atmos. Meas. Tech., 4(3), 445–461, doi:10.5194/amt-4-445-2011, 2011.

Lavi, A., Vermeuel, M. P., Novak, G. A. and Bertram, T. H.: The sensitivity of benzene cluster cation chemical ionization mass spectrometry to select biogenic terpenes, Atmos. Meas. Tech. Discuss., 3251–3262, doi:10.5194/amt-2017-408, 2017.

Lee, C., Sultana, C. M., Collins, D. B., Santander, M. V, Axson, J. L., Malfatti, F., Cornwell, G. C., Grandquist, J. R., Deane, G. B., Stokes, M. D., Azam, F., Grassian, V. H. and Prather, K. a.: Advancing Model Systems for Fundamental Laboratory Studies of Sea Spray Aerosol Using the Microbial Loop, J. Phys. Chem. A, 150805131932006, doi:10.1021/acs.jpca.5b03488, 2015.

Lee, H. D., Ray, K. K. and Tivanski, A. V.: Solid, Semisolid, and Liquid Phase States of Individual Submicrometer Particles Directly Probed Using Atomic Force Microscopy, Anal. Chem.,

89(23), 12720–12726, doi:10.1021/acs.analchem.7b02755, 2017.

Lee, H. D., Kaluarachchi, C. P., Hasenecz, E. S., Zhu, J. Z., Popa, E., Stone, E. A. and Tivanski, A. V.: Effect of dry or wet substrate deposition on the organic volume fraction of core-shell aerosol particles, Atmos. Meas. Tech., 12(3), 2033–2042, doi:10.5194/amt-12-2033-2019, 2019.

Lee, H. D., Morris, H. S., Laskina, O., Sultana, C. M., Lee, C., Jayarathne, T., Cox, J. L., Wang, X., Hasenecz, E. S., Demott, P. J., Bertram, T. H., Cappa, C. D., Stone, E. A., Prather, K. A., Grassian, V. H. and Tivanski, A. V.: Organic Enrichment, Physical Phase State, and Surface Tension Depression of Nascent Core-Shell Sea Spray Aerosols during Two Phytoplankton Blooms, ACS Earth Sp. Chem., 4(4), 650–660, doi:10.1021/acsearthspacechem.0c00032, 2020a.

Lee, H. D., Wigley, S., Lee, C., Or, V. W., Hasenecz, E. S., Stone, E. A., Grassian, V. H., Prather, K. A. and Tivanski, A. V.: Physicochemical Mixing State of Sea Spray Aerosols: Morphologies Exhibit Size Dependence, ACS Earth Sp. Chem., 4(9), 1604–1611, doi:10.1021/acsearthspacechem.0c00153, 2020b.

Levine, N. M.: Putting the spotlight on organic sulfur, Science (80-.)., 354(6311), 418–419, doi:10.1126/science.aai8650, 2016.

Lewis, E. R. and Schwartz, S. E.: Sea Salt Aerosol Production: Mechanisms, Methods, Measurements, and Models--A Critical Review, American Geophysical Union, Washington D.C., 2004.

Lopez-Hilfiker, F. D., Pospisilova, V., Huang, W., Kalberer, M., Mohr, C., Stefenelli, G., Thornton, J. A., Baltensperger, U., Prevot, A. S. H. and Slowik, J. G.: An Extractive Electrospray Ionization Time-of-Flight Mass Spectrometer (EESI-TOF) for online measurement of atmospheric aerosol particles, Atmos. Meas. Tech., 1–40, doi:10.5194/amt-2019-45, 2019.

Lopez-Yglesias, X. F., Yeung, M. C., Dey, S. E., Brechtel, F. J. and Chan, C. K.: Performance evaluation of the Brechtel Mfg. Humidified Tandem Differential Mobility Analyzer (BMI HTDMA) for studying hygroscopic properties of aerosol particles, Aerosol Sci. Technol., 48(9), 969–980, doi:10.1080/02786826.2014.952366, 2014.

Mael, L. E., Busse, H. and Grassian, V. H.: Measurements of Immersion Freezing and Heterogeneous Chemistry of Atmospherically Relevant Single Particles with Micro-Raman Spectroscopy, Anal. Chem., 91(17), 11138–11145, doi:10.1021/acs.analchem.9b01819, 2019.

Marie, D., Partensky, F., Jacquet, S. and Vaulot, D.: Enumeration and cell cycle analysis of natural populations of marine picoplankton by flow cytometry using the nucleic acid stain SYBR Green I, Appl. Environ. Microbiol., 63(1), 186–193, doi:10.1128/aem.63.1.186-193.1997, 1997.

Mayer, K. J., Wang, X., Santander, M. V, Mitts, B. A., Sauer, J. S., Sultana, C. M., Cappa, C. D. and Prather, K. A.: Secondary Marine Aerosol Plays a Dominant Role over Primary Sea Spray Aerosol in Cloud Formation, ACS Cent. Sci., Accepted, doi:10.1021/acscentsci.0c00793, 2020.

Michaud, J. M., Thompson, L. R., Kaul, D., Espinoza, J. L., Richter, R. A., Xu, Z. Z., Lee, C., Pham, K. M., Beall, C. M., Malfatti, F., Azam, F., Knight, R., Burkart, M. D., Dupont, C. L. and Prather, K. A.: Taxon-specific aerosolization of bacteria and viruses in an experimental ocean-atmosphere mesocosm, Nat. Commun., 9(1), doi:10.1038/s41467-018-04409-z, 2018.

Noble, R. T. and Fuhrman, J. A.: Use of SYBR Green I for rapid epifluorescence counts of marine viruses and bacteria, Aquat. Microb. Ecol., 14(2), 113–118, doi:10.3354/ame014113, 1998.

Novak, G. A. and Bertram, T. H.: Reactive VOC Production from Photochemical and Heterogeneous Reactions Occurring at the Air-Ocean Interface, Acc. Chem. Res., 53(5), 1014–1023, doi:10.1021/acs.accounts.0c00095, 2020.

O'Dowd, C. D. and de Leeuw, G.: Marine aerosol production: a review of the current knowledge, Philos. Trans. R. Soc. A Math. Phys. Eng. Sci., 365(1856), 1753–1774, doi:10.1098/rsta.2007.2043, 2007.

Olson, R. J., Chisholm, S. W., Zettler, E. R. and Armbrust, E. V.: Pigments, size, and distributions of Synechococcus in the North Atlantic and Pacific Oceans, Limnol. Oceanogr., 35(1), 45–58, doi:10.4319/lo.1990.35.1.0045, 1990.

Or, V. W., Estillore, A. D., Tivanski, A. V. and Grassian, V. H.: Lab on a tip: Atomic force microscopy-photothermal infrared spectroscopy of atmospherically relevant organic/inorganic aerosol particles in the nanometer to micrometer size range, Analyst, 143(12), 2765–2774, doi:10.1039/c8an00171e, 2018.

Orenstein, E. C., Ratelle, D., Briseño-Avena, C., Carter, M., Franks, P. J. S., Jaffe, J. S. and Roberts, P. L. D.: The Scripps Plankton Camera system: a framework and platform for in situ microscopy, Limnol. Oceanogr. Methods, submitted, doi:10.1002/lom3.10394, 2020.

Patterson, J. P., Collins, D. B., Michaud, J. M., Axson, J. L., Sultana, C. M., Moser, T., Dommer, A. C., Conner, J., Grassian, V. H., Stokes, M. D., Deane, G. B., Evans, J. E., Burkart, M. D., Prather, K. A. and Gianneschi, N. C.: Sea Spray Aerosol Structure and Composition Using Cryogenic Transmission Electron Microscopy., ACS Cent. Sci., 2(1), 40–47, doi:10.1021/acscentsci.5b00344, 2016.

Perkins, R. J., Gillette, S. M., Hill, T. C. J. and Demott, P. J.: The Labile Nature of Ice Nucleation by Arizona Test Dust, ACS Earth Sp. Chem., 4(1), 133–141, doi:10.1021/acsearthspacechem.9b00304, 2020.

Peters, T. M. and Leith, D.: Concentration measurement and counting efficiency of the aerodynamic particle sizer 3321, J. Aerosol Sci., 34(5), 627–634, doi:10.1016/S0021-8502(03)00030-2, 2003.

Petras, D., Koester, I., Da Silva, R., Stephens, B. M., Haas, A. F., Nelson, C. E., Kelly, L. W., Aluwihare, L. I. and Dorrestein, P. C.: High-Resolution Liquid Chromatography Tandem Mass Spectrometry Enables Large Scale Molecular Characterization of Dissolved Organic Matter , Front. Mar. Sci. , 4, 405 [online] Available from: https://www.frontiersin.org/article/10.3389/fmars.2017.00405, 2017.

Pomeroy, L. R., le Williams, P. J. B., Azam, F. and Hobbie, J. E.: The Microbial Loop, Oceanography, 20(SPL.ISS. 2), 28–33, doi:10.5670/oceanog.2007.45, 2007.

Prather, K. a, Bertram, T. H., Grassian, V. H., Deane, G. B., Stokes, M. D., Demott, P. J., Aluwihare, L. I., Palenik, B. P., Azam, F., Seinfeld, J. H., Moffet, R. C., Molina, M. J., Cappa, C. D., Geiger, F. M., Roberts, G. C., Russell, L. M., Ault, A. P., Baltrusaitis, J., Collins, D. B., Corrigan, C. E., Cuadra-Rodriguez, L. a, Ebben, C. J., Forestieri, S. D., Guasco, T. L., Hersey, S. P., Kim, M. J., Lambert, W. F., Modini, R. L., Mui, W., Pedler, B. E., Ruppel, M. J., Ryder, O. S., Schoepp, N. G., Sullivan, R. C. and Zhao, D.: Bringing the ocean into the laboratory to probe the chemical complexity of sea spray aerosol., Proc. Natl. Acad. Sci. U. S. A., 110(19), 7550–5, doi:10.1073/pnas.1300262110, 2013.

Ray, K. K., Lee, H. D., Gutierrez, M. A., Chang, F. J. and Tivanski, A. V.: Correlating 3D Morphology, Phase State, and Viscoelastic Properties of Individual Substrate-Deposited Particles, Anal. Chem., 91(12), 7621–7630, doi:10.1021/acs.analchem.9b00333, 2019.

Roberts, G. C. and Nenes, a.: A Continuous-Flow Streamwise Thermal-Gradient CCN Chamber for Atmospheric Measurements, Aerosol Sci. Technol., 39(3), 206–221, doi:10.1080/027868290913988, 2005.

Roveretto, M., Li, M., Hayeck, N., Brüggemann, M., Emmelin, C., Perrier, S. and George, C.: Real-Time Detection of Gas-Phase Organohalogens from Aqueous Photochemistry Using Orbitrap Mass Spectrometry, ACS Earth Sp. Chem., 3(3), 329–334, doi:10.1021/acsearthspacechem.8b00209, 2019.

Ryder, O. S., Campbell, N. R., Morris, H., Forestieri, S., Ruppel, M. J., Cappa, C., Tivanski, A., Prather, K. and Bertram, T. H.: Role of Organic Coatings in Regulating N2O5 Reactive Uptake to Sea Spray Aerosol, J. Phys. Chem. A, 119(48), 11683–11692, doi:10.1021/acs.jpca.5b08892, 2015.

Saukko, E., Lambe, A. T., Massoli, P., Koop, T., Wright, J. P., Croasdale, D. R., Pedernera, D. A., Onasch, T. B., Laaksonen, A., Davidovits, P., Worsnop, D. R. and Virtanen, A.: Humidity-dependent phase state of SOA particles from biogenic and anthropogenic precursors, Atmos. Chem. Phys., 12(16), 7517–7529, doi:10.5194/acp-12-7517-2012, 2012.

Schneider, S. R., Collins, D. B., Lim, C. Y., Zhu, L. and Abbatt, J. P. D.: Formation of Secondary

Organic Aerosol from the Heterogeneous Oxidation by Ozone of a Phytoplankton Culture, ACS Earth Sp. Chem., 3(10), 2298–2306, doi:10.1021/acsearthspacechem.9b00201, 2019.

Shen, S., Jaques, P. A., Zhu, Y., Geller, M. D. and Sioutas, C.: Evaluation of the SMPS-APS system as a continuous monitor for measuring PM2.5, PM10 and coarse (PM2.5-10) concentrations, Atmos. Environ., 36(24), 3939–3950, doi:10.1016/S1352-2310(02)00330-8, 2002.

Smith, J. N., Moore, K. F., McMurry, P. H. and Eisele, F. L.: Atmospheric Measurements of Sub-20 nm Diameter Particle Chemical Composition by Thermal Desorption Chemical Ionization Mass Spectrometry, Aerosol Sci. Technol., 38(2), 100–110, doi:10.1080/02786820490249036, 2004.

Stokes, M. D., Deane, G. B., Prather, K., Bertram, T. H., Ruppel, M. J., Ryder, O. S., Brady, J. M. and Zhao, D.: A Marine Aerosol Reference Tank system as a breaking wave analogue for the production of foam and sea-spray aerosols, Atmos. Meas. Tech., 6(4), 1085–1094, doi:10.5194/amt-6-1085-2013, 2013.

Stokes, M. D., Deane, G., Collins, D. B., Cappa, C., Bertram, T., Dommer, A., Schill, S., Forestieri, S. and Survilo, M.: A miniature Marine Aerosol Reference Tank (miniMART) as a compact breaking wave analogue, Atmos. Meas. Tech., 9(9), 4257–4267, doi:10.5194/amt-9-4257-2016, 2016.

Trueblood, J. V., Alves, M. R., Power, D., Santander, M. V., Cochran, R. E., Prather, K. A. and Grassian, V. H.: Shedding Light on Photosensitized Reactions within Marine-Relevant Organic Thin Films, ACS Earth Sp. Chem., 3(8), 1614–1623, doi:10.1021/acsearthspacechem.9b00066, 2019a.

Trueblood, J. V., Wang, X., Or, V. W., Alves, M. R., Santander, M. V., Prather, K. A. and Grassian, V. H.: The Old and the New: Aging of Sea Spray Aerosol and Formation of Secondary Marine Aerosol through OH Oxidation Reactions, ACS Earth Sp. Chem., 3(10), 2307–2314, doi:10.1021/acsearthspacechem.9b00087, 2019b.

Utermöhl, H.: Neue Wege in der quantitativen Erfassung des Plankton.(Mit besonderer Berücksichtigung des Ultraplanktons.), SIL Proceedings, 1922-2010, 5(2), 567–596, doi:10.1080/03680770.1931.11898492, 1931.

Voisin, D., Smith, J. N., Sakurai, H., McMurry, P. H. and Eisele, F. L.: Thermal desorption chemical ionization mass spectrometer for ultrafine particle chemical composition, Aerosol Sci. Technol., 37(6), 471–475, doi:10.1080/02786820300959, 2003.

Wakeham, S. G., Canuel, E. A. and Doering, P. H.: Geochemistry of volatile organic compounds in seawater: Mesocosm experiments with 14C-model compounds, Geochim. Cosmochim. Acta, 50(6), 1163–1172, doi:10.1016/0016-7037(86)90399-6, 1986.

Wang, X., Sultana, C. M., Trueblood, J., Hill, T. C. J., Malfatti, F., Lee, C., Laskina, O., Moore,

K. A., Beall, C. M., McCluskey, C. S., Cornwell, G. C., Zhou, Y., Cox, J. L., Pendergraft, M. A., Santander, M. V., Bertram, T. H., Cappa, C. D., Azam, F., DeMott, P. J., Grassian, V. H. and Prather, K. A.: Microbial Control of Sea Spray Aerosol Composition: A Tale of Two Blooms, ACS Cent. Sci., 1(3), 124–131, doi:10.1021/acscentsci.5b00148, 2015.

Wolfe, G. M., Nicely, J. M., St. Clair, J. M., Hanisco, T. F., Liao, J., Oman, L. D., Brune, W. B., Miller, D., Thames, A., González Abad, G., Ryerson, T. B., Thompson, C. R., Peischl, J., McKain, K., Sweeney, C., Wennberg, P. O., Kim, M., Crounse, J. D., Hall, S. R., Ullmann, K., Diskin, G., Bui, P., Chang, C. and Dean-Day, J.: Mapping hydroxyl variability throughout the global remote troposphere via synthesis of airborne and satellite formaldehyde observations, Proc. Natl. Acad. Sci., 116(23), 11171 LP – 11180, doi:10.1073/pnas.1821661116, 2019.

Chapter 7. CAICE Studies: Insights from a Decade of Ocean-Atmosphere Experiments in the Laboratory

7.1 Conspectus

Ocean-atmosphere interactions control the composition of the atmosphere, hydrological cycle, and temperature of our planet, as well as affect human and ecosystem health. Our understanding of the impact of ocean emissions on atmospheric chemistry and climate is limited relative to terrestrial systems, despite the fact oceans cover the majority (71%) of the Earth. As a result, the impact of marine aerosols on clouds represents one of the largest uncertainties in our understanding of climate, which is limiting our ability to accurately predict the future temperatures of our planet. The emission of gases and particles from the ocean surface constitutes an important chemical link between the ocean and atmosphere, and is mediated by marine biological, physical and chemical processes. It is challenging to isolate the role of biological ocean processes on atmospheric chemistry in the real world, which contains a mixture of terrestrial and anthropogenic emissions. One decade ago, the NSF Center for Aerosol Impacts on Chemistry of the Environment (CAICE) took a unique ocean-in-the-laboratory approach to study the factors controlling the chemical composition of marine aerosols and their effects on clouds and climate. CAICE studies have demonstrated that the complex interplay of phytoplankton, bacteria, and viruses exerts significant control over sea spray aerosol composition and the production of volatile organic compounds. In addition, CAICE experiments have explored the physical production mechanisms and their impact on the properties of marine cloud condensation nuclei and ice nucleating particles, thus shedding light on connections between the oceans and cloud formation. As these ocean-in-the-laboratory experiments become more sophisticated, they allow for further exploration of the complexity of the processes that control atmospheric emissions from the ocean, as well as

incorporating the effects of atmospheric aging and secondary oxidation processes. In the face of unprecedented global climate change, these results provide key insights into how our oceans and atmosphere are responding to human-induced changes to our planet.

This account presents results from a decade of research by chemists in the NSF Center for Aerosol Impacts on Chemistry of the Environment. The mission of CAICE involves taking a multidisciplinary approach to transform the ability to accurately predict the impact of marine aerosols on our environment by bringing the full real-world chemical complexity of the ocean/atmosphere into the laboratory. Towards this end, CAICE has successfully advanced the study of the ocean-atmosphere system under controlled laboratory settings through the stepwise simulation of physical production mechanisms and incorporation of marine microorganisms, building to systems which replicate real-world chemical complexity. This powerful approach has already made substantial progress in advancing our understanding of how ocean biology and physical processes affect the composition of nascent SSA, as well as yielded insights that help explain longstanding discrepancies in field observations in the marine environment. CAICE research is now using laboratory studies to assess how real-world complexity, such as warming temperatures, ocean acidification, wind speed, biology, and anthropogenic perturbations, impacts the evolution of sea spray aerosol properties, as well as shapes the composition of the marine atmosphere.

7.2 Introduction

Marine aerosols constitute an important chemical link between the oceans and the atmosphere. Aerosols affect climate directly by scattering incoming solar radiation and indirectly by affecting cloud properties (Carslaw et al., 2009). Aerosols can serve as cloud condensation nuclei (CCN), which influences the size and number of droplets in a cloud, thus affecting

precipitation and interactions with radiation (Andreae et al., 2005),(Rosenfeld et al., 2014). In addition, some aerosols may serve as ice nuclei (IN), facilitating the formation of ice crystals in mixed-phase clouds (Kanji et al., 2017),(Wilson et al., 2015). Aerosol-cloud interactions constitute the largest source of uncertainty in our understanding of the Earth's radiative budget,(Boucher et al., 2013) with a large contribution from the understanding of natural aerosols (Carslaw et al., 2013).

The climate impacts of marine aerosols are of particular interest, as oceans cover 71% of the Earth's surface. Primary sea spray aerosol (SSA) is generated by bubble-bursting at the ocean surface as a result of breaking waves. Secondary marine aerosol (SMA) is formed from the oxidation of volatile gases emitted from the oceans,(O'Dowd and de Leeuw, 2007) which can result in the formation of new particles through nucleation processes (Covert et al., 1992),(Vaattovaara et al., 2006). Alternatively, secondary species can condense onto existing particles in the marine atmosphere, such as SSA, influencing their chemical composition and properties (Fitzgerald, 1991). Biological activity in seawater exerts significant control over the chemical composition of SSA,(O'Dowd et al., 2004),(Wang et al., 2015) as well as the emission of gas-phase precursors which form SMA (Andreae and Raemdonck, 1983),(Arnold et al., 2009).

A major challenge in the study of marine aerosols and gases is disentangling the multitude of factors which influence their composition and properties: biological activity in seawater; transport of terrestrial and anthropogenic aerosols and gases to marine regions; heterogeneous and photochemical aging processes; physical parameters such as wind speed, temperature, and relative humidity; and secondary aerosol formation and growth processes. These numerous confounding variables make it challenging to disentangle the individual contributions from each of these processes, which impedes our ability to model and predict the properties of marine aerosols.

Ocean-atmosphere experiments conducted in the laboratory have the significant advantage of allowing for the isolated study of individual processes which control marine aerosol composition, properties, and production flux. Here, we discuss ocean-atmosphere experiments addressing the aforementioned challenges. Through the implementation of technologies designed to produce marine aerosols as naturally as possible, we outline the various directions of new inquiry opened by the ocean-atmosphere experimental approach as well as the successes already achieved (Figure 7.1). Lastly, we introduce the future of ocean-atmosphere experiments through the lens of an under-development facility which seeks to improve upon previous designs and allows for the study of external perturbations on the natural marine environment including high speed winds and cold ocean temperatures.

7.3 Making Waves: Sea Spray Aerosol Generation

Multiple CAICE innovations have advanced our understanding of atmospheric chemistry through ocean-in-the-laboratory approaches. Initial experiments focused on using accurate production methods to generate realistic SSA in controlled laboratory settings. In the past, many studies have used sintered glass filters to produce SSA by forcing air through the filters to produce bubbles, which rise to the surface and burst, producing SSA (Quinn et al., 2015),(Sellegri et al., 2006). However, a major drawback of these methods is that they produce a very narrow range of bubble sizes, which skews the resulting SSA size distribution and produces a persistent surface foam (Collins et al., 2014). In order to produce realistic SSA, it is necessary to simulate the action of real breaking ocean waves, which intermittently entrain air beneath the ocean surface via the action of plunging sheets of water, producing a wide range of bubble sizes. To accurately capture this process in the laboratory, CAICE has pioneered the use of wave channels for laboratory studies of marine aerosols (Prather et al., 2013). Traditionally used for experiments in physical

oceanography, these large channels often hold over 10,000 L of seawater and produce waves using computer-controlled reciprocating paddles (Figure 7.2A), which send artificial waves to break on an artificial beach. To facilitate studies of marine aerosols, CAICE researchers transformed an existing wave channel into an ocean-atmosphere simulator by sealing it with lids to create an enclosed headspace along the full length of the channel. Clean, particle-free air is provided to the headspace by a specialized filtration system. These modifications have enabled the study of sea spray aerosol generated by real breaking waves in natural seawater under the cleanest possible conditions, isolated from anthropogenic and terrestrial influences. An advantage of their large size, wave channels allow for many analytical instruments in the same location to sample both seawater properties as well as gases and aerosols in the headspace. These large-scale experiments have discovered numerous processes which govern and contribute to the transfer of molecules from the ocean to the atmosphere (Cochran et al., 2017; Wang et al., 2015).

Despite serving as the "gold standard" for ocean/atmosphere experiments, drawbacks of the use of wave channels are the size and cost, which limit widespread usage. This has been addressed by the development of smaller SSA generation devices which produce realistic bubble and aerosol size distributions without requiring the use of a full-sized wave channel. The Marine Aerosol Reference Tank (MART) is a CAICE-developed 210 L acrylic tank which generates an intermittent plunging sheet of water to produce a bubble plume which replicates the size distribution and has a temporal evolution similar to bubble plumes measured in the ocean and in wave tanks (Figure 7.2B) (Stokes et al., 2013). These bubbles rupture at the water surface, producing SSA closely matching the size distribution produced by breaking waves in wave channels and the natural environment (Figure 7.2D). The enclosed MART headspace, containing both aerosols and gases, can then be sampled by various offline and online methods at particle

concentrations (~500 #/cm3) needed for most measurement techniques. Replication of the proper SSA size distribution has been a crucial advancement in answering questions such as the impact of changing biology on SSA flux and hygroscopicity.(Collins et al., 2016) Other questions, difficult to study in the field, such as the influence of seawater temperature on SSA production, have also been investigated using the MART (Forestieri et al., 2018). Natural or artificial seawater added to the MART can be biologically stimulated through nutrient and culture additions to grow a representative range of natural marine microorganisms. The versatility of the MART as an accurate SSA production device make it useful not only for investigations of the influences of ocean biology, but the physiochemical properties of aerosols as well (Ault et al., 2013; Lee et al., 2015; Ryder et al., 2015a). The MART has been widely adopted as the de facto method for generating realistic SSA size distributions and has been utilized by researchers outside of CAICE for studies on physical production mechanisms,(Harb and Foroutan, 2019) health effects,(van Acker et al., 2020; Asselman et al., 2019) and ship-based measurements of marine aerosols (Bates et al., 2020).

An undesirable side-effect of the centrifugal pump currently used in the MART is potential physical damage to the marine microorganisms via pump shear, which distorts the biological communities towards the most hardy species (Collins, 2014). To facilitate smaller scale experiments and preserve fragile microorganisms, a smaller MART which uses a gentler plunging mechanism was developed. The miniMART features a 19 L acrylic tank where a small plunging waterfall is generated through the action of a water wheel (Figure 7.2C) (Stokes et al., 2016). Similarly, bubble plumes and short-lived foams are generated which produce bubble size distributions and sea spray aerosol closely matching the size distribution found in the natural ocean. Through the miniMART, multiple findings regarding the behavior of surface partitioned

organics, marine enzymes, and ice nuclei have been obtained (Hasenecz et al., 2019). The wave channel, MART, and miniMART represent the ability to perform ocean-atmosphere experiments across four orders of magnitude of water volume, giving massive flexibility towards the design of experiments which vary in scale, expense, and complexity. Tradeoffs in constraints involving the air flow, number of SSA produced, ease of cleaning, experimental footprint, transport of water, and other logistical factors must be considered. At the wave channel level, the operational environment and level of effort is similar to that of a field campaign, whereas the miniMART can be easily used to conduct smaller scale experiments by a single investigator in the laboratory.

7.4 Building the Biological Complexity of Ocean-Atmosphere-Simulations

The initial ocean-atmosphere experiments conducted in CAICE focused on accurately producing SSA in the laboratory, both with regards to size distributions and chemical complexity. This was accomplished initially using a wave channel to generate realistic SSA from natural seawater, and later by the development of the MART and miniMART. Following the development of physical production methods, the next goal of CAICE was to understand how biological activity in the oceans modulates and controls the properties of SSA. To this end, a novel mesocosm experiment was conducted in the wave channel to simulate the biological and chemical complexity of the real ocean.1 During this 5-day mesocosm, cultures of marine phytoplankton and bacteria were added to the seawater in the wave channel. The major findings of this study in 2011 were that biogenic organic species have profound impacts on the chemical composition and properties of SSA. However, as the cultures were added to the seawater sequentially, this experiment did not adequately simulate the full progression of a real oceanic phytoplankton bloom. The next major ocean-atmosphere experiment within CAICE was the Investigation into Marine Particle Chemistry and Transfer Science (IMPACTS) experiment in 2014. During this campaign, a phytoplankton

bloom was induced in natural seawater by adding nutrients to the wave channel and measuring the evolution of SSA composition and properties over the full bloom life cycle. A major goal was to replicate the microbial loop—a process which occurs naturally in the oceans wherein marine phytoplankton, bacteria, and viruses interact dynamically over the course of a bloom cycle (Azam et al., 1983).

During IMPACTS, marked differences were observed in SSA properties over two subsequent blooms, including the aerosol composition, organic speciation, and INP production, which has been attributed to differences in the phytoplankton and bacterial dynamics in the system (Wang, 2017). The role of enzymes, specifically lipase, produced by marine microorganisms was found to transform the available pool of aqueous organic carbon to a more soluble state (Wang et al., 2015). The effects of the microbial transformation of the marine organic carbon were later observed in the composition of aerosols produced through wave breaking. Specifically, the fraction of aliphatic-rich SSA was observed to be enhanced during periods of high phytoplankton productivity and low bacterial activity. This trend was found to be reversed in cases where phytoplankton activity was high with commensurately high bacterial activity. This discovery stimulated further research into the role of lipase as an effector of aerosol composition inside individual droplets, uncovering a new mechanism for the transformation of organic compounds after aerosolization (Malfatti et al., 2019). These results together advance an important narrative that the competition between phytoplankton production and bacterial degradation exert control on the composition of marine aerosols which contrasts with attempts to predict aerosol composition using chlorophyll-a (chl-a) alone (Quinn et al., 2014; Rinaldi et al., 2013).

Beyond their influence on the array of organic matter, the diversity of marine bacteria and viruses aerosolized from IMPACTS seawater was characterized using state-of-the-art sequencing

approaches (Michaud et al., 2018). This research uncovered new information about specific microorganisms that are preferentially transferred from seawater to aerosols, while also connecting the physiochemical structure of the microorganisms to their efficiency of aerosolization. Aerosolized taxa also included notable species of infectious concern such as Legionella, E. coli, Corynebacterium, and Mycobacterium. The implications of taxon-specific aerosolization from marine environments are multifold: where ice nucleation efficiency of different marine organisms can influence cloud formation, and certain taxa may have significant impacts on human health. These findings highlight how biological complexity in the oceans affects marine aerosol composition and atmospheric chemistry.

Further experiments simulating the influence of biological complexity on SSA properties have been conducted using MARTs. The Biological Effects on Air-Sea Transfer (BEAST) experiment investigated the influence of marine bacteria and viruses on SSA composition and organosulfur gas production. Results from BEAST have shed insight on the bacterial turnover of marine saccharides and their transfer to the aerosol phase (Hasenecz et al., 2020). In the same experiment, the production of non-dimethyl sulfide organosulfur gases, methanethiol and dimethyl disulfide was found to be significantly enhanced, with flux ratios of (MeSH+DMDS/DMS) which ranged from 0.2-35, significantly higher than those observed in field studies.(Sauer et al., 2020) The unexpected production of these reactive gases was connected to both the turnover in bacterial assemblages as well as possible changes in metabolic pathways influencing the transformation of these dissolved gases. These findings have further reinforced the importance of accounting for the community structure and activity of marine microorganisms.

7.5 Probing the Chemical Complexity of Sea Spray Aerosol

The ability to produce realistic SSA in the laboratory from natural seawater across a wide range of biological conditions, with no contamination from terrestrial gases and aerosols, has greatly expanded our understanding of the chemical complexity of SSA. Studies have investigated the chemical composition of freshly emitted SSA including, morphology and structure, individual particle mixing state, and reactivity with atmospheric trace gases. Early results from wave channel experiments indicated that SSA is an external mixture, made up of four distinct particle types including sea salt, mixed sea salt/organic, organic, and biological particles. In a landmark study on the composition of SSA, the presence of whole bacteria, viruses, phytoplankton, and marine vesicles was discovered using cryo-electron microscopy performed on MART and wave channel generated aerosols.(Patterson et al., 2016) The molecular diversity of SSA has also been shown to be sensitive to biological activity and vary over time in response to the dynamics of phytoplankton and heterotrophic bacteria in seawater (Cochran et al., 2017).

Results from laboratory ocean-atmosphere experiments within CAICE have shown that nascent SSA is enriched with organic compounds relative to both bulk seawater and the sea surface microlayer (SSML). For example, saccharides were observed to be enriched in submicron SSA from 14 to 1314-fold relative to seawater (Jayarathne et al., 2016). Analysis of SSA by high resolution mass spectrometry has shown that the molecular composition of nascent SSA is size dependent, and that organic surfactants such as fatty acids are selectively transferred to smaller particles (Cochran et al., 2016). Further studies have shown that the size-selective transfer of organic material from seawater to the aerosol phase is largely driven by the mechanics of bubble bursting. Briefly, the bursting of the bubble cap produces film drops, which are enriched with hydrophobic materials which partition to the air-water interface, while jet drops are produced by the collapse of the bubble cavity. These two different SSA production mechanisms result in an

externally mixed aerosol population, with two distinct chemical compositions.1 While it was previously believed that film drops contributed primarily to the submicron aerosol and jet drops contributed to the supermicron mode, CAICE experiments have shown that jet drops can produce up to 43% of submicron SSA (Wang et al., 2017).

The mixing state and chemical complexity of SSA has been shown to have a significant influence over heterogenous reactions with atmospheric trace gases. These findings have significant implications for atmospheric chemistry and climate models, as many currently approximate the properties of SSA as that of pure NaCl. The reactions of SSA with reactive nitrogen species (i.e. N_2O_5, HNO_3) have been of particular interest, given their impact on the global NOx budget. CAICE laboratory studies of the reaction between individual nascent SSA particles with nitric acid have shown a wide range of behavior, from no reaction to complete reaction, due to both particle type and heterogeneity within individual particles (Ault et al., 2014b). The analysis of individual SSA particles using transmission electron microscopy (TEM) has shown that particles undergo ion redistribution after reaction with nitric acid, which indicates particle structure plays an important role in controlling heterogeneous reactivity (Ault et al., 2013).

In addition, studies on the reactive uptake of N_2O_5 by laboratory-generated SSA have also been conducted within CAICE (Ryder et al., 2015a). These experiments used a MART to generate SSA from both natural ocean water and artificial seawater, which was sequentially doped with molecular mimics of seawater organics, and found that organic films do not impede the reactive uptake of N_2O_5 at high relative humidity. Studies on the uptake N_2O_5 at the air-sea interface have found that aromatic compounds (i.e. phenol and humic acid) present at an air-liquid interface can suppress the yield of $ClNO_2$ by acting as competitive reactants with chloride (Ryder et al., 2015b). Notably, the usage of low-complexity seawater mimics failed to reproduce the uptake properties

observed both in the field and with MART generated aerosols, showing the need for experiments that maintain the high complexity of the marine environment. These results highlight the utility of ocean-atmosphere simulators, which can be used to generate model SSA containing selected compounds in order to simplify and understand the specific variables which contribute to the full complexity of the real environment.

7.6 Climate-Relevant Properties of Marine Aerosols

Aerosol-cloud interactions are the largest source of uncertainty in our understanding of the climate system (Boucher et al., 2013). The oceans have been identified as a major source of ice nucleating particles (INP), however, terrestrial contributions from dust and other sources dominate in regions where there is long-range transport of these aerosols, including over the oceans (McCluskey et al., 2018b, 2018a) (McCluskey et al., 2018b, 2018a). Marine INP are now known, partially due to findings by CAICE, to be excellent ice nucleators, however the rarity of marine INPs (about 5 in 10^5 particles at -30˚C) makes understanding their composition very difficult (DeMott et al., 2015). In order to study marine INP, measurements must be conducted in extremely remote sampling locations. By isolating ocean from terrestrial influences in the laboratory, it was possible to definitively identify and measure the properties of INP emitted from the oceans (DeMott et al., 2015), (McCluskey et al., 2017). The usage of more representative SSA production techniques like the MART and wave channel have shown that the production method is important to INP release (DeMott et al., 2015). Further studies on marine INP have focused on developing a molecular-level understanding of the sources of these particles and how they are influenced by the activity of different marine microorganisms such as phytoplankton and bacteria (Mccluskey et al., 2018),(DeMott et al., 2018).

Laboratory ocean-atmosphere experiments have lent clarity to the debate over what drives the correlations between cloud droplet number and seawater chlorophyll-a concentrations observed in remote sensing studies (McCoy et al., 2015). It was hypothesized that biological activity in seawater could either affect the CCN activity and production flux of SSA, or it could result in increased SMA formation. Research within CAICE has shown that biological activity in seawater has a weak effect on the CCN activity of freshly emitted SSA, and that the observed changes cannot account for the observed influence on cloud properties (Collins et al., 2016). Using a miniMART, Forestieri and coworkers observed a strong relationship between SSA production and water temperature for artificial seawater, which is consistent with parameterizations in the literature (Forestieri et al., 2018). However, for natural seawater, they observed seemingly random, irreproducible variability in SSA production, which evolved over the course of several days. This variability was attributed to temporal changes in the water composition, possibly related to organic or biological components of the natural seawater not present in the artificial mimics. While some conflicting data regarding SSA flux has been reported, (Alpert et al., 2015; Christiansen et al., 2019; Forestieri et al., 2018, Collins et al., 2013) recently Bates and coworkers utilized a MART deployed during a ship-based study in the North Atlantic and concluded that variability in the flux of SSA was not linked to the activity of marine phytoplankton (Bates et al., 2020). In summary, influence of biological activity on SSA flux, and by extension CCN concentrations, remains highly uncertain.

Further experiments within CAICE have shown that the changes in SSA flux and hygroscopicity during a phytoplankton bloom cycle cannot explain the observed correlations between chl-a and cloud properties. During four subsequent phytoplankton bloom cycles, we found a weakly negative correlation between the flux of SSA from a MART (as evidenced by the

integrated number concentrations) and the seawater chl-a concentrations, a proxy for biological activity (Figure 7.3a). In addition, the shape of the size distribution remained relatively constant throughout the experiments (Figure 7.5). While some variability is observed in the production of SSA during these experiments, it does not appear to be driven by phytoplankton alone. In addition, no correlation was observed between chl-a and the apparent hygroscopicity parameter, which remained relatively unchanged the course of all four bloom cycles ($\kappa app = 1.02 \pm 0.04$, Figure 7.3b). In summary, while there appears to be some degree of natural variability in both the flux and hygroscopicity of SSA, ocean-atmosphere experiments using MARTs have conclusively shown that this variability is not directly related to marine phytoplankton concentrations, as indicated by the chl-a concentrations. The relative insensitivity of SSA flux and hygroscopicity to biological activity suggests that the observed correlations between cloud properties and phytoplankton blooms is driven by secondary aerosol formation, either through the formation of new SMA particles or the condensation of secondary species onto existing particles, thus increasing their size and ability to act as CCN.

7.7 Beyond Primary SSA: Marine Gas Emissions and Atmospheric Reactions

CAICE ocean-atmosphere experiments have, in the past, primarily focused on the factors controlling the properties of freshly emitted SSA; however, in the real marine atmosphere, SSA particles are transformed by aging processes, such as photochemistry, oxidation, and reactions with trace gases. Understanding how the composition and properties of SSA transform over hours, days, or even weeks of atmospheric processing is critical for accurately representing them within climate models. In addition, the oceans are a source of volatile organic compounds (VOCs), which may lead to the formation of secondary marine aerosol. While a great deal of attention has been paid to the formation of sulfate aerosols from dimethyl sulfide oxidation, the role of other reactive

trace gases which may contribute to secondary aerosol formation in the marine atmosphere have not been fully explored. Currently, a major research focus within CAICE is determining the biotic and abiotic factors which control the production of marine VOCs, as well as the properties and composition of secondary aerosols formed from their oxidation, and their potential impacts on cloud properties and climate.

Future steps towards replicating the real marine atmosphere in the laboratory have been the incorporation of oxidation and atmospheric aging processes. To accomplish this, Potential Aerosol Mass Oxidative Flow Reactors (PAM-OFRs) have been coupled with both MARTs and the wave channel to generate secondary marine aerosol and simulate the aging of primary SSA. The PAM-OFR system has been described elsewhere (Kang et al., 2007; Lambe et al., 2011). Briefly, the OFR uses UV lamps (λ = 185 nm and 254 nm) to generate high concentrations of OH radical, which react with the sampled air as it flows through the reactor. This results in the formation of new particles, as well as the oxidation of primary aerosols. In contrast to environmental chambers, the short residence time (~100-300 sec) allows for the near real-time measurements of secondary aerosol formation and aged SSA on a dynamic system such as a phytoplankton bloom, which can evolve and change rapidly. Previously, the PAM-OFR has been primarily used to study terrestrial and anthropogenic systems;(Palm et al., 2016) however, results from CAICE have shown the utility of this technique for the study of marine systems (Mayer et al., 2020; Trueblood et al., 2019). The adoption of OFRs for marine aerosol research has pushed the boundaries of ocean-in-the-laboratory experiments and allowed us to further probe the links between biological activity in the ocean and atmospheric chemistry.

As CAICE research has shown the controlling influence of biological activity on marine aerosol formation involves secondary processes, new ways to understand the production of marine

gases have become essential. A particular advantage of ocean-atmosphere experiments is the lack of solar flux and oxidants which can break down volatile gases very quickly. For example, during BEAST, the lack of these factors in the MART allowed for effective measurement of methanethiol and dimethyl disulfide; gaseous species which have high absorption and •OH reactive cross sections which keep their steady state concentrations low in the natural environment. Future CAICE ocean-atmosphere experiments will continue to take advantage of this property to better understand the production of labile volatile species far more difficult to observe in the natural environment. Additionally, community structure, stress, solar irradiation, signaling, grazing, nutrient availability, and other factors are relevant and important to the production of gases by microorganisms in the marine environment (Achyuthan et al., 2017; Carpenter et al., 2012). The role of bacteria in the formation of marine alkyl nitrate production was a significant CAICE finding enabled by the usage of ocean-atmosphere analogs.(Kim et al., 2015) By eliminating solar flux, this production was narrowed down to the marine organisms present, something not yet demonstrated in field studies. The role of metabolic partitioning along multiple pathways which lead to the production of marine gases, especially organosulfur species, is a central focus of CAICE, as the production of these gases in the marine environment is both highly variable and poorly understood (Kettle et al., 2001). Building a comprehensive list of marine VOCs and their relative fluxes at different biological states is a key CAICE focus which is currently under investigation. Furthermore, given the vast wealth of biological speciation data obtained during large mesocosm experiments, connecting the production of marine gases to specific biological actors is a new research area within CAICE.

7.8 Outlook

Over the past decade, CAICE studies of isolated ocean-atmosphere interactions have greatly expanded our understanding of marine aerosols and their complex chemical properties. These experiments bridge the gap between field observations and traditional laboratory studies by building up real-world complexity under controlled conditions. New directions in marine aerosol research have been opened by findings using the unique ocean-atmosphere in the laboratory approach, including investigations into enzyme-aerosol activity, formation of unique vesicle macrostructures, heterogenous reactions, and detection of previously under-appreciated reactive biogenic gas phase species (Ault et al., 2013; Kim et al., 2015; Malfatti et al., 2019; Patterson et al., 2016).

The Sea Spray Chemistry and Particle Evolution (SeaSCAPE) campaign was the most recent CAICE study conducted using a wave channel. This campaign focused on simulating atmospheric oxidation processes on both SSA and gases emitted from seawater during a phytoplankton bloom cycle. In addition to the oxidation experiments, comprehensive measurements were made of nascent SSA. Briefly, these measurements include aerosol chemical composition, size distributions, phase and morphology, hygroscopicity, IN activity, and trace gas speciation. The SeaSCAPE campaign will directly measure how rapid atmospheric processing transforms the properties of marine aerosols, enabled by laboratory ocean-atmosphere experiments. While significant progress has been made, critical gaps remain in our ability to fully simulate the marine environment, such as capturing the full temporal scale of oxidation and aging processes. These challenges must be addressed by modeling and the development of new innovative experimental proxies.

Future ocean-atmosphere experiments in CAICE will take the next step and center around the development of the Scripps Ocean Atmosphere Research Simulator (SOARS), shown in Figure

7.4. Once completed (planned by summer 2021), this first-of-its-kind facility will enable unique multidisciplinary experiments simulating a wide range of biological, physical, and chemical factors which influence the marine atmosphere. As a fully temperature-controlled wind-wave channel, SOARS will provide control of waves, windspeed (up to gale force winds), diurnal light cycling, and both water and air temperature (from polar to tropical conditions). An integrated environmental reaction chamber will allow for the simulation of atmospheric oxidation and aging of particles and gases under both pristine and polluted conditions. The ability to simulate these different physical and chemical processes under controlled conditions in the laboratory will allow for experiments which simulate the full complexity of the real marine environment. Experiments using the SOARS facility will explore the full extent of biological influence on marine aerosol production and properties under past and future climate scenarios. In addition, this facility will allow for studies of how anthropogenic air and water pollution, climate change, and ocean acidification affect ocean biology and the marine atmosphere.

It is critical to develop tools for improving our understanding of the impacts of natural ecosystems as the Earth undergoes unprecedented change. Over the past decade, CAICE has developed unique infrastructure and positioned itself at the forefront in innovating a range of ocean-atmosphere experimental systems and analytical methods to directly unravel the impacts of humans and natural emissions on the marine atmosphere.

7.9 Acknowledgements

This material is based upon work supported by the National Science Foundation through the Center for Aerosol Impacts on the Chemistry of the Environment, an NSF Center for Chemical Innovation (CHE-1801971).

Chapter 7, in full, is a reprint of material that has been published in Accounts of Chemical Research. Mayer, K.J., Sauer, J.S., Dinasquet, J., Prather, K.A. (2020). “CAICE Studies: Insights from a Decade of Ocean-Atmosphere Experiments in the Laboratory.” Accounts of Chemical Research (2020) Kathryn Mayer, and the dissertation author are the primary investigators and author of this manuscript

7.10 Figures

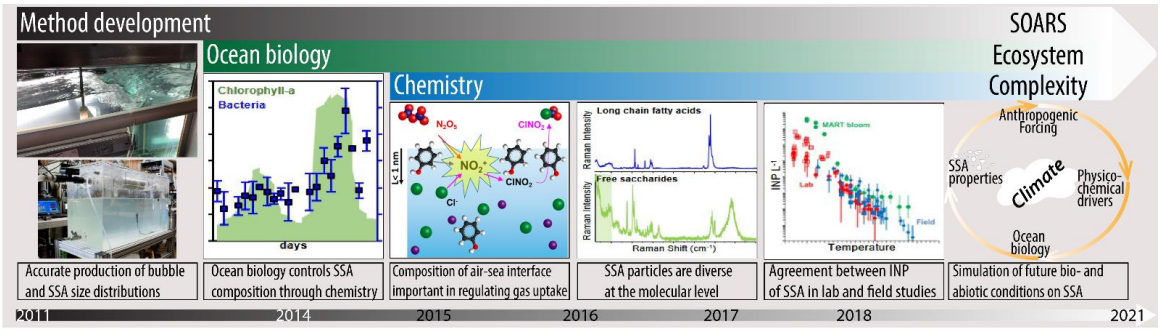

Figure 7.1. Timeline of CAICE achievements, through the innovation and development of a new ocean-atmosphere interaction facility and major experimental results obtained using these systems. CAICE seeks to accurately predict the impact of marine aerosols on our environment by bringing the full real-world chemical complexity to the laboratory. Towards this end, the team has successfully replicated the complexity of the ocean-atmosphere, by accurately reproducing bubble and SSA size distribution and the microbiology of the system. The CAICE in-development SOARS simulator will assess the impact of the full system complexity on atmospheric chemistry. Adapted with permission from Ref. 2 and Ref. 20. Copyright 2015 American Chemical Society. (SSA: Sea spray aerosols, IN: Ice nucleation, SOARS: Scripps Ocean Atmosphere Research Simulator)

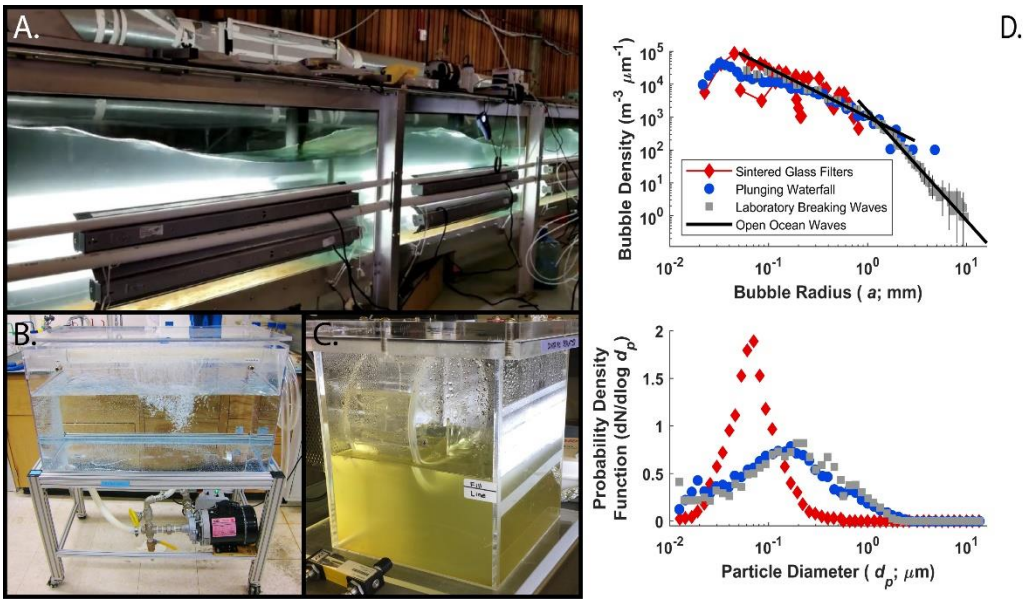

Figure 7.2. CAICE's ocean-atmosphere simulators: 13,000 L wave channel (A), 210 L Marine Aerosol Reference Tank - MART (B) and 19 L miniMART (C). Panel (D) shows the bubble size distributions and normalized aerosol size distributions with laboratory and plunging waterfall in reference to open ocean waves. Reproduced with permission from ref. 20. Copyright 2015 American Chemical Society.

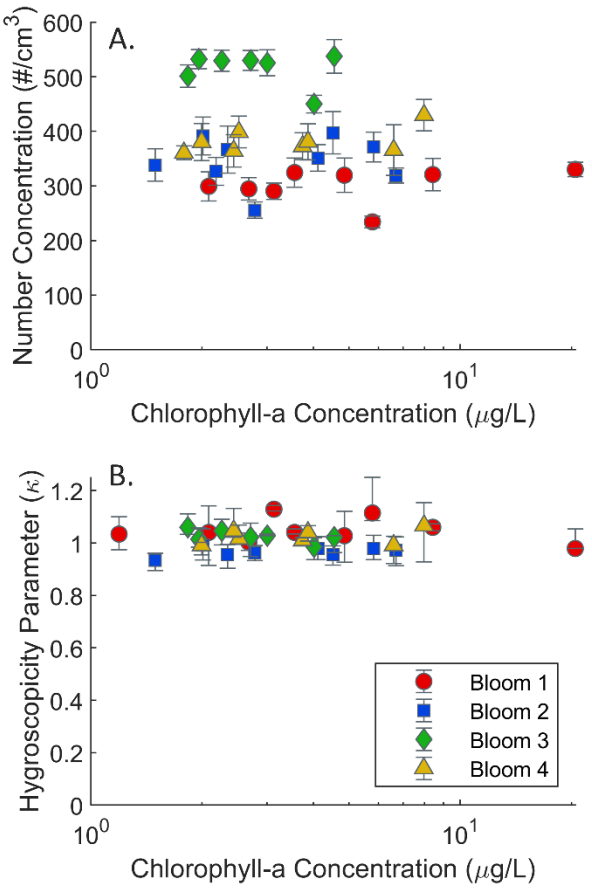

Figure 7.3. a) Number concentrations of MART-generated SSA versus seawater chl-a concentrations during four phytoplankton bloom experiments. As the air flowrate through the MART headspace is kept constant, the number concentration is directly proportional to the flux of SSA. b) Apparent hygroscopicity parameters (kapp) of MART-generated SSA during the four phytoplankton bloom experiments. These results show the relative insensitivity of both SSA flux and CCN activity with regards to biological activity in seawater, as represented by the chl-a concentrations. Detailed methods and experimental details are reported in the supplemental, as well as the daily data (Figures 7.6 and 7.8), aerosol size distributions (Figure 7.5) and CCN activation curves (Figure 7.7).

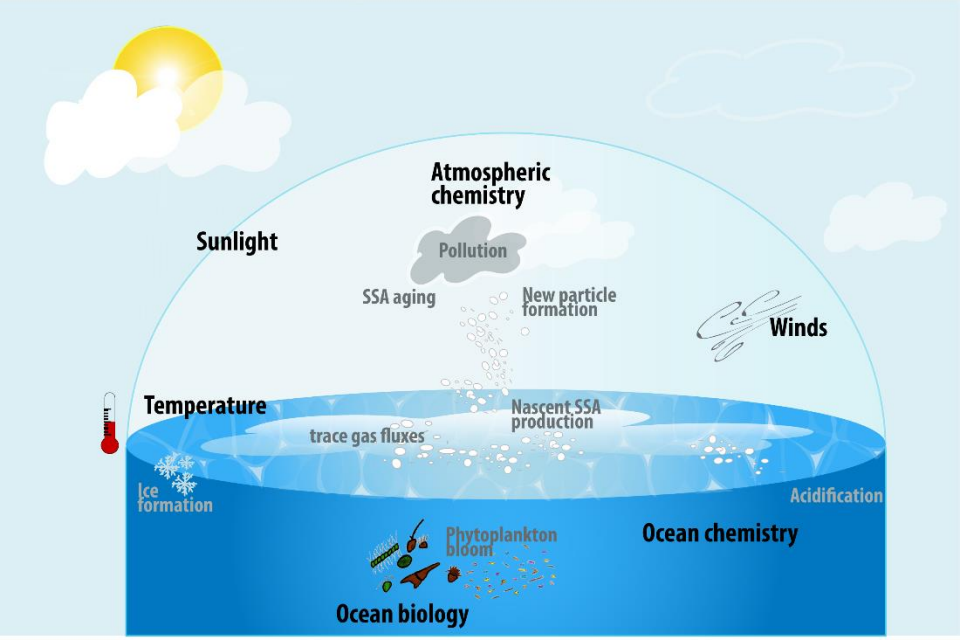

Figure 7.4. Representation of the Scripps Ocean Atmosphere Research Simulator (SOARS) which enables the ability to simulate biotic, as well as physical and non-biotic chemical processes of the marine environment within the laboratory. The facility will provide the possibility to modulate the light intensity (through artificial lights and natural lights), temperature of the atmosphere and water (with the ability to form sea-ice), wind and waves, ocean biology (e.g. inducing a phytoplankton bloom, manipulating bacterial and viral populations), ocean chemistry (e.g. ocean acidification), as well as the atmospheric composition through aging of sea spray aerosol and trace gases in the smog chamber.

7.11 Supplementary information

Sea spray aerosol (SSA) was generated using a marine aerosol reference tank (MART) during four mesocosm bloom experiments. The blooms were grown in natural seawater collected from Scripps Pier (32.86 N, -117.25 W) in a 2,400 L outdoor tank, which received natural sunlight. Algae growth media (Guillard's f/2) was added to the seawater to induce a phytoplankton bloom (Guillard 1962). Silicates were added to Blooms 1,2, and 4, but were omitted from Bloom 3 to encourage the growth of non-diatom species. Chlorophyll-A (chl-a) concentrations were measured daily to track the progress of the bloom cycle using a handheld fluorometer (AquaFluor, Turner Designs Inc.). During each day of the bloom experiments, 120 L of seawater was transferred to the MART for SSA measurements. Afterwards, the seawater was returned to the outdoor tank.

Aerosols were dried prior to measurement using a silica diffusion dryer. SSA size distributions were measured using a scanning mobility particle sizer (SMPS 3398, TSI Inc.) and an aerodynamic particle sizer (APS 3321, TSI Inc.). The aerodynamic diameters measured by the APS were converted to physical diameters using an effective density of $\rho = 1.8\ g \cdot cm^{-3}$. The SMPS mobility diameter is assumed to be equivalent to the physical diameter.

Size-resolved CCN measurements were made using a continuous flow stream-wise thermal gradient cloud condensation nuclei counter (CCN-100, Droplet Measurement Technologies, Inc). Briefly, SSA was size selected using a differential mobility analyzer (DMA 3081, TSI Inc) and the flow split evenly between the CCN counter and condensation particle counter (W-CPC 3787, TSI Inc). The size-selected diameter was kept constant at Dd = 50 nm and the CCN counter scanned over a range of supersaturations. The apparent hygroscopicity parameter (κapp) was calculated using the κ-Köhler equation (Petters 1971). The surface tension of the air-surface interface was assumed to be that of pure water, $\sigma_{s/a} = 0.072\ J \cdot m$.

7.12 Supplementary tables

Table 7.1 Summary nutrient additions to mesocosm experiments

Experiment	**Nutrient Addition**	**Silicates**	**Maximum chl-a concentration**
Bloom 1	f/20	Yes	20.5 μg/L
Bloom 2	f/100	Yes	6.7 μg/L
Bloom 3	f/100	No	4.6 μg/L
Bloom 4	f/100	Yes	8.0 μg/L

7.13 Supplementary Figures

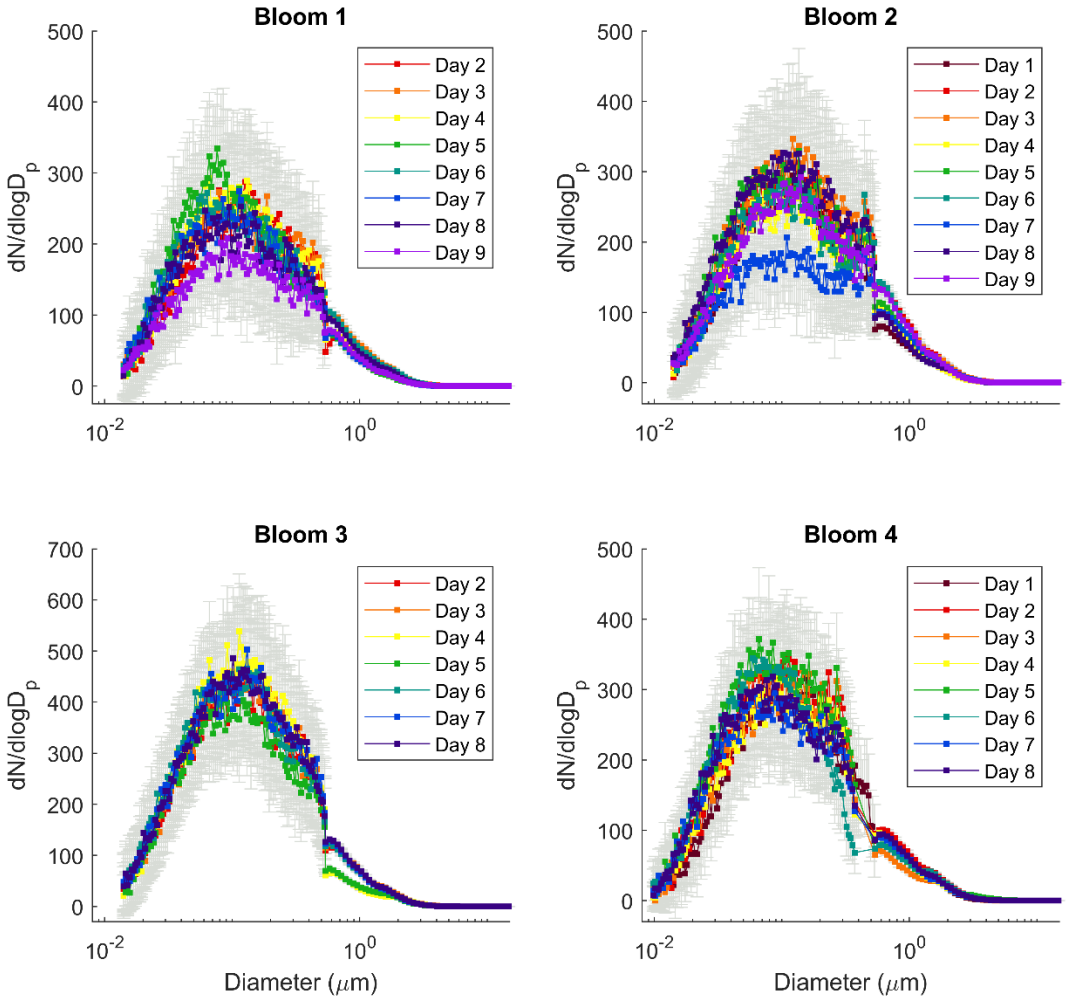

Figure 7.5. Size distributions of MART-generated SSA during each day of the four mesocosm experiments. Error bars are shown in grey and represent ± 1σ.

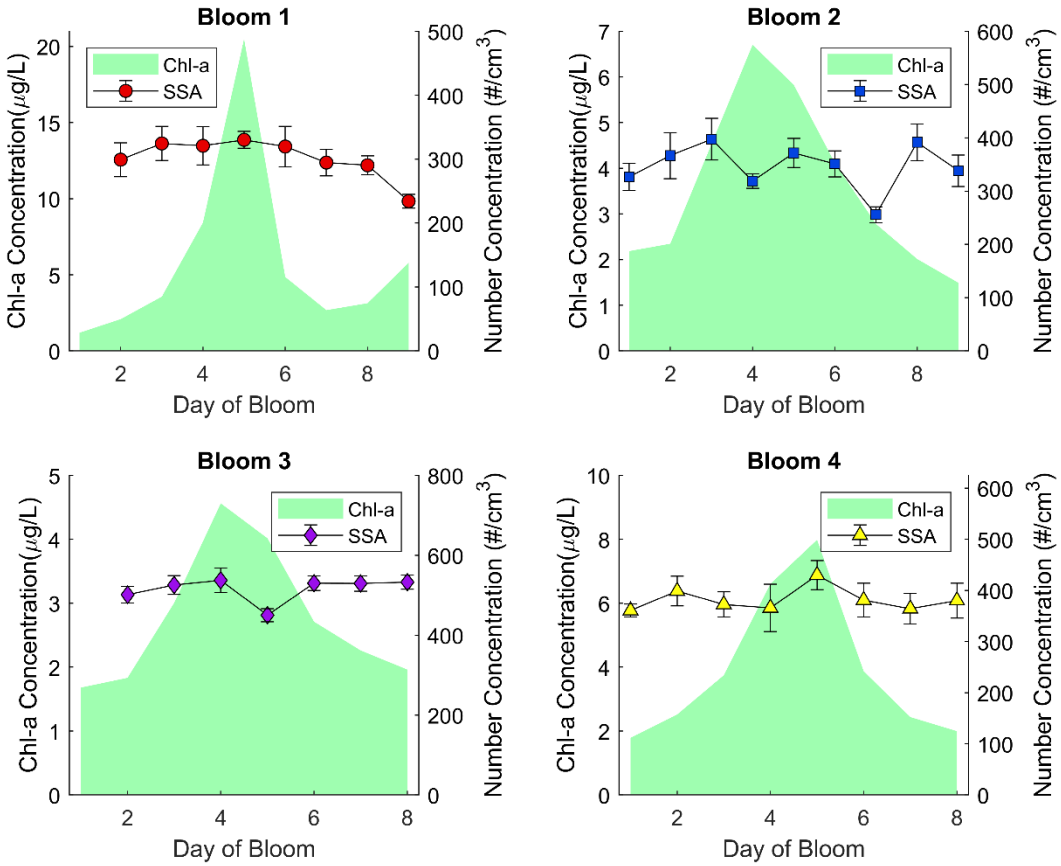

Figure 7.6. Time series of seawater chlorophyll-a concentrations and SSA number concentrations over the course of each bloom experiment. The number concentrations were calculated from the aerosol size distributions shown in Figure 7.5. Error bars represent ± 1σ.

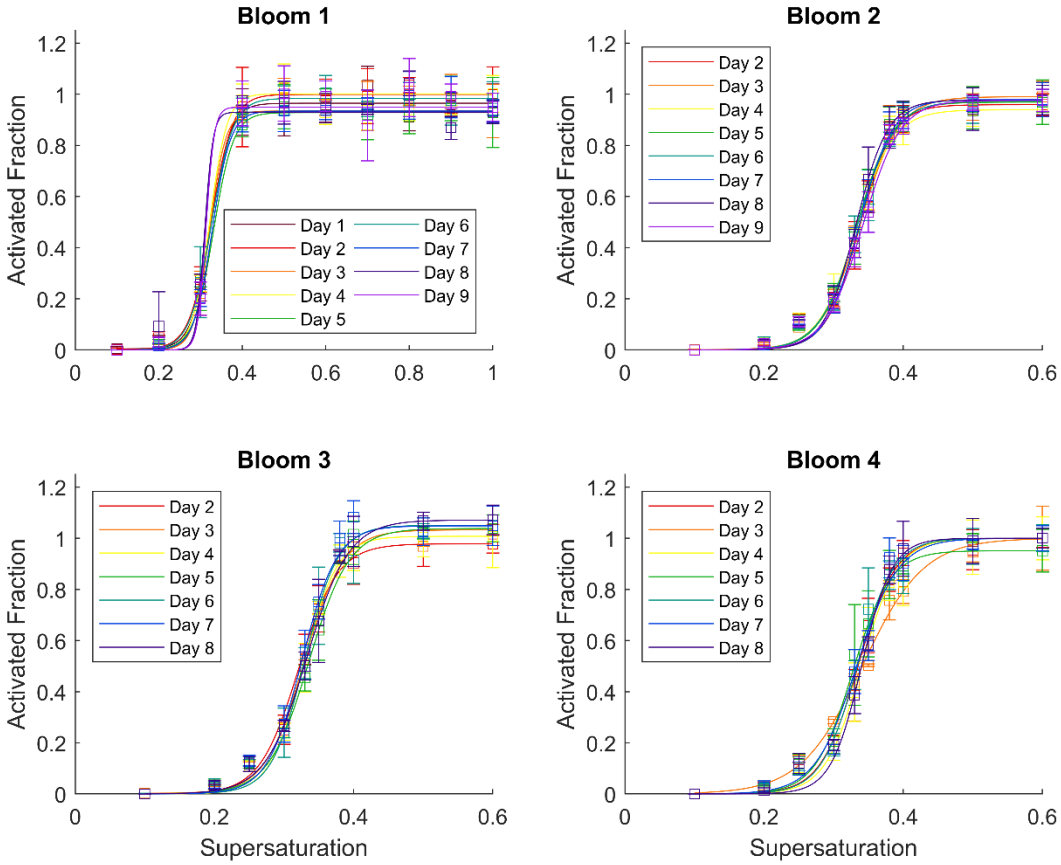

Figure 7.7. Daily SR-CCN activation curves for SSA (Dd = 50 nm) from each day of the bloom experiments. The activated fraction is the ratio of CCN/CN, as measured by the CCN-counter and CPC respectively. Sigmoid curves were fitted to the data and are shown as solid lines. Error bars represent ± 1σ. Time series of seawater chlorophyll-a concentrations and SSA number concentrations over the course of each bloom experiment. The number concentrations were calculated from the aerosol size distributions shown in Figure 7.5. Error bars represent ± 1σ.

.

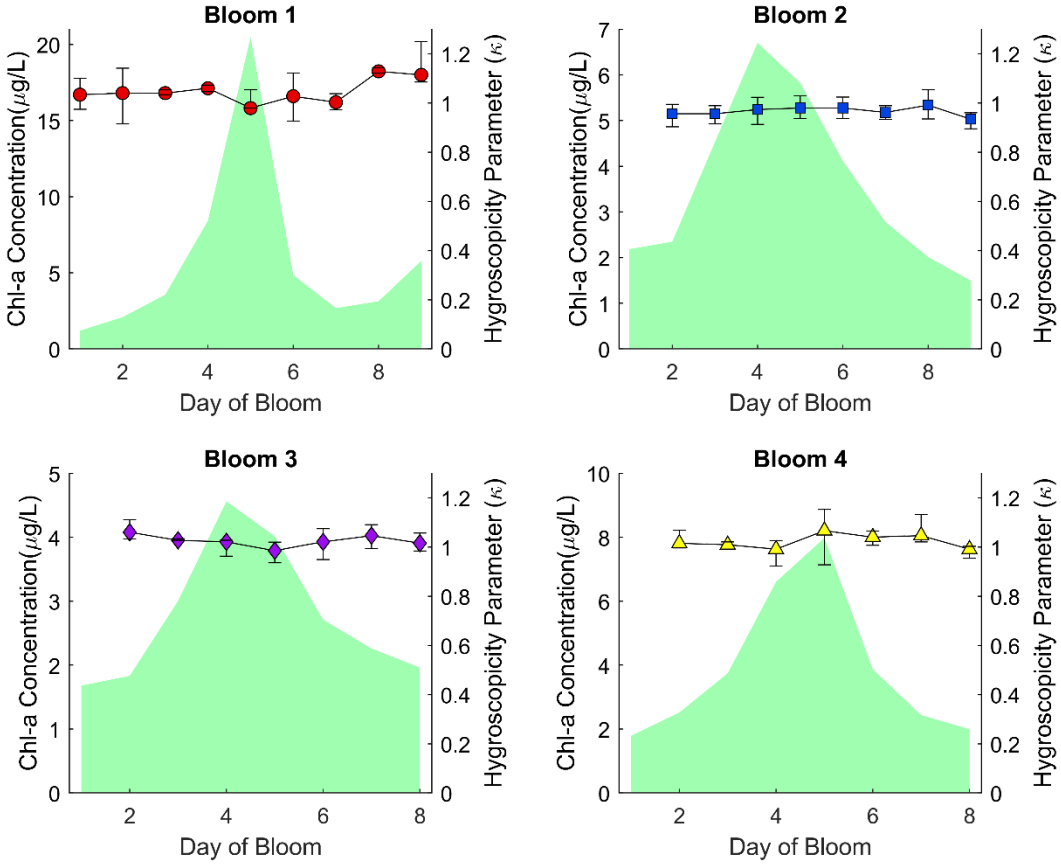

Figure 7.8. Time series of the apparent hygroscopicity parameter (κapp) for SSA (Dd = 50 nm) measured during each day of the bloom. Error bars were calculated from the uncertainty in the measured activated fractions (± 1σ). The observed changes in SSA CCN activity were quite small over the course off all bloom experiments and the mean hygroscopicity parameter was κapp= 1.02 ± 0.04. These results demonstrate the insensitivity of the CCN activity of small SSA to biological activity in seawater, as represented by the chl-a concentrations.

7.14 References

Achyuthan, K. E., Harper, J. C., Manginell, R. P. and Moorman, M. W.: Volatile metabolites emission by in vivo microalgae—an overlooked opportunity?, Metabolites, 7(3), doi:10.3390/metabo7030039, 2017.

Van Acker, E., de Rijcke, M., Asselman, J., Beck, I. M., Huysman, S., Vanhaecke, L., de Schamphelaere, K. A. C. and Janssen, C. R.: Aerosolizable marine phycotoxins and human health effects: In vitro support for the biogenics hypothesis, Mar. Drugs, 18(1), doi:10.3390/md18010046, 2020.

Alpert, P. A., Kilthau, W. P., Bothe, D. W., Radway, J. C., Aller, J. Y. and Knopf, D. A.: The influence of marine microbial activities on aerosol production: A laboratory mesocosm study, J. Geophys. Res. Atmos., 120(17), 8841–8860, doi:10.1002/2015JD023469, 2015.

Andreae, M. O., Jones, C. D. and Cox, P. M.: Strong present-day aerosol cooling implies a hot future., Nature, 435(7046), 1187–90, doi:10.1038/nature03671, 2005.

ANDREAE, M. O. and RAEMDONCK, H.: Dimethyl Sulfide in the Surface Ocean and the Marine Atmosphere: A Global View, Science (80-.)., 221(4612), 744 LP – 747, doi:10.1126/science.221.4612.744, 1983.

Arnold, S. R., Spracklen, D. V., Williams, J., Yassaa, N., Sciare, J., Bonsang, B., Gros, V., Peeken, I., Lewis, a. C., Alvain, S. and Moulin, C.: Evaluation of the global oceanic isoprene source and its impacts on marine organic carbon aerosol, Atmos. Chem. Phys., 9(4), 1253–1262, doi:10.5194/acpd-8-16445-2008, 2009.

Asselman, J., Van Acker, E., De Rijcke, M., Tilleman, L., Van Nieuwerburgh, F., Mees, J., De Schamphelaere, K. A. C. and Janssen, C. R.: Marine biogenics in sea spray aerosols interact with the mTOR signaling pathway, Sci. Rep., 9(1), 1–10, doi:10.1038/s41598-018-36866-3, 2019.

Ault, A. P., Guasco, T. L., Ryder, O. S., Baltrusaitis, J., Cuadra-Rodriguez, L. A., Collins, D. B., Ruppel, M. J., Bertram, T. H., Prather, K. A. and Grassian, V. H.: Inside versus outside: Ion redistribution in nitric acid reacted sea spray aerosol particles as determined by single particle analysis, J. Am. Chem. Soc., 135(39), 14528–14531, doi:10.1021/ja407117x, 2013.

Ault, A. P., Guasco, T. L., Baltrusaitis, J., Ryder, O. S., Trueblood, J. V., Collins, D. B., Ruppel, M. J., Cuadra-Rodriguez, L. A., Prather, K. A. and Grassian, V. H.: Heterogeneous reactivity of nitric acid with nascent sea spray aerosol: Large differences observed between and within individual particles, J. Phys. Chem. Lett., 5(15), 2493–2500, doi:10.1021/jz5008802, 2014a.

Ault, A. P., Guasco, T. L., Baltrusaitis, J., Ryder, O. S., Trueblood, J. V., Collins, D. B., Ruppel, M. J., Cuadra-Rodriguez, L. A., Prather, K. A. and Grassian, V. H.: Heterogeneous reactivity of nitric acid with nascent sea spray aerosol: Large differences observed between and within individual particles, J. Phys. Chem. Lett., 5(15), 2493–2500, doi:10.1021/jz5008802, 2014b.

Azam, F., Fenchel, T., Field, J., Gray, J., Meyer-Reil, L. and Thingstad, F.: The Ecological Role of Water-Column Microbes in the Sea, Mar. Ecol. Prog. Ser., 10, 257–263, doi:10.3354/meps010257, 1983.

Bates, T. S., Quinn, P. K., Coffman, D. J., Johnson, J. E., Upchurch, L., Saliba, G., Lewis, S., Graff, J., Russell, L. M. and Behrenfeld, M. J.: Variability in Marine Plankton Ecosystems Are Not Observed in Freshly Emitted Sea Spray Aerosol Over the North Atlantic Ocean, Geophys. Res. Lett., 47(1), doi:10.1029/2019GL085938, 2020.

Boucher, O., Randall, D., Artaxo, P., Bretherton, C., Feingold, G., Forster, P., Kerminen, V.-M. V.-M., Kondo, Y., Liao, H., Lohmann, U., Rasch, P., Satheesh, S. K., Sherwood, S., Stevens, B., Zhang, X. Y. and Zhan, X. Y.: Clouds and Aerosols, Clim. Chang. 2013 Phys. Sci. Basis. Contrib. Work. Gr. I to Fifth Assess. Rep. Intergov. Panel Clim. Chang., 571–657, doi:10.1017/CBO9781107415324.016, 2013.

Carpenter, L. J., Archer, S. D. and Beale, R.: Ocean-atmosphere trace gas exchange, Chem. Soc. Rev., 41(19), 6473–6506, doi:10.1039/c2cs35121h, 2012.

Carslaw, K. S., Boucher, O., Spracklen, D. V., Mann, G. W., Rae, J. G. L., Woodward, S. and Kulmala, M.: Atmospheric aerosols in the earth system: a review of interactions and feedbacks, Atmos. Chem. Phys. Discuss., 9(3), 11087–11183, doi:10.5194/acpd-9-11087-2009, 2009.

Carslaw, K. S., Lee, L. a, Reddington, C. L., Pringle, K. J., Rap, a, Forster, P. M., Mann, G. W., Spracklen, D. V, Woodhouse, M. T., Regayre, L. a and Pierce, J. R.: Large contribution of natural aerosols to uncertainty in indirect forcing., Nature, 503(7474), 67–71, doi:10.1038/nature12674, 2013.

Christiansen, S., Salter, M. E., Gorokhova, E., Nguyen, Q. T. and Bilde, M.: Sea Spray Aerosol Formation: Laboratory Results on the Role of Air Entrainment, Water Temperature, and Phytoplankton Biomass, Environ. Sci. Technol., doi:10.1021/acs.est.9b04078, 2019.

Cochran, R. E., Laskina, O., Jayarathne, T., Laskin, A., Laskin, J., Lin, P., Sultana, C., Lee, C., Moore, K. A., Cappa, C. D., Bertram, T. H., Prather, K. A., Grassian, V. H. and Stone, E. A.: Analysis of Organic Anionic Surfactants in Fine and Coarse Fractions of Freshly Emitted Sea Spray Aerosol, Environ. Sci. Technol., 50(5), 2477–2486, doi:10.1021/acs.est.5b04053, 2016.

Cochran, R. E., Laskina, O., Trueblood, J. V., Estillore, A. D., Morris, H. S., Jayarathne, T., Sultana, C. M., Lee, C., Lin, P., Laskin, J., Laskin, A., Dowling, J. A., Qin, Z., Cappa, C.

D., Bertram, T. H., Tivanski, A. V., Stone, E. A., Prather, K. A. and Grassian, V. H.: Molecular Diversity of Sea Spray Aerosol Particles: Impact of Ocean Biology on Particle Composition and Hygroscopicity, Chem, 2(5), 655–667, doi:10.1016/j.chempr.2017.03.007, 2017.

Collins, D. B., Ault, A. P., Moffet, R. C., Ruppel, M. J., Cuadra-Rodriguez, L. A., Guasco, T. L., Corrigan, C. E., Pedler, B. E., Azam, F., Aluwihare, L. I., Bertram, T. H., Roberts, G. C., Grassian, V. H. and Prather, K. A.: Impact of marine biogeochemistry on the chemical mixing state and cloud forming ability of nascent sea spray aerosol, J. Geophys. Res. Atmos., 118(15), 8553–8565, doi:10.1002/jgrd.50598, 2013.

Collins, D. B., Zhao, D. F., Ruppel, M. J., Laskina, O., Grandquist, J. R., Modini, R. L., Stokes, M. D., Russell, L. M., Bertram, T. H., Grassian, V. H., Deane, G. B. and Prather, K. A.: Direct aerosol chemical composition measurements to evaluate the physicochemical differences between controlled sea spray aerosol generation schemes, Atmos. Meas. Tech., 7(11), 3667–3683, doi:10.5194/amt-7-3667-2014, 2014.

Collins, D. B., Bertram, T. H., Sultana, C. M., Lee, C., Axson, J. L. and Prather, K. A.: Phytoplankton blooms weakly influence the cloud forming ability of sea spray aerosol, Geophys. Res. Lett., 9975–9983, doi:10.1002/2016GL069922, 2016.

Covert, D. S., Kapustin, V. N., Quinn, P. K. and Bates, T. S.: New particle formation in the marine boundary layer, J. Geophys. Res., 97(D18), 20581, doi:10.1029/92JD02074, 1992.

DeMott, P. J., Hill, T. C. J., McCluskey, C. S., Prather, K. A., Collins, D. B., Sullivan, R. C., Ruppel, M. J., Mason, R. H., Irish, V. E., Lee, T., Hwang, C. Y., Rhee, T. S., Snider, J. R., McMeeking, G. R., Dhaniyala, S., Lewis, E. R., Wentzell, J. J. B., Abbatt, J., Lee, C., Sultana, C. M., Ault, A. P., Axson, J. L., Diaz Martinez, M., Venero, I., Santos-Figueroa, G., Stokes, M. D., Deane, G. B., Mayol-Bracero, O. L., Grassian, V. H., Bertram, T. H., Bertram, A. K., Moffett, B. F. and Franc, G. D.: Sea spray aerosol as a unique source of ice nucleating particles, Proc. Natl. Acad. Sci., 113(21), 201514034, doi:10.1073/pnas.1514034112, 2015.

DeMott, P. J., Mason, R. H., McCluskey, C. S., Hill, T. C. J., Perkins, R. J., Desyaterik, Y., Bertram, A. K., Trueblood, J. V., Grassian, V. H., Qiu, Y., Molinero, V., Tobo, Y., Sultana, C. M., Lee, C. and Prather, K. A.: Ice nucleation by particles containing long-chain fatty acids of relevance to freezing by sea spray aerosols, Environ. Sci. Process. Impacts, 20(11), 1559–1569, doi:10.1039/c8em00386f, 2018.

Fitzgerald, J. W.: Marine aerosols: A review, Atmos. Environ. Part A, Gen. Top., 25(3–4), 533–545, doi:10.1016/0960-1686(91)90050-H, 1991.

Forestieri, S. D., Moore, K. A., Martinez Borrero, R., Wang, A., Stokes, M. D. and Cappa, C. D.: Temperature and Composition Dependence of Sea Spray Aerosol Production, Geophys. Res. Lett., 45(14), 7218–7225, doi:10.1029/2018GL078193, 2018.

Guillard, R. L. and Ryther, J. H.: Studies of Marine Planktonic Diatoms, Can. J. Microbiol., 8, 229–239, 1962.

Harb, C. and Foroutan, H.: A Systematic Analysis of the Salinity Effect on Air Bubbles Evolution: Laboratory Experiments in a Breaking Wave Analog, J. Geophys. Res. Ocean., 124(11), 7355–7374, doi:10.1029/2019JC015337, 2019.

Hasenecz, E. S., Kaluarachchi, C. P., Lee, H. D., Tivanski, A. V. and Stone, E. A.: Saccharide Transfer to Sea Spray Aerosol Enhanced by Surface Activity, Calcium, and Protein Interactions, ACS Earth Sp. Chem., 3(11), 2539–2548, doi:10.1021/acsearthspacechem.9b00197, 2019.

Hasenecz, E. S., Jayarathne, T., Pendergraft, M. A., Santander, M. V., Mayer, K. J., Sauer, J., Lee, C., Gibson, W. S., Kruse, S. M., Malfatti, F., Prather, K. A. and Stone, E. A.: Marine Bacteria Affect Saccharide Enrichment in Sea Spray Aerosol during a Phytoplankton Bloom, ACS Earth Sp. Chem., 4(9), 1638–1649, doi:10.1021/acsearthspacechem.0c00167, 2020.

Jayarathne, T., Sultana, C. M., Lee, C., Malfatti, F., Cox, J. L., Pendergraft, M. A., Moore, K. A., Azam, F., Tivanski, A. V., Cappa, C. D., Bertram, T. H., Grassian, V. H., Prather, K. A. and Stone, E. A.: Enrichment of Saccharides and Divalent Cations in Sea Spray Aerosol during Two Phytoplankton Blooms, Environ. Sci. Technol., 50(21), 11511–11520, doi:10.1021/acs.est.6b02988, 2016.

Kang, E., Root, M. J. and Brune, W. H.: Introducing the concept of Potential Aerosol Mass (PAM), Atmos. Chem. Phys. Discuss., 7(4), 9925–9972, doi:10.5194/acpd-7-9925-2007, 2007.

Kanji, Z. A., Ladino, L. A., Wex, H., Boose, Y., Burkert-Kohn, M., Cziczo, D. J. and Krämer, M.: Overview of Ice Nucleating Particles, Meteorol. Monogr., 58, 1.1-1.33, doi:10.1175/AMSMONOGRAPHS-D-16-0006.1, 2017.

Kettle, A. J., Rhee, T. S., Von Hobe, M., Poulton, A., Aiken, J. and Andreae, M. O.: Assessing the flux of different volatile sulfur gases from the ocean to the atmosphere, J. Geophys. Res. Atmos., 106(D11), 12193–12209, doi:10.1029/2000JD900630, 2001.

Kim, M. J., Michaud, J. M., Williams, R., Sherwood, B. P., Pomeroy, R., Azam, F., Burkart, M. and Bertram, T. H.: Bacterial-driven production of nitrates in seawater, Geophys. Res. Lett., 42(2), 1–8, doi:10.1002/2014GL062865.Received, 2015.

Lambe, A. T., Onasch, T. B., Massoli, P., Croasdale, D. R., Wright, J. P., Ahern, A. T., Williams, L. R., Worsnop, D. R., Brune, W. H. and Davidovits, P.: Laboratory studies of the chemical composition and cloud condensation nuclei (CCN) activity of secondary organic aerosol (SOA) and oxidized primary organic aerosol (OPOA), Atmos. Chem. Phys., 11(17), 8913–8928, doi:10.5194/acp-11-8913-2011, 2011.

Lee, C., Sultana, C. M., Collins, D. B., Santander, M. V., Axson, J. L., Malfatti, F., Cornwell, G. C., Grandquist, J. R., Deane, G. B., Stokes, M. D., Azam, F., Grassian, V. H. and Prather, K. a.: Advancing Model Systems for Fundamental Laboratory Studies of Sea Spray Aerosol Using the Microbial Loop, J. Phys. Chem. A, 150805131932006, doi:10.1021/acs.jpca.5b03488, 2015.

Malfatti, F., Lee, C., Tinta, T., Pendergraft, M. A., Celussi, M., Zhou, Y., Sultana, C. M., Rotter, A., Axson, J. L., Collins, D. B., Santander, M. V., Anides Morales, A. L., Aluwihare, L. I., Riemer, N., Grassian, V. H., Azam, F. and Prather, K. A.: Detection of Active Microbial Enzymes in Nascent Sea Spray Aerosol: Implications for Atmospheric Chemistry and Climate, Environ. Sci. Technol. Lett., 6(3), 171–177, doi:10.1021/acs.estlett.8b00699, 2019.

Mayer, K. J., Wang, X., Santander, M. V, Mitts, B. A., Sauer, J. S., Sultana, C. M., Cappa, C. D. and Prather, K. A.: Secondary Marine Aerosol Production Strongly Influenced by Biological Activity in Seawater, ACS Cent. Sci., (1), 2020.

Mccluskey, C. S., Hill, E. T. C. J., Sultana, C. M., Laskina, O., Trueblood, J., Santander, M. V., Beall, C. M., Michaud, J. M., Kreidenweis, S. M., Prather, K. A., Grassian, V. and Demott, P. J.: A mesocosm double feature: Insights into the chemical makeup of marine ice nucleating particles, J. Atmos. Sci., 75(7), 2405–2423, doi:10.1175/JAS-D-17-0155.1, 2018.

McCluskey, C. S., Hill, T. C. J., Malfatti, F., Sultana, C. M., Lee, C., Santander, M. V., Beall, C. M., Moore, K. A., Cornwell, G. C., Collins, D. B., Prather, K. A., Jayarathne, T., Stone, E. A., Azam, F., Kreidenweis, S. M. and DeMott, P. J.: A dynamic link between ice nucleating particles released in nascent sea spray aerosol and oceanic biological activity during two mesocosm experiments, J. Atmos. Sci., 74(1), 151–166, doi:10.1175/JAS-D-16-0087.1, 2017.

McCluskey, C. S., Ovadnevaite, J., Rinaldi, M., Atkinson, J., Belosi, F., Ceburnis, D., Marullo, S., Hill, T. C. J., Lohmann, U., Kanji, Z. A., O'Dowd, C., Kreidenweis, S. M. and DeMott, P. J.: Marine and Terrestrial Organic Ice-Nucleating Particles in Pristine Marine to Continentally Influenced Northeast Atlantic Air Masses, J. Geophys. Res. Atmos., 123(11), 6196–6212, doi:10.1029/2017JD028033, 2018a.

McCluskey, C. S., Hill, T. C. J., Humphries, R. S., Rauker, A. M., Moreau, S., Strutton, P. G., Chambers, S. D., Williams, A. G., McRobert, I., Ward, J., Keywood, M. D., Harnwell, J., Ponsonby, W., Loh, Z. M., Krummel, P. B., Protat, A., Kreidenweis, S. M. and DeMott, P. J.: Observations of Ice Nucleating Particles Over Southern Ocean Waters, Geophys. Res. Lett., 45(21), 11,989-11,997, doi:10.1029/2018GL079981, 2018b.

McCoy, D. T., Burrows, S. M., Wood, R., Grosvenor, D. P., Elliott, S. M., Ma, P.-L., Rasch, P. J. and Hartmann, D. L.: Natural aerosols explain seasonal and spatial patterns of Southern Ocean cloud albedo., Sci. Adv., 1(6), e1500157, doi:10.1126/sciadv.1500157, 2015.

Michaud, J. M., Thompson, L. R., Kaul, D., Espinoza, J. L., Richter, R. A., Xu, Z. Z., Lee, C., Pham, K. M., Beall, C. M., Malfatti, F., Azam, F., Knight, R., Burkart, M. D., Dupont, C. L. and Prather, K. A.: Taxon-specific aerosolization of bacteria and viruses in an experimental ocean-atmosphere mesocosm, Nat. Commun., 9(1), doi:10.1038/s41467-018-04409-z, 2018.

O'Dowd, C. D. and de Leeuw, G.: Marine aerosol production: a review of the current knowledge, Philos. Trans. R. Soc. A Math. Phys. Eng. Sci., 365(1856), 1753–1774, doi:10.1098/rsta.2007.2043, 2007.

O'Dowd, C. D., Facchini, M. C., Cavalli, F., Ceburnis, D., Mircea, M., Decesari, S., Fuzzi, S., Young, J. Y. and Putaud, J. P.: Biogenically driven organic contribution to marine aerosol, Nature, 431(7009), 676–680, doi:10.1038/nature02959, 2004.

Palm, B. B., Campuzano-Jost, P., Ortega, A. M., Day, D. A., Kaser, L., Jud, W., Karl, T., Hansel, A., Hunter, J. F., Cross, E. S., Kroll, J. H., Peng, Z., Brune, W. H. and Jimenez, J. L.: In situ secondary organic aerosol formation from ambient pine forest air using an oxidation flow reactor, Atmos. Chem. Phys., 16(5), 2943–2970, doi:10.5194/acp-16-2943-2016, 2016.

Patterson, J. P., Collins, D. B., Michaud, J. M., Axson, J. L., Sultana, C. M., Moser, T., Dommer, A. C., Conner, J., Grassian, V. H., Stokes, M. D., Deane, G. B., Evans, J. E., Burkart, M. D., Prather, K. A. and Gianneschi, N. C.: Sea spray aerosol structure and composition using cryogenic transmission electron microscopy, ACS Cent. Sci., 2(1), 40–47, doi:10.1021/acscentsci.5b00344, 2016.

Petters, M. D. and Kreidenweis, S. M.: A single parameter representation of hygroscopic growth and cloud condensation nucleus activity-Part 3: Including surfactant partitioning, Atmos. Chem. Phys., 13(2), 1081–1091, doi:10.5194/acp-13-1081-2013, 2013.

Prather, K. a, Bertram, T. H., Grassian, V. H., Deane, G. B., Stokes, M. D., Demott, P. J., Aluwihare, L. I., Palenik, B. P., Azam, F., Seinfeld, J. H., Moffet, R. C., Molina, M. J., Cappa, C. D., Geiger, F. M., Roberts, G. C., Russell, L. M., Ault, A. P., Baltrusaitis, J., Collins, D. B., Corrigan, C. E., Cuadra-Rodriguez, L. a, Ebben, C. J., Forestieri, S. D., Guasco, T. L., Hersey, S. P., Kim, M. J., Lambert, W. F., Modini, R. L., Mui, W., Pedler, B. E., Ruppel, M. J., Ryder, O. S., Schoepp, N. G., Sullivan, R. C. and Zhao, D.: Bringing the ocean into the laboratory to probe the chemical complexity of sea spray aerosol., Proc. Natl. Acad. Sci. U. S. A., 110(19), 7550–5, doi:10.1073/pnas.1300262110, 2013.

Quinn, P. K., Bates, T. S., Schulz, K. S., Coffman, D. J., Frossard, A. A., Russell, L. M., Keene, W. C. and Kieber, D. J.: Contribution of sea surface carbon pool to organic matter enrichment in sea spray aerosol, Nat. Geosci., 7(3), 228–232, doi:10.1038/ngeo2092, 2014.

Quinn, P. K., Collins, D. B., Grassian, V. H., Prather, K. A. and Bates, T. S.: Chemistry and Related Properties of Freshly Emitted Sea Spray Aerosol, Chem. Rev., 115(10), 4383–4399, doi:10.1021/cr500713g, 2015.

Rinaldi, M., Fuzzi, S., Decesari, S., Marullo, S., Santoleri, R., Provenzale, A., Von Hardenberg, J., Ceburnis, D., Vaishya, A., O'Dowd, C. D. and Facchini, M. C.: Is chlorophyll-a the best surrogate for organic matter enrichment in submicron primary marine aerosol?, J. Geophys. Res. Atmos., 118(10), 4964–4973, doi:10.1002/jgrd.50417, 2013.

Rosenfeld, D., Sherwood, S., Wood, R. and Donner, L.: Climate Effects of Aerosol-Cloud Interactions, Science (80-.)., 343(January), 379–380, doi:10.1126/science.1247490, 2014.

Ryder, O. S., Campbell, N. R., Morris, H., Forestieri, S., Ruppel, M. J., Cappa, C., Tivanski, A., Prather, K. and Bertram, T. H.: Role of Organic Coatings in Regulating N2O5 Reactive Uptake to Sea Spray Aerosol, J. Phys. Chem. A, 119(48), 11683–11692, doi:10.1021/acs.jpca.5b08892, 2015a.

Ryder, O. S., Campbell, N. R., Shaloski, M., Al-Mashat, H., Nathanson, G. M. and Bertram, T. H.: Role of Organics in Regulating ClNO2 Production at the Air-Sea Interface, J. Phys. Chem. A, 119(31), 8519–8526, doi:10.1021/jp5129673, 2015b.

Sauer, J. S., Minich, J. J., Dinasquet, J., Malfatti, F., Mayer, K. J., Santander, M. V, Pendergraft, M., Mitts, B. A., Lee, C., Wang, X., Rico, B., Knight, R., Bertram, T. H. and Prather, K. A.: Production of Dimethyl Sulfide , Methanethiol , and Dimethyl Disulfide During Controlled Phytoplankton - Bacterial Mesocosm Experiments, J. Geophys. Res. Biogeoscience, Submitted, 2020.

Sellegri, K., O'Dowd, C. D., Yoon, Y. J., Jennings, S. G. and de Leeuw, G.: Surfactants and submicron sea spray generation, J. Geophys. Res. Atmos., 111(22), 1–12, doi:10.1029/2005JD006658, 2006.

Stokes, M. D., Deane, G. B., Prather, K., Bertram, T. H., Ruppel, M. J., Ryder, O. S., Brady, J. M. and Zhao, D.: A Marine Aerosol Reference Tank system as a breaking wave analogue for the production of foam and sea-spray aerosols, Atmos. Meas. Tech., 6(4), 1085–1094, doi:10.5194/amt-6-1085-2013, 2013.

Stokes, M. D., Deane, G., Collins, D. B., Cappa, C., Bertram, T., Dommer, A., Schill, S., Forestieri, S. and Survilo, M.: A miniature Marine Aerosol Reference Tank (miniMART) as a compact breaking wave analogue, Atmos. Meas. Tech., 9(9), 4257–4267, doi:10.5194/amt-9-4257-2016, 2016.

Trueblood, J. V., Wang, X., Or, V. W., Alves, M. R., Santander, M. V., Prather, K. A. and Grassian, V. H.: The Old and the New: Aging of Sea Spray Aerosol and Formation of Secondary Marine Aerosol through OH Oxidation Reactions, ACS Earth Sp. Chem., 3(10), 2307–2314, doi:10.1021/acsearthspacechem.9b00087, 2019.

Vaattovaara, P., Huttunen, P. E., Yoon, Y. J., Joutsensaari, J., Lehtinen, K. E. J., O'Dowd, C. D. and Laaksonen, A.: The composition of nucleation and Aitken modes particles during coastal nucleation events: evidence for marine secondary organic contribution, Atmos. Chem. Phys. Discuss., 6(2), 3337–3379, doi:10.5194/acpd-6-3337-2006, 2006.

Wang, X., Sultana, C. M., Trueblood, J., Hill, T. C. J., Malfatti, F., Lee, C., Laskina, O., Moore, K. A., Beall, C. M., McCluskey, C. S., Cornwell, G. C., Zhou, Y., Cox, J. L., Pendergraft, M. A., Santander, M. V., Bertram, T. H., Cappa, C. D., Azam, F., DeMott, P. J., Grassian, V. H. and Prather, K. A.: Microbial Control of Sea Spray Aerosol Composition: A Tale of Two Blooms, ACS Cent. Sci., 1(3), 124–131, doi:10.1021/acscentsci.5b00148, 2015.

Wang, X., Deane, G. B., Moore, K. A., Ryder, O. S., Stokes, M. D., Beall, C. M., Collins, D. B., Santander, M. V., Burrows, S. M., Sultana, C. M. and Prather, K. A.: The role of jet and film drops in controlling the mixing state of submicron sea spray aerosol particles, Proc. Natl. Acad. Sci. U. S. A., 114(27), 6978–6983, doi:10.1073/pnas.1702420114, 2017.

Wilson, T. W., Ladino, L. A., Alpert, P. A., Breckels, M. N., Brooks, I. M., Browse, J., Burrows, S. M., Carslaw, K. S., Huffman, J. A., Judd, C., Kilthau, W. P., Mason, R. H., McFiggans, G., Miller, L. A., Nájera, J. J., Polishchuk, E., Rae, S., Schiller, C. L., Si, M., Temprado, J. V., Whale, T. F., Wong, J. P. S., Wurl, O., Yakobi-Hancock, J. D., Abbatt, J. P. D., Aller, J. Y., Bertram, A. K., Knopf, D. A. and Murray, B. J.: A marine biogenic source of atmospheric ice-nucleating particles, Nature, 525(7568), 234–238, doi:10.1038/nature14986, 2015.

Chapter 8. Conclusions

8.1 Synopsis

This dissertation investigates the production of chemical metabolites by algae as they proceed through their life cycles and are affected by external conditions. Chapter 2 describes measurements of gaseous compounds from marine mesocosm experiments which showed the unexpected production of non-dimethyl sulfide organosulfur gases. Chapter 3 demonstrates the usage of 3 complementary mass spectrometric technique to identify algal metabolites associated with grazing. Chapter 4 demonstrates the capabilities of chemical ionization mass spectrometry to monitor algae gas production in real time as algae are infected with deleterious grazers. This dissertation also investigates the chemical complexity of the marine environment though the measurement and simulation of the ocean-atmosphere interface. Chapter 5 applies a new ionization method, liquid sampling atmospheric pressure glow discharge, towards the analysis of highly saline organic samples. Chapter 6 outlines a recent experimental intensive which utilized a newly characterized wave channel device for multiple marine mesocosm experiments. Finally, Chapter 7 is a review of the ocean-atmosphere experimental approach, demonstrating the progress made by replicating the ocean's biological and chemical complexity in the laboratory.

8.2 Conclusions

8.2.1 Production of dimethyl sulfide, methanethiol, and dimethyl disulfide during controlled phytoplankton-bacterial mesocosm experiments

This study examined the production of volatile organosulfur compounds (OSCs) during marine mesocosm experiments to better understand factors which control dimethylsulfoniopropionate (DMSP) breakdown ratios between dimethyl sulfide (DMS) and the less common methanethiol (MeSH) and dimethyl disulfide (DMDS) (Reisch et al., 2011). Benzene

cluster cation chemical ionization mass spectrometry was used to measure daily headspace concentrations of OSCs in the headspace of marine aerosol reference tanks (MARTs) filled with coastal seawater as they proceeded through 3 separate mesocosm blooms. DMDS and MeSH were observed to be significantly elevated, with (MeSH+DMDS)/DMS flux ratios up to 30 in comparison limited series of literature field measurements which are normally below 0.07 (Kettle et al., 2001; Leck and Rodhe, 1991; Turner et al., 1995). DMDS, generally a very dilute OSC in the natural marine environment compared to observations in this work, was shown with control experiments to be produced by a mixture of instrumental artifacts which amounted to 35% of the production, with the remaining DMDS formed naturally within the MART, either through abiotic MeSH dimerization or by an unknown biotic mechanism.

The unexpected production of large quantities MeSH and DMDS stimulated investigations into the bacterial assemblage and functional genes present during each mesocosm. 16S amplicon sequencing identified a wide variety of DMS, MeSH, and DMDS correlated bacteria, with many taxa which are known to possess functional genes related to DMSP metabolism. The gammaproteobacteria methylophaga spp., observed to increase during the end of mesocosm 1 during high MeSH production, is well known to participate in DMS oxidation which produces MeSH.(Boden et al., 2010) Measurements of aqueous DMSP catabolic genes, dddP and dmdA which are the first steps towards the formation of DMS and MeSH respectively (Zeng et al., 2016), showed ample counts of dddP but were sparse for dmdA suggesting alternative enzymatic pathways or routes of sulfur metabolism may have been active such as the catabolism of DMS to MeSH suggested above.

Given the high ratios of MeSH and DMDS to DMS, the atmospheric impacts of this work indicate that in some cases, up to 40% of atmospheric sulfate could originate from MeSH and

DMDS in coastal areas with similar biological and chemical drivers to those encountered in this work, which compares to 10% for measurements obtained from the field (Kettle et al., 2001). The findings in this paper advance the understanding of marine OSC production by introducing and characterizing a scenario in which the production of non-DMS OSCs was substantially different that field observations, showing that significant complexity in this marine biogeochemical system remains to be understood.

8.2.2 Multi-scale examination of grazer-induced changes in molecular signatures of cyanobacteria

This study sought to investigate the molecular fingerprints generated by mixtures of cyanobacteria and amoeba grazers using a complementary set of mass spectrometric techniques suited for the solid, liquid, and gas phase. Imaging mass spectrometry (IMS) performed on agar lawns of Synechococcus elongatus PCC 7942 infected by a heterolobosean amoeba (HGG1) measured several m/z's which corresponded with healthy algae as well as specific markers of grazing activity. Some grazing metabolites were determined to be specific to algae-grazer pairs, while others were generally attributable to the grazing process. Notably, many m/z's decreased in intensity as a response to grazing as productive algal cells were lost.

To provide a putative identity of metabolites observed in IMS, liquid chromatography tandem mass spectrometry (LC-MS/MS) was performed on aqueous samples of healthy and grazer-infected algae. Molecular networking (Wang et al., 2016) of LC-MS/MS data was used to identify metabolites and also investigate associations between them. This analysis showed that chlorophyll-a and its breakdown products were responsive indicators of algal grazing, with losses of Mg^{2+}, phytol, and methyl formate being key chemical transformations between chlorophyll-a and the grazing-induced breakdown products.

Given the observations of chlorophyll-a breakdown products connected by losses of phytol and methyl formate, an investigation of the gas phase species produced by grazer-impacted algae was undertaken using gas chromatography mass spectrometry and chemical ionization mass spectrometry. These analyses were unable to observe methyl formate in grazer-infected algal cultures, which is likely due to either chemical degradation of methyl formate to methanol and formic acid, or rapid uptake by grazers (Francisco, 2003; Jogunola et al., 2011; Stirling and Dalton, 1980). A phytol breakdown product, phytol ketone, was observed in the gas phase to change in response to grazing, however these changes were not straightforward to interpret as the loss in algae biomass combined with grazer consumption, led to an overall loss in phytol ketone intensity as opposed to increases predicted by IMS and LC-MS/MS. Despite mixed results for phytol ketone and methyl formate, headspace analysis observed numerous other gas species which changed in response to grazing, either increasing or decreasing in intensity, showing promise for using gas analysis as a diagnostic method for early grazer detection (Reese et al., 2019). This work adds detail regarding the changes in metabolite production during algal grazing, showing that while the connections between breakdown products can be identified, translating that information to gas phase production is not immediately straightforward and requires more investigation.

8.2.3 Early Detection of Algal Grazing with Rapid, Continuous Measurements of Volatile Gases

A chemical ionization time of flight mass spectrometer (CI-TOFMS) was utilized for continuous, high frequency (1 Hz) gas phase monitoring of 3 cyanobacterial cultures as they grew in healthy conditions and then were subsequently infected with a ciliate grazer. Contemporaneously with gas phase composition measurements, this study was the first time the quantity of algal biomass and grazer cell counts were measured to connect the dynamics of algal

senescence and grazer productivity with volatile gas production. CI-TOFMS analysis identified over 40 unique ions which varied in intensity over the algae life cycle and in response to grazer activity. Notable species, m/z 18 (ammonia), m/z 137 (monoterpenes), and m/z 70 (C_4H_7N) were observed to change drastically (>10σ) 17-44 hours after grazer addition, which contrasted detection by microscopy which took 68-94 hours to observe grazer cells in the algal cultures.

Interestingly, the duration of time between grazer addition and CI-TOFMS detection of grazers via volatile gases was found to be variant across each of the 3 algae-grazer experiments, with faster gas phase detection occurring in sampling vessels where algal biomass was higher. This interesting result stimulated an analysis of the time series behavior of gas production by algae with respect to biomass. While it was expected that larger total changes in gas phase composition would be expected for higher algal biomasses, we also found that the relative change in gas intensities were greater, indicating the algal response to grazing was more pronounced. These results add a new element to investigations of algal gas responses to grazers, showing that the metabolic and biological state of the algal culture affects its response to grazing.

Lastly, an analysis of CI-TOFMS performance was undertaken to characterize the instrument's ability to monitor multiple sampling vessels in a short period. Utilizing the automated sampling schedule which switched from clean zero air to the algae-containing vessel, the ion equilibration time ($1/e^2$) was obtained. For non-ammonia volatile gases measured by the CI-TOFMS, the average time for gases to equilibrate on the CI-TOFMS inlet was ~6 seconds, with more basic gases and ammonia requiring longer due to their high solubility which causes them to dissolve into water microlayers present on sampling tubing (Liu et al., 2019). Nevertheless, using the longest 1/e2 time, CI-TOFMS analysis using the experimental conditions in this work could monitor up to 10 culturing vessels per hour. These experiments together show that CI-TOFMS is

a promising method for monitoring algae for the presence of grazers, however the impacts of algal biomass on response need to be better understood.

8.2.4 Liquid sampling atmospheric pressure glow discharge ionization as a technique for the characterization of salt-containing organic samples

The liquid sampling atmospheric pressure glow discharge (LS-APGD) ion source, previously developed for the analysis of inorganic species using high resolution mass spectrometry (HRMS) (Hoegg et al., 2016), was repurposed for the analysis high salinity organic samples derived from the marine environment. The ionization source's behavior was first benchmarked using a triglyceride reference mixture, composed of multiple medium to long chain triglycerides which were analyzed across a variety of probe conditions and salinities from 0.01 to 100mM NaCl. This analysis found that the LS-APGD was highly sensitive to the sample mixture and capable of analyzing saline samples up to 0.5M NaCl compared to the predominant method of liquid sample ionization for HRMS, electrospray ionization (ESI) which could not generate informative spectra over 1mM NaCl. An important factor was discovered during the triglyceride mixture analysis which showed significantly diminished fragmentation of triglycerides at salinities above 1mM NaCl. This stabilization was attributed to the energetically favorable complexation of sodium cations by the triglyceride, which has been observed in previous studies of collisionally induced fragmentation of adducted triglycerides (Duffin et al., 1991; Grossert et al., 2014). This study showed that the salt-tolerant features of the LS-APGD do not mean a lack of dependence on salt concentration towards the sensitivity of response, and therefore samples must be calibrated at the salinity for which they are analyzed in the LS-APGD.

The LS-APGD was then challenged with an analysis of highly complex marine dissolved organic matter (mDOM) samples run in both saltless and 50mM added NaCl and compared to the

same analyses typically performed using ESI. The LS-APGD was able to generate similar quantities and diversity of ions as ESI, but in addition, its ability to measure mDOM at elevated salt concentrations was also clearly better than ESI. This analysis was further applied to the first direct analysis of organic rich untreated seawater without pre-processing or salt removal which is routinely used for ESI analysis. The usage of LS-APGD for salt-containing organic samples opens many new opportunities for better charactering the marine environment in its native state.

8.2.5 The sea spray chemistry and particle evolution study (SeaSCAPE): overview and experimental methods

In Summer 2019, an intensive experiment utilizing the Scripps Institution of Oceanography wave channel was undertaken to study the chemical and biological dynamics of the ocean atmosphere interface. This experiment brought 13,000 L of coastal seawater indoors where it naturally evolved after the addition of nutrients to stimulate a mesocosm. The biological progress of this mesocosm proceeded with a large peak of productive phytoplankton biomass which receded with the onset of heterotrophic bacteria later. The evolution of phytoplankton assemblages started from a diatom dominated community structure towards a mixed population of microzooplankton and mixed aggregates during the later phase of the bloom, likely responsible for the increases in dissolved organic matter observed to increase over the mesocosm duration.

As wave channels have been used previously for ocean-atmosphere simulations, but have only been characterized to a limited extent (Prather et al., 2013), experiments studying the wave channel's sea spray aerosol (SSA) production characteristics, cleanliness, air flow, and ideal sampling locations were undertaken. These experiments identified an ideal sampling port location and depth, informed by maximum aerosol particle concentrations, however SSA concentrations were found to be highly variable on a diurnal cycle. SSA particle counts information, combined

with high-variance measurements of wave channel headspace velocity indicate that turbulent air flow conditions likely exist in the wave channel which impose important constraints on sampling procedures. The wave channel headspace was shown to be vulnerable to the introduction of anthropogenic gaseous contaminants which penetrated through the air handling system. To rectify this challenge, the usage of an isolated sampling vessel for marine gases was demonstrated to avoid these contaminants while still allowing sampling of the chemically and biologically representative wave channel.

8.2.6 CAICE studies: insights from a decade of ocean-atmosphere experiments in the laboratory

The merits, achievements, and current limitations of the ocean-atmosphere experimental approach were discussed. Marine aerosol reference tanks and wave channels are contrasted with previously used SSA generation methods to show the improvements in chemically and morphologically representative SSA generation (Collins et al., 2014; Prather et al., 2013; Stokes et al., 2013). The ability of ocean-atmosphere simulators to enable the connection of marine biology to atmospheric aerosols and atmospheric chemistry through mesocosm experiments is shown. Further discoveries made possible by the ocean-atmosphere approach include the impact of marine enzymes on seawater and aerosol composition, the heterogeneous chemical reactivity of SSA (Ault et al., 2014), trace gas production (Kim et al., 2015), mechanisms of microorganism aerosolization (Michaud et al., 2018), and quantitative measurements of ice nucleating particles (DeMott et al., 2015). Modern improvements to the ocean-atmosphere experimental approach are discussed which show the need for the addition of more complexity which include oxidative and anthropogenic perturbations to mesocosm experiments to better simulate the natural environment.

8.3 Future directions

8.3.1 Further studies on the origin and fate of marine organosulfur species

Chapter 2 investigated the production of methanethiol (MeSH), dimethyl sulfide (DMS), and dimethyl disulfide (DMDS) during three marine mesocosm experiments. Chapter 2 showed that the production of MeSH was possibly due to the oxidative consumption of DMS by heterotrophic bacteria, while DMDS was formed through an unknown process likely caused by aqueous MeSH dimerization. The factors controlling the consumption of DMS by marine heterotrophic bacteria needs to be understood with greater clarity, specifically regarding the fate of MeSH generated from DMS catabolism (Kiene and Bates, 1990). Ascertaining the factors which control MeSH uptake and uptake inhibition will allow for better predictions of MeSH:DMS ratios in the natural environment, especially in productive coastal zones where this ratio is more variable (Kettle et al., 2001). While MeSH dimerization to DMDS has been observed in some aqueous solutions and on metallic surfaces (Chin and Lindsay, 1994), the natural dimerization rate of MeSH in seawater or on particles in seawater is unknown and should be determined through careful measurements of dissolved MeSH by GC/MS or CIMS

8.3.2 Cataloging, characterizing, and understanding metabolites produced from algae-grazer interactions

Chapter 3 combined mass spectrometric analyses from the solid, liquid, and gas phase to identify metabolites produced from systems where algae were infected by an amoeba grazer. While results shown in Chapter 3 implicate the grazing-induced degradation of chlorophyll-a, the expected volatile breakdown products, methyl formate and phytol were unobserved. The biochemistry of chlorophyll-a breakdown is complex and poorly understood (Hortensteiner, 1999). Further research is necessary to understand whether these compounds are assimilated by grazers or further broken down into other metabolites (Rontani and Volkman, 2003). While a large fraction

of algal cell biomass can be chlorophyll-a, other metabolites, such as proteins and lipids are sought by grazers. Further investigations of the IMS dataset for non-chlorophyll-a metabolites produced in response to grazing is warranted.

Chapter 4 utilized chemical ionization time-of-flight mass spectrometry to monitor the production of volatile metabolites produced by grazer infected algae at much higher sampling frequencies than analyses in Chapter 3. This analysis found connections between algal biomass and the intensity and speed of volatile gas responses to grazing. Algal signaling and allelopathy to grazing is poorly understood. (Bacellar Mendes and Vermelho, 2013; Zuo, 2019). Better understanding the factors which control the rate at which algae respond to grazing via signaling should be studied as the response rate may inform better practices for pest control. Many algae, especially cyanobacteria, adjust culture pH in response to changes to state of health.(Watson, 2003) As many volatile gases, especially those that are acidic or basic, have volatility that is dependent on pH (Zhang et al., 2017), further investigations into the role of changing algal culture pH and observations of gases should be studied as the ability to detect these gases reliably during grazing could be impacted.

In this study, the chemical ionization reagent gas utilized was $(H_2O)_nH^+$, which tends to ionize low-oxidized organic compounds and amines. The usage of an alternative ion chemistry, such as $(C_6H_6)^+$ which could identify other algal volatile gases such as organosulfur species which may respond faster or in other informative ways to grazing should be investigated.

8.3.3 Taking advantage of a salt tolerant high-resolution mass spectrometer

Chapter 5 of this dissertation utilized liquid sampling atmospheric pressure glow discharge ionization to analyze organic samples of marine salinity for high resolution mass spectrometry. These results were limited to the analysis of a triglyceride reference mixture and marine dissolved

organic matter, however other high-salt sample types such as sea spray aerosol have yet to be investigated. While the impacts of salt concentration on ionization efficiency and fragmentation of triglycerides were characterized, the impacts of salt on ionization of other common marine molecular classes such as amino acids and polysaccharides should be further explored to understand their ionization dynamics in the presence of salts. As noted in Chapter 5, utilization of LS-APGD at high sample salinities (>0.1M) tended to cause buildup of salt material on the mass spectrometer inlet which eventually disrupted analysis. Modifications to the LS-APGD to circumvent this issue would provide valuable opportunities to directly analyze seawater samples should be attempted.

8.3.4 Better replicating the complexity of ocean-atmosphere interactions

Chapter 6 of this dissertation focuses on the characterization of the Scripps Institution of Oceanography wave channel and an overview of the SeaSCAPE experimental intensive. This work found significant variability in SSA particle concentrations that varied during daily sampling as well as by sampling location along the channel. Measurements into the air flow characteristics, especially turbulence, in the wave channel should be pursued to contextualize the observed variability in SSA sampling and make further improvements. Wave channel headspace cleanliness from anthropogenic organic gases such as benzene and toluene as well as NOx was another factor that was challenging to maintain during SeaSCAPE. Focus on future work should investigate technologies for the removal of volatile organic compounds from high volume air flows, specifically targeting the easiest to remove species, aromatics and highly oxidizable gases, which most significantly affect the production of secondary organic aerosol in oxidative chambers.

Chapter 7 of this dissertation was a review of the ocean-atmosphere experimental approach developed in CAICE. Numerous findings have been made for SSA generated with this method,

however future work needs to focus on the quantity and types of volatile organic gases produced by natural marine biology. Furthermore, the chemical, biological, and physical complexity still needs to be increased in ocean-atmosphere simulators to better resemble the natural environment. New ocean atmosphere simulators should study the impacts of wind, temperature, natural and anthropogenic oxidants, water acidity, and increasing trophic levels of biology on marine gas and aerosol production.

8.4 References

Ault, A. P., Guasco, T. L., Baltrusaitis, J., Ryder, O. S., Trueblood, J. V, Collins, D. B., Ruppel, M. J., Cuadra-Rodriguez, L. A., Prather, K. A. and Grassian, V. H.: Heterogeneous reactivity of nitric acid with nascent sea spray aerosol: Large differences observed between and within individual particles, J. Phys. Chem. Lett., 5(15), 2493–2500, doi:10.1021/jz5008802, 2014.

Bacellar Mendes, L. and Vermelho, A.: Allelopathy as a potential strategy to improve microalgae cultivation, Biotechnol. Biofuels, 6(1), 152, doi:10.1186/1754-6834-6-152, 2013.

Boden, R., Kelly, D. P., Murrell, J. C. and Schäfer, H.: Oxidation of dimethylsulfide to tetrathionate by Methylophaga thiooxidans sp. nov.: A new link in the sulfur cycle, Environ. Microbiol., 12(10), 2688–2699, doi:10.1111/j.1462-2920.2010.02238.x, 2010.

Chin, H. W. and Lindsay, R. C.: Mechanisms of Formation of Volatile Sulfur Compounds following the Action of Cysteine Sulfoxide Lyases, J. Agric. Food Chem., 42(7), 1529–1536, doi:10.1021/jf00043a026, 1994.

Collins, D. B., Zhao, D. F., Ruppel, M. J., Laskina, O., Grandquist, J. R., Modini, R. L., Stokes, M. D., Russell, L. M., Bertram, T. H., Grassian, V. H., Deane, G. B. and Prather, K. A.: Direct aerosol chemical composition measurements to evaluate the physicochemical differences between controlled sea spray aerosol generation schemes, Atmos. Meas. Tech., 7(11), 3667–3683, doi:10.5194/amt-7-3667-2014, 2014.

DeMott, P. J., Hill, T. C. J., McCluskey, C. S., Prather, K. A., Collins, D. B., Sullivan, R. C., Ruppel, M. J., Mason, R. H., Irish, V. E., Lee, T., Hwang, C. Y., Rhee, T. S., Snider, J. R., McMeeking, G. R., Dhaniyala, S., Lewis, E. R., Wentzell, J. J. B., Abbatt, J., Lee, C., Sultana, C. M., Ault, A. P., Axson, J. L., Diaz Martinez, M., Venero, I., Santos-Figueroa, G., Stokes, M. D., Deane, G. B., Mayol-Bracero, O. L., Grassian, V. H., Bertram, T. H., Bertram, A. K., Moffett, B. F. and Franc, G. D.: Sea spray aerosol as a unique source of ice nucleating particles, Proc. Natl. Acad. Sci., 113(21), 201514034, doi:10.1073/pnas.1514034112, 2015.

Duffin, K. L., Henion, J. D. and Shieh, J. J.: Electrospray and Tandem Mass Spectrometry Characterization of Acylglycerol Mixtures That Are Dissolved in Nonpolar Solvents, Anal. Chem., 63(17), 1781–1788, doi:10.1021/ac00017a023, 1991.

Francisco, J. S.: Mechanistic study of the gas-phase decomposition of methyl formate, J. Am. Chem. Soc., 125(34), 10475–10480, doi:10.1021/ja0117682, 2003.

Grossert, J. S., Herrera, L. C., Ramaley, L. and Melanson, J. E.: Studying the chemistry of cationized triacylglycerols using electrospray ionization mass spectrometry and density functional theory computations, J. Am. Soc. Mass Spectrom., 25(8), 1421–1440, doi:10.1007/s13361-014-0917-9, 2014.

Hoegg, E. D., Barinaga, C. J., Hager, G. J., Hart, G. L., Koppenaal, D. W. and Marcus, R. K.: Preliminary Figures of Merit for Isotope Ratio Measurements: The Liquid Sampling-Atmospheric Pressure Glow Discharge Microplasma Ionization Source Coupled to an Orbitrap Mass Analyzer, J. Am. Soc. Mass Spectrom., 27(8), 1393–1403, doi:10.1007/s13361-016-1402-4, 2016.

Hortensteiner, S.: Chlorophyll breakdown in higher plants and algae, Cell. Mol. Life Sci., 56, 330–347, doi:https://doi.org/10.1007/s000180050434, 1999.

Jogunola, O., Salmi, T., Waärnå, J., Mikkola, J. P. and Tirronen, E.: Kinetics of methyl formate hydrolysis in the absence and presence of a complexing agent, Ind. Eng. Chem. Res., 50(1), 267–276, doi:10.1021/ie101045k, 2011.

Kettle, A. J., Rhee, T. S., Von Hobe, M., Poulton, A., Aiken, J. and Andreae, M. O.: Assessing the flux of different volatile sulfur gases from the ocean to the atmosphere, J. Geophys. Res. Atmos., 106(D11), 12193–12209, doi:10.1029/2000JD900630, 2001.

Kiene, R. P. and Bates, T. S.: Biological removal of dimethyl sulphide from sea water, Nature, 345(6277), 702–705, doi:10.1038/345702a0, 1990.

Kim, M. J., Michaud, J. M., Williams, R., Sherwood, B. P., Pomeroy, R., Azam, F., Burkart, M. and Bertram, T. H.: Bacterial-driven production of nitrates in seawater, Geophys. Res. Lett., 42(2), 1–8, doi:10.1002/2014GL062865., 2015.

Leck, C. and Rodhe, H.: Emissions of marine biogenic sulfur to the atmosphere of northern Europe, J. Atmos. Chem., 12(1), 63–86, doi:10.1007/BF00053934, 1991.

Liu, X., Deming, B., Pagonis, D., Day, D. A., Palm, B. B., Talukdar, R., Roberts, J. M., Veres, P. R., Krechmer, J. E., Thornton, J. A., De Gouw, J. A., Ziemann, P. J. and Jimenez, J. L.: Effects of gas-wall interactions on measurements of semivolatile compounds and small polar molecules, Atmos. Meas. Tech., 12(6), 3137–3149, doi:10.5194/amt-12-3137-2019, 2019.

Michaud, J. M., Thompson, L. R., Kaul, D., Espinoza, J. L., Richter, R. A., Xu, Z. Z., Lee, C., Pham, K. M., Beall, C. M., Malfatti, F., Azam, F., Knight, R., Burkart, M. D., Dupont, C. L. and Prather, K. A.: Taxon-specific aerosolization of bacteria and viruses in an experimental ocean-atmosphere mesocosm, Nat. Commun., 9(1), doi:10.1038/s41467-018-04409-z, 2018.

Prather, K. a, Bertram, T. H., Grassian, V. H., Deane, G. B., Stokes, M. D., Demott, P. J., Aluwihare, L. I., Palenik, B. P., Azam, F., Seinfeld, J. H., Moffet, R. C., Molina, M. J., Cappa, C. D., Geiger, F. M., Roberts, G. C., Russell, L. M., Ault, A. P., Baltrusaitis, J., Collins, D. B., Corrigan, C. E., Cuadra-Rodriguez, L. a, Ebben, C. J., Forestieri, S. D., Guasco, T. L., Hersey, S. P., Kim, M. J., Lambert, W. F., Modini, R. L., Mui, W., Pedler, B. E., Ruppel, M. J., Ryder, O. S., Schoepp, N. G., Sullivan, R. C. and Zhao, D.: Bringing

the ocean into the laboratory to probe the chemical complexity of sea spray aerosol., Proc. Natl. Acad. Sci. U. S. A., 110(19), 7550–5, doi:10.1073/pnas.1300262110, 2013.

Reese, K. L., Fisher, C. L., Lane, P. D., Jaryenneh, J. D., Moorman, M. W., Jones, A. D., Frank, M. and Lane, T. W.: Chemical Profiling of Volatile Organic Compounds in the Headspace of Algal Cultures as Early Biomarkers of Algal Pond Crashes, Sci. Rep., 9(1), 1–10, doi:10.1038/s41598-019-50125-z, 2019.

Reisch, C. R., Moran, M. A. and Whitman, W. B.: Bacterial catabolism of dimethylsulfoniopropionate (DMSP), Front. Microbiol., 2, 1–12, doi:10.3389/fmicb.2011.00172, 2011.

Rontani, J.-F. and Volkman, J. K.: Phytol degredation products as biogeochemical tracers in aquatic environments, Plant Cell., 34, 1–35, 2003.

Stirling, D. I. and Dalton, H.: Oxidation of dimethyl ether, methyl formate and bromomethane by Methylococcus capsulatus (Bath), J. Gen. Microbiol., 116(2), 277–283, doi:10.1099/00221287-116-2-277, 1980.

Stokes, M. D., Deane, G. B., Prather, K., Bertram, T. H., Ruppel, M. J., Ryder, O. S., Brady, J. M. and Zhao, D.: A Marine Aerosol Reference Tank system as a breaking wave analogue for the production of foam and sea-spray aerosols, Atmos. Meas. Tech., 6(4), 1085–1094, doi:10.5194/amt-6-1085-2013, 2013.

Turner, S. M., Nightingale, P. D., Broadgate, W. and Liss, P. S.: The distribution of dimethyl sulphide and dimethylsulphoniopropionate in Antarctic waters and sea ice, Deep. Res. Part II, 42(4–5), 1059–1080, doi:10.1016/0967-0645(95)00066-Y, 1995.

Wang, M., Carver, J. J., Phelan, V. V., Sanchez, L. M., Garg, N., Peng, Y., Nguyen, D. D., Watrous, J., Kapono, C. A., Luzzatto-Knaan, T., Porto, C., Bouslimani, A., Melnik, A. V., Meehan, M. J., Liu, W. T., Crüsemann, M., Boudreau, P. D., Esquenazi, E., Sandoval-Calderón, M., Kersten, R. D., Pace, L. A., Quinn, R. A., Duncan, K. R., Hsu, C. C., Floros, D. J., Gavilan, R. G., Kleigrewe, K., Northen, T., Dutton, R. J., Parrot, D., Carlson, E. E., Aigle, B., Michelsen, C. F., Jelsbak, L., Sohlenkamp, C., Pevzner, P., Edlund, A., McLean, J., Piel, J., Murphy, B. T., Gerwick, L., Liaw, C. C., Yang, Y. L., Humpf, H. U., Maansson, M., Keyzers, R. A., Sims, A. C., Johnson, A. R., Sidebottom, A. M., Sedio, B. E., Klitgaard, A., Larson, C. B., Boya, C. A. P., Torres-Mendoza, D., Gonzalez, D. J., Silva, D. B., Marques, L. M., Demarque, D. P., Pociute, E., O'Neill, E. C., Briand, E., Helfrich, E. J. N., Granatosky, E. A., Glukhov, E., Ryffel, F., Houson, H., Mohimani, H., Kharbush, J. J., Zeng, Y., Vorholt, J. A., Kurita, K. L., Charusanti, P., McPhail, K. L., Nielsen, K. F., Vuong, L., Elfeki, M., Traxler, M. F., Engene, N., Koyama, N., Vining, O. B., Baric, R., Silva, R. R., Mascuch, S. J., Tomasi, S., Jenkins, S., Macherla, V., Hoffman, T., Agarwal, V., Williams, P. G., Dai, J., Neupane, R., Gurr, J., Rodríguez, A. M. C., Lamsa, A., Zhang, C., Dorrestein, K., Duggan, B. M., Almaliti, J., Allard, P. M., et al.: Sharing and community curation of mass spectrometry data with Global Natural Products Social Molecular Networking, Nat. Biotechnol., 34(8), 828–837, doi:10.1038/nbt.3597, 2016.

Watson, S. B.: Cyanobacterial and eukaryotic algal odour compounds: Signals or by-products? A review of their biological activity, Phycologia, 42(4), 332–350, doi:10.2216/i0031-8884-42-4-332.1, 2003.

Zeng, Y. X., Qiao, Z. Y., Yu, Y., Li, H. R. and Luo, W.: Diversity of bacterial dimethylsulfoniopropionate degradation genes in surface seawater of Arctic Kongsfjorden, Sci. Rep., 6, 1–9, doi:10.1038/srep33031, 2016.

Zhang, X., Chingin, K., Zhong, D., Liang, J., Ouyang, Y. and Chen, H.: On the chemistry of 1-pyrroline in solution and in the gas phase, Sci. Rep., 7(1), 1–8, doi:10.1038/s41598-017-08217-1, 2017.

Zuo, Z.: Why algae release volatile organic compounds - The emission and roles, Front. Microbiol., 10(MAR), 1–7, doi:10.3389/fmicb.2019.00491, 2019.